IOP PUBLISHING NONLINEARITY

Nonlinearity **21** (2008) R1–R118 doi:10.1088/0951-7715/21/1/R01

INVITED ARTICLE

Wigner's dynamical transition state theory in phase space: classical and quantum

Holger Waalkens[1,2], **Roman Schubert**[1] **and Stephen Wiggins**[1]

[1] School of Mathematics, University of Bristol, University Walk, Bristol BS8 1TW, UK
[2] Department of Mathematics, University of Groningen, Nijenborgh 9, 9747 AG Groningen, The Netherlands

E-mail: h.waalkens@math.rug.nl, roman.schubert@bristol.ac.uk and s.wiggins@bristol.ac.uk

Received 1 August 2007, in final form 1 November 2007
Published 7 December 2007
Online at stacks.iop.org/Non/21/R1

Recommended by J P Keating

Abstract

We develop Wigner's approach to a dynamical transition state theory in phase space in both the classical and quantum mechanical settings. The key to our development is the construction of a normal form for describing the dynamics in the neighbourhood of a specific type of saddle point that governs the evolution from reactants to products in high dimensional systems. In the classical case this is the standard Poincaré–Birkhoff normal form. In the quantum case we develop a normal form based on the Weyl calculus and an explicit algorithm for computing this quantum normal form. The classical normal form allows us to discover and compute the phase space structures that govern classical reaction dynamics. From this knowledge we are able to provide a direct construction of an energy dependent dividing surface in phase space having the properties that trajectories do not locally 're-cross' the surface and the directional flux across the surface is minimal. Using this, we are able to give a formula for the directional flux through the dividing surface that goes beyond the harmonic approximation. We relate this construction to the flux–flux autocorrelation function which is a standard ingredient in the expression for the reaction rate in the chemistry community. We also give a classical mechanical interpretation of the activated complex as a normally hyperbolic invariant manifold (NHIM), and further describe the structure of the NHIM. The quantum normal form provides us with an efficient algorithm to compute quantum reaction rates and we relate this algorithm to the quantum version of the flux–flux autocorrelation function formalism. The significance of the classical phase space structures for the quantum mechanics of reactions is elucidated by studying the phase space distribution of scattering states. The quantum normal form also provides an efficient way of computing Gamov–Siegert resonances. We relate these resonances to the lifetimes of the quantum activated complex. We consider several one, two and three degree-of-freedom

systems and show explicitly how calculations of the above quantities can be carried out. Our theoretical framework is valid for Hamiltonian systems with an arbitrary number of degrees of freedom and we demonstrate that in several situations it gives rise to algorithms that are computationally more efficient than existing methods.

PACS numbers: 82.20.Ln, 05.45.−a, 34.10.+x

1. Introduction

The subject of this paper is *transition state theory*—classical and quantum. Transition state theory (TST) (sometimes also referred to as 'activated complex theory' or the 'theory of absolute reaction rates') is widely regarded as the most important theoretical and computational approach to analysing chemical reactions, both from a qualitative and a quantitative point of view. The central ideas of TST are so fundamental that in recent years TST has been recognized as a very natural and fruitful approach in areas far beyond its origin of conception in chemistry. For example, it has been used in atomic physics [JFU00], studies of the rearrangements of clusters [KB99, KB02], solid state and semi-conductor physics [JTDF84, Eck95], diffusion dynamics in materials [VMG02], cosmology [dOdAST02] and celestial mechanics [JRL+02, WBW05b].

The literature on TST is vast, which befits the importance, utility, breadth, scope and success of the theory. Searching ISI Web of Knowledge on the phrase 'transition state theory' yields more than 17 600 hits. Searching Google with the same phrase gives more than 41 000 000 hits. There have been numerous reviews of TST, and the relatively recent review of [TGK96] is an excellent source for earlier reviews, historical accounts, books, pedagogical papers and handbook chapters dealing with TST. Moreover, [TGK96] is notable from the point of view that in little more that 10 years it has attracted more than 458 citations (and it also contains 844 references)!

Certainly the existence of this vast literature begs the question 'why does there need to be yet another paper on the theoretical foundations of TST, what new could it possibly add?' The one word answer to this question is 'dynamics'. Advances in experimental techniques over the past twenty years, such as, e.g. femtosecond laser spectroscopy, transition state spectroscopy and single molecule techniques [Neu92, PZ95, Zew00], now provide us with 'real time' dynamical information on the progress of a chemical reaction from 'reactants' to 'products'. At the same time, these new experimental techniques, as well as advances in computational capabilities, have resulted in a growing realization among chemists of the ubiquity of nonergodic behaviour in complex molecular systems, see, e.g. [SY04, BHC05, BHC06, Car05]. All of these results point to a need to develop a framework for studying and understanding dynamics in high dimensional dynamical systems and recently developed tools in computational and applied dynamical systems theory are giving new insights and results in the study of the dynamics of molecular systems with three or more degrees of freedom. In particular, we will show how these recent advances in analytical and computational techniques can enable us to realize Wigner's *dynamical* picture of transition state theory in *phase space* for systems with three or more degrees of freedom. However, to set this in context we first need to describe a bit of the historical background and setting of TST.

Transition state theory was created in the 1930s, with most of the credit being given to Eyring, Polanyi and Wigner, who are referred to as the 'founding trinity of TST' in Miller's important review on chemical reaction rates [Mil98b]. Nevertheless, important contributions were also made by Evans, Farkas, Szilard, Horiuti, Pelzer and Marcelin, and these are described in the discussions of the historical development of the subject given in [LK83, PT05a].

The approach to TST taken by Eyring [Eyr35] emphasized thermodynamics (see the perspective paper of [Pet00]). The approach of Wigner [Wig38] on the other hand is based on classical mechanics (see the perspective paper of [Gar00]). It is the dynamical approach of Wigner that is the focus of this paper. Despite the fact that the original framework of TST is classical mechanics, it is natural to consider quantum mechanical versions of this approach to reaction dynamics. We will first describe the classical mechanical setting, and then consider the quantum mechanical version, and we will emphasize how much of the structure and philosophy of the classical approach influences the quantum approach.

1.1. Transition state theory: classical dynamics

To begin with, we first examine the assumptions of classical TST, as set out by Wigner. Wigner begins by stating that he considers chemical reactions in a setting where the equilibrium Maxwell–Boltzmann velocity and energy distributions are maintained (see [Mah74] for a detailed discussion of this point) and for which the potential energy surface is known [Gar00]. He then gives the following assumptions from which he derives TST:

1. the motion of the nuclei occurs on the Born–Oppenheimer potential energy surface ('electronic adiabaticity' of the reaction)
2. classical mechanics adequately describes the motion of the nuclei
3. there exists a hypersurface in phase space dividing the energy surface into a region of reactants and a region of products having the property that all trajectories that pass from reactants to products must cross this dividing surface precisely once.

It is important to note that Wigner clearly developed his ideas in *phase space*, the arena for dynamics. It is important to keep this in mind since a great deal of later developments occur in *configuration space*, in which certain dynamical properties are obscured.

From the modelling point of view, the first two assumptions are of a very different nature from the third. The first two are central to developing the model, or *dynamical system* (i.e. determining the potential energy surface and Hamiltonian function). As a result, once a dynamical system describing the reaction has been developed the third 'assumption' cannot really have the status of an assumption. Rather, such a hypersurface satisfying these properties must be shown to exist for the dynamical system. Of course, in practice this is exactly how the theory is utilized. One starts with a dynamical system describing the reaction, and then one attempts to construct a 'dividing surface' having the required characteristics. It is precisely this third 'assumption' that is at the heart of this paper and from which, as we shall see, many dynamical consequences flow.

We will be concerned with dynamics on a fixed energy surface. In this paper 'energy' means the total energy of the system, e.g. the sum of the kinetic and potential energies. More mathematically, the energy surface is the level set of the Hamiltonian function[3]. This is important to keep in mind because in not an insignificant portion of the relevant literature the meaning of the phrase 'energy surface' is actually the 'potential energy surface', and a great

[3] Hamiltonian functions can be more general than the sum of the kinetic and potential energy terms. They could contain magnetic terms or Coriolis terms, for example. Nevertheless, we will still refer to the level set of the Hamiltonian function as the 'energy surface'.

deal of effort is expended in attempting to infer dynamical phenomena from the 'topography' of the potential energy surface. Certainly for one degree-of-freedom (DoF) Hamiltonian systems (i.e. one configuration space coordinate and one associated momentum) one can understand all possible dynamics from the shape of the potential energy surface. This is definitely not true for more than one DoF (or else dynamical phenomena such as 'chaos' would have been discovered many years earlier). However, two DoF Hamiltonian systems, where the Hamiltonian is the sum of the kinetic and potential energies, do allow for certain constructions based solely on the potential energy surface that imply important dynamical phenomena. We will survey these later in this introduction. We emphasize that similar constructions using the potential energy surface for systems having more than 2 DoF simply do not work in the same way as they do for 2 DoF.

Now to realize assumption 3, on a fixed energy surface, we need to choose a dividing surface that will 'separate' the energy surface into two parts ('two parts' is a bit too simplistic, but we will come back to that later)—one part corresponding to the reactants and the other to products. The dividing surface would have the additional (dynamical) property that trajectories evolving from reactants to products cross it only once. Again, these reactant and product regions are typically defined via the potential energy surface. They are often interpreted as 'potential wells' (i.e. local minima of the potential energy function) that are 'separated' by a 'saddle point' and a surface (in configuration space) passing through a neighbourhood of the saddle point serves as the dividing surface [Pec81]. We will show that for systems with three or more DoF such a configuration space approach, in several different ways, does not allow one to realize Wigner's original construction of TST. In fact, this is a central message of this paper. It can be misleading, and even wrong, to attempt to infer dynamical phenomena from the topography of the potential energy surface.

In the series of papers [WWJU01, UJP+01, WBW04a, WW04, WBW04b, WBW05a, WBW05c] the fundamental framework for phase space TST is developed. The starting point is classical mechanics and a Hamiltonian function describing the system (the same as [Wig38]). The Hamiltonian can be expressed in any convenient set of coordinates, have any number, d, degrees of freedom (DoF) and does *not* have to be of the form 'kinetic plus potential energy', e.g. it can include rotational or magnetic terms.

With the Hamiltonian function in hand, the next step is to locate particular saddle-like equilibrium points of the associated Hamilton's equations that are of a certain type. Namely, the matrix associated with the linearization of Hamilton's equations about the equilibrium has a pair of real eigenvalues of opposite signs ($\pm\lambda$) and $2d-2$ purely imaginary eigenvalues occurring in complex conjugate pairs ($\pm i\omega_k$, $k = 2, \ldots, d$). Such equilibria are called saddle-centre-...-centres, and structures associated with these equilibria provide the fundamental mechanism for 'transformation' in a large, and diverse, number of applications (some listed at the beginning of this introduction), whose *dynamical* consequences have remained a mystery.

Of course, locating saddles is in the spirit of classical transition state theory, but there is an important difference here. We are concerned with the *dynamical consequences* of certain types of saddles of Hamilton's equations in phase space. The usual approach is to consider saddles of the potential energy surface (the setting of the 'landscape paradigm' [Wal04]). However, if the Hamiltonian has the form of the sum of the kinetic energy and the potential energy, then there is a correspondence between the rank one saddles of the potential energy surface and the saddle-centre-...-centre type equilibria of Hamilton's equations. But here we emphasize the phase space setting and the influence of this saddle in the dynamical arena of phase space. We reiterate that a central point of ours is that it is difficult, and often misleading, to try to infer dynamics from properties of configuration space.

Next we seek to understand the phase space geometry near this saddle-centre-...-centre (henceforth referred to as a 'saddle') equilibrium point of Hamilton's equations. An understanding of the geometry will give rise to a set of coordinates that will enable us to explicitly compute the phase space structures that govern transport and to quantify their influence on trajectories. This set of coordinates is realized in an algorithmic manner through the use of the Poincaré–Birkhoff normal form procedure. These *normal form coordinates* are central to our theory and the resulting analytical and computational techniques. In particular, they enable us to show that 'near' the saddle the energy surface has what we call the 'bottleneck property' which facilitates the construction of an energy dependent dividing surface. This dividing surface has the 'no-recrossing' property and the flux across the dividing surface is 'minimal' (in a sense that we will make precise). Moreover, the coordinates also naturally give rise to a 'dynamical reaction path'. We want to describe these notions in a bit more detail and place them in the context of the chemistry literature.

Further, we note that historically it has been well recognized that the computation of quantities associated with chemical reactions is greatly facilitated by adopting a 'good' set of coordinates [JR61, EM74, Mil76, Mil77]. In particular, if the Hamiltonian is separable, i.e. there is a set of *configuration space coordinates* in terms of which the equations of motion decouple, then the choice of a dividing surface with the no-recrossing property is trivial [Gar00]. This situation is extremely special and therefore almost irrelevant for chemical reactions. However, the normal form method shows that such a decoupling can always be obtained in the neighbourhood of the dividing surface through the symplectic ('canonical') transformation of the full phase space coordinates (i.e. a symplectic transformation mixing the configuration space coordinates and the conjugate momenta). The normal form thus is a constructive way of obtaining 'good' coordinates in phase space.

The bottleneck property of the energy surface and the energy dependent dividing surface. The geometry or 'shape' of a fixed energy surface has received little attention, as opposed to consideration of the geometry or 'shape' of *potential* energy surfaces. This is unfortunate since an understanding of the geometry of the energy surface is essential for constraining and interpreting the possible global dynamics. Nevertheless, the lack of attention to this issue is understandable since such considerations give rise to extremely difficult mathematical problems. As an example, the importance of an understanding of the topology of the energy surface for an understanding of the dynamics of the three body problem was emphasized by Poincaré [Poi93a, Poi93b, Poi93c], and work on this problem has involved some of the giants of mathematics of the 20th century and has resulted in the creation of many new areas of mathematical research. Very recent results on the three body problem, as well as a discussion of the history of the subject, can be found in [MMW98], and a discussion of the developments of an appropriate computational framework for studying such questions for general Hamiltonian systems can be found in [KMM04]. We would expect that similar studies of the structure of the energy surfaces for standard Hamiltonian's arising in studies of reaction dynamics will be similarly fruitful and lead to new global dynamical insights.

However, there are 'local' results that describe the geometry of the energy surface that are very relevant to studies of reaction dynamics and TST. In particular, for a range of energies above that of the saddle, the $(2d-1)$-dimensional energy surface locally has the structure of the product of a $(2d-2)$-dimensional sphere with the real line, $S^{2d-2} \times \mathbb{R}$. We say that in this region of the phase space the energy surface has the 'bottleneck property' because it is (locally) separated into two pieces: $S^{2d-2} \times \mathbb{R}^+$ and $S^{2d-2} \times \mathbb{R}^-$, and $S^{2d-2} \times \{0\}$ is the dividing surface that separates these two pieces of the energy surface, and we identify the two pieces separated by this dividing surface as 'reactants' and 'products'. It will turn out that $\mathbb{R}$

corresponds to a natural (energy dependent) 'reaction coordinate' and S^{2d-2} will correspond to (energy dependent) unstable bath modes, or vibrations 'normal' to the reaction coordinate.

It should be clear that the geometry of the energy surface, as the energy varies, is an important feature of reaction dynamics. In particular, the geometry changes with energy and the 'bottleneck', $S^{2d-2} \times \mathbb{R}$, may deform into a more complicated shape as the energy is further increased above that of the saddle. This can lead to the 'breakdown' of the validity of transition state theory in the sense that we are not able to construct a dividing surface separating reactants from products that is not recrossed. We note that an 'energy limit' for TST has been discussed in [GL77, SK78]. Looking at it another way, the energy surface deforms in such a way that the distinction between reactants and products becomes unclear. This is one way in which TST can 'break down'. We will mention one other way after we have introduced the notion of a normally hyperbolic invariant manifold.

The 'no-recrossing' property and minimal flux. The dividing surface described above can be realized through the normal form computations and transformations [WWJU01, UJP+01]. The high dimensional spherical geometry, S^{2d-2}, is significant in several ways. A sphere is separated into two parts along its equator, which in this high dimensional case is given by S^{2d-3}, the $(2d-3)$-dimensional sphere[4]. The Hamiltonian vector field is transverse to each hemisphere, but in an opposite sense for each hemisphere. This indicates the evolution from reactants to products through one hemisphere, and the evolution from products to reactants through the other hemisphere. Transversality of the Hamiltonian vector field to a hemisphere is the mathematical property one needs to show that there are 'no local recrossing of trajectories', as is shown in [UJP+01] and in this paper. The Hamiltonian vector field is tangent to the equator of the sphere[5]. Mathematically, this is the condition for the equator, S^{2d-3}, to be an invariant manifold. More precisely, it is saddle-like in stability and an example of a *normally hyperbolic invariant manifold*, or NHIM [Wig94, WWJU01, UJP+01]. The NHIM has the physical interpretation as the 'activated complex'—an unstable super molecule poised between reactants and products.

Except for the equator, S^{2d-3} (which is a normally hyperbolic invariant manifold), the dividing surface thus is locally a 'surface of no return' in the sense that all trajectories that start on the dividing surface exit a neighbourhood of the dividing surface [UJP+01]. Most importantly for reaction dynamics, the energy surface has the 'bottleneck property'. That is, our dividing surface locally divides the energy surface into two, disjoint components, which correspond to reactants and products. Therefore the *only* way a trajectory can pass from one of these components of the energy surface to the other is to pass through the dividing surface. The issue of 'recrossing' is an important part of the choice of the dividing surface. Truhlar [Tru98] distinguishes two types of recrossing: *local* and *global* recrossing. Local recrossing cannot occur with our choice of dividing surface. However, global recrossing is a very different matter. If the energy surface is compact (i.e. closed and bounded, for our purposes) then the Poincaré recurrence theorem [Arn78] implies that global recrossing must occur for almost all trajectories crossing the dividing surface. Moreover, the existence of homoclinic orbits and heteroclinic cycles may also be an intrinsic feature of the dynamics [WBW04a, WBW04b, WBW05a, WBW05b, WBW05c]. Their existence also implies that global recrossing cannot be avoided regardless of the choice of transition state; in other words,

[4] Think of the familiar, and easily visualizable, case of the two-dimensional sphere, S^2. It is separated into two hemispheres by its equator, a sphere of one less dimension, S^1.

[5] If the Hamiltonian vector field is transverse to one hemisphere, transverse to the other hemisphere in the opposite directional sense, and it varies smoothly in phase space, then we can view the equator as where the Hamiltonian vector field 'changes direction'.

global recrossing is a fundamental property of the dynamics and its presence does not therefore indicate the limitations of any particular method for constructing a dividing surface.

Wigner [Wig38] pointed out that the effect of trajectories recrossing the dividing surface would result in 'too high values of the reaction rate'. This observation naturally leads to the notion of *variational transition state theory*, where the idea is to vary the choice of dividing the surface in such a way that the flux across the dividing surface attains a minimum value (see [Kec67] and the review paper of [TG84]). The latter review paper contains 206 references and has more than 390 citations, which is indicative of the fact that variational transition state theory is a huge subject in its own right. Much of the work that falls under the heading of 'variational transition state theory' involves dividing surfaces in configuration space (see [JJ01, BJ05] for a systematic development of this approach). These beautiful results obtained by our predecessors can with modern day mathematical tools be formulated differently, leading to more general results. The beginnings of a general framework for such an approach was first given by [Mac91], and this was used in [WW04] to show that the dividing surfaces computed by the normal form approach described in [WWJU01, UJP+01] have 'minimal flux'. It is worth re-emphasizing, that our dividing surface construction and our flux calculations are carried out in phase space, not configuration space. The work in [WW04] implies that one cannot find a surface in configuration space for systems with more than 2 DoF that is free of *local* recrossing, and therefore has minimal flux (*unless* the system is given in coordinates in which the Hamiltonian is separable or has some very special symmetries).

It is worth pointing out here that flux across a dividing surface is a 'local property' with respect to the given surface, i.e. it does not require integration of trajectories for its computation. If one makes a 'bad' choice of dividing surface that is not free of *local* recrossing then one must compute trajectories to correct for the local recrossing effect (in the chemistry literature these are referred to as 'dynamical corrections' to the rate, see [MM97,Pri05] for specific examples of the effect of recrossing and how it is treated). This is particularly apparent when one carefully examines a standard ingredient in the reaction rate in use in the chemistry community—the flux–flux autocorrelation function for which we show that the use of our dividing surface and phase space approach allows the computation of this function without the long time integration of trajectories.

In summary, our work on the geometry of reaction dynamics allows for a careful analysis and realization of Wigner's [Wig38] dynamical version for transition state theory. The dynamical foundations of Wigner's transition state theory received a great deal of attention in the 1970s in a series of seminal papers by Child, McLafferty, Pechukas and Pollak [PM73, PP77, PP78, PP79a, PP79b, PCP80, PC80, CP80, Pec81], and there is a wealth of dynamical ideas in these works. However, it is important to realize that these works focus almost entirely on 2 DoF, and most of the results have not been generalized to 3 or more DoF. Nevertheless, for 2 DoF they show how to construct a dividing surface without recrossing from the projection of a periodic orbit, the Lyapunov orbit associated with a saddle equilibrium point, to configuration space—the so-called *periodic orbit dividing surface* (PODS) [PM73, PP78]. In addition to this construction being limited to 2 DoF systems, the Hamiltonian must be of type 'kinetic plus potential'—Coriolis terms due to a rotating coordinate system or a magnetic field are not allowed.

The generalization to more than two degrees of freedom and to more general Hamiltonians has posed a major problem for decades. The reasons for the problems are twofold. On the one hand, a construction based on configuration space, as in the case of the PODS, simply does not work for systems with more than two degrees of freedom, as discussed in [WW04]. On the other hand, it was not clear what replaces the periodic orbit in higher dimension. For more than two degrees of freedom a periodic orbit lacks sufficient dimensionality to serve as

a building block for the construction of a dividing surface. In fact, a completely new object, a so-called *normally hyperbolic invariant manifold* (NHIM) [Wig94], takes the place of the periodic orbit in two degrees of freedom. It is interesting to recall a remark of Pechukas from his influential review paper [Pec81]:

> It is easy to guess that generalized transition states in problems with more degrees of freedom must be unstable invariant classical manifolds of the appropriate dimension, but to our knowledge no calculations have been done.

Our work gives a precise characterization of these invariant manifolds in terms of the NHIM, as well as shows exactly what calculations are required to realize them in specific systems.[6] The NHIM is not only the building block for the construction of a dividing surface in arbitrary dimension, but it also forms the basis for locating the transition pathways for reactions in terms of the stable and unstable manifolds of the NHIM [WBW04b].

Finally, we remarked earlier that one way in which TST can 'break down' is through deformation of the energy surface. Another way in which it may break down is through *bifurcation of the NHIM*. For 2 DoF systems the NHIM is a periodic orbit and bifurcation theory for periodic orbits in Hamiltonian systems is well developed [Mey70, MH92]. Bifurcation of the NHIM in 2 DoF systems can lead to stable motions that 'trap' trajectories in the transition region. This has been observed in [CP80, MM97]. At present there exists no general bifurcation theory for NHIMs in systems with d DoF, $d \geqslant 3$, and this poses a limitation to the range of validity of our approach. In this case the relevant NHIMs are $(2d-3)$-dimensional and contain their own nontrivial dynamics. The development of bifurcation theory for such objects promises to be a challenging and interesting mathematical problem that should yield new insights into reaction dynamics.

The dynamical reaction path. Thus far we have described the geometry of the energy surface near a saddle and the nature of the dividing surface that separates the energy surface near the saddle into two regions corresponding to reactants and products. Now we want to describe in more detail how trajectories approach, and move away from, the dividing surface. For this purpose the notion of the *reaction path* arises.

Traditionally, the *reaction path* of a polyatomic molecule is the steepest descent path on the potential energy surface (if mass-weighted Cartesian coordinates are used) connecting saddle points and minima [MHA80]. Hence, it is a configuration space notion derived from properties of the potential energy surface that is used to describe a specific dynamical phenomenon. Similarly to TST, the literature related to reaction paths is vast. Searching ISI Web of Knowledge on the phrase 'reaction path' yields more than 6600 hits. Searching Google with the same phrase gives more than 7900 000 hits. It is often assumed that a reacting trajectory, when projected into configuration space, will be 'close' to this reaction path, and much work is concerned with developing configuration space coordinates (and their associated conjugate

[6] It is perhaps worth pointing out that when reading the chemistry literature mathematicians might experience some confusion surrounding the phrases 'transition state' and 'dividing surface'. In some parts of the literature they are used synonymously. In other parts, they have a very different meaning, as can be seen from the above quote of Pechukas. A dividing surface *cannot* be an invariant manifold, or else trajectories could not cross the surface (trajectories on an invariant manifold remain on that manifold for all time). The confusion probably arose out of the PODS theory. In that situation the dividing surface and the invariant manifold (the periodic orbit) project to the same line in configuration space. The projection of a reactive trajectory to configuration space intersects this line in configuration space. In the three-dimensional energy surface, however, the trajectory intersects the dividing surface and not the periodic orbit. The dividing surface is a two-dimensional sphere, S^2, in this case (i.e. it is of one dimension less than the three-dimensional energy surface) and the periodic orbit is an invariant one-dimensional sphere, S^1, that forms the equator of the sphere. The same situation holds for more than two DoF. The equator of our dividing surface is a normally hyperbolic invariant manifold (but a periodic orbit does not have sufficient dimensions to satisfy this requirement).

momenta) in which the dynamical equations that describe evolution 'close' to this reaction path can be expressed (see, e.g., [Mar66a,Mar66b,Mar68,MHA80,Mil83,Nat92b,Nat92a,NGT+91, Nat91, Nat04, GGB01, GGB04, GB05]). However, despite its fundamental importance in the historical development of the subject of reaction dynamics, one might question the relationship of this configuration based reaction path to the actual path taken in the course of the dynamical evolution from reactants to products. In fact, in recent years numerous experiments have shown that the actual dynamics may exhibit significant deviations from the 'classical reaction path' [PCC+05, SSH02, AYAD03, LCZ+07, TLL+04, Bow06, HK06, PMOE06].

In this paper we show that the coordinates given by normal form theory also give rise to an intrinsic *dynamical reaction path*, which is a trajectory on the energy surface. Its construction follows from the dynamical properties associated with the NHIM ('activated complex'). The NHIM has stable and unstable manifolds which, as we will explain in detail, have the structure of spherical cylinders, $S^{2d-3} \times \mathbb{R}$, and form the phase space conduits for reaction in the sense that they enclose the reactive trajectories. Our dynamical reaction path forms the centre line of these spherical cylinders and gives rise to a phase space description of an invariant 'modal partitioning' along the reaction path corresponding to energy in the reacting mode and energies in the (nonlinear) vibrational modes normal to the reaction path.

1.2. Transition state theory: quantum dynamics

Historically a great deal of effort—mostly in the chemistry community—has been devoted to developing a quantum mechanical version of transition state theory (see the work by Miller and coworkers [Mil98a]). Nonetheless, a quantum mechanical formulation of transition state theory is still considered an open problem (see the recent review by Pollak and Talkner [PT05b]). The nature of the difficulties is summed up succinctly by Miller [Mil98b]:

> —the conclusion of it all is that there is no uniquely well-defined quantum version of TST in the sense that there is in classical mechanics. This is because tunnelling along the reaction coordinate necessarily requires one to solve the (quantum) dynamics for some finite region about the TS dividing surface, and if one does this fully quantum mechanically there is no 'theory' left, i.e. one has a full dimensional quantum treatment which is ipso facto exact, a quantum simulation.

Part of the problem leading to this statement originates from (classical) transition state theory where the necessary theoretical framework to realize transition state theory for multi-dimensional systems as described in this paper has been developed only very recently. In particular, this realization of classical TST requires one to work in *phase space* (as opposed to configuration space). This also has consequences for the development of a quantum version of transition state theory (which should reduce to classical TST in the classical limit and have all the computational benefits of a 'local' theory as in the classical case). Again due to the lack of a theoretical framework, most approaches to developing a quantum version of transition state theory involve attempts to achieve a separation of the Schrödinger equation that describes the chemical reaction. However, as in the classical case this separation does not exist. In contrast to this, we will develop a quantum version of TST which is built in a systematic way on the classical theory presented in this paper.

In the classical case the key idea to realize TST is to transform the Hamilton function describing the reaction to normal form. In the quantum case we will establish a quantum version of the classical normal form theory, and from this all of the quantum reaction dynamics quantities will flow. In particular, the classical phase space structures that we found will play a central role in the computation of quantum mechanical reaction quantities. Quantum

mechanical computations are notable for suffering from the 'curse of dimensionality.' We will see that the property of integrability which follows from the normal form in the classical case will have a quantum manifestation that renders computations of 'local' reaction quantities tractable for high dimensional systems. This leads to very efficient algorithms for computing, e.g. quantum mechanical cumulative reaction probabilities and resonances.

Classical normal form theory is a standard technique of dynamical systems theory, and there are many textbooks and tutorial papers that describe the subject. However, quantum normal form theory is probably much less familiar in both the dynamical systems community as well as the chemistry community. It is therefore useful to provide a discussion of the background, context and historical development of the subject.

Symplectic transformations like those involved in the classical normal form theory also have a long history in the study of partial differential equations. In the theory of *microlocal analysis* they form one of the core techniques introduced in the late 1960s and early 1970s in the fundamental papers by Egorov, Hörmander and Duistermaat, [Ego69, Hör71, DH72]. These ideas lead naturally to the consideration of normal forms for partial differential equations, and these were used to study the solvability and the singularities of solutions. The basic idea is the following. One can associate with a linear partial differential operator a function on phase space by substituting momenta for the partial differentials. The resulting function is called the *symbol* of the operator. One can now use a symplectic transformation to find coordinates in which the symbol has a particularly simple form. The crucial point now is that the tools from microlocal analysis allow one to quantize such a symplectic transformation. The result is a unitary operator which is called a *Fourier integral operator* and yields the transformation of the original partial differential operator corresponding to the symplectic transformation of its symbol (plus small error terms). This is the content of Egorov's theorem [Ego69]. If the transformed symbol assumes a simple form, then the the transformed operator assumes a simple form too and its properties can be studied more easily. This construction was the basis for many developments in the theory of linear partial differential equations in the 1970s, such as the study of the solvability and the propagation of singularities (see, e.g., the compendium by Hörmander [Hör85a, Hör85b]).

In quantum mechanics the relation between operators and symbols mentioned above is the relation between the Hamilton operator, which defines a quantum mechanical system, and the corresponding classical Hamilton function, which defines the classical dynamical system corresponding to the quantum system. The operator thus is the quantization of the symbol, and microlocal analysis provides us with a powerful set of tools to analyse quantum systems. These ideas were applied, e.g. in the seminal work by Colin de Verdière on modes and quasimodes [CdV77], where he constructed classical and quantum normal forms around invariant tori in phase space which still is an active area of research (see, e.g., the recent work by Cargo *et al* [CGSL$^+$05]).

In transition state theory the classical Hamiltonian relevant for reaction type dynamics has an equilibrium point, and as we have discussed in the first part of the introduction one can use symplectic transformations to bring the Hamilton function to a normal form in the neighbourhood of the equilibrium point. The tools from microlocal analysis will allow us to quantize this symplectic transformation and bring the Hamilton operator into a normal form, too. The problem of quantum normal forms near equilibrium points of the symbol has been studied quite extensively already. But most of this work concerns *stable* equilibrium points (see [BV90, EGH91, Sjö92, BGP99]). Here the aim is to construct a quantum normal form in order to study energy spectra and eigenfunctions with very high precision. In the physics literature [Rob84, Ali85, Eck86, FE88a, FE88b] the same question was studied based on the Lie approach to classical normal forms. In the early works there has been some

confusion about the ordering problem in quantization, but these problems have been resolved by Crehan [Cre90].

The case of an unstable equilibrium point (or more precisely an equilibrium of saddle-centre-. . .-centre type), which occurs in transition state theory, has received much less attention in the literature so far. In this case one expects the operator to have continuous spectrum, and so instead of computing eigenvalues one is looking for resonances. Resonances are complex eigenvalues. Their imaginary parts are related to the finite lifetime of quantum states in the neighbourhood of the unstable equilibrium point. Since the problem is no longer self-adjoint, the determination of resonances is in general a much more difficult problem than that of eigenvalues (see [Zwo99] for a review). The case of a Hamilton operator for which the symbol has an unstable equilibrium is one of the few cases where resonances can be computed to high accuracy using a complex Bohr–Sommerfeld quantization. For 2 DoF systems, this was developed in [GS87, Sjö03] (for references in the chemistry literature, see, e.g. [SM91, Moi98] where resonances are known as Gamov–Siegert eigenvalues). The methods were then extended to systems with more DoF by Sjöstrand in [Sjö87], and building on this work more complete results were obtained by Kaidi and Kerdelhué [KK00] who derived quantization conditions for the resonances which are valid to all orders in the semiclassical parameter $\hbar$ and are based on a quantum normal form. In [IS02] this was embedded into the study of more general normal forms for Fourier integral operators.

The development and study of the quantum normal form near an equilibrium point of saddle-centre-. . .-centre type is one of the main aims in the quantum part of this paper. As mentioned above, the quantum normal form has already been used to study resonances in the literature before. We will see that the quantum normal form provides us with much more information which includes cumulative reaction probabilities and a detailed understanding of the dynamical mechanism of quantum reactions. To this end we will relate the quantum states described by the quantum normal form to the phase space structures that control classical reaction dynamics. In the classical case the NHIM is the manifestation of the activated complex. Due to the Heisenberg uncertainty relation, there is no such invariant structure in quantum mechanics. In fact the resonances will describe how the quantum activated complex decays.

In order to use the quantum normal form to study concrete chemical reactions we have to be able to compute it explicitly, i.e. we need an explicit algorithm analogous to the classical normal form. The mathematical treatments in [Sjö87, KK00] do not give us such an algorithm. Therefore we develop a quantized version of the classical normal form algorithm which is similar to the quantum normal form for stable equilibrium points in [Cre90, EGH91, BGP99]. We give a complete exposition of our algorithm to compute the quantum normal form. At the level of symbols, the classical and quantum normal form algorithms are almost identical. The essential differences are that the Poisson bracket is replaced by the Moyal bracket, and rather than dealing with polynomial functions of the phase space coordinates, we deal with polynomial functions of the phase space coordinates and $\hbar$.

The outline of this paper is as follows. In section 2 we start by reviewing classical normal form theory. We show in detail how to construct symplectic transformations from the flows of Hamiltonian vector fields. The theory is presented in such a way that it allows for a direct comparison with the quantum normal form that we develop in section 3. This section includes a careful review of the necessary tools from the symbol calculus which are required to quantize symplectic transformations. In section 4 we discuss the phase space structures which govern classical reaction dynamics and show how these phase space structures can be realized with the help of the classical normal form. This includes the construction of a dividing surface, the role of the NHIM and its stable and unstable manifolds, the foliation of the NHIM by invariant tori and its relation to the activated complex, the definition of dynamical reaction

paths and a formula for the directional flux through the dividing surface. In this section we also relate the theory presented to the flux–flux autocorrelation function formalism that can be found in the chemistry literature. Section 5 is the quantum mechanical analogue of section 4. We here use the quantum normal form to study quantum reaction dynamics. We show how to construct a local S-matrix from the quantum normal form and how this leads to an efficient algorithm to compute the cumulative reaction probability (the quantum analogue of the classical flux). We study the distributions of the scattering states in phase space and relate them to the phase space structures governing classical reaction dynamics. We also relate the quantum normal form computation of the cumulative reaction probability to the quantum version of the flux–flux autocorrelation function formalism. In section 6 we study quantum resonances that correspond to the (classical) activated complex. We show how the resonances describe the quantum mechanical lifetimes of the activated complex. We study the phase space distributions of the corresponding resonance states and interpret these distributions in terms of the phase space structures associated with the classical dynamics of reactions. In section 7 we illustrate the efficiency of the classical and quantum normal form algorithms for computing fluxes, cumulative reaction probabilities and resonances by applying the theory presented to several examples with one, two and three degrees of freedom.

2. Classical normal form theory

In this section we summazise the main elements of classical Poincaré–Birkhoff normal form theory for Hamiltonian functions. This is a well-known theory and has been the subject of many review papers and books [Dep69, DF76, AKN88, MH92, Mur03]. The main reason for summarizing the essential results here is that the reader can clearly see the classical and quantum normal form theories 'side by side'. In this way the classical–quantum correspondence is most apparent. This is explicitly illustrated by developing the classical normal form theory in a way that is rather different from that found in the literature. This difference allows us to explicitly show that the structure of the classical and the quantum normal form theories is very similar. At the same time, we emphasize that the classical normal form theory is an essential tool for both discovering and computing the necessary geometric structures in phase space with which we construct our phase space transition state theory in section 4.

This section is organized as follows. In section 2.1 we show how functions on phase space transform under symplectic coordinate transformations, which are constructed as Hamiltonian flows. In section 2.2 we define what a (classical) normal form is and show how the formalism developed in section 2.1 can be used to transform a Hamiltonian function into normal form to any desired order of its Taylor expansion about an equilibrium point. The general scheme is discussed in detail in section 2.3 for the case of a saddle-centre-. . .-centre equilibrium point.

2.1. Transformation of phase space functions through symplectic coordinate transformations

The essence of classical normal form theory is to find a new set of coordinates, i.e. a change of variables, that transforms the Hamiltonian to a 'simpler' form (and we will explicitly define what we mean by 'simpler' shortly). Since we are dealing with Hamiltonian functions we want the coordinate transformation to preserve the Hamiltonian structure, and this will be accomplished if the transformation is *symplectic* [Arn78, AM78]. A standard approach to constructing symplectic transformations is through the use of Lie transforms (see, e.g., [Mur03]), which we now review. Before proceeding we note that there are issues related to differentiability of functions, existence and uniqueness of solutions of ordinary differential equations, etc. However, we will proceed formally and assume that our functions have as

many derivatives as required and that solutions of ordinary differential equations exist, and are sufficiently differentiable, on domains of interest. Our purpose here is to develop methods and an algorithm. Its applicability must be verified for specific problems.

A function W on phase space $\mathbb{R}^d \times \mathbb{R}^d$ defines a Hamiltonian vector field

$$X_W = \sum_{k=1}^{d} \left(\frac{\partial W}{\partial p_k} \frac{\partial}{\partial q_k} - \frac{\partial W}{\partial q_k} \frac{\partial}{\partial p_k} \right), \tag{2.1}$$

and at a point $z = (q, p) = (q_1, \ldots, q_d, p_1, \ldots, p_d)$ in phase space this vector field takes the value

$$X_W(z) = \left(\frac{\partial W(z)}{\partial p_1}, \ldots, \frac{\partial W(z)}{\partial p_d}, -\frac{\partial W(z)}{\partial q_1}, \ldots, -\frac{\partial W(z)}{\partial q_d} \right). \tag{2.2}$$

The solutions of the ordinary differential equation ('Hamilton's equations')

$$\frac{\mathrm{d}}{\mathrm{d}\epsilon} z(\epsilon) = X_W(z(\epsilon)) \tag{2.3}$$

define a Hamiltonian flow, $z \mapsto z(\epsilon) := \Phi_W^\epsilon(z)$, which satisfies the properties

- $\Phi_W^{\epsilon_1} \circ \Phi_W^{\epsilon_2} = \Phi_W^{\epsilon_1 + \epsilon_2}$,
- $\Phi_W^{\epsilon} \circ \Phi_W^{-\epsilon} = \mathrm{id}$,
- $\Phi_W^{0} = \mathrm{id}$,

where id denotes the identity map, and

$$\frac{\mathrm{d}}{\mathrm{d}\epsilon} \Phi_W^\epsilon(z) = X_W(\Phi^\epsilon(z)). \tag{2.4}$$

Most importantly for us, the Hamiltonian flow Φ_W^ϵ defines a symplectic, or 'canonical', coordinate transformation of the phase space onto itself [Arn78]. This is significant because symplectic coordinate transformations preserve the Hamiltonian structure. The Hamiltonian W is referred to as the *generating function* for the symplectic transformation Φ_W^ϵ.

We now consider the transformation of a (scalar valued) function on phase space under such a symplectic transformation. More precisely, for a phase space function A and a symplectic coordinate transformation defined from the flow generated by Hamilton's equations $z(\epsilon) = \Phi_W^\epsilon(z)$, the transformation of the function under this symplectic transformation is given by

$$A(\epsilon) = A \circ \Phi_W^{-\epsilon}, \tag{2.5}$$

or, in coordinates,

$$A(\epsilon)\big(z(\epsilon)\big) = A(z). \tag{2.6}$$

For our purposes we want to develop $A(\epsilon)$ as a (formal) power series in ϵ. We begin by computing the first derivative of $A(\epsilon)$ with respect to ϵ giving

$$\frac{\mathrm{d}}{\mathrm{d}\epsilon} A(\epsilon) = -\langle \nabla A, X_W \rangle \circ \Phi_W^{-\epsilon} = \{W, A\} \circ \Phi_W^{-\epsilon}, \tag{2.7}$$

where $\nabla A \equiv (\partial A/\partial q_1, \ldots, \partial A/\partial q_d, \partial A/\partial p_1, \ldots, \partial A/\partial p_d)$ is the gradient of A, $\langle \cdot, \cdot \rangle$ is the standard scalar product in $\mathbb{R}^{2d}$ and

$$\{W, A\} = \sum_{k=1}^{d} \left(\frac{\partial W}{\partial q_k} \frac{\partial A}{\partial p_k} - \frac{\partial W}{\partial p_k} \frac{\partial A}{\partial q_k} \right) = -\{A, W\}, \tag{2.8}$$

is the Poisson bracket of W and A. Using the fact that W is invariant under the flow Φ_W^ϵ (i.e. $W(\Phi_W^{-\epsilon}) = W(\Phi_W^0)$, or, in other words, the Hamiltonian W is constant along trajectories of the vector field X_W generated by W) we can rewrite (2.7) as

$$\frac{\mathrm{d}}{\mathrm{d}\epsilon}A(\epsilon) = \{W, A(\epsilon)\}. \tag{2.9}$$

The Poisson bracket gives us a convenient way of representing the derivatives of a function along trajectories of Hamilton's equations. We simplify the notation further by defining the adjoint operator

$$\mathrm{ad}_W : A \mapsto \mathrm{ad}_W A := \{W, A\} \tag{2.10}$$

associated with a generating function W. We can now differentiate (2.9) again to obtain the second order derivative with respect to ϵ,

$$\frac{\mathrm{d}^2}{\mathrm{d}\epsilon^2}A(\epsilon) = \frac{\mathrm{d}}{\mathrm{d}\epsilon}\left(\frac{\mathrm{d}}{\mathrm{d}\epsilon}A(\epsilon)\right) = \left\{W, \frac{\mathrm{d}}{\mathrm{d}\epsilon}A(\epsilon)\right\} = \{W, \{W, A(\epsilon)\}\} =: [\mathrm{ad}_W]^2 A(\epsilon). \tag{2.11}$$

Continuing this procedure for higher order derivatives gives

$$\begin{aligned}\frac{\mathrm{d}^n}{\mathrm{d}\epsilon^n}A(\epsilon) &= \frac{\mathrm{d}}{\mathrm{d}\epsilon}\left(\frac{\mathrm{d}^{n-1}}{\mathrm{d}\epsilon^{n-1}}A(\epsilon)\right) = \left\{W, \left\{\cdots\left\{W, \frac{\mathrm{d}}{\mathrm{d}\epsilon}A(\epsilon)\right\}\cdots\right\}\right\} \\ &= \{W, \{\cdots\{W, \{W, A(\epsilon)\}\}\cdots\}\} =: [\mathrm{ad}_W]^n A(\epsilon).\end{aligned} \tag{2.12}$$

Using these results, we obtain the Taylor expansion of $A(\epsilon)$ about $\epsilon = 0$,

$$A(\epsilon) = \sum_{n=0}^{\infty} \frac{\epsilon^n}{n!}\frac{\mathrm{d}^n}{\mathrm{d}\epsilon^n}A(\epsilon)|_{\epsilon=0} = \sum_{n=0}^{\infty}\frac{\epsilon^n}{n!}[\mathrm{ad}_W]^n A, \tag{2.13}$$

where $A(0) = A$ and $[\mathrm{ad}_W]^n A$ are defined as in equations (2.9)–(2.12) with $[\mathrm{ad}_W]^0 A = A$.

Equation (2.13) gives the Taylor expansion with respect to the flow parameter or 'time' ϵ for a phase space function A that is transformed by a symplectic transformation defined by the Hamiltonian flow generated by the function W. It will form the basis of the classical normal form method where the idea is to 'simplify' (or 'normalize') a function which, for us, will be a specific Hamiltonian through the choice of an 'appropriately chosen' sequence of symplectic transformations that simplify the Hamiltonian 'order by order' of its Taylor expansion with respect to the phase space coordinates $z = (q, p)$. First, we need to make clear that the normal form procedure that we develop here is valid *in a neighbourhood of an equilibrium point*. This means that the normal form is a local object whose dynamics have meaning for the original Hamiltonian only in a neighbourhood of an equilibrium point. In order to describe the terms in the Taylor expansion of a given order in the phase space coordinates more precisely we introduce the vector spaces $\mathcal{W}_{\mathrm{cl}}^s$, $s \in \mathbb{N}_0$, of polynomials which are homogeneous of order s. The space $\mathcal{W}_{\mathrm{cl}}^s$ is spanned (over $\mathbb{C}$) by all monomials of the form

$$q^\alpha p^\beta := \prod_{k=1}^{d} q_k^{\alpha_k} p_k^{\beta_k}, \qquad \text{where } |\alpha| + |\beta| := \sum_{k=1}^{d} \alpha_k + \beta_k = s. \tag{2.14}$$

The following two lemmata are the key tools used in the computation of the classical normal form.

Lemma 1. *Let $W \in \mathcal{W}_{\mathrm{cl}}^{s'}$, $A \in \mathcal{W}_{\mathrm{cl}}^s$ with $s, s' \geqslant 1$, then*

$$\{W, A\} \in \mathcal{W}_{\mathrm{cl}}^{s+s'-2}, \tag{2.15}$$

and for $n \geqslant 0$,

$$[\mathrm{ad}_W]^n A \in \mathcal{W}_{\mathrm{cl}}^{n(s'-2)+s} \tag{2.16}$$

if $n(s'-2)+s \geqslant 0$ and $\left[\mathrm{ad}_W\right]^n A = 0$ otherwise.

Proof. This lemma can be proven by direct calculation. □

This lemma is key to the proof of lemma 2.

Lemma 2. *Let* $W \in \mathcal{W}_{\rm cl}^{s'}$ *with* $s' \geqslant 3$ *and*

$$A = \sum_{s=0}^{\infty} A_s \tag{2.17}$$

with $A_s \in \mathcal{W}_{\rm cl}^{s}$. *Then*

$$A' := A \circ \Phi_W^{-1} = \sum_{n=0}^{\infty} \frac{1}{n!} [\mathrm{ad}_W]^n A = \sum_{s=0}^{\infty} A'_s, \tag{2.18}$$

where

$$A'_s = \sum_{n=0}^{[\frac{s}{s'-2}]} \frac{1}{n!} [\mathrm{ad}_W]^n A_{s-n(s'-2)}, \tag{2.19}$$

where $[s/(s'-2)]$ *denotes the integer part of* $s/(s'-2)$.

Proof. Using (2.17), we write out the next to last term in (2.18) as a series of series as follows (where we have also changed the summation index from s to j in order to avoid possible confusion):

$$\sum_{n=0}^{\infty} \frac{1}{n!} [\mathrm{ad}_W]^n A = \sum_{n=0}^{\infty} \frac{1}{n!} [\mathrm{ad}_W]^n \sum_{j=0}^{\infty} A_j = \sum_{j=0}^{\infty} A_j + \sum_{j=0}^{\infty} \mathrm{ad}_W A_j + \sum_{j=0}^{\infty} \frac{1}{2} [\mathrm{ad}_W]^2 A_j$$
$$+ \sum_{j=0}^{\infty} \frac{1}{3!} [\mathrm{ad}_W]^3 A_j + \ldots + \sum_{j=0}^{\infty} \frac{1}{n!} [\mathrm{ad}_W]^n A_j + \ldots . \tag{2.20}$$

We now want to inspect each series in the series and extract the order s term from each one. Then summing these terms will give the series (2.19). Using lemma 1, we find

$$[\mathrm{ad}_W]^n A_j \in \mathcal{W}_{\rm cl}^{n(s'-2)+j}. \tag{2.21}$$

Now we wish to choose j such that

$$[\mathrm{ad}_W]^n A_j \in \mathcal{W}_{\rm cl}^{s}. \tag{2.22}$$

Comparing (2.21) and (2.22), this is true for

$$j = s - n(s'-2). \tag{2.23}$$

Hence it follows that

$$A'_s = \sum_{n=0}^{[\frac{s}{s'-2}]} \frac{1}{n!} [\mathrm{ad}_W]^n A_{s-n(s'-2)}. \tag{2.24}$$

□

2.2. Definition and computation of the classical normal form

We will now define when a Hamilton function is in classical normal form. Here we use the adjective 'classical' to distinguish the normal form in the case of classical mechanics from the normal form that we will define for the case of quantum mechanics in section 3. As we will see, in general a Hamilton function is not in normal form. However, as we will show in detail, the formalism reviewed in the previous section can be used to construct an explicit algorithm which allows one to transform a Hamilton function to normal form to any desired order of its Taylor expansion.

The starting point is a Hamilton function with an equilibrium point at $z = z_0$, i.e. $\nabla H(z_0) = 0$. Let $H_2(z) := \frac{1}{2}\langle z - z_0, \mathrm{D}^2 H(z_0)(z - z_0)\rangle$ be the quadratic part of the Taylor expansion of H about z_0[7]. We then make the following

Definition 1. *We say that H is in classical normal form with respect to the equilibrium point z_0 if*

$$\mathrm{ad}_{H_2} H \equiv \{H_2, H\} = 0. \tag{2.25}$$

It follows from this definition that if H is in normal form then H_2 will be an integral of the motion generated by the Hamilton function H and moreover, as we will see below, depending on the structure of H_2, further integrals of the motion will exist. A consequence of the existence of integrals of motion is the structuring, or *foliation*, of the phase space by lower dimensional surfaces or *manifolds* that are invariant under the dynamics. If we choose initial conditions for Hamilton's equations then these initial conditions will determine values of the integrals of motion. The full solution of Hamilton's equation will then be contained in the manifold given by the common level set of the integrals corresponding to the initial values. This way the integrals of the motion confine the possible dynamics. Moreover, the existence of integrals of the motion significantly simplifies the study of the dynamics.

In general a Hamilton function is not in normal form. However, we will use the formalism and results developed in the previous section to transform a Hamiltonian to normal form in a neighbourhood of the equilibrium point to a certain order of its Taylor expansion about the equilibrium point. As we will see, the transformed Hamiltonian function truncated at this order will lead to a very accurate description of the motion in the neighbourhood of the equilibrium point. (What we mean by 'accurate description' is discussed in section 4.5.)

We develop the following procedure. We begin with our 'original Hamiltonian'

$$H = H^{(0)}, \tag{2.26}$$

and we construct a consecutive sequence of symplectic transformations

$$H^{(0)} \to H^{(1)} \to H^{(2)} \to H^{(3)} \to \cdots \to H^{(N)}, \tag{2.27}$$

where N is a sufficiently large integer which will be the order at which we will truncate the normal form series.

The first step in the sequence (2.27) is obtained by shifting the critical point z_0 to the origin of a new coordinate system. We set

$$z^{(1)} = z - z_0. \tag{2.28}$$

The Hamiltonian function $H^{(1)}$ is the representation of $H^{(0)}$ in terms of the new coordinates $z^{(1)}$, i.e.

$$H^{(1)}(z^{(1)}) = H^{(0)}(z^{(1)} + z_0). \tag{2.29}$$

[7] Here , $\mathrm{D}^2 H(z_0)$ denotes the Hessian of H at z_0, i.e. the matrix of second derivatives $(\partial_{z_i}\partial_{z_j} H(z_0))_{ij}$.

Once the equilibrium point is shifted to the origin, our normal form procedure will require us to work with the Taylor expansion of the Hamiltonian $H^{(1)}$ about the origin in a 'term-by-term' fashion. Let

$$H^{(1)} = E_0 + \sum_{s=2}^{\infty} H_s^{(1)}, \tag{2.30}$$

where

$$H_s^{(1)}(q, p) := \sum_{|\alpha|+|\beta|=s} \frac{1}{\alpha!\beta!} \partial_q^\alpha \partial_p^\beta H^{(1)}(0, 0) q^\alpha p^\beta \tag{2.31}$$

are the terms of order s. Here we employ the usual multi-index notation; for $\alpha \equiv (\alpha_1, \cdots, \alpha_d) \in N_0^d$ we have $|\alpha| \equiv \alpha_1 + \cdots + \alpha_d$, $\alpha! \equiv \alpha_1!\alpha_2! \cdots \alpha_d!$, $q^\alpha \equiv q_1^{\alpha_1} q_2^{\alpha_2} \cdots q_d^{\alpha_d}$ and $\partial_q^\alpha \equiv \partial^{\alpha_1}/\partial q_1^{\alpha_1} \cdots \partial^{\alpha_d}/\partial q_d^{\alpha_d}$ (for $\beta \in N_0^d$ and $p \in \mathbb{R}^d$, the notation is analogous). Since (2.30) is a Taylor expansion of a Hamiltonian about an equilibrium point at the origin it follows that $H_1^{(1)} = 0$. In particular, $H_0^{(1)} \equiv E_0$ is the 'energy' of the equilibrium point.

At the next step in the sequence (2.27) we choose a linear symplectic transformation such that $H_2^{(2)}$ assumes a 'simple form'. In other words, we seek a transformation that simplifies the quadratic part of the Hamiltonian or, equivalently, the linear part of the Hamiltonian vector field. This is accomplished by choosing an appropriate symplectic $2d \times 2d$ matrix M, i.e. a matrix statisfying $M^T J M = J$, where J is the standard $2d \times 2d$ symplectic matrix

$$J = \begin{pmatrix} 0 & \mathrm{id} \\ -\mathrm{id} & 0 \end{pmatrix} \tag{2.32}$$

whose blocks consist of $d \times d$ zero matrices and $d \times d$ identity matrices. We then set

$$z^{(2)} = M z^{(1)}, \tag{2.33}$$

and the corresponding transformed Hamiltonian is given by

$$H^{(2)}(z^{(2)}) = H^{(1)}(M^{-1} z^{(2)}). \tag{2.34}$$

Which form of $H_2^{(2)}$ can be considered to be 'simple' depends on the nature of the particular equilibrium point (i.e. the eigenvalues and eigenvectors associated with the matrix obtained by linearizing Hamilton's equations about the origin). The main benefit of having $H_2^{(2)}$ in a 'simple' form is that this will simplify the explicit implementation of the algorithm to normalize the higher order terms, $n \geqslant 3$, i.e. how to choose the next steps in the sequence (2.27). Therefore, 'simplify' could mean that we would seek a transformation that would diagonalize the linear part of Hamilton's equations, or transform it to 'real Jordan canonical form' in the case of complex eigenvalues. Clearly, constructing such a transformation is a problem in linear algebra for which there is a large literature. However, the symplectic case tends to bring with it new difficulties, both in the analytical and computational areas (see, e.g., [CK99]). In the next section we will see how to simplify the linear part of Hamilton's equations for our particular case of interest, i.e. a saddle-centre-. . .-centre equilibrium point satisfying a certain 'nonresonance' condition. However, it is important to realize that the normal form *algorithm* does not depend on the specific form taken by the linear part of Hamilton's equations.

Up to this point we have located an equilibrium point of interest, translated it to the origin, Taylor expanded the resulting transformed Hamiltonian $H^{(1)}$ about the origin (for which $H_1^{(1)} = 0$), and constructed a linear symplectic transformation in such a way that the quadratic part of the resulting transformed Hamiltonian, $H_2^{(2)}$, is 'simple'. Now we are ready to describe how to normalize the terms of order three and higher, i.e. how to define the next steps in the sequence (2.27). To accomplish these transformations we will use the formalism

reviewed in section 2.1 and successively transform the Hamiltonian by the time one maps of the flows generated by Hamiltonian vector fields. More precisely, for $n \geqslant 3$, $H^{(n)}$ is computed from $H^{(n-1)}$ according to

$$H^{(n)} = H^{(n-1)} \circ \Phi_{W_n}^{-1} = \sum_{k=0}^{\infty} \frac{1}{k!} [\mathrm{ad}_{W_n}]^k H^{(n-1)} \tag{2.35}$$

with a generating function $W_n \in \mathcal{W}_{\mathrm{cl}}^n$. The order s term of the Taylor expansion of $H^{(n)}$ expressed as a series involving terms in the Taylor expansion of $H^{(n-1)}$ and W_n is obtained by substituting the Taylor expansion of $H^{(n-1)}$ into (2.35) and using lemma 2. This gives

$$H_s^{(n)} = \sum_{k=0}^{\left[\frac{s}{n-2}\right]} \frac{1}{k!} [\mathrm{ad}_{W_n}]^k H_{s-k(n-2)}^{(n-1)}, \qquad n \geqslant 3. \tag{2.36}$$

The corresponding transformation of phase space coordinates is then given by

$$z^{(n)} = \Phi_{W_n}^1(z^{(n-1)}), \qquad n \geqslant 3. \tag{2.37}$$

We note that in fact also the affine linear symplectic coordinate transformations (2.28) and (2.33) which formed the first two steps in the sequence (2.27) can be formally expressed as time one maps of Hamiltonian flows with generating function $W_1 \in \mathcal{W}_{\mathrm{cl}}^1$ and $W_2 \in \mathcal{W}_{\mathrm{cl}}^2$, respectively. A generating function W_1 whose time one map achieves the translation (2.28) is given by

$$W_1(z) = -\langle z_0, Jz \rangle, \tag{2.38}$$

where J is the standard $2d \times 2d$ symplectic matrix defined in equation (2.32). This gives

$$z^{(1)} = \Phi_{W_1}^1(z) = z - z_0. \tag{2.39}$$

In this case the upper limit of the sum in (2.36) is infinity. It is in general not straightforward to explicitly give an expression for a generating function $W_2 \in \mathcal{W}_{\mathrm{cl}}^2$ whose time one map achieves the linear symplectic transformation (2.33) for a given symplectic matrix M. But such a W_2 always exists[8]. For $n = 2$ in equation (2.36) the upper limit of the sum is again infinity. In the next section we will provide a matrix M which achieves the simplification of the quadratic part of the Hamiltonian function for the case of a saddle-centre-...-centre equilibrium point satisfying a nonresonance condition without specifying the corresponding W_2. Note however that it is M and not necessarily W_2 which is required for our normalization procedure.

Let us now proceed with the nonlinear symplectic transformations generated by polynomials $W_n \in \mathcal{W}_{\mathrm{cl}}^n$ with $n \geqslant 3$ to achieve the third and higher steps in the sequence (2.27). The first thing to note is that these transformations will not alter the zeroth order term, E_0, and we will also have $H_1^{(1)} = H_1^{(n)} = 0$, $n \geqslant 3$. The zeroth order term is unaltered since the upper limit in the sum (2.36) is zero for $s = 0$. The first order term stays zero because for $s \leqslant 1$ in combination with $n > 3$ and $s = 0$ in combination with $n = 3$, the upper limit in the sum (2.36) is again zero. For $n = 3$ in combination with $s = 1$, the upper limit is 1. However, the $k = 1$ term, $\mathrm{ad}_{W_3} H_0^{(2)}$, in the sum (2.36) is zero because $H_0^{(2)}$ is the constant E_0 and hence vanishes when ad_{W_3} is applied to it.

Moreover, the quadratic part of the Hamiltonian $H_2^{(2)}$ will not be modified by the transformations generated by W_n, $n \geqslant 3$. We will show this directly from our formalism.

[8] This follows from two facts. Firstly, the group of linear symplectic transformations is connected, and therefore the image of the exponentiation of its Lie algebra is connected, too. Secondly, this Lie algebra is isomorphic to the vector space of quadratic polynomials endowed with the Poisson bracket [Fol89]. Therefore the set of all time one maps generated by quadratic elements of $\mathcal{W}_{\mathrm{cl}}^2$ is the whole symplectic group.

Lemma 3. $H_2^{(n)} = H_2^{(2)}, \quad n \geqslant 3.$

Proof. The idea is to use (2.35) to transform from $H^{(n-1)}$ to $H^{(n)}$, and then to show that $H_2^{(n)} = H_2^{(n-1)}$ for $n \geqslant 3$.

We separate out the constant and quadratic parts of $H^{(n-1)}$ as

$$H^{(n-1)} = E_0 + H_2^{(n-1)} + \sum_{s=3}^{\infty} H_s^{(n-1)}, \tag{2.40}$$

and then we substitute this into (2.35) to obtain

$$H^{(n)} = \sum_{k=0}^{\infty} \frac{1}{k!} [\mathrm{ad}_{W_n}]^k E_0 + \sum_{k=0}^{\infty} \frac{1}{k!} [\mathrm{ad}_{W_n}]^k H_2^{(n-1)} + \sum_{k=0}^{\infty} \frac{1}{k!} [\mathrm{ad}_{W_n}]^k \sum_{s=3}^{\infty} H_s^{(n-1)}. \tag{2.41}$$

Note that the first series in this expression only admits the $k = 0$ term, E_0. We consider the case $n \geqslant 3$. In this case, the third series, using lemma 1, only admits terms of order larger than or equal to three. Hence, all of the quadratic terms must be in the second series. Using lemma 1, the kth term in that series is contained in $\mathcal{W}_{\mathrm{cl}}^{k(n-2)+2}$. Therefore the only quadratic term occurs for $k = 0$, which is $H_2^{(n-1)}$. □

Lemma 3 motivates the definition of the operator

$$\mathcal{D} := \mathrm{ad}_{H_2^{(2)}} = \{H_2^{(2)}, \cdot\}. \tag{2.42}$$

In fact, $\mathcal{D}$ will simply be a convenient shorthand notation for the operator $\mathrm{ad}_{H_2} = \{H_2, \cdot\}$ in the definition of the the normal form in Definition 1 in terms of the coordinates $z^{(2)}$. The operator $\mathcal{D}$ plays a crucial role in the computation of the normal form transformation.

The other important point to realize when transforming $H^{(n-1)}$ to $H^{(n)}$ with $\Phi_{W_n}^{-1}$, $W_n \in \mathcal{W}_{\mathrm{cl}}^n$, is that all terms of order smaller than n are unchanged (however, the terms of order larger than n are modified by the nth order normalization transformation). This is essential for the success of the iterative process and we provide a proof of this result now.

Lemma 4. *For $n \geqslant 3$ and $0 \leqslant s < n$, $H_s^{(n)} = H_s^{(n-1)}$.*

Proof. First, it is important to consider the upper limit of the sum (2.36). For $0 \leqslant s \leqslant n-3$ it is zero, which indicates that for these values of s only the $k = 0$ term is nonzero. Hence, we have

$$H_s^{(n)} = H_s^{(n-1)}, \qquad 0 \leqslant s \leqslant n-3. \tag{2.43}$$

Next we separately consider the cases $s = n-2$ and $s = n-1$. Using (2.36) we find for $s = n-2$,

$$H_{n-2}^{(n)} = H_{n-2}^{(n-1)} + \mathrm{ad}_{W_n} H_0^{(n-1)} = H_{n-2}^{(n-1)} \tag{2.44}$$

since $H_0^{(n-1)} = E_0 = \mathrm{const}$. For $s = n-1$, (2.36) gives

$$H_{n-1}^{(n)} = H_{n-1}^{(n-1)} + \mathrm{ad}_{W_n} H_1^{(n-1)} + \delta_{n,3} \tfrac{1}{2} [\mathrm{ad}_{W_n}]^2 H_0^{(n-1)} = H_{n-1}^{(n-1)} \tag{2.45}$$

since $H_1^{(n-1)} = 0$ and $H_0^{(n-1)} = E_0 = \mathrm{const}$. The Kronecker symbol in the last term of the second expression shows that this term occurs only for $n = 3$. □

Now if we consider the nth order term in $H^{(n)}$ this will show us how to choose W_n, $n \geqslant 3$.

Lemma 5 (Homological equation). *For $s = n \geqslant 3$,*

$$H_n^{(n)} = H_n^{(n-1)} - \mathcal{D} W_n. \tag{2.46}$$

Proof. This result is also obtained from (2.36), with a careful consideration of the upper limit of the sum. The case $n \geqslant 5$ is the most straightforward. In this case only $k = 0$ and $k = 1$ contribute in the sum, and using (2.8), we immediately obtain that

$$H_n^{(n)} = H_n^{(n-1)} + \mathrm{ad}_{W_n} H_2^{(2)} = H_n^{(n-1)} - \mathrm{ad}_{H_2^{(2)}} W_n = H_n^{(n-1)} - \mathcal{D}W_n. \tag{2.47}$$

The special cases $s = n = 4$ and $s = n = 3$ must be considered. These will give rise to some additional terms in (2.36). However, as for lemma 4, these will be zero if we take into account $H_1^{(n-1)} = 0$ and $[\mathrm{ad}_{W_n}]^k E_0 = 0$ for integers $k > 0$, $n \geqslant 3$. □

Equation (2.47) is known as the *homological equation*. We want to solve the homological equation, i.e. find a function $W_n \in \mathcal{W}_{\mathrm{cl}}^n$, in such a way that $H^{(n)}$ is in normal form up to order n. To this end note that it follows from lemma 1 that $\mathcal{D}$ defines a *linear* map of $\mathcal{W}_{\mathrm{cl}}^n$ into $\mathcal{W}_{\mathrm{cl}}^n$, i.e. *for each n*,

$$\mathcal{D} : \mathcal{W}_{\mathrm{cl}}^n \to \mathcal{W}_{\mathrm{cl}}^n. \tag{2.48}$$

In order to have $H^{(n)}$ in normal form up to order n we have to require $\mathcal{D}\, H_n^{(n)} = 0$. Looking at the homological equation (2.47) this means we need to find a function $W_n \in \mathcal{W}_{\mathrm{cl}}^n$ such that $H_n^{(n)} = H_n^{(n-1)} - \mathcal{D}\, W_n$ is in the kernel of the restriction of $\mathcal{D}$ to $\mathcal{W}_{\mathrm{cl}}^n$, i.e.

$$H_n^{(n)} = H_n^{(n-1)} - \mathcal{D}W_n \in \mathrm{Ker}\mathcal{D}|_{\mathcal{W}_{\mathrm{cl}}^n}. \tag{2.49}$$

Definition 2. *We will call the homological equation (2.46) solvable if for any $n \geqslant 3$ there exists for any $H_n \in \mathcal{W}_{\mathrm{cl}}^n$ an $W_n \in \mathcal{W}_{\mathrm{cl}}^n$ such that*

$$H_n - \mathcal{D}\, W_n \in \mathrm{Ker}\mathcal{D}|_{\mathcal{W}_{\mathrm{cl}}^n}. \tag{2.50}$$

Whether the homological equation is solvable and how such a W_n can be found depends on the structure of $\mathcal{D}$, i.e. on the structure of the matrix associated with the linearization of the vector field about the equilibrium point. In the next subsection we will show that the homological equation is solvable in the case of a saddle-centre-. . .-centre equilibrium point and explain how W_n can be found.

We summarize the results of this section in the following theorem.

Theorem 1. *Assume that a Hamiltonian function H has an equilibrium point at $z_0 \in \mathbb{R}^d \times \mathbb{R}^d$, and that the homological equation is solvable. Then for every $N \in \mathbb{N}$ there is a symplectic transformation Φ_N such that*

$$H \circ \Phi_N^{-1} = H_{\mathrm{CNF}}^{(N)} + O_{N+1}, \tag{2.51}$$

where $H_{\mathrm{CNF}}^{(N)}$ is in normal form (with respect to $z = (0, 0)$) and O_{N+1} is of order $N + 1$, i.e. there exists an open neighbourhood U of $z = (0, 0)$ and a constant $c > 0$ such that

$$|O_{N+1}(\epsilon z)| < c\epsilon^{N+1} \tag{2.52}$$

for $z \in U$ and $\epsilon < 1$.

Proof. Following the scheme described in this section we normalize the Hamilton function H order by order according to the sequence (2.27). We start by choosing a new coordinate system $z^{(1)} = z - z_0$ which has the equilibrium point z_0 at the origin (see (2.28)), and Taylor expand the Hamilton function $H^{(1)}$, which we obtain from expressing H in the new coordinates $z^{(1)}$ (see equation (2.29)), about $z^{(1)} = 0$ to order N. The remainder which we denote by $R_{N+1}^{(1)}$ is then of order $N + 1$.

We then choose a symplectic $2d \times 2d$ matrix M to define a linear symplectic transformation to new coordinates $z^{(2)} = M\, z^{(1)}$ in terms of which the quadratic part of the transformed Hamilton function $H^{(2)}$ (see equation (2.34)) assumes a simple form. As mentioned above, the

choice of M depends on the nature of the equilibrium point and will simplify the calculation of the steps for $n \geqslant 3$ in the sequence (2.27). Apart from this, however, the choice of the symplectic matrix M is not important. We thus get

$$H^{(2)} = E_0 + \sum_{s=2}^{N} H_s^{(2)} + R_{N+1}^{(2)}, \tag{2.53}$$

where $H_s^{(2)}(z^{(2)}) = H_s^{(1)}(M^{-1} z^{(2)})$, i.e. $H_s^{(2)} \in \mathcal{W}_{\mathrm{cl}}^s$ for $s = 2, \ldots, N$, and the remainder term $R_{N+1}^{(2)}$ given by $R_{N+1}^{(2)}(z^{(2)}) = R_{N+1}^{(1)}(M^{-1} z^{(2)})$ is again of order $N+1$.

Having simplified the quadratic part, we proceed inductively by subsequently choosing generating functions $W_n \in \mathcal{W}_{\mathrm{cl}}^n$, which at each order n, $n = 3, \ldots, N$, solve the homological equation (2.46) and determine $H^{(n)}$ from $H^{(n-1)}$ as follows. For $n \geqslant 3$, $H^{(n-1)}$ is of the form

$$H^{(n-1)} = \sum_{s=0}^{N} H_s^{(n-1)} + R_{N+1}^{(n-1)}, \tag{2.54}$$

where $H_s^{(n-1)} \in \mathcal{W}_{\mathrm{cl}}^s$ and $R_{N+1}^{(n-1)}$ is of order $N+1$. Using this decomposition of $H^{(n-1)}$ we can write for $H^{(n)} = H^{(n-1)} \circ \Phi_{W_n}^{-1}$,

$$H^{(n)} = \sum_{s=0}^{N} H_s^{(n-1)} \circ \Phi_{W_n}^{-1} + R_{N+1}^{(n-1)} \circ \Phi_{W_n}^{-1} \tag{2.55}$$

$$= \sum_{s=0}^{N} \sum_{k=0}^{\infty} \frac{1}{k!} [\mathrm{ad}_{W_n}]^k H_s^{(n-1)} + R_{N+1}^{(n-1)} \circ \Phi_{W_n}^{-1} \tag{2.56}$$

$$= \sum_{s=0}^{N} \sum_{k=0}^{[\frac{N-s}{n-2}]} \frac{1}{k!} [\mathrm{ad}_{W_n}]^k H_s^{(n-1)} + R_{N+1}^{(n)}, \tag{2.57}$$

where

$$R_{N+1}^{(n)} = R_{N+1}^{(n-1)} \circ \Phi_{W_n}^{-1} + \sum_{s=0}^{N} \sum_{k=\left[\frac{N-s}{n-2}\right]+1}^{\infty} \frac{1}{k!} [\mathrm{ad}_{W_n}]^k H_s^{(n-1)}. \tag{2.58}$$

Here we have used equation (2.35) to get (2.56). To obtain (2.57) from (2.56) we removed all those terms from the double sum in (2.56) contained in the $\mathcal{W}_{\mathrm{cl}}^s$ with $s \geqslant N+1$ and absorbed them in the new remainder term $R_{N+1}^{(n)}$ in (2.58). Since the symplectic transformations $\Phi_{W_n}^1$ are near identity transformations for $n \geqslant 3$ the remainder term $R_{N+1}^{(n)}$ is again of order $N+1$.

After the step $n = N$ the terms of order less than or equal to N of the Hamilton function $H^{(N)}$ are then in normal form (with respect to $z = (0,0)$). The symplectic transformation Φ_N in equation (2.51) and the corresponding new coordinates $z^{(N)}$ are then given by

$$z^{(N)} \equiv \Phi_N(z) = \Phi_{W_N}^1 \circ \cdots \circ \Phi_{W_3}^1(z^{(2)}), \qquad z^{(2)} = M z^{(1)}, \qquad z^{(1)} = z - z_0. \tag{2.59}$$

□

From the point of view of applications the definition of the normal form in definition 1 is not very practical since it requires one to carry out the procedure described in the proof of theorem 1 for $N \to \infty$. In general, it is well known that such normal form transformations do not converge, except in special cases [SM71, Bru71, Rüs67, PM03]. For applications it is more practical to consider the *truncated normal form*.

Definition 3 (*N*th order classical normal form). *Consider a Hamilton function H with an equilibrium point $z_0 \in \mathbb{R}^d \times \mathbb{R}^d$ which, for $N \in \mathbb{N}$, we normalize as described in theorem 1. Then we refer to $H_{\mathrm{CNF}}^{(N)}$ in equation (2.51) as the Nth order classical normal form (CNF) of H.*

Note that in order to compute the Nth order normal form it is sufficient to carry out the Taylor expansion of the Hamiltonian up to order N. The remainder term can be neglected immediately since the procedure described in the proof of theorem 1 shows that no terms from the remainder term will enter the Nth order normal form.

Of course, the normal form procedure presented in this section raises such questions as 'what is the error associated with truncating the normal form at some finite order?' After all, one is interested in the dynamics associated with the full, original Hamiltonian. Another obvious question is 'what is the optimum order at which to truncate the normal form so that errors are minimized?' There is no general theory that can be used to answer such questions. They must be addressed on a problem-by-problem basis. Fortunately, truncating the normal form does give extremely accurate results in a number of problems [WBW04a, WBW04b, WBW05b], and we will consider this in more detail in section 4.5.

2.3. Nature and computation of the normal form in a neighbourhood of an equilibrium point of saddle-centre-...-centre stability type

We now describe the computation of the normal form in the classical situation of interest to us; in the neighbourhood of an equilibrium point of saddle-centre-...-centre stability type. This means that the matrix associated with the linearization of Hamilton's equations about the equilibrium point has two real eigenvalues, $\pm\lambda$, and $d-1$ complex conjugate pairs of pure imaginary eigenvalues, $\pm \mathrm{i}\,\omega_k$, $k = 2, \ldots, d$. Moreover, we will assume that the ω_k, $k = 2, \ldots, d$, are nonresonant in the sense that they are linearly independent over the integers, i.e. $k_2\,\omega_2 + \cdots + k_d\,\omega_d \neq 0$ for all $(k_2, \ldots, k_d) \in \mathbb{Z}^{d-1} - \{0\}$ (note that the more stringent diophantine condition for nonresonance [AKN88] is not required for our work).

But first, we locate the equilibrium point of interest, denote it by $z_0 = (q_0, p_0)$, and translate it to the origin using the generating function given in (2.38). The Taylor series of the corresponding Hamiltonian then has the form

$$H^{(1)}(z^{(1)}) = E_0 + H_2^{(1)}(z^{(1)}) + \sum_{s=3}^{\infty} H_s^{(1)}(z^{(1)}). \tag{2.60}$$

We next construct a linear symplectic transformation $M : \mathbb{R}^{2d} \mapsto \mathbb{R}^{2d}$ such that for $z^{(2)} = M\,z^{(1)}$, we have

$$H_2^{(2)}(z^{(2)}) = \lambda p_1^{(2)} q_1^{(2)} + \sum_{k=2}^{d} \frac{\omega_k}{2}((p_k^{(2)})^2 + q_k^{(2)})^2). \tag{2.61}$$

We note that for some purposes it is convenient to consider also a slightly modified version of the coordinates $z^{(2)} = (q^{(2)}, p^{(2)})$ which for later reference we will denote by $(Q^{(2)}, P^{(2)})$. The coordinates $(q^{(2)}, p^{(2)})$ and $(Q^{(2)}, P^{(2)})$ agree in the centre components, i.e. $Q_k^{(2)} = q_k^{(2)}$ and $P_k^{(2)} = p_k^{(2)}$ for $k = 2, \ldots, d$, but are rotated versus each other by an angle of 45° in the saddle plane, i.e.

$$Q_1^{(2)} = \frac{1}{\sqrt{2}}(q_1^{(2)} - p_1^{(2)}), \qquad P_1^{(2)} = \frac{1}{\sqrt{2}}(q_1^{(2)} + p_1^{(2)}). \tag{2.62}$$

Note that the transformation from $(q^{(2)}, p^{(2)})$ to $(Q^{(2)}, P^{(2)})$ is symplectic. In terms of $(Q^{(2)}, P^{(2)})$ the quadratic part of the Hamiltonian assumes the form

$$H_2^{(2)}(Q^{(2)}, P^{(2)}) = \frac{\lambda}{2}((P_1^{(2)})^2 - Q_1^{(2)})^2) + \sum_{k=2}^{d} \frac{\omega_k}{2}((P_k^{(2)})^2 + Q_k^{(2)})^2). \tag{2.63}$$

The quadratic part then consists of the sum of one inverted harmonic oscillator (or 'parabolic barrier') and $d-1$ harmonic oscillators.

In order to construct the $2d \times 2d$ matrix M above we label the eigenvalues of $J\,\mathrm{D}^2 H(z_0)$ (which is the matrix corresponding to the linearization of Hamilton's vector field around the equilibrium point) in such a way that

$$e_1 = -e_{1+d} = \lambda, \qquad e_k = -e_{k+d} = \mathrm{i}\omega_k, \qquad k = 2, \ldots, d, \tag{2.64}$$

and then use the corresponding eigenvectors $v_1, \ldots, v_{2d}$ to form the columns of the matrix M according to

$$M = (c_1 v_1, c_2 \mathrm{Re} v_2, \ldots, c_d \mathrm{Re} v_d, c_1 v_{1+d}, c_2 \mathrm{Im} v_2, \ldots, c_d \mathrm{Im} v_d), \tag{2.65}$$

where $c_1, \ldots, c_d$ are scalars defined as

$$c_1^{-2} := \langle v_1, J v_{1+d} \rangle, \qquad c_k^{-2} := \langle \mathrm{Re} v_k, J \mathrm{Im} v_k \rangle, \qquad k = 2, \ldots, d. \tag{2.66}$$

The constants $c_1, \ldots, c_d$ guarantee that the matrix M will be symplectic, i.e. M will satisfy $M^{\mathrm{T}} J M = J$. Here we have assumed that the eigenvectors v_1 and v_{1+d} have been chosen in such a way that $\langle v_1, J v_{1+d} \rangle$ is positive (if $\langle v_1, J v_{1+d} \rangle < 0$ then we multiply v_{1+d} by -1). It is not difficult to see that c_k^{-2}, $k = 2, \ldots, d$, are automatically positive if the frequencies ω_k are positive[9]. Using the fact that $\langle v_n, J v_k \rangle = 0$ for n and k from the distinct sets $\{1, 1+d\}$, $\{2, 2+d\}, \ldots, \{d, 2d\}$, it is easily verified that the matrix M satisfies $M^{\mathrm{T}} J M = J$.

2.3.1. Solution of the homological equation. Given a Hamiltonian function whose quadratic part is of the form (2.61), the solution of the homological equation derived in lemma 5 for any order $n \geqslant 3$ is extremely simple and transparent if we first perform the following symplectic complex linear change of coordinates $z^{(n)} = (q^{(n)}, p^{(n)}) \mapsto (x, \xi)$ which has the components $x_1 = q_1^{(n)}$, $\xi_1 = p_1^{(n)}$ and

$$x_k := \frac{1}{\sqrt{2}}(q_k^{(n)} - \mathrm{i} p_k^{(n)}), \qquad \xi_k := \frac{1}{\sqrt{2}}(p_k^{(n)} - \mathrm{i} q_k^{(n)}), \qquad k = 2, \ldots, d. \tag{2.67}$$

Here, and for the rest of this section, we omit the superscript (n) for x and ξ for the sake of a simpler and less cumbersome notation.

In terms of the phase space coordinates (x, ξ), the linear map $\mathcal{D}$ takes the form

$$\mathcal{D} = \lambda(\xi_1 \partial_{\xi_1} - x_1 \partial_{x_1}) + \sum_{k=2}^{d} \mathrm{i}\omega_k(\xi_k \partial_{\xi_k} - x_k \partial_{x_k}). \tag{2.68}$$

The form of (2.68) is significant for two reasons. One is that when the monomials of order n defined in (2.14) are expressed in terms of the coordinates (x, ξ) they form a basis for $\mathcal{W}_{\mathrm{cl}}^n$. We have

$$\mathcal{W}_{\mathrm{cl}}^n = \mathrm{span}\left\{ x^\alpha \xi^\beta := \prod_{k=1}^{d} x_k^{\alpha_k} \xi_k^{\beta_k} : \quad |\alpha| + |\beta| := \sum_{k=1}^{d} \alpha_k + \beta_k = n \right\}. \tag{2.69}$$

[9] In fact, if one of the d_k^{-2} is negative then this means that the corresponding frequency is negative; this is a case which we have excluded, although it can be dealt with in a way that is similar to the procedure described in this paper.

Secondly, in this basis the linear map (2.68) is diagonal. In fact, using (2.68), we see that the image under $\mathcal{D}$ of a monomial $x^\alpha \xi^\beta \in \mathcal{W}^n_{\rm cl}$ is

$$\mathcal{D}\prod_{k=1}^{d} x_k^{\alpha_k}\xi_k^{\beta_k} = \left(\lambda(\beta_1-\alpha_1)+\sum_{k=2}^{d} \mathrm{i}\omega_k(\beta_k-\alpha_k)\right)\prod_{k=1}^{d} x_k^{\alpha_k}\xi_k^{\beta_k}. \tag{2.70}$$

These monomials thus are eigenvectors of (2.68).

Since the map $\mathcal{D}$ can be diagonalized it follows in a trivial way that $\mathcal{W}^n_{\rm cl}$ can be represented as the direct sum of the kernel of $\mathcal{D}$ acting on $\mathcal{W}^n_{\rm cl}$, $\mathrm{Ker}\mathcal{D}|_{\mathcal{W}^n_{\rm cl}}$, and the image of $\mathcal{D}$ acting on $\mathcal{W}^n_{\rm cl}$, $\mathrm{Im}\mathcal{D}|_{\mathcal{W}^n_{\rm cl}}$, i.e.

$$\mathcal{W}^n_{\rm cl} = \mathrm{Ker}\mathcal{D}|_{\mathcal{W}^n_{\rm cl}} \oplus \mathrm{Im}\mathcal{D}|_{\mathcal{W}^n_{\rm cl}}. \tag{2.71}$$

Now we can express $H_n^{(n-1)}$ as

$$H_n^{(n-1)} = H_{n;\mathrm{Ker}}^{(n-1)} + H_{n;\mathrm{Im}}^{(n-1)}, \tag{2.72}$$

where $H_{n;\mathrm{Ker}}^{(n-1)} \in \mathrm{Ker}\mathcal{D}|_{\mathcal{W}^n_{\rm cl}}$ and $H_{n;\mathrm{Im}}^{(n-1)} \in \mathrm{Im}\mathcal{D}|_{\mathcal{W}^n_{\rm cl}}$. We can then choose W_n such that

$$\mathcal{D}W_n = H_{n;\mathrm{Im}}^{(n-1)}, \tag{2.73}$$

and therefore by (2.46)

$$H_n^{(n)} = H_{n;\mathrm{Ker}}^{(n-1)}. \tag{2.74}$$

The choice of W_n is not unique since one can always add terms from the kernel of $\mathcal{D}|_{\mathcal{W}^n_{\rm cl}}$. However, we will require $W_n \in \mathrm{Im}\mathcal{D}|_{\mathcal{W}^n_{\rm cl}}$, i.e. we will invert $\mathcal{D}$ on its image $\mathrm{Im}\mathcal{D}|_{\mathcal{W}^n_{\rm cl}}$, which renders the choice of W_n unique.

Using our assumption that the frequencies $\omega_2, \ldots, \omega_d$ are nonresonant, i.e. linearly independent over $\mathbb{Z}$, we see from (2.70) that a monomial $x^\alpha\xi^\beta$ is mapped to zero if and only if $\alpha_k = \beta_k$ for all $k = 1, \ldots, d$. In particular $\mathrm{Ker}\mathcal{D}|_{\mathcal{W}^s_{\rm cl}} = \{0\}$ if s is odd. This implies that coordinate transformations can be constructed such that all odd order terms are eliminated. Moreover, for s even, the terms that *cannot* be eliminated are those which are sums of monomials for which x_k and ξ_k have equal integer exponents for all $k = 1, \ldots, d$.

Concretely, we can compute W_n according to (2.73) as follows. We assume that $H_{n;\mathrm{Im}}^{(n-1)}$ is the linear combination of L monomials of order n,

$$H_{n;\mathrm{Im}}^{(n-1)} = \sum_{l=1}^{L} h_l \prod_{k=1}^{d} x_k^{\alpha_{k;l}}\xi_k^{\beta_{k;l}}, \tag{2.75}$$

with $\sum_{k=1}^{d}\alpha_{k;l}+\beta_{k;l} = n$ for all $l = 1, \ldots, L$, and for all $l = 1, \ldots, L$, there is at least one $k = 1, \ldots, d$ for which $\alpha_{k;l} \neq \beta_{k;l}$ (i.e. the vectors $(\alpha_{1;l}, \ldots, \alpha_{d;l})$ and $(\beta_{1;l}, \ldots, \beta_{d;l})$ are different for all $l = 1, \ldots, L$). Upon inspecting (2.70), and using (2.73), we see that a generating function W_n that solves the homological equation is given by

$$W_n = \sum_{l=1}^{L} \frac{h_l}{\lambda(\beta_{1;l}-\alpha_{1;l})+\sum_{k=2}^{d}\mathrm{i}\omega_k(\beta_{k;l}-\alpha_{k;l})} \prod_{k=1}^{d} x_{k;l}^{\alpha_{k;l}}\xi_{k;l}^{\beta_{k;l}}. \tag{2.76}$$

As mentioned above this solution of the homological equation is unique if we require W_n to be in $\mathrm{Im}\mathcal{D}|_{\mathcal{W}^n_{\rm cl}}$.

2.3.2. Integrals of the classical motion from the Nth order classical normal form. The Nth order classical normal form $H^{(N)}_{\mathrm{CNF}}$ is a polynomial in the Nth order phase space coordinates (2.59) which, in order to keep the notation in this section simple, we will denote by (q, p), i.e. we will omit superscripts (N) on the phase space coordinates. As discussed in the previous section, it follows that if we perform the symplectic complex linear change of coordinates $x_1 = q_1, \xi_1 = p_1$ and

$$x_k := \frac{1}{\sqrt{2}}(q_k - \mathrm{i}p_k), \qquad \xi_k := \frac{1}{\sqrt{2}}(p_k - \mathrm{i}q_k), \qquad k = 2, \ldots, d, \tag{2.77}$$

then the coordinate pairs x_k and ξ_k will have equal integer exponents for all $k = 1, \ldots, d$ in each monomial of $H^{(N)}_{\mathrm{CNF}}$. As a consequence the functions

$$I = p_1 q_1 = \xi_1 x_1, \qquad J_k = \tfrac{1}{2}(p_k^2 + q_k^2) = \mathrm{i}\xi_k x_k, \qquad k = 2, \ldots, d, \tag{2.78}$$

are integrals of the motion generated by $H^{(N)}_{\mathrm{CNF}}$. This assertion is simple to verify with the following computations:

$$\frac{\mathrm{d}}{\mathrm{d}t} I = \{I, H^{(N)}_{\mathrm{CNF}}\} = 0, \qquad \frac{\mathrm{d}}{\mathrm{d}t} J_k = \{J_k, H^{(N)}_{\mathrm{CNF}}\} = 0, \qquad k = 2, \ldots, d. \tag{2.79}$$

The integrals of the motion I and J_k can be used to define action angle variables. We therefore define the conjugate angles

$$\varphi_1 = \begin{cases} \tanh^{-1}\left(\dfrac{q_1 + p_1}{q_1 - p_1}\right), & p_1 q_1 < 0, \\ \tanh^{-1}\left(\dfrac{q_1 - p_1}{q_1 + p_1}\right), & p_1 q_1 > 0, \end{cases} \tag{2.80}$$

$$\varphi_k = \arg(p_k + \mathrm{i}q_k), \qquad k = 2, \ldots, d.$$

It is not difficult to see that the map $(q, p) \mapsto (\varphi_1, \ldots, \varphi_d, I, J_2, \ldots, J_d)$ is symplectic.

For $k = 2, \ldots, d$, the ranges of the φ_k are $[0, 2\pi)$ and the ranges of the J_k are $[0, \infty)$. The maps $(q_k, p_k) \mapsto (\varphi_k, J_k)$ are singular at $q_k = p_k = 0$ where the angles φ_k are not defined. Away from the singularities the maps are one to one. In contrast, the range of both φ_1 and I is $\mathbb{R}$ (φ_1 thus is not an angle in the usual sense). The map $(q_1, p_1) \mapsto (\varphi_1, I_1)$ is singular on the lines $p_1 = 0$ and $q_1 = 0$ which map to $I = 0$ with $\varphi_1 = \infty$ and $\varphi_1 = -\infty$, respectively. Even away from the singularities each (φ_1, I) has still two preimages (q_1, p_1) which correspond to the two branches of the hyperbola $I = p_1 q_1$. The coordinate lines of the action angle variables are shown in figure 1.

We note that in terms of the coordinates (Q, P) with $(Q_k, P_k) = (q_k, p_k)$, $k = 2, \ldots, d$, and

$$Q_1 = \frac{1}{\sqrt{2}}(q_1 - p_1), \qquad P_1 = \frac{1}{\sqrt{2}}(q_1 + p_1), \tag{2.81}$$

the integrals $J_k, k = 2, \ldots, d$, are of the same form while I changes to

$$I = \tfrac{1}{2}(P_1^2 - Q_1^2). \tag{2.82}$$

The angles φ_k, $k = 1, \ldots, d$, are cyclic, i.e. the Hamilton function $H^{(N)}_{\mathrm{CNF}}$ effectively depends only on the integrals I and $J_k, k = 2, \ldots, d$. To indicate this and for later reference we introduce the function $K^{(N)}_{\mathrm{CNF}}$ defined via

$$H^{(N)}_{\mathrm{CNF}} = K^{(N)}_{\mathrm{CNF}}(I, J_2, \ldots, J_d) = E_0 + \lambda I + \omega_2 J_2 + \cdots + \omega_d J_d + \text{higher order terms}. \tag{2.83}$$

Here the higher order terms are of order greater than 1 and less than or equal to $[N/2]$ in the integrals, where $[N/2]$ denotes the integer part of $N/2$. Note that since the Hamiltonian in normal form does not have any odd order terms, only the case of even N is of interest.

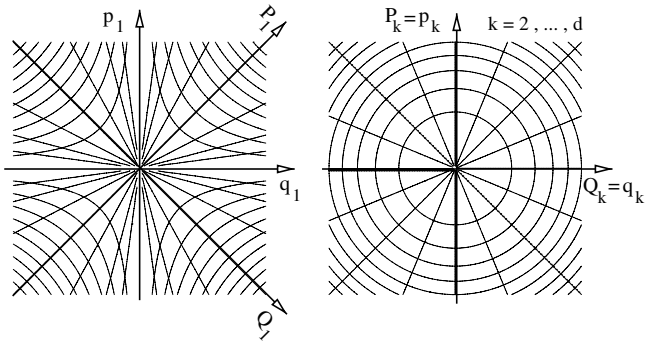

Figure 1. The left figure shows contour lines of the action angle variables I and φ_1 (hyperbolae and straight lines, respectively) in the saddle plane with coordinates (q_1, p_1) and (Q_1, P_1) which are rotated versus each other by 45°. The right figure shows contour lines of the action angle variables J_k and φ_k, $k = 2, \ldots, d$ (circles and straight lines, respectively) in the centre planes with coordinates $(q_k, p_k) = (Q_k, P_k)$.

As we will see, the classical integrals of motion are extremely useful for characterizing, and realizing, classical phase space structures. However, the obvious question arises and must be answered. These are constants of the motion for the Nth order classical normal form $H^{(N)}_{\mathrm{CNF}}$. How close to being constant are they on trajectories of the full Hamiltonian? Also, we will use them to construct certain invariant manifolds for the Nth order classical normal form $H^{(N)}_{\mathrm{CNF}}$. How close to being invariant will these manifolds be for the full Hamiltonian? These questions must be asked, and answered, on a problem-by-problem basis. A number of studies have recently shown that for moderate N (e.g. 10–14), these integrals are 'very close' to constant for the full Hamiltonian dynamics for most practical purposes and that the invariant manifolds constructed from them are 'almost invariant' for the full Hamiltonian dynamics.

We emphasize again that in this section we omitted superscripts (N) on the coordinates in order to keep the notation simple and that the integrals of the motion of the Nth order normal form only assume the simple form in (2.78) if they are expressed in terms of the Nth order normal form coordinates (2.59).

3. Quantum normal form theory

In this section we develop a normal form theory for quantum mechanics that is algorithmically the same as the one presented for classical mechanics in the previous section, section 2. However, the objects manipulated by the algorithm in the quantum mechanical case are different, and this is what we now describe.

In quantum mechanics the role of a Hamilton function in classical mechanics is played by a self-adjoint operator, the Hamilton operator. While the Hamilton function in classical mechanics acts on a phase space, which was $\mathbb{R}^{2d}$ in section 2, a Hamilton operator acts on a Hilbert space, which will be $L^2(\mathbb{R}^d)$ in our case.

The quantum mechanical analogue of a symplectic transformation in classical mechanics is a unitary transformation. The conjugation of a Hamilton operator $\hat{H}$ by a unitary operator $\hat{U}$ gives the new operator

$$\hat{H}' = \hat{U}^* \hat{H} \hat{U}, \tag{3.1}$$

where $\hat{U}^*$ denotes the adjoint of $\hat{U}$. The operator $\hat{H}'$ is again self-adjoint and has the same spectral properties as the original Hamilton operator $\hat{H}$. We will use unitary transformations

to simplify the Hamilton operator in the same way that we used symplectic transformations to simplify the classical Hamilton function. In the classical setting the symplectic transformations were obtained as the time one maps of a Hamiltonian flow, where the Hamiltonian, W, was referred to as the generating function. In the quantum mechanical setting we will analogously consider a self-adjoint operator $\hat{W}$ which gives the unitary operator

$$\hat{U} = \mathrm{e}^{-\frac{\mathrm{i}}{\hbar}\hat{W}}. \tag{3.2}$$

The operator $\hat{W}$ is called the generator of $\hat{U}$. Analogous to the development of (2.7) and the results that follow, we now consider the one-parameter family of self-adjoint operators defined by

$$\hat{H}(\epsilon) := \mathrm{e}^{\frac{\mathrm{i}}{\hbar}\epsilon\hat{W}}\hat{H}\mathrm{e}^{-\frac{\mathrm{i}}{\hbar}\epsilon\hat{W}}, \tag{3.3}$$

where the parameter ϵ is real. Note that $\hat{H}' = \hat{U}^*\hat{H}\hat{U} = \hat{H}(\epsilon = 1)$, and $\hat{H} = \hat{H}(\epsilon = 0)$. If we differentiate (3.3) with respect to ϵ we obtain the Heisenberg equation

$$\frac{\mathrm{d}}{\mathrm{d}\epsilon}\hat{H}(\epsilon) = \frac{\mathrm{i}}{\hbar}[\hat{W}, \hat{H}(\epsilon)], \tag{3.4}$$

where $[\cdot, \cdot]$ denotes the commutator which, for two operators $\hat{A}$, $\hat{B}$, is defined as $[\hat{A}, \hat{B}] = \hat{A}\hat{B} - \hat{B}\hat{A}$. Therefore $\hat{H}'$ can be obtained from the solution of (3.4) with initial condition $\hat{H}(\epsilon = 0) = \hat{H}$. Equation (3.4) will play the same role for the development of the quantum normal form as equation (2.9) played for the classical normal form. This is consistent with the usual quantum–classical correspondence where the commutator $\frac{\mathrm{i}}{\hbar}[\cdot, \cdot]$ is related to the Poisson bracket $\{\cdot, \cdot\}$. In the next section we will make this correspondence more precise.

One of the key properties of the classical normal form in the neighbourhood of a nonresonant saddle-centre-. . .-centre equilibrium point is that the Hamilton function in normal form is a function of the classical integrals, see (2.83). We will see in section 4 that this feature will help us to understand the local classical dynamics and identify the phase space structures that control the dynamics near a nonresonant saddle-centre-. . .-centre equilibrium point. In the quantum mechanical case the classical integrals will correspond to 'elementary' operators with well-known spectral properties. Analogous to symplectic transformations in the classical case, we will use unitary transformations in the quantum mechanical case to bring the Hamilton operator into a simpler form in which it will be a function of these elementary operators only. In the same manner as in the classical case, this simplification will be obtained 'order by order'. To give notions like 'order' and 'equilibrium point' a meaning for quantum operators and also to derive an explicit algorithm to achieve the desired simplification we will have to relate quantum operators to classical phase space functions and vice versa. This is the subject of the following section, section 3.1. The formalism developed in section 3.1 is then used in section 3.2 to transform Hamilton operators through conjugation by unitary operators. In section 3.3 we will define when a Hamilton operator is in quantum normal form, and show how a given Hamilton operator can be transformed to quantum normal form to any desired order. In section 3.4 we study the nature of the quantum normal form for our case of interest, which is in a neighbourhood of a nonresonant saddle-centre-. . .-centre equilibrium point of a corresponding classical Hamiltonian system. As a first explicit example, we show how the quantum normal form can be computed for one-dimensional potential barriers in section 3.5.

3.1. The classical–quantum correspondence

The basis for our quantization of the classical normal form described in section 2.2 is the Weyl quantization and the associated Weyl calculus. Before we use the Weyl calculus to define the quantum normal form in section 3.3 we want to give some background on the general

theory, which provides a systematic way of formulating the quantum–classical correspondence. General references for the material in this section that contain much more detail and background are [Fol89, DS99, Mar02].

3.1.1. Weyl quantization. A quantization is a rule which associates operators on a Hilbert space with functions on a phase space. We will use here the Weyl quantization, which is the one most commonly used. Let q_k and p_k, $k = 1, \ldots, d$, be the components of the position and momentum vectors q and p, respectively. These are quantized in such a way that they act on a wavefunction $\psi(q)$ according to

$$\hat{q}_k \psi(q) = q_k \psi(q), \qquad \hat{p}_k \psi(q) = \frac{\hbar}{\mathrm{i}} \frac{\partial \psi(q)}{\partial q_k}. \tag{3.5}$$

The Weyl quantization extends these prescriptions to general functions of (q, p) by requiring that, for $\xi_q, \xi_p \in \mathbb{R}^d$, the quantization of the exponential function

$$\mathrm{e}^{\frac{\mathrm{i}}{\hbar}(\langle \xi_p, q\rangle + \langle \xi_q, p\rangle)} \tag{3.6}$$

is the phase space translation operator

$$\hat{T}_{\xi_q, \xi_p} = \mathrm{e}^{\frac{\mathrm{i}}{\hbar}(\langle \xi_p, \hat{q}\rangle + \langle \xi_q, \hat{p}\rangle)}. \tag{3.7}$$

Using Fourier inversion we can represent a function on phase space as

$$A(q, p) = \frac{1}{(2\pi\hbar)^{2d}} \int_{\mathbb{R}^d}\int_{\mathbb{R}^d} \bar{A}(\xi_q, \xi_p) \mathrm{e}^{\frac{\mathrm{i}}{\hbar}(\langle \xi_p, q\rangle + \langle \xi_q, p\rangle)} \, \mathrm{d}\xi_q \, \mathrm{d}\xi_p, \tag{3.8}$$

where

$$\bar{A}(\xi_q, \xi_p) = \int_{\mathbb{R}^d}\int_{\mathbb{R}^d} A(q, p) \mathrm{e}^{-\frac{\mathrm{i}}{\hbar}(\langle \xi_p, q\rangle + \langle \xi_q, p\rangle)} \, \mathrm{d}q \, \mathrm{d}p \tag{3.9}$$

is the Fourier transform of A. The *Weyl quantization* $\mathrm{Op}[A]$ of A is then defined by replacing the factor $\mathrm{e}^{\frac{\mathrm{i}}{\hbar}(\langle \xi_p, q\rangle + \langle \xi_q, p\rangle)}$ in the integral (3.8) by the operator $\hat{T}_{\xi_q, \xi_p}$, i.e.

$$\mathrm{Op}[A] = \frac{1}{(2\pi\hbar)^{2d}} \int_{\mathbb{R}^d}\int_{\mathbb{R}^d} \overline{A}(\xi_q, \xi_p) \hat{T}_{\xi_q, \xi_p} \, \mathrm{d}\xi_q \, \mathrm{d}\xi_p. \tag{3.10}$$

In order to manipulate these operators and understand their mathematical properties we will need the appropriate definitions and notation. We will say that $A \in \mathcal{S}_\hbar(\mathbb{R}^d \times \mathbb{R}^d)$ if A depends smoothly on $(\hbar, q, p)$ and if for all $\alpha, \beta \in \mathbb{N}^d$ and $k \in \mathbb{N}$ there exists a constant $C_{\alpha,\beta,k}$ such that

$$(1 + |q| + |p|)^k |\partial_q^\alpha \partial_p^\beta A(\hbar, q, p)| \leqslant C_{\alpha,\beta,k}. \tag{3.11}$$

The space $\mathcal{S}_\hbar(\mathbb{R}^d \times \mathbb{R}^d)$ is similar to the usual Schwartz space. The only difference is that we allow the functions to depend additionally on the parameter $\hbar$ in a smooth way. For $A \in \mathcal{S}_\hbar(\mathbb{R}^d \times \mathbb{R}^d)$ the Fourier transform is again a Schwartz function and so the Weyl quantization (3.10) gives a well-defined bounded operator. But the quantization can be extended to larger classes of functions. One such larger standard class of functions for which the Weyl quantization is well behaved is $S^m(\mathbb{R}^d \times \mathbb{R}^d)$ for some $m \in \mathbb{R}$. Here $A \in S^m(\mathbb{R}^d \times \mathbb{R}^d)$ if A satisfies the estimates

$$|\partial_q^\alpha \partial_p^\beta A(\hbar, q, p)| \leqslant C_{\alpha,\beta}(1 + |q| + |p|)^m \qquad \text{for all } \alpha, \beta \in \mathbb{N}^d. \tag{3.12}$$

If $A \in S^m(\mathbb{R}^d \times \mathbb{R}^d)$ then $\mathrm{Op}[A] : \mathcal{S}_\hbar(\mathbb{R}^d) \to \mathcal{S}_\hbar(\mathbb{R}^d)$ (see, e.g., [DS99]). Here $\mathcal{S}_\hbar(\mathbb{R}^d)$ is defined analogously to $\mathcal{S}_\hbar(\mathbb{R}^d \times \mathbb{R}^d)$ in (3.11). The function A is called the (Weyl) *symbol* of the operator $\mathrm{Op}[A]$. If the symbol A also depends on the parameter $\hbar$ we will usually assume that, for small $\hbar$, A has an asymptotic expansion in integer powers of $\hbar$,

$$A(\hbar, q, p) \sim A_0(q, p) + \hbar A_1(q, p) + \hbar^2 A_2(q, p) + \cdots. \tag{3.13}$$

Here the leading order term $A_0(q, p)$ is then called the *principal symbol* and it is interpreted as the classical phase space function corresponding to $\mathrm{Op}[A]$.

The quantization (3.10) can also be inverted. Let $\hat{A}$ be an operator; then

$$A(\hbar, q, p) := \mathrm{Tr}(\hat{T}^*(q, p)\hat{A}), \tag{3.14}$$

is the Weyl symbol of $\hat{A}$, i.e. we have $\mathrm{Op}[A] = \hat{A}$, with Tr denoting the trace and $\hat{T}^*$ denoting the adjoint of $\hat{T}$.

The advantage of this representation of operators is that many properties of the operators are nicely reflected in their symbols. For later reference we collect two such relations:

1. For the adjoint operator one has $\mathrm{Op}[A]^* = \mathrm{Op}[A^*]$, where A^* denotes the complex conjugate symbol of A. Hence, a real valued symbol gives a symmetric operator.
2. If $A \in S^0(\mathbb{R}^d \times \mathbb{R}^d)$, i.e. the symbol and all its derivatives are bounded, then the corresponding operator is bounded as an operator on $L^2(\mathbb{R}^d)$. This is known as the Calderon–Vaillancourt theorem [DS99]. This implies in particular that a real valued symbol $A \in S^0(\mathbb{R}^d \times \mathbb{R}^d)$ gives a self-adjoint operator $\mathrm{Op}[A]$.

For example, the symbol $J = (p^2 + q^2)/2$ on $\mathbb{R} \times \mathbb{R}$ is in $S^2(\mathbb{R} \times \mathbb{R})$. Its principal symbol is $(p^2 + q^2)/2$ and the Weyl quantization gives

$$\mathrm{Op}[J] = -\frac{\hbar^2}{2}\frac{\mathrm{d}^2}{\mathrm{d}q^2} + \frac{1}{2}q^2. \tag{3.15}$$

Similarly, the symbol $I = p\,q$ is in $S^2(\mathbb{R} \times \mathbb{R})$ with principal symbol $p\,q$ and is quantized as

$$\mathrm{Op}[I] = \frac{\hbar}{\mathrm{i}}\left(q\frac{\mathrm{d}}{\mathrm{d}q} + \frac{1}{2}\right). \tag{3.16}$$

These are the quantizations of the classical integrals obtained in section 2.3.2, and they will form the building blocks of the quantum normal form associated with a saddle-centre-. . .-centre equilibrium point in section 3.4.

3.1.2. The Moyal bracket. The main idea behind the introduction of symbols of operators is that one can use the symbols to study properties of the operators, as we have already indicated in the last subsection. Since the symbols are functions they are in general much easier to study than operators. One can probably say that the single most useful fact about pseudodifferential operators, i.e. operators whose symbols satisfy estimates like (3.12), is that they form an algebra, i.e. the product of two such operators is again of this type, and that one can compute the symbol of a product from the symbols of the operators which are multiplied.

The quantum normal form algorithm we will develop will rely essentially on this product formula for symbols. Given two functions A, B, one can find a function $A * B$ such that $\mathrm{Op}[A]\mathrm{Op}[B] = \mathrm{Op}[A * B]$, see [DS99]. This so-called *star product* of A and B is given by

$$A * B(q, p) = A(q, p) \exp\left(\mathrm{i}\frac{\hbar}{2}[\langle \overleftarrow{\partial}_q, \overrightarrow{\partial}_p\rangle - \langle \overrightarrow{\partial}_q, \overleftarrow{\partial}_p\rangle]\right) B(q, p), \tag{3.17}$$

where the arrows indicate whether the partial differentiation acts to the left (on A) or to the right (on B). For the precise meaning of the expression on the right-hand side of this equation we refer the reader to [Fol89, DS99, Mar02]. However, by expanding the exponential we obtain the more explicit asymptotic expansion in powers of $\hbar$ that will suffice for our purposes

$$\begin{aligned} A * B(q, p) &\sim \sum_{k=0}^{\infty} \frac{1}{k!}\left(\frac{\mathrm{i}\hbar}{2}\right)^k A(q, p)[\langle \overleftarrow{\partial}_q, \overrightarrow{\partial}_p\rangle - \langle \overrightarrow{\partial}_q, \overleftarrow{\partial}_p\rangle]^k B(q, p) \\ &= A(q, p)B(q, p) + \frac{\mathrm{i}\hbar}{2}\{A, B\}(q, p) + \cdots, \end{aligned} \tag{3.18}$$

where $\{\cdot,\cdot\}$ again denotes the Poisson bracket defined in (2.8). In particular, if $A \in S^m(\mathbb{R}^d \times \mathbb{R}^d)$ and $B \in S^{m'}(\mathbb{R}^d \times \mathbb{R}^d)$ then $A * B \in S^{m+m'}(\mathbb{R}^d \times \mathbb{R}^d)$ [Fol89, DS99, Mar02]. It is worth mentioning that even if A and B are independent of $\hbar$, the product $A * B$ will in general depend on $\hbar$ with the principal symbol being given by $A\,B$, i.e. the usual product of the functions A and B.

From the Heisenberg equation (3.4) we see that the commutator plays an important role when one wants to conjugate an operator with a one-parameter family of unitary operators. Applying the product formula (3.17) to the expression for the commutator of $\mathrm{Op}[A]$ and $\mathrm{Op}[B]$,

$$\mathrm{Op}[A]\mathrm{Op}[B] - \mathrm{Op}[B]\mathrm{Op}[A] = \mathrm{Op}[A * B] - \mathrm{Op}[B * A] = \mathrm{Op}[A * B - B * A], \tag{3.19}$$

we obtain the formula for the symbol of a commutator

$$(A * B - B * A)(q, p) = \frac{\hbar}{\mathrm{i}}\{A, B\}_M(q, p), \tag{3.20}$$

where $\{\cdot,\cdot\}_M$ is the *Moyal bracket* which is defined as

$$\{A, B\}_M(q, p) = \frac{2}{\hbar}A(q, p)\sin\left(\frac{\hbar}{2}[\langle \overleftarrow{\partial}_p, \overrightarrow{\partial}_q\rangle - \langle \overrightarrow{\partial}_p, \overleftarrow{\partial}_q\rangle]\right)B(q, p). \tag{3.21}$$

For the precise interpretation of the right-hand side of this equation we again refer the reader to [Fol89, DS99, Mar02]. However, as above, by expanding the sine we can obtain an explicit asymptotic expansion for small $\hbar$ that will suffice for our purposes,

$$\{A, B\}_M(q, p) \sim \sum_{k=0}^{\infty}\left(\frac{\hbar}{2}\right)^{2k}\frac{(-1)^k}{(2k+1)!}A(q, p)[\langle \overleftarrow{\partial}_p, \overrightarrow{\partial}_q\rangle - \langle \overrightarrow{\partial}_p, \overleftarrow{\partial}_q\rangle]^{(2k+1)}B(q, p). \tag{3.22}$$

Note that in the case where one of the functions A, B is a polynomial the sum terminates at some finite k and gives the exact expression for the Moyal product. In what follows, all our explicit calculations will use from the Weyl quantization only the asymptotic formula (3.22) for the Moyal product. Since we will work only with finite Taylor series, the asymptotic expansion will always terminate and give the exact result.

From (3.22) we see that

$$\{A, B\}_M(q, p) = \{A, B\}(q, p) + O(\hbar^2), \tag{3.23}$$

i.e. in leading order the Moyal bracket is equal to the Poisson bracket, and moreover, if at least one of the functions A, B is a second order polynomial then

$$\{A, B\}_M(q, p) = \{A, B\}(q, p). \tag{3.24}$$

3.1.3. Localizing in phase space. One important application of the product formula (3.17) is that it allows operators to be localized in phase space, a technique often called *micro-localization*, which in fact gave the whole field of microlocal analysis its name. Let $\rho \in S^0(\mathbb{R}^d \times \mathbb{R}^d)$ be a cutoff function, i.e. there is a set $U \subset \mathbb{R}^d \times \mathbb{R}^d$ such that

$$\rho|_U = 1 \tag{3.25}$$

and ρ has support in a small neighbourhood of U. Then we will call $\mathrm{Op}[\rho]$ a cutoff operator (associated with U), and we can use it to split any operator $\mathrm{Op}[H]$ into two parts

$$\mathrm{Op}[H] = \mathrm{Op}[\rho]\mathrm{Op}[H] + (1 - \mathrm{Op}[\rho])\mathrm{Op}[H] = \mathrm{Op}[H_{\mathrm{loc}}] + \mathrm{Op}[H_{\mathrm{rem}}] \tag{3.26}$$

where $H_{\mathrm{loc}} = \rho * H$ and $H_{\mathrm{rem}} = H - \rho * H$. By the product formula (3.17) the symbol H_{loc} is concentrated near the support of ρ and H_{rem} is concentrated on the complement of the support of ρ. In this sense the usual procedure to localize the study of functions and dynamical systems by multiplication with cutoff functions can be quantized. In particular we have

$H_{\mathrm{loc}} = \rho H + O(\hbar)$, so the leading order is actually the classical localization. If $\mathrm{Op}[\rho]$ is a cutoff operator associated with some phase space region U we will call $\mathrm{Op}[H_{\mathrm{loc}}] = \mathrm{Op}[\rho]\mathrm{Op}[H]$ the localization of H to U.

The localization appears to be a very natural object to consider with regard to the application we are interested in, namely the study of the dynamics of a chemical reaction which is described by a Hamilton operator $\mathrm{Op}[H]$ whose principal symbol has a saddle-centre-...-centre equilibrium point. The neighbourhood of the equilibrium point is the most important region for the chemical reactions. This is where the reactants combine to form the activated complex which then decays into the products. So it is natural to use the above procedure to localize the Hamiltonian to a neighbourhood of the equilibrium point in phase space. In fact, we will derive the quantization of the classical normal form procedure for a Hamiltonian which is localized.

The localization has another advantage which is of a more technical nature. The Hamilton operators we will encounter have symbols with polynomial growth in p and q for large p and q, and this leads to some technical complications concerning questions like self-adjointness and unitarity. If we localize our Hamiltonians by multiplication with a cutoff operator we end up working with operators with bounded symbols only, for which self-adjointness is easy to show. This will make many proofs technically much easier.

3.2. Transformation of operators through conjugation with unitary operators using the Weyl calculus

We will now apply the Weyl calculus to the problem outlined in the beginning of this section. For an operator $\hat{A} = \mathrm{Op}[A]$ with symbol A we consider its conjugation by a unitary operator $\hat{U} = \mathrm{e}^{\frac{\mathrm{i}}{\hbar}\hat{W}}$, where $\hat{W} = \mathrm{Op}[W]$ has symbol W. Our aim is to find the symbol A' such that

$$\mathrm{Op}[A'] = \mathrm{e}^{\frac{\mathrm{i}}{\hbar}\mathrm{Op}[W]}\mathrm{Op}[A]\mathrm{e}^{-\frac{\mathrm{i}}{\hbar}\mathrm{Op}[W]}. \tag{3.27}$$

If we introduce the one-parameter family of operators

$$\hat{A}(\epsilon) = \mathrm{Op}[A(\epsilon)] = \mathrm{e}^{\frac{\mathrm{i}}{\hbar}\epsilon\mathrm{Op}[W]}\mathrm{Op}[A]\mathrm{e}^{-\frac{\mathrm{i}}{\hbar}\epsilon\mathrm{Op}[W]} \tag{3.28}$$

then $A' = A(\epsilon = 1)$ and the Heisenberg equation (3.4) can be written in terms of the Moyal bracket as an equation for the symbol $A(\epsilon)$,

$$\frac{\mathrm{d}}{\mathrm{d}\epsilon}A(\epsilon) = \{W, A(\epsilon)\}_M. \tag{3.29}$$

In order to obtain A' we thus have to solve (3.29) with initial condition $A(0) = A$. Note the similarity between (3.29) and (2.9) in section 2.1 which expresses the correspondence between the Heisenberg equation (3.4) and the classical equation (2.9) in the framework of the Weyl calculus.

We will now discuss methods of how to solve equation (3.29) for certain choices of W. Recall that if W is a polynomial of order less than or equal to two, then the Moyal bracket reduces to the Poisson bracket (see (3.24)) and hence equation (3.29) reduces to (2.9), and we recalled earlier in our development of the classical normal form theory that polynomials of order less than or equal to two generate affine linear symplectic transformations (see section 2.2 and reference [Fol89]). The following lemma tells us that the symbols of operators transform in the same way as classical phase space functions under such transformations.

Lemma 6 (Exact Egorov). *Assume $W(q, p)$ is a polynomial of order less than or equal to 2 with real valued coefficients, and let Φ_W^1 be the time one map of the Hamiltonian flow generated by W (see (2.5)). Then*

$$\hat{U} = \mathrm{e}^{-\frac{\mathrm{i}}{\hbar}\mathrm{Op}[W]} \tag{3.30}$$

is unitary, and for every $A \in S^m(\mathbb{R}^d \times \mathbb{R}^d)$*, we have*

$$e^{\frac{i}{\hbar}\mathrm{Op}[W]}\mathrm{Op}[A]e^{-\frac{i}{\hbar}\mathrm{Op}[W]} = \mathrm{Op}[A'] \tag{3.31}$$

with $A' \in S^m(\mathbb{R}^d \times \mathbb{R}^d)$ *given by*

$$A' = A \circ \Phi_W^{-1}. \tag{3.32}$$

Proof. For the full proof we refer the reader to the appendix to chapter 7 in [DS99]. The main ideas are as follows. It is well known that $\mathrm{Op}[W]$ is essentially self-adjoint (see e.g. [DS99]), and therefore $\hat{U}$ is unitary. In order to find H' we have to solve (3.29). Since W is a polynomial of order two or less than two equation (3.29) reduces to (2.9). From equation (2.5) we see that $A(\epsilon) = A \circ \Phi_W^{-\epsilon}$, and at $\epsilon = 1$ we obtain (3.32). Now if W is a polynomial of order less than or equal to two, then Φ_W^{-1} is an affine linear transformation. Hence if $A \in S^m(\mathbb{R}^d \times \mathbb{R}^d)$, then $A' \in S^m(\mathbb{R}^d \times \mathbb{R}^d)$. □

This result is called 'exact Egorov' because there is a more general theorem due to Egorov [Ego69] which states that, for a large class of W, a similar result holds asymptotically for $\hbar \to 0$. However, only for polynomials of degree equal to or less than two, do the higher order terms in $\hbar$ vanish.

For later reference we consider the following example. For $(q, p) \in \mathbb{R}^2$, let

$$W(q, p) = -\frac{\pi}{4}\frac{1}{2}(p^2 + q^2), \tag{3.33}$$

which is the Hamilton function of an harmonic oscillator. The factor $-\pi/4$ is introduced for convenience. The function W generates the vector field

$$X_W(q, p) = (\partial_p W(q, p), -\partial_q W(q, p)) = \frac{\pi}{4}(-p, q). \tag{3.34}$$

The corresponding flow is given by

$$(q(\epsilon), p(\epsilon)) = \Phi_W^{\epsilon}(q, p) = \left(\cos\left(\epsilon\frac{\pi}{4}\right)q - \sin\left(\epsilon\frac{\pi}{4}\right)p, \sin\left(\epsilon\frac{\pi}{4}\right)q + \cos\left(\epsilon\frac{\pi}{4}\right)p\right). \tag{3.35}$$

The harmonic oscillator thus generates rotations in the (q, p)-plane. In particular, the time one map of the flow generated by W gives the map from the coordinates (q, p) to the new coordinates

$$(Q, P) = \Phi_W^1(q, p) = \frac{1}{\sqrt{2}}(q - p, q + p), \tag{3.36}$$

which we have already considered in section 2.3. Transforming $I(q, p) = pq$ under this flow we get

$$I'(Q, P) = I \circ \Phi_W^{-1}(Q, P) = \tfrac{1}{2}(P^2 - Q^2), \tag{3.37}$$

which gives the operator

$$\mathrm{Op}[I'] = -\frac{\hbar^2}{2}\frac{\mathrm{d}^2}{\mathrm{d}Q^2} - \frac{1}{2}Q^2. \tag{3.38}$$

We will refer to $\mathrm{Op}[I']$ as the Q representation of $\mathrm{Op}[I]$, and for later reference we denote the unitary transformation which classically generates the 45° rotation (3.36) as

$$\hat{U}_{\mathrm{r}} = e^{-\frac{i}{\hbar}\mathrm{Op}[W]}, \tag{3.39}$$

where W is given by (3.33).

Having discussed this particular example of an application of lemma 6 (exact Egorov) we now turn to the case of higher order polynomials in W. To this end we will develop a power series approach analogous to what we described in section 2.1. This will provide higher order approximations in $\hbar$ as well as give an explicit expression for the symbol of the transformed in (3.27) in the case where W or A are polynomials.

We begin by simplifying the notation and define the Moyal-adjoint action. For two smooth functions W and A, we define analogously to the adjoint action in (2.10) the Moyal-adjoint action as

$$\mathrm{Mad}_W A := \{W, A\}_M. \tag{3.40}$$

Using the Moyal adjoint equation (3.29) becomes

$$\frac{\mathrm{d}A(\epsilon)}{\mathrm{d}\epsilon} = \mathrm{Mad}_W A(\epsilon). \tag{3.41}$$

We compute higher order derivatives of $A(\epsilon)$ with respect to ϵ in a manner analogous to (2.11) and (2.12). We successively differentiate (3.29) and apply the notation (3.40) to obtain

$$\frac{\mathrm{d}^n}{\mathrm{d}\epsilon^n} A(\epsilon) = [\mathrm{Mad}_W]^n A(\epsilon). \tag{3.42}$$

Hence, the (formal) Taylor series in ϵ around $\epsilon = 0$ is given by

$$A(\epsilon) = \sum_{n=0}^{\infty} \frac{\epsilon^n}{n!} [\mathrm{Mad}_W]^n A, \tag{3.43}$$

and setting $\epsilon = 1$ we obtain the formal sum

$$A' = \sum_{n=0}^{\infty} \frac{1}{n!} [\mathrm{Mad}_W]^n A. \tag{3.44}$$

This expression is completely analogous to (2.13), and as we will see in more detail, can be used in a similar fashion to compute the symbol A' up to any desired order in $\hbar$ and (q, p). In particular, analogously to equation (2.13), it gives the Taylor expansion with respect to ϵ, evaluated at $\epsilon = 1$, for the symbol A' of the operator obtained after conjugation of the operator defined by the symbol A by the unitary transformation generated by W. This formula forms the basis of the quantum normal form method where the idea is to 'simplify' (or 'normalize') the symbol whose quantization will then correspond to the normal form of the Hamilton operator. As in the classical case, the computation of the Taylor expansion is carried out 'order by order' using power series expansions of the symbol in (q, p) and $\hbar$. The series is expanded about an equilibrium point of the principal symbol, and therefore the quantum normal form will be valid in a neighbourhood of this point. Hence, as in the classical case, the quantum normal form is a 'local object' whose operator nature requires more technical details for a rigorous characterization of its properties (cf section 3.1.3 and definition 4), and we will describe these in more detail in the following.

Therefore similar to the mathematical formalism required for computing the classical normal form, normalizing the symbol of the operator that will correspond to the quantum normal form will require us to manipulate monomials which in addition to (q, p) now also have factors of $\hbar$. In order to describe this we adopt a notation introduced by Crehan [Cre90] and define the spaces

$$\mathcal{W}^s_{\mathrm{qm}} = \mathrm{span}\left\{\hbar^j q^\alpha p^\beta := \hbar^j \prod_{k=1}^{d} q_k^{\alpha_k} p_k^{\beta_k} \ : \ |\alpha| + |\beta| + 2j = s\right\}. \tag{3.45}$$

These spaces $\mathcal{W}^s_{\rm qm}$ are closely related to the spaces $\mathcal{W}^s_{\rm cl}$ spanned by the polynomials (2.14) in the classical case. In fact we have

$$\mathcal{W}^s_{\rm qm} = \bigoplus_{k=0}^{[s/2]} \hbar^k \mathcal{W}^{s-2k}_{\rm cl}, \tag{3.46}$$

where $[s/2]$ denotes the integer part of $s/2$.

Below we want to use functions $W \in \mathcal{W}^s_{\rm qm}$ in order to construct unitary operators of the form $\mathrm{e}^{-\frac{\mathrm{i}}{\hbar}\mathrm{Op}[W]}$. However, the quantization of a function $W \in \mathcal{W}^s_{\rm qm}$ will give an unbounded operator and this makes the discussion of self-adjointness of $\mathrm{Op}[W]$, and hence the unitarity of $\mathrm{e}^{-\frac{\mathrm{i}}{\hbar}\mathrm{Op}[W]}$, more complicated. But since we are interested in the local quantum dynamics generated by a Hamilton operator in the neighbourhood of an equilibrium point of its principal symbol it will be sufficient to have a local version of the spaces $\mathcal{W}^s_{\rm qm}$. We thus apply the localization procedure from section 3.1.3. We say that $W \in \mathcal{W}^s_{\rm qm;loc}$ if $W \in \mathcal{S}_\hbar(\mathbb{R}^d \times \mathbb{R}^d)$ and there is an open neighbourhood U of $z_0 = 0 \in \mathbb{R}^d \times \mathbb{R}^d$ such that

$$W|_U \in \mathcal{W}^s_{\rm qm}. \tag{3.47}$$

The quantization of elements of $\mathcal{W}^s_{\rm qm;loc}$ will then give bounded operators. Therefore, if $W \in \mathcal{W}^s_{\rm qm;loc}$ is real valued then $\mathrm{Op}[W]$ will be self-adjoint and thus $\hat{U} = \mathrm{e}^{-\frac{\mathrm{i}}{\hbar}\mathrm{Op}[W]}$ will be unitary.

We will frequently use Taylor expansions and want to modify them in such a way that the terms in the expansion are in $\mathcal{W}^s_{\rm qm;loc}$. In order to make our discussion of this property precise we will need the following definition.

Definition 4. *We will say a function $O_N \in \mathcal{S}_\hbar(\mathbb{R}^d \times \mathbb{R}^d)$ is a remainder of order N (around $(q, p) = (0, 0)$) if there is an open neighbourhood U of $(q, p) = (0, 0)$ and $c > 0$ such that*

$$|O_N(\varepsilon^2\hbar, \varepsilon q, \varepsilon p)| < c\varepsilon^N \tag{3.48}$$

for $\hbar < 1$, $(q, p) \in U$ and $\varepsilon < 1$.

We then can formulate

Lemma 7. *Let $A \in \mathcal{S}_\hbar(\mathbb{R}^d \times \mathbb{R}^d)$, then there exist $A_s \in \mathcal{W}^s_{\rm qm;loc}$ such that for any $N \in \mathbb{N}$ there is a remainder $O_N \in \mathcal{S}_\hbar(\mathbb{R}^d \times \mathbb{R}^d)$ of order N such that*

$$A = \sum_{s=0}^{N-1} A_s + O_N. \tag{3.49}$$

Proof. Let us take the ordinary Taylor expansion of $A(\hbar, q, p)$ around $(\hbar, q, p) = (0, 0, 0)$ and order the terms according to the definition of order in (3.45). This gives us an expansion $A = \sum_{s=0}^{N-1} \tilde{A}_s + R_N$ with

$$\tilde{A}_s = \sum_{|\alpha|+|\beta|+2j=s} \frac{1}{j!\alpha!\beta!} \partial_\hbar^k \partial_q^\alpha \partial_p^\beta A(0, q_0, p_0) q^\alpha p^\beta \hbar^j \in \mathcal{W}^s_{\rm qm} \tag{3.50}$$

and $R_N(\varepsilon^2\hbar, \varepsilon q, \varepsilon p) = O(\varepsilon^N)$. Now choose a function $\rho \in \mathcal{S}_\hbar(\mathbb{R}^d \times \mathbb{R}^d)$ with $\rho|_U \equiv 1$ for some open neighbourhood U of 0, and set $A_s := \rho\tilde{A}_s$. Then it follows directly that $A_s \in \mathcal{W}^s_{\rm qm;loc}$ and $O_N := A - \sum_{s=0}^{N-1} A_s \in \mathcal{S}_\hbar(\mathbb{R}^d \times \mathbb{R}^d)$ is a remainder of order N. □

The main reason for defining the order s according to (3.45), i.e. the reason for double counting the powers of $\hbar$, is that it behaves nicely with respect to the Moyal product. This is reflected in the following lemmata. The first one is the analogue of lemma 1 in the classical case.

Lemma 8. *Let* $W \in \mathcal{W}^{s'}_{\mathrm{qm;loc}}$, $A \in \mathcal{W}^{s}_{\mathrm{qm;loc}}$, $s, s' \geqslant 1$, *then*

$$\{W, A\}_M \in \mathcal{W}^{s+s'-2}_{\mathrm{qm;loc}}, \tag{3.51}$$

and for $n \geqslant 0$,

$$[\mathrm{Mad}_W]^n A \in \mathcal{W}^{n(s'-2)+s}_{\mathrm{qm;loc}}, \tag{3.52}$$

if $n(s'-2)+s \geqslant 0$ *and* $\left[\mathrm{Mad}_W\right]^n A = 0$ *otherwise.*

Proof. We can write the Moyal bracket (3.22) as

$$\{W, A\}_M = \sum_k \left(\frac{\hbar}{2}\right)^{2k} \frac{(-1)^k}{(2k+1)!} D^{(2k+1)}(W, A)(q, p) \tag{3.53}$$

with the bi-differential operators

$$D^{(2k+1)}(W, A)(q, p) := W(q, p)[\langle \overleftarrow{\partial}_p, \overrightarrow{\partial}_q \rangle - \langle \overrightarrow{\partial}_p, \overleftarrow{\partial}_q \rangle]^{(2k+1)} A(q, p), \tag{3.54}$$

Now the bi-differential operator $D^{(2k+1)}$ is of order $2k+1$ in the arguments involving A and W individually, and therefore

$$D^{(2k+1)} : \mathcal{W}^{s}_{\mathrm{qm;loc}} \times \mathcal{W}^{s'}_{\mathrm{qm;loc}} \to \mathcal{W}^{s-(2k+1)+s'-(2k+1)}_{\mathrm{qm;loc}}. \tag{3.55}$$

On the other hand, multiplication by $\hbar^{2k}$ maps $\mathcal{W}^{s-(2k+1)+s'-(2k+1)}_{\mathrm{qm;loc}}$ to $\mathcal{W}^{s-(2k+1)+s'-(2k+1)+4k}_{\mathrm{qm;loc}} = \mathcal{W}^{s+s'-2}_{\mathrm{qm;loc}}$, and therefore every term in the series (3.53) is in $\mathcal{W}^{s+s'-2}_{\mathrm{qm;loc}}$. But the order of W and A as polynomials in (q, p) near $(q, p) = (0, 0)$ is at most s and s', respectively, and therefore the terms in the series (3.53) vanish near $(q, p) = (0, 0)$ for $2k+1 > \min(s, s')$. Hence

$$\{W, A\}_M \in \mathcal{W}^{s+s'-2}_{\mathrm{qm;loc}}. \tag{3.56}$$

The second result then follows by induction. □

We can now turn our attention to the computation of the symbol of a conjugated operator when the generator of the unitary operator has order larger than 2. The computation will proceed in two steps; in the first lemma we show that conjugation respects the class of symbols we are working with.

Lemma 9. *Let* $W \in \mathcal{W}^{s}_{\mathrm{qm;loc}}$ *and* $A \in \mathcal{S}_\hbar(\mathbb{R}^d \times \mathbb{R}^d)$, *then there exists an* $A' \in \mathcal{S}_\hbar(\mathbb{R}^d \times \mathbb{R}^d)$ *such that* $\mathrm{Op}[A'] = \mathrm{e}^{\frac{\mathrm{i}}{\hbar}\mathrm{Op}[W]}\mathrm{Op}[A]\mathrm{e}^{-\frac{\mathrm{i}}{\hbar}\mathrm{Op}[W]}$.

The techniques for proving this lemma are different from the ones we use in the rest of the paper. In order not to interrupt the flow of the paper, we therefore present the proof in appendix A.

By lemma 9 we know that the symbol of $\mathrm{e}^{\frac{\mathrm{i}}{\hbar}\mathrm{Op}[W]}\mathrm{Op}[A]\mathrm{e}^{-\frac{\mathrm{i}}{\hbar}\mathrm{Op}[W]}$ is a function in $\mathcal{S}_\hbar(\mathbb{R}^d \times \mathbb{R}^d)$. With the help of lemma 8 we can reorder the terms in the formal expansion (3.44) to turn it into a well-defined Taylor expansion in the sense of lemma 7. This is the content of the following lemma which can be considered to be the analogue of lemma 2 in the classical case.

Lemma 10. *Let* $W \in \mathcal{W}^{s'}_{\mathrm{qm;loc}}$, $s' \geqslant 3$, *and* $A \in \mathcal{S}_\hbar(\mathbb{R}^d \times \mathbb{R}^d)$ *with Taylor expansion* $A = \sum_{s=0}^{\infty} A_s$, $A_s \in \mathcal{W}^{s}_{\mathrm{qm;loc}}$. *Then the symbol* A' *of* $\mathrm{e}^{\frac{\mathrm{i}}{\hbar}\mathrm{Op}[W]}\mathrm{Op}[A]\mathrm{e}^{-\frac{\mathrm{i}}{\hbar}\mathrm{Op}[W]}$ *has the Taylor expansion*

$$A' = \sum_{s=0}^{\infty} A'_s \tag{3.57}$$

with

$$A'_s = \sum_{n=0}^{[\frac{s}{s'-2}]} \frac{1}{n!} [\mathrm{Mad}_W]^n A_{s-n(s'-2)} \in \mathcal{W}^s_{\mathrm{qm;loc}}, \tag{3.58}$$

i.e. for every $N \in \mathbb{N}$ *there exists a remainder* $O_N \in \mathcal{S}_\hbar(\mathbb{R}^d \times \mathbb{R}^d)$ *of order* N *such that*

$$A' = \sum_{s=0}^{N-1} A'_s + O_N. \tag{3.59}$$

Proof. By lemma 9 we know that $A' \in \mathcal{S}_\hbar(\mathbb{R}^d \times \mathbb{R}^d)$, and we have to compute its Taylor series. With (3.42) we can use the Taylor expansion of $A'(\epsilon)$ to write

$$A' = \sum_{n=0}^{N-1} \frac{1}{n!} \big[\mathrm{Mad}_W\big]^n A + O'_N \tag{3.60}$$

with

$$O'_N = \frac{1}{(N-1)!} \int_0^1 (1-\epsilon)^{N-1} \big[\mathrm{Mad}_W\big]^N A'(\epsilon)\, \mathrm{d}\epsilon, \tag{3.61}$$

being just the standard remainder formula for Taylor expansions. Since $A'(\epsilon) \in \mathcal{S}_\hbar(\mathbb{R}^d \times \mathbb{R}^d) = \mathcal{W}^0_{\mathrm{qm;loc}}$ we have by lemma 8 that $O'_N \in \mathcal{S}_\hbar(\mathbb{R}^d \times \mathbb{R}^d)$ is a remainder of order N. If we next insert the Taylor expansion for A we get

$$A' = \sum_{l=0}^{N-1} \sum_{n=0}^{N-1} \frac{1}{n!} \big[\mathrm{Mad}_W\big]^n A_l + O_N, \tag{3.62}$$

where $O_N \in \mathcal{S}_\hbar(\mathbb{R}^d \times \mathbb{R}^d)$ denotes the collection of all the remainder terms of order N. Using lemma 8 we can collect all the terms of order k in the sum which gives (3.58). To this end one can proceed completely analogously to the proof of lemma 2 and we therefore omit the details. □

3.3. Definition and computation of the quantum normal form

We will now define when a Hamilton operator is in quantum normal form. Similarly to the case of the classical normal form, in general a Hamilton operator is not in quantum normal form. However, as we will show, the formalism based on the Weyl calculus developed in the previous two sections can be used to construct an explicit algorithm which will allow us to transform a Hamilton operator to normal form to any desired order of its symbol. The algorithm will consist of two parts. The first part operates on the level of the symbols of operators, and this part of the algorithm will be very similar to the normalization algorithm in the classical case. In the second part the symbols are quantized, i.e. the operators corresponding to the symbols will be determined.

The starting point is a Hamilton operator $\mathrm{Op}[H]$ which is the Weyl quantization of a symbol $H(\hbar, q, p)$. Assume that the Hamiltonian dynamical system defined by the *principal symbol* has an *equilibrium point* at $z_0 = (q_0, p_0)$, i.e. the gradient of the principal symbol vanishes at z_0. Let $H_2(z) \in \mathcal{W}^2_{\mathrm{qm}}$ denote the second order term of the Taylor expansion of the symbol H about z_0 and $\mathrm{Op}[H_2]$ its Weyl quantization. We now make the

Definition 5 (Quantum normal form). *We say that* $\mathrm{Op}[H]$ *is in quantum normal form with respect to the equilibrium point* z_0 *of its principal symbol if*

$$[\mathrm{Op}[H_2], \mathrm{Op}[H]] = 0, \tag{3.63}$$

or equivalently in terms of the symbol,

$$\mathrm{ad}_{H_2} H \equiv \{H_2, H\} = 0. \tag{3.64}$$

The equivalence of the two equations in definition 5 derives from the fact that the Moyal bracket reduces to the Poisson bracket if one of its arguments is quadratic. Moreover, we remark that H_2 and the quadratic part of the principal symbol differ at most by a term that consists of $\hbar$ with a constant prefactor. Since the Poisson bracket vanishes if one of its two arguments is a constant it does not make a difference in definition 5 if H_2 in (3.64) were replaced by the second order term of the Taylor expansion of the principal symbol.

As in the case of a Hamilton function being in classical normal form the property of a Hamilton operator to be in quantum normal form has strong implications which in the quantum case lead to a considerable simplification of the study of the spectral properties of the operator. To this end recall that two commuting operators have a joint set of eigenfunctions. Hence, if an operator is in quantum normal form the study of its spectral properties will be simplified considerably, since the spectrum and eigenfunctions of an operator $\mathrm{Op}[H_2]$ with a symbol of order 2 are well known.

Similarly to the classical case a Hamilton operator is in general not in quantum normal form. However, we will now show how the formalism developed in the previous two sections can be used to transform a Hamilton operator to quantum normal form to any desired order of its symbol. Similarly to the classical case we will truncate the symbol at a certain order and show that the corresponding Hamilton operator will lead to a very good approximation of many interesting spectral properties of the original Hamilton operator.

We develop the following procedure. Let $H = H^{(0)}$ denote the symbol of our original Hamilton operator. We will construct a consecutive sequence of transformations of the symbol according to

$$H =: H^{(0)} \to H^{(1)} \to H^{(2)} \to H^{(3)} \to \cdots \to H^{(N)} \tag{3.65}$$

by requiring the symbol $H^{(n)}$, for $n \geqslant 1$, to derive from the symbol $H^{(n-1)}$ by conjugating $\mathrm{Op}[H^{(n-1)}]$ with a unitary transformation according to

$$\mathrm{Op}[H^{(n)}] = \mathrm{e}^{\frac{\mathrm{i}}{\hbar}\mathrm{Op}[W_n]}\mathrm{Op}[H^{(n-1)}]\mathrm{e}^{-\frac{\mathrm{i}}{\hbar}\mathrm{Op}[W_n]}, \tag{3.66}$$

where the symbol W_n of the generator of the unitary transformation is in $\mathcal{W}^n_{\mathrm{qm;loc}}$. As in the series of symplectic transformations in the classical case in (2.27), N in (3.65) is again a sufficiently large integer at which we will truncate the quantum normal form computation. The algorithm for normalizing the symbol will be identical to the classical case. The key difference is that the Poisson bracket of the classical case is replaced by the Moyal bracket in the quantum case. With this replacement, the mathematical manipulations leading to normalization of the symbol are virtually identical.

To this end, using (3.44) we see that, analogously to (2.35) in the classical case, we have

$$H^{(n)} = \sum_{k=0}^{\infty} \frac{1}{k!}\big[\mathrm{Mad}_{W_n}\big]^k H^{(n-1)}. \tag{3.67}$$

As in the classical case the first two steps, $n = 1, 2$, in (3.65) differ somewhat in nature from the steps for $n \geqslant 3$. The first step serves to shift the equilibrium point to the origin and the second step serves to simplify the quadratic part of the symbol. It follows from lemma 6

(exact Egorov) that we achieve these affine linear transformations by choosing the symbols W_1 and W_2 identical to the generators of the corresponding symplectic transformations in the classical case. We thus have

$$H^{(1)}(\hbar, z) = H^{(0)}(\hbar, z + z_0) \tag{3.68}$$

and

$$H^{(2)}(\hbar, z) = H^{(1)}(\hbar, M^{-1}z), \tag{3.69}$$

where M is a suitable symplectic $2d \times 2d$ matrix which achieves the simplification of the quadratic part of the symbol analogously to the classical case. It is important to note that we do not explicitly need the generators W_1 and W_2 which, as mentioned in section 2.2, might be difficult to compute.

Before we proceed with the normalization of the higher order terms, $n \geqslant 3$, we will assume that we localize around the equilibrium point which is now at the origin, see section 3.1.3, i.e. by multiplying $H^{(2)}$ by a suitable cutoff function concentrated about the origin we can assume $H^{(2)} \in \mathcal{S}_\hbar(\mathbb{R}^d \times \mathbb{R}^d)$ and the terms $H_s^{(2)}$ of the Taylor expansion of $H^{(2)}$ to be in $\mathcal{W}^s_{\mathrm{qm;loc}}$.

For the higher order terms, $n \geqslant 3$, we find by (3.58) in lemma 10 that the terms $H_s^{(n)}$ can be computed from the terms of the power series of $H^{(n-1)}$ according to

$$H_s^{(n)} = \sum_{k=0}^{[\frac{s}{n-2}]} \frac{1}{k!}[\mathrm{Mad}_{W_n}]^k H^{(n-1)}_{s-k(n-2)}. \tag{3.70}$$

The normalization procedure for the terms of order $n \geqslant 3$ of the symbol has very similar properties as the corresponding procedure in the classical case. In particular a transformation at a given order does not affect lower order terms. This is made more precise in the following lemmata that are the analogues of lemmas 3 and 4 for the classical case from section 2.2.

Lemma 11. $H_2^{(n)} = H_2^{(2)}$, $n \geqslant 3$.

Proof. The proof is completely analogous to the proof of lemma 3 and is therefore omitted. □

As in the classical case, lemma 11 motivates the adoption of the following notation for the operator

$$\mathcal{D} := \mathrm{ad}_{H_2^{(2)}} = \{H_2^{(2)}, \cdot\}. \tag{3.71}$$

Lemma 12. *For $n \geqslant 3$ and $0 \leqslant s < n$, $H_s^{(n)} = H_s^{(n-1)}$.*

Proof. The proof is completely analogous to the proof of lemma 4 and is therefore omitted. □

As in the classical case the nth order term in $H_n^{(n)}$ indicates how to choose W_n for $n \geqslant 3$.

Lemma 13 (Quantum homological equation). *For $s = n \geqslant 3$,*

$$H_n^{(n)} = H_n^{(n-1)} - \mathcal{D}W_n, \tag{3.72}$$

Proof. The proof is completely analogous to the proof of lemma 5 and is therefore omitted. □

The homological equation (3.72) is solved in exactly the same way as the homological equation in the classical normal form computation described in section 2.3.1. The only difference is that we now deal with a symbol that in contrast to the classical Hamilton function in general depends on $\hbar$. But due to the splitting $\mathcal{W}^s_{\mathrm{qm}} = \bigoplus_{k=0}^{[s/2]} \hbar^k \mathcal{W}^{s-2k}_{\mathrm{cl}}$, see (3.46), the

results on the solution of the classical homological equation can be transferred directly. In particular the notion of solvability introduced in definition 2 carries over verbatim.

We note that so far we have only shown how to transform the Hamilton operator to quantum normal form on the level of its symbol. We have not yet discussed the implications for the corresponding transformed operator. As we will see, similarly to the question of how to explicitly solve the homological equation, the nature of the transformed Hamilton operator depends on the type of equilibrium point of the principal symbol. In the next section, section 3.4, we will discuss this in detail for the case of a nonresonant saddle-centre-. . .-centre equilibrium point.

We summarize our findings in the following theorem.

Theorem 2. *Assume the principal symbol of* $\mathrm{Op}[H]$ *has an equilibrium point at* $z_0 \in \mathbb{R}^d \times \mathbb{R}^d$, *and that the homological equation is solvable in the sense of definition 2. Then for every* $N \in \mathbb{N}$ *there is a unitary transformation* $\hat{U}_N$ *such that*

$$\hat{U}_N^* \mathrm{Op}[H] \hat{U}_N = \mathrm{Op}[H_{\mathrm{QNF}}^{(N)}] + \mathrm{Op}[O_{N+1}], \tag{3.73}$$

where $\mathrm{Op}[H_{\mathrm{QNF}}^{(N)}]$ *is in quantum normal form (with respect to 0) and* O_{N+1} *is of order* $N + 1$.

Proof. As we have seen in this section the conjugations of a Hamilton operator by unitary transformations to transform it to quantum normal form can be carried out on the level of the symbols of the operators involved. This makes the proof of theorem 2 very similar to the proof of theorem 1 in the classical case. In fact, the proof of theorem 1 carries over verbatim when one replaces the Poisson bracket by the Moyal bracket. Then lemma 3 is replaced by lemma 11 and lemma 4 by lemma 12.

Using the scheme (3.65) with (3.66) then gives the unitary transformation $\hat{U}_N$ in (3.73) as

$$\hat{U}_N = \mathrm{e}^{-\frac{\mathrm{i}}{\hbar}\mathrm{Op}[W_1]} \mathrm{e}^{-\frac{\mathrm{i}}{\hbar}\mathrm{Op}[W_2]} \mathrm{e}^{-\frac{\mathrm{i}}{\hbar}\mathrm{Op}[W_3]} \cdots \mathrm{e}^{-\frac{\mathrm{i}}{\hbar}\mathrm{Op}[W_N]}. \tag{3.74}$$

The first two generators, W_1 and W_2, are chosen exactly as in the classical normal form algorithm, see (3.68) and the following paragraph, and by lemma 6 (exact Egorov) this induces the same transformation of the symbols as in the classical case. The other generators $W_n, n \geqslant 3$, are then chosen recursively as solutions of the homological equation, see lemma 13, where after each step we have to determine $H^{(n)}$ up to order N from (3.70). □

Similarly to the classical case the definition of the quantum normal form in definition 5 is of little value for practical purposes since we cannot expect the quantum normal computation to converge if we carry it out for $N \to \infty$ as required by definition 5. For applications it is more useful to consider the *truncated quantum normal form*.

Definition 6 (*N*th order quantum normal form). *Consider a Hamilton operator* $\mathrm{Op}[H]$ *whose principal symbol has an equilibrium point at* $z_0 \in \mathbb{R}^d \times \mathbb{R}^d$ *which, for* $N \in \mathbb{N}$, *we normalize according to theorem 2. Then we refer to the operator* $\mathrm{Op}[H_{\mathrm{QNF}}^{(N)}]$ *in equation (3.73) as the* N*th order quantum normal form (QNF) of* $\mathrm{Op}[H]$.

We have seen that the procedure to construct the quantum normal form is very similar to the procedure to compute the classical normal form. In particular the homological equations (2.46) and (3.72) which determine the choice of the successive transformations (2.27) and (3.65), respectively, look identical since the Poisson bracket reduces to the Moyal bracket if one of its arguments is a polynomial of order less than or equal to 2. However, it is important to point out that this does not mean that the Moyal bracket completely disappears from the procedure in the quantum case. In fact, while the normalization transformation at a given order does not modify lower order terms, it does modify all higher order terms, and the Moyal bracket

plays an important role in this, see (3.70). Consequently the terms in the Taylor expansions of $H^{(n)}$ and the generators W_n will in general depend on $\hbar$.

Since the Moyal bracket tends to the Poisson bracket in the limit $\hbar \to 0$ we expect that the symbol of the quantum normal form should tend to the classical normal form, too. This is indeed the case.

Proposition 1. *The principal symbol of the Nth order quantum normal* $\mathrm{Op}[H^{(N)}_{\mathrm{QNF}}]$ *is the classical normal form of order N, i.e.*

$$H^{(N)}_{\mathrm{QNF}}(\hbar, q, p) = H^{(N)}_{\mathrm{CNF}}(q, p) + O(\hbar). \tag{3.75}$$

Proof. This follows from an inspection of the construction of the classical and quantum normal forms. The first two steps are identical by lemma 6 (exact Egorov). The homological equation determining the choices of the W_n is also identical. What is different however is the transformation of the higher order terms, $k > n$. Here we have equation (2.36) in the classical case and equation (3.70) in the quantum case, and these equations differ by the use of the adjoint versus the Moyal adjoint. But since $\mathrm{Mad}_W A = \mathrm{ad}_W A + O(\hbar)$ and therefore

$$\mathrm{Mad}^k_W A = \mathrm{ad}^k_W A + O(\hbar) \tag{3.76}$$

the differences in the higher order terms between the classical and the quantum transformation schemes are always of order $\hbar$. This implies that the differences between the symbol of the quantum normal form and the classical normal form are of order $\hbar$. □

3.4. Nature and computation of the quantum normal form in a neighbourhood of an equilibrium point of the principal symbol of saddle-centre-. . .-centre type

We now describe how the quantum normal form of a Hamilton operator can be computed in the case where the principal symbol has an equilibrium point of saddle-centre-. . .-centre type, i.e. the matrix associated with the linearization of the Hamiltonian vector field generated by the principal symbol has two real eigenvalues, $\pm\lambda$, and $d-1$ complex conjugate pairs of imaginary eigenvalues $\pm \mathrm{i}\,\omega_k$, $k = 2, \ldots d$. We will assume that the ω_k, $k = 2, \ldots d$, are nonresonant in the sense that they are linearly independent over the integers, i.e. $k_2\omega_2 + \cdots + k_d\omega_d \neq 0$ for all $(k_2, \ldots k_d) \in \mathbb{Z}^{d-1} - \{0\}$.

As mentioned in the previous section it follows from lemma 6 (exact Egorov) that we can use the same affine linear symplectic transformations that we used in the classical case in section 2 to shift the equilibrium point to the origin of the coordinate system and to simplify the second order term of the symbol. We thus have

$$H^{(2)} = E_0 + H^{(2)}_2 + \sum_{s=3}^{\infty} H^{(2)}_s, \tag{3.77}$$

where

$$H^{(2)}_2(\hbar, q, p) = \lambda q_1 p_1 + \sum_{k=2}^{d} \frac{\omega_k}{2}(p_k^2 + q_k^2) + c\hbar, \tag{3.78}$$

where c is some real constant.

We note that in terms of the coordinates (Q, P) we defined in section 2.3 $H^{(2)}_2$ is given by

$$H^{(2)}_2(\hbar, q, p) = \frac{\lambda}{2}(P_1^2 - Q_1^2) + \sum_{k=2}^{d} \frac{\omega_k}{2}(P_k^2 + Q_k^2) + c\hbar, \tag{3.79}$$

which is the analogue of equation (2.63) in the classical case.

3.4.1. Solution of the homological equation. We will solve the homological equation in the spaces $\mathcal{W}^n_{\mathrm{qm}}$. The solution will then be localized by multiplication with a cutoff function afterwards to obtain elements in $\mathcal{W}^n_{\mathrm{qm;loc}}$. This will ensure that the quantizations of these symbols are bounded and generate unitary operators.

In order to solve the homological equation in lemma 13 we perform the linear symplectic complex change of coordinates $(q, p) \mapsto (x, \xi)$ given by $x_1 = q_1, \xi_1 = p_1$ and

$$x_k := \frac{1}{\sqrt{2}}(q_k - \mathrm{i}p_k), \qquad \xi_k := \frac{1}{\sqrt{2}}(p_k - \mathrm{i}q_k), \qquad k = 2, \ldots, d. \tag{3.80}$$

In terms of these coordinates the operator $\mathcal{D}$ defined in (3.71) assumes the simple form

$$\mathcal{D} = \lambda(\xi_1\partial_{\xi_1} - x_1\partial_{x_1}) + \sum_{k=2}^{d} \mathrm{i}\omega_k(\xi_k\partial_{\xi_k} - x_k\partial_{x_k}). \tag{3.81}$$

In terms of these coordinates the spaces $\mathcal{W}^n_{\mathrm{qm}}$ defined in (3.45) are given by

$$\mathcal{W}^n_{\mathrm{qm}} = \mathrm{span}\left\{\hbar^j x^\alpha \xi^\beta := \hbar^j \prod_{k=1}^{d} x_k^{\alpha_k}\xi_k^{\beta_k} \;:\; |\alpha| + |\beta| + 2j = n\right\}, \tag{3.82}$$

and the operator $\mathcal{D}$ acts on an element $\hbar^j x^\alpha \xi^\beta \in \mathcal{W}^n_{\mathrm{qm}}$ according to

$$\mathcal{D}\hbar^j \prod_{k=1}^{d} x_k^{\alpha_k}\xi_k^{\beta_k} = \left(\lambda(\beta_1 - \alpha_1) + \sum_{k=2}^{d} \mathrm{i}\omega_k(\beta_k - \alpha_k)\right)\hbar^j \prod_{k=1}^{d} x_k^{\alpha_k}\xi_k^{\beta_k}. \tag{3.83}$$

This means that the map $\mathcal{D}$ can again be diagonalized and similarly to the classical case we have that $\mathcal{W}^n_{\mathrm{qm}}$ is given by the direct sum of the kernel of $\mathcal{D}$ acting on $\mathcal{W}^n_{\mathrm{qm}}$, $\mathrm{Ker}\mathcal{D}|_{\mathcal{W}^n_{\mathrm{qm}}}$ and the image of $\mathcal{D}$ acting on $\mathcal{W}^n_{\mathrm{qm}}$, $\mathrm{Im}\mathcal{D}|_{\mathcal{W}^n_{\mathrm{qm}}}$, i.e.

$$\mathcal{W}^n_{\mathrm{qm}} = \mathrm{Ker}\mathcal{D}|_{\mathcal{W}^n_{\mathrm{qm}}} \oplus \mathrm{Im}\mathcal{D}|_{\mathcal{W}^n_{\mathrm{qm}}}. \tag{3.84}$$

Now we can express $H_n^{(n-1)}$ as

$$H_n^{(n-1)} = H_{n;\mathrm{Ker}}^{(n-1)} + H_{n;\mathrm{Im}}^{(n-1)}, \tag{3.85}$$

where $H_{n;\mathrm{Ker}}^{(n-1)} \in \mathrm{Ker}\mathcal{D}|_{\mathcal{W}^n_{\mathrm{qm}}}$ and $H_{n;\mathrm{Im}}^{(n-1)} \in \mathrm{Im}\mathcal{D}|_{\mathcal{W}^n_{\mathrm{qm}}}$. We can therefore choose W_n such that

$$\mathcal{D}W_n = H_{n;\mathrm{Im}}^{(n-1)}, \tag{3.86}$$

and therefore

$$H_n^{(n)} = H_{n;\mathrm{Ker}}^{(n-1)}. \tag{3.87}$$

Similarly to the classical case the choice of W_n is not unique since one can always add terms from the kernel of $\mathcal{D}|_{\mathcal{W}^n_{\mathrm{qm}}}$. However, we will require $W_n \in \mathrm{Im}\mathcal{D}|_{\mathcal{W}^n_{\mathrm{qm}}}$, i.e. we will invert $\mathcal{D}$ on its image $\mathrm{Im}\mathcal{D}|_{\mathcal{W}^n_{\mathrm{qm}}}$.

Using our assumption that the frequencies $\omega_2, \ldots, \omega_d$ are nonresonant, i.e. linearly independent over $\mathbb{Z}$, we see from (3.83) that a monomial $\hbar^j x^\alpha \xi^\beta$ is mapped to zero if and only if $\alpha_k = \beta_k$, $k = 1, \ldots, d$. In particular $\mathrm{Ker}\mathcal{D}|_{\mathcal{W}^s_{\mathrm{qm}}} = \{0\}$ if s is odd. This implies that unitary transformations can be constructed such that all odd order terms in the symbol of the conjugated Hamilton operator are eliminated. Moreover, for s even, the terms that *cannot* be eliminated are those which are sums of monomials for which $x_k^{(s)}$ and $\xi_k^{(s)}$ have equal integer exponents for all $k = 1, \ldots, d$.

Concretely, we can compute W_n from (3.86) as follows. We assume that $H_{n;\mathrm{Im}}^{(n-1)}$ is the linear combination of L monomials of order n,

$$H_{n;\mathrm{Im}}^{(n-1)} = \sum_{l=1}^{L} h_l \hbar^{j_l} \prod_{k=1}^{d} x_k^{\alpha_{k;l}}\xi_k^{\beta_{k;l}}, \tag{3.88}$$

with $2j_l + \sum_{k=1}^{d} \alpha_{k;l} + \beta_{k;l} = n$ for all $l = 1, \ldots, L$, and for all $l = 1, \ldots, L$, there is at least one $k = 1, \ldots, d$ for which $\alpha_{k;l} \neq \beta_{k;l}$ (i.e. the vectors $(\alpha_{1;l}, \ldots, \alpha_{d;l})$ and $(\beta_{1;l}, \ldots, \beta_{d;l})$ are different for all $l = 1, \ldots, L$). Upon inspecting (3.83), and using (3.86), we see that a suitable generating function is given by

$$W_n = \sum_{l=1}^{L} \frac{h_l}{\lambda(\beta_{1;l} - \alpha_{1;l}) + \sum_{k=2}^{d} \mathrm{i}\omega_k(\beta_{k;l} - \alpha_{k;l})} \hbar^{j_l} \prod_{k=1}^{d} x_{k;l}^{\alpha_{k;l}} \xi_{k;l}^{\beta_{k;l}}. \tag{3.89}$$

As mentioned above this solution of the homological equation is unique if we require W_n to be in $\mathrm{Im}\mathcal{D}|_{\mathcal{W}_{\mathrm{qm}}^n}$.

3.4.2. Structure of the Hamilton operator in Nth order quantum normal form. In the previous section we have seen how to obtain the quantum normal form to order N in the case where the equilibrium point is of saddle-centre-...-centre type. So far these computations have been carried out on the level of the symbols of the Hamilton operators. We now discuss the implications for the structure of the corresponding Hamilton operator in quantum normal form itself.

In the classical case in sections 2.3.1 and 2.3.2 we have shown that in each monomial of the Hamilton function in Nth order classical normal form the coordinate pairs (x_k, ξ_k) (or equivalently (q_k, p_k)), $k = 1, \ldots, d$, occur with equal integer exponents and that this implies that the Hamilton function in Nth order classical normal form is effectively a function of d integrals, see equation (2.83).

In the previous section we saw that in the monomials that form the symbol of a Hamilton operator in Nth order quantum normal form the coordinate pairs (x_k, ξ_k) (or equivalently (q_k, p_k)), $k = 1, \ldots, d$, again have equal integer exponents. Hence, the symbol is effectively a function of $I = p_1 q_1$, $J_k = \frac{1}{2}(p_k^2 + q_k^2)$, $k = 2, \ldots, d$. We will now show that analogously to (2.83) the Hamilton operator in Nth order quantum normal form is a function of the d operators

$$\hat{I} := \mathrm{Op}[I], \qquad \hat{J}_k := \mathrm{Op}[J_k], \qquad k = 2, \ldots, d, \tag{3.90}$$

see equations (3.15) and (3.16). To this end recall that the Hamilton operator in quantum normal form is localized near the equilibrium point. We will say that two operators $\mathrm{Op}[A]$ and $\mathrm{Op}[B]$ are equal near a point $z = (q, p)$ in phase space if their symbols A and B are equal in a neighbourhood of z. To indicate this we write

$$\mathrm{Op}[A] \equiv_z \mathrm{Op}[B]. \tag{3.91}$$

Theorem 3. *Let $\mathrm{Op}[H_{\mathrm{QNF}}^{(N)}]$ be a Hamilton operator in Nth order quantum normal form with respect to an equilibrium point of its principal symbol of saddle-centre-...-centre type, and assume furthermore that the frequencies $\omega_2, \ldots, \omega_d$ associated with the $d-1$ centres are linearly independent over $\mathbb{Z}$. Then there exists a polynomial $K_{\mathrm{QNF}}^{(N)} : \mathbb{R}^d \to \mathbb{R}$ of order $[N/2]$ such that*

$$\mathrm{Op}[H_{\mathrm{QNF}}] \equiv_0 K_{\mathrm{QNF}}^{(N)}(\hat{I}, \hat{J}_2, \ldots, \hat{J}_d). \tag{3.92}$$

In this theorem $[N/2]$ denotes the integer part of $N/2$. The proof of this theorem is based on the following

Lemma 14. *Let $I = pq$, $J = \frac{1}{2}(p^2 + q^2)$, and $\hat{I} = \mathrm{Op}[I]$, $\hat{J} = \mathrm{Op}[J]$, respectively, then there are integers $\Gamma_{n,k}$ such that for any $n \in \mathbb{N}$,*

$$\mathrm{Op}[I^n] = \sum_{k=0}^{[n/2]} (-1)^k \Gamma_{n,k} \left(\frac{\hbar}{2}\right)^{2k} \hat{I}^{n-2k} \tag{3.93}$$

and

$$\mathrm{Op}[J^n] = \sum_{k=0}^{[n/2]} \Gamma_{n,k} \left(\frac{\hbar}{2}\right)^{2k} \hat{J}^{n-2k}. \tag{3.94}$$

Here $[n/2]$ *denotes the integer part of* $n/2$*, and the coefficients* $\Gamma_{n,k}$ *are determined by the recursion relation*

$$\Gamma_{n+1,k} = \Gamma_{n,k} + n^2 \Gamma_{n-1,k-1} \qquad \text{for } k \geqslant 1 \tag{3.95}$$

and $\Gamma_{n,0} = 1$.

Proof. We start by considering the case of $I = pq$. The strategy will be to use the Weyl calculus to determine the symbol of $\mathrm{Op}[I^n]$ as a function of I, and then to invert this relation. The symbol of $\mathrm{Op}[I^n]$ is $I^{*n} := I * I * \cdots * I$, the n-fold star product of I. Using $I = pq$ and the definition of the star product in (3.17) we find the recursion relation

$$I * I^n = I^{n+1} + \left(\frac{\hbar}{2}\right)^2 n^2 I^{n-1}. \tag{3.96}$$

This can be rewritten as

$$\mathrm{Op}[I^{n+1}] = \hat{I}\mathrm{Op}[I^n] - \left(\frac{\hbar}{2}\right)^2 n^2 \mathrm{Op}[I^{n-1}], \tag{3.97}$$

which can be used to determine the $\hat{I}^n := \mathrm{Op}[I^n]$ recursively. If we insert the ansatz (3.93) into the recursion relation (3.97) we find the recursion for the coefficients (3.95).

In order to show the validity of equation (3.94) we apply the same strategy and find instead of (3.97)

$$\mathrm{Op}[J^{n+1}] = \hat{J}\mathrm{Op}[J^n] + \left(\frac{\hbar}{2}\right)^2 n^2 \mathrm{Op}[J^{n-1}], \tag{3.98}$$

and inserting now (3.94) as an ansatz into this equation leads again to the relation (3.95) for the coefficients. □

We note that the closed formulae for $\hat{I}^n$ and $\hat{J}_k^n$ given in [Cre90] are not correct. We now prove theorem 3.

Proof of theorem 3. It follows from our construction that the symbol of a Hamilton operator in quantum normal form is near $(q, p) = (0, 0)$ a polynomial in I, J_k, $k = 2, \ldots, d$, that can be written in the following form:

$$H_{\mathrm{QNF}}^{(N)} = \sum_{l=1}^{L} h_l \hbar^{j_l} I^{\alpha_{1;l}} J_2^{\alpha_{2;l}} \cdots J_d^{\alpha_{d;l}}, \tag{3.99}$$

where $2j_l + 2\sum_{k=1}^{d} \alpha_{k;l} \leqslant N$, or equivalently $j_l + \sum_{k=1}^{d} \alpha_{k;l} \leqslant N/2$, for all $l = 1, \ldots, L$. For $\mathrm{Op}[H_{\mathrm{QNF}}^{(N)}]$ we thus find

$$\mathrm{Op}[H_{\mathrm{QNF}}^{(N)}] = \sum_{l=1}^{L} h_l \hbar^{j_l} \mathrm{Op}[I^{\alpha_{1;l}}]\mathrm{Op}[J_2^{\alpha_{2;l}}] \cdots \mathrm{Op}[J_d^{\alpha_{d;l}}]. \tag{3.100}$$

If we insert the expansions from lemma 14 into (3.100) we obtain

$$\mathrm{Op}[H_{\mathrm{QNF}}^{(N)}] = \sum_{l=1}^{L} h_l \hbar^{j_l} \sum_{k_1=0}^{[\alpha_{1;l}/2]} \sum_{k_2=0}^{[\alpha_{2;l}/2]} \cdots \sum_{k_d=0}^{[\alpha_{d;l}/2]} (-1)^{\alpha_{1;l}} \Gamma_{\alpha_{1;l},k_1} \cdots \Gamma_{\alpha_{d;l},k_d}$$
$$\times \left(\frac{\hbar}{2}\right)^{2(k_1+\ldots+k_d)} \hat{I}^{\alpha_{1;l}-2k_1} \hat{J}_2^{\alpha_{2;l}-2k_2} \cdots \hat{J}_d^{\alpha_{d;l}-2k_d}. \tag{3.101}$$

Since $j_l + \sum_{k=1}^{d} \alpha_{k;l} \leqslant N/2$ for all $l = 1, \ldots, L$ it follows that the RHS of (3.101) is a polynomial of order $[N/2]$ in $\hat{I}, \hat{J}_2, \ldots, \hat{J}_d$. This polynomial defines the function $K_{\mathrm{QNF}}^{(N)}$.

We note that for $\hbar \to 0$ the polynomial $K_{\mathrm{QNF}}^{(N)}$ tends to the polynomial $K_{\mathrm{CNF}}^{(N)}$ defined in (2.83) that gives the Nth order classical normal form as a function of the integrals I and J_k, $k = 2, \ldots, d$. Though this is obvious from the proof of theorem 3 it is worth mentioning that in general the coefficients in the polynomial $K_{\mathrm{QNF}}^{(N)}$ differ from the polynomial that is obtained from writing $H_{\mathrm{QNF}}^{(N)}$ as a function of I and J_k, $k = 2, \ldots, d$. We will see this in the example presented in section 3.5.

Theorem 3 is a crucial result. It tells us that the truncated quantum normal form simply is a polynomial in the operators $\hat{I}$ and $\hat{J}_k$, $k = 2, \ldots, d$, whose spectral properties are well known. As we will see in more detail in sections 5 and 6 this will allow us to compute quantum reaction rates and quantum resonances with high efficiency.

3.5. Quantum normal form for one-dimensional potential barriers

In the following we present the explicit computation of the quantum normal form for Hamilton operators of one-dimensional systems of type 'kinetic plus potential' where the potential has a maximum. It is important to point out that the applicability of the normal form algorithms—both classical and quantum—is not restricted to systems of the form 'kinetic plus potential' (i.e. for example, Coriolis terms in the Hamiltonian function or Hamilton operator due to a magnetic field or a rotating coordinate frame are allowed). Since even for this simple one-dimensional problem the expressions for the symbols and operators involved soon become very lengthy we will carry out the quantum normal form algorithm only to order 4. We note that we implemented the normalization algorithm in the programming language C++. In our object-oriented implementation the number of dimensions and the order of truncation of the normal form can be chosen arbitrarily. This C++ program will be used to compute the high order quantum normal forms for the more complicated examples given in section 7.

For now let us consider a Hamilton operator of the form

$$\hat{H} = -\frac{\hbar^2}{2m}\frac{\mathrm{d}^2}{\mathrm{d}q^2} + V(q), \tag{3.102}$$

where the potential V is assumed to have a (nondegenerate) maximum at $q = q_0$. The Weyl symbol of $\hat{H}$ is given by

$$H(\hbar, q, p) = \frac{1}{2m}p^2 + V(q), \tag{3.103}$$

i.e. $\mathrm{Op}[H] = \hat{H}$. Since the symbol H does not depend on $\hbar$, the symbol agrees with the principal symbol. Hamilton's equations for the Hamiltonian function given by H then have an equilibrum point at $(q, p) = (q_0, 0)$ which is of saddle stability type, i.e. the matrix associated with the linearization of the Hamiltonian vector field about the equilibrium point has a pair of real eigenvalues $\pm\lambda$. Here λ is given by

$$\lambda = \sqrt{-\frac{1}{m}V''(q_0)}. \tag{3.104}$$

The first two steps in the sequence of transformations (3.65) serve to shift the equilibrium point of the (principal) symbol to the origin and to simplify the quadratic part of the symbol. As mentioned in section 3.3, it follows from lemma 6 (exact Egorov) that the transformations of the symbol H to achieve these goals agree with the corresponding classical transformations.

Classically, we shift the equilibrium point to the origin of the coordinate system by transforming the coordinates according to

$$(q, p) \mapsto (q - q_0, p). \tag{3.105}$$

For completeness, we note that this transformation can be obtained from the time one map of the flow generated by the first order polynomial

$$W_1(q, p) = -q_0 p, \tag{3.106}$$

i.e. $\Phi^1_{W_1}(q, p) = (q - q_0, p)$. The Weyl quantization of W_1 is given by

$$\mathrm{Op}[W_1] = q_0 \,\mathrm{i}\hbar \frac{\mathrm{d}}{\mathrm{d}q}. \tag{3.107}$$

It follows from lemma 6 that

$$\mathrm{e}^{\frac{\mathrm{i}}{\hbar}\mathrm{Op}[W_1]}\mathrm{Op}[H]\mathrm{e}^{-\frac{\mathrm{i}}{\hbar}\mathrm{Op}[W_1]} \tag{3.108}$$

has the symbol

$$H^{(1)}(\hbar, q, p) = H \circ \Phi^{-1}_{W_1}(\hbar, q, p) = H(\hbar, q + q_0, p) = \frac{1}{2m} p^2 + V(q + q_0). \tag{3.109}$$

We now want to find a unitary transformation such that the quadratic part of the symbol $H^{(2)}$ of the transformed Hamilton operator assumes the form

$$H^{(2)}_2(\hbar, q, p) = \lambda\, p\, q. \tag{3.110}$$

Classically, this is achieved by the transformation

$$(q, p) \mapsto \left(\sqrt{m\lambda}\, q, \frac{1}{\sqrt{m\lambda}} p\right) \tag{3.111}$$

followed by the 45° rotation

$$(q, p) \mapsto \left(\frac{1}{\sqrt{2}}(p + q), \frac{1}{\sqrt{2}}(p - q)\right). \tag{3.112}$$

Both these transformations are symplectic.

Again for completeness, we note that the transformation (3.111) can be obtained from the time one map of the flow generated by

$$W_2(q, p) = \ln(\sqrt{m\lambda})\, p\, q, \tag{3.113}$$

i.e.

$$\Phi^1_{W_2}(q, p) = \left(\sqrt{m\lambda}\, q, \frac{1}{\sqrt{m\lambda}} p\right). \tag{3.114}$$

The Weyl quantization of W_2 is given by

$$\mathrm{Op}[W_2] = \ln(\sqrt{m\lambda})\, \frac{\hbar}{\mathrm{i}} \left(q \frac{\mathrm{d}}{\mathrm{d}q} + \frac{1}{2}\right), \tag{3.115}$$

see equation (3.16). The transformation (3.112) can be obtained from the time one map of the flow generated by

$$W'_2(q, p) = \frac{\pi}{4} \frac{1}{2}(q^2 + p^2), \tag{3.116}$$

which gives

$$\Phi^1_{W'_2}(q, p) = \left(\frac{1}{\sqrt{2}}(p + q), \frac{1}{\sqrt{2}}(p - q)\right), \tag{3.117}$$

see the example after lemma 6 (exact Egorov), (3.33). The Weyl quantization of W_2' is given by

$$\mathrm{Op}[W_2'] = \frac{\pi}{2}\Big(-\frac{\hbar^2}{2}\frac{\mathrm{d}^2}{\mathrm{d}q^2} + \frac{1}{2}q^2\Big), \tag{3.118}$$

see equation (3.15).

Using lemma 6 it follows that the symbol of

$$\mathrm{Op}[H^{(2)}] = \mathrm{e}^{\frac{\mathrm{i}}{\hbar}\mathrm{Op}[W_2']}\mathrm{e}^{\frac{\mathrm{i}}{\hbar}\mathrm{Op}[W_2]}\mathrm{Op}[H^{(1)}]\mathrm{e}^{-\frac{\mathrm{i}}{\hbar}\mathrm{Op}[W_2]}\mathrm{e}^{-\frac{\mathrm{i}}{\hbar}\mathrm{Op}[W_2']} \tag{3.119}$$

is given by

$$\begin{aligned} H^{(2)}(\hbar, q, p) &= H^{(1)} \circ \Phi_{W_2'}^{-1} \circ \Phi_{W_2}^{-1}(\hbar, q, p) \\ &= V_0 + \lambda qp + \sum_{k=3}^{\infty}\sum_{n=0}^{k} V_{n;k-n}\, p^n q^{k-n} =: \sum_{k=0}^{\infty} H_k^{(2)}(\hbar, q, p), \end{aligned} \tag{3.120}$$

where

$$H_0^{(2)}(\hbar, q, p) = V_0 := V(q_0), \qquad H_1^{(2)}(\hbar, q, p) = 0, \qquad H_2^{(2)}(\hbar, q, p) = \lambda pq. \tag{3.121}$$

The coefficients of the monomials in (3.120) of cubic or higher degree are

$$V_{n;\,j} = (-1)^n \frac{1}{n!\,j!}\frac{1}{(2m\lambda)^{(n+j)/2}}\frac{\mathrm{d}^{n+j}V(q_0)}{\mathrm{d}q^{n+j}}, \qquad n + j \geqslant 3. \tag{3.122}$$

So far, i.e. up to order 2, the transformations involved in the quantum normal form algorithm agree with their counterparts in the classical normal form algorithm. We now want to study the next steps in the sequence (3.65) which give the quantum normal form of order three and four. To make these transformations well defined we from now on assume that we use the scheme outlined in section 3.1.3 to localize the Hamilton operator $H^{(2)}$ and the operators which will generate the required unitary transformations about the origin. The monomials in the third and fourth order polynomials $H_3^{(2)}$ and $H_4^{(2)}$ have coefficients

$$V_{3;0} = -V_{0;3} = -\frac{1}{3}V_{2;1} = \frac{1}{3}V_{1;2} = -\frac{1}{6}\frac{1}{(2m\lambda)^{3/2}}V''(q_0), \tag{3.123}$$

$$V_{4;0} = V_{0;4} = -\frac{1}{4}V_{3;1} = -\frac{1}{4}V_{1;3} = \frac{1}{6}V_{2;2} = \frac{1}{24}\frac{1}{(2m\lambda)^2}V''(q_0), \tag{3.124}$$

respectively, where the primes denote derivatives.

It follows from equation (3.70) that for $W_3 \in \mathcal{W}^3_{\mathrm{qm;loc}}$, the symbol of the transformed operator

$$\mathrm{Op}[H^{(3)}] = \mathrm{e}^{\frac{\mathrm{i}}{\hbar}\mathrm{Op}[W_3]}\mathrm{Op}[H^{(2)}]\mathrm{e}^{-\frac{\mathrm{i}}{\hbar}\mathrm{Op}[W_3]} \tag{3.125}$$

is given by

$$H^{(3)} = H_0^{(3)} + H_1^{(3)} + H_2^{(3)} + H_3^{(3)} + H_4^{(3)} + \cdots, \tag{3.126}$$

where following lemma 12, the terms $H_k^{(3)}$ and $H_k^{(2)}$ agree for $k \leqslant 2$, and

$$H_3^{(3)} = H_3^{(2)} + \mathrm{Mad}_{W_3} H_2^{(2)} = H_3^{(2)} + \{W_3, H_2^{(2)}\}, \tag{3.127}$$

$$H_4^{(3)} = H_4^{(2)} + \mathrm{Mad}_{W_3} H_3^{(2)} + \frac{1}{2}[\mathrm{Mad}_{W_3}]^2 H_2^{(2)}. \tag{3.128}$$

Equation (3.127) is the homological equation. Introducing the operator

$$\mathcal{D} = \{H_2^{(2)}, \cdot\} \tag{3.129}$$

the homological equation takes the form

$$H_3^{(3)} = H_3^{(2)} - \mathcal{D}W_3, \tag{3.130}$$

which agrees with the form of the homological equation in lemma 13. Following section 3.4 we need to solve the homological equation, i.e. choose W_3, such that $\mathcal{D}H_3^{(3)} = 0$. Since $\mathcal{W}_{\rm qm}^3 = {\rm Im}\mathcal{D}|_{\mathcal{W}_{\rm qm}^3}$, or equivalently ${\rm Ker}\mathcal{D}|_{\mathcal{W}_{\rm qm}^3} = \{0\}$, we have to choose W_3 such that $H_3^{(3)} = 0$. From (3.127) we see that this is achieved by setting

$$W_3(\hbar, q, p) = -\sum_{n=0}^{3} \frac{1}{\lambda(2n-3)} V_{n;3-n} p^n q^{3-n}, \tag{3.131}$$

$$= -\frac{V_{3;0}}{3\lambda}(p^3 - 9p^2q - 9pq^2 + q^3). \tag{3.132}$$

Inserting this W_3 into (3.128) gives

$$H_4^{(3)}(\hbar, q, p) = V_{4;0}(p^4 - 4p^3q + 6p^2q^2 - 4pq^3 + q^4) - \frac{V_{3;0}^2}{\lambda}(3p^4 + 12p^3q - 30p^2q^2 + 12pq^3 + 3q^4 - 4\hbar^2). \tag{3.133}$$

Note the occurrence of the term involving $\hbar^2$. It is a consequence of the second term on the right-hand side of (3.128) which involves the Moyal bracket of two polynomials which are of degree higher than two for which the Moyal bracket no longer coincides with the Poisson bracket.

Using equation (3.70) again we see that for $W_4 \in \mathcal{W}_{\rm qm;loc}^4$, the symbol of the transformed operator

$${\rm Op}[H^{(4)}] = {\rm e}^{\frac{\rm i}{\hbar}{\rm Op}[W_4]}{\rm Op}[H^{(3)}]{\rm e}^{-\frac{\rm i}{\hbar}{\rm Op}[W_4]} \tag{3.134}$$

is given by

$$H^{(4)} = H_0^{(4)} + H_1^{(4)} + H_2^{(4)} + H_3^{(4)} + H_4^{(4)} + \cdots, \tag{3.135}$$

where it again follows from lemma 12 that $H_k^{(4)} = H_k^{(3)}$ for $k \leqslant 3$. For $k = 4$ we obtain the homological equation

$$H_4^{(4)} = H_4^{(3)} + {\rm Mad}_{W_4} H_2^{(3)} = H_4^{(3)} - \mathcal{D}W_4. \tag{3.136}$$

We need to choose W_4 such that $\mathcal{D}H_4^{(4)} = 0$. We therefore decompose $H_4^{(3)}$ according to

$$H_4^{(3)} = H_{4;{\rm Ker}}^{(3)} + H_{4;{\rm Im}}^{(3)}, \tag{3.137}$$

where $H_{4;{\rm Ker}}^{(3)} \in {\rm Ker}\mathcal{D}|_{\mathcal{W}_{\rm qm}^4}$ and $H_{4;{\rm Im}}^{(3)} \in {\rm Im}\mathcal{D}|_{\mathcal{W}_{\rm qm}^4}$. It follows from section 3.4 that $H_{4;{\rm Ker}}^{(3)}$ consists of all monomials of $H_4^{(3)}$ in which p and q have the same integer exponent and $H_{4;{\rm Im}}^{(3)}$ consists of all monomials of $H_4^{(3)}$ in which p and q have different integer exponents. We thus have

$$H_{4;{\rm Ker}}^{(3)} = 6V_{4;0}p^2q^2 + \frac{V_{3;0}^2}{\lambda}(30p^2q^2 + 4\hbar^2) \tag{3.138}$$

and

$$H_{4;{\rm Im}}^{(3)} = V_{4;0}(p^4 - 4p^3q - 4pq^3 + q^4) - \frac{V_{3;0}^2}{\lambda}(3p^4 + 12p^3q + 12pq^3 + 3q^4). \tag{3.139}$$

To achieve $\mathcal{D}H_4^{(4)} = 0$ we choose

$$W_4(\hbar, q, p) = \frac{V_{3;0}}{4\lambda^2}(3p^4 + 24p^3q - 24pq^3 - 3q^4) - \frac{V_{4;0}}{4\lambda}(p^4 - 8p^3q + 8pq^3 - q^4). \tag{3.140}$$

We thus get

$$H^{(4)}(\hbar, q, p) = V_0 + \lambda pq + 6\, V_{4;0} p^2 q^2 + \frac{V_{3;0}^2}{\lambda}(30 p^2 q^2 + 4\hbar^2) + O_5, \tag{3.141}$$

where the remainder O_5 is defined according to definition 4. Neglecting O_5 gives the symbol of the 4th order quantum normal form. In order to get the corresponding operator we have to replace the factors $I = pq$ by the operator $\hat{I} = \mathrm{Op}[I]$. To this end we use the recurrence (3.93) in lemma 14 to get

$$\mathrm{Op}[I^2] = \hat{I}^2 - \frac{\hbar^2}{4}. \tag{3.142}$$

The 4th order quantum normal form of the operator $\hat{H}$ in (3.102) is thus given by

$$K_{\mathrm{QNF}}^{(4)}(\hat{I}) = V_0 + \lambda \hat{I} + \left(30\frac{V_{3;0}^2}{\lambda} + 6V_{4;0}\right)\hat{I}^2 - \frac{\hbar^2}{2}\left(7\frac{V_{3;0}^2}{\lambda} + 3V_{4;0}\right) \tag{3.143}$$

$$= V_0 + \lambda \hat{I} + \frac{1}{16m^2\lambda^2}\left(\frac{5}{3m\lambda^2}\big(V''(q_0)\big)^2 + V''(q_0)\right)\hat{I}^2 - \frac{1}{64m^2\lambda^2}\left(\frac{7}{9m\lambda^2}\big(V''(q_0)\big)^2 + V''(q_0)\right)\hbar^2. \tag{3.144}$$

This gives the first correction term to the well known quadratic approximation which consists of approximating the potential barrier by an inverted parabola. The corresponding classical normal form is given by

$$K_{\mathrm{CNF}}^{(4)}(I) = V_0 + \lambda I + \frac{1}{16m^2\lambda^2}\left(\frac{5}{3m\lambda^2}\big(V''(q_0)\big)^2 + V''(q_0)\right) I^2. \tag{3.145}$$

We see that the polynomial $K_{\mathrm{QNF}}^{(4)}$ (in $\hat{I}$) has two more terms than the polynomial $K_{\mathrm{CNF}}^{(4)}$ (in I). These are the terms involving $\hbar$, and their occurrence is due to the Moyal bracket (see the comment following equation (3.133) which enters the quantum normal form computation on the level of the symbols and the Weyl quantization of powers of the classical integral $I = p\,q$ (see (3.142)) which is required to obtain the Hamilton operator from its symbol.

4. Classical reaction dynamics and reaction probabilities

In this section we give an overview of the theory of reaction dynamics that is firmly rooted in the dynamical arena of phase space and has recently been developed in [WWJU01, UJP+01, WBW04b, WW04, WBW05a, WBW05b, WBW05c]. This section is organized as follows. In section 4.1 we describe the geometric structures in *phase space* near an equilibrium point of saddle-centre-. . .-centre stability type (see section 2.3) that control the classical dynamics of reactions. These phase space structures are 'realized' through the classical normal form, and details of this are given in section 4.2 where we also provide a detailed discussion of how these phase space structures constrain trajectories of Hamilton's equations. In section 4.3 we describe how the integrability of the truncated normal form gives rise to the foliation of the phase space near the saddle by Lagrangian manifolds. This will be of central importance for the quantum mechanics of reactions as we will see in section 5. In section 4.4 we will show how the normal form can be used to compute the directional flux through the dividing surface. As we will see the normal form obtained from truncating the normal form algorithm at a suitable order gives a very accurate description of the local dynamics. Means to verify the accuracy are discussed in section 4.5. While the normal form technique is 'locally applicable'

in a neighbourhood of the reaction region, in section 4.6 we discuss how the local structures mentioned above can be globalized in a way that their influence on reactions outside this 'local' region can be determined. Finally, in section 4.7 we comment on the flux–flux autocorrelation function formalism to compute classical reaction probabilities that is frequently utilized in the chemistry literature, its relation to our phase space theory and the computational benefits of our approach over the flux–flux autocorrelation function formalism.

4.1. Phase space structures that control classical reaction dynamics: an overview of the geometry

Our starting point is an equilibrium point of Hamilton's equations of saddle-centre-...-centre stability type. Near (and we will discuss what we mean by 'near' in section 4.5) such equilibrium points there exist lower dimensional manifolds that completely dictate the dynamics of the evolution of trajectories from reactants to products (or vice versa). The normal form theory developed in section 2 provides a transformation to a new set of coordinates, referred to as the *normal form coordinates*, in which these manifolds can be identified and explicitly computed, and then mapped back into the original, 'physical' coordinates via the normal form transformation. In this section we give a brief description of these phase space structures, and in section 4.2 we describe how they constrain trajectories.

We let E_0 denote the energy of the saddle, and we consider a fixed energy $E > E_0$ (and 'sufficiently close' to E_0). We also restrict our attention to a certain neighbourhood U, local to the equilibrium point. We defer a discussion of exactly how this region is chosen to section 4.5; suffice it to say for now that the region is chosen so that an integrable nonlinear approximation to the dynamics yields structures to within a given desired accuracy.

Near this equilibrium point the $(2d-1)$-dimensional energy surface in the $2d$-dimensional phase space $\mathbb{R}^{2d}$ has the structure of a 'spherical cylinder' $S^{2d-2} \times \mathbb{R}$, i.e. the Cartesian product of a $(2d-2)$-dimensional sphere S^{2d-2} and a line $\mathbb{R}$. The dividing surface that we construct locally separates the energy surface into two components; 'reactants' and 'products'. This dividing surface which we denote by $S_{\mathrm{ds}}^{2d-2}(E)$ has the structure of a $(2d-2)$-dimensional sphere S^{2d-2}. It can be shown to have the following properties:

- The only way that trajectories can evolve from the reactants component to the products component (and vice versa), without leaving the local region U, is by crossing $S_{\mathrm{ds}}^{2d-2}(E)$. We refer to this property of $S_{\mathrm{ds}}^{2d-2}(E)$ as the 'bottleneck property'[10].
- The dividing surface that we construct is free of local recrossings; any trajectory which crosses $S_{\mathrm{ds}}^{2d-2}(E)$ must leave the neighbourhood U before it might possibly cross $S_{\mathrm{ds}}^{2d-2}(E)$ again.
- A consequence of the previous property of the dividing surface is that it minimizes the (directional) flux. It is thus the optimal dividing surface sought for in variational transition state theory [WW04].

The dividing surface $S_{\mathrm{ds}}^{2d-2}(E)$ itself is divided into two hemispheres: the *forward reactive hemisphere* $B_{\mathrm{ds,\,f}}^{2d-2}(E)$, and the *backward reactive hemisphere* $B_{\mathrm{ds,\,b}}^{2d-2}(E)$. The hemispheres $B_{\mathrm{ds,\,f}}^{2d-2}(E)$ and $B_{\mathrm{ds,\,b}}^{2d-2}(E)$ are topological $(2d-2)$-balls. These two hemispheres are separated by the equator of $S_{\mathrm{ds}}^{2d-2}(E)$, which itself is a sphere of dimension $(2d-3)$. On $B_{\mathrm{ds,\,f}}^{2d-2}(E)$ and $B_{\mathrm{ds,\,b}}^{2d-2}(E)$ the Hamiltonian vector field is transversal to each of these surfaces. This transversality is the mathematical manifestation of 'no recrossing'. Heuristically, 'transversal'

[10] Here we inserted the restriction 'without leaving the local region U' to exclude the case where the dividing surface does not divide the full (global) energy surface into two disjoint components. For example, two regions in an energy surface might be connected by channels associated with two different saddle-centre-...-centre equilibrium points.

means that the Hamiltonian vector field 'pierces' the surfaces, i.e. there is no point where it is tangential to the surface. Now the Hamiltonian vector field pierces the surfaces $B^{2d-2}_{\mathrm{ds,\,f}}(E)$ and $B^{2d-2}_{\mathrm{ds,\,b}}(E)$ in opposite directions. Since the vector field varies smoothly from point to point, it must be tangential to the equator on which $B^{2d-2}_{\mathrm{ds,\,f}}(E)$ and $B^{2d-2}_{\mathrm{ds,\,b}}(E)$ are joined. More mathematically, the fact that the Hamiltonian vector field is tangential to the equator means that the equator is an *invariant manifold*. In fact, it is a so-called *normally hyperbolic invariant manifold* (NHIM) [Wig94], denoted by $S^{2d-3}_{\mathrm{NHIM}}(E)$, where normal hyperbolicity means that the expansion and contraction rates transverse to the manifold dominate those tangent to the manifold, and there are an equal number of independent expanding and contracting directions transverse to the manifold at each point on the manifold. This implies that it is 'saddle like' in terms of stability (in our set-up there is one expanding direction and one contracting direction normal to the NHIM at each point on the NHIM). Heuristically, one can think of it as a 'big saddle like surface'. In fact, the $(2d-3)$-dimensional NHIM is the energy surface of an invariant subsystem which has $d-1$ degrees of freedom, i.e. one degree of freedom less than the full system. In chemistry terminology this subsystem is the 'activated complex', which may be thought of as representing an oscillating (unstable) 'supermolecule' poised between reactants and products [Eyr35, Pec81, Mil98a].

Normally hyperbolic invariant manifolds have stable and unstable manifolds, which themselves are invariant manifolds. In particular, the NHIM, $S^{2d-3}_{\mathrm{NHIM}}(E)$, has $(2d-2)$-dimensional stable and unstable manifolds $W^s(E)$ and $W^u(E)$ which are isoenergetic, i.e. contained in the energy surface. These invariant manifolds have the topology of spherical cylinders $S^{2d-3}\times\mathbb{R}$. Since they are of codimension one in the energy surface, i.e. they are of one dimension less than the energy surface, they act as impenetrable barriers. The importance of these particular geometrical structures is that all reactive trajectories (both forward and backward) must lie inside regions of the energy surface that are enclosed by the NHIM's stable and unstable manifolds. This can be described more precisely by first noting that $W^s(E)$ and $W^u(E)$ each have two branches that 'join' at the NHIM. We call these branches the *forward* and *backward* branches of $W^s(E)$ and $W^u(E)$, and denote them by $W^s_{\mathrm{f}}(E)$, $W^s_{\mathrm{b}}(E)$, $W^u_{\mathrm{f}}(E)$ and $W^u_{\mathrm{b}}(E)$, respectively. We call the union of the forward branches, $W_{\mathrm{f}}(E) := W^s_{\mathrm{f}}(E)\cup W^u_{\mathrm{f}}(E)$, the *forward reactive spherical cylinder*. Trajectories with initial conditions enclosed by $W_{\mathrm{f}}(E)$ in the reactants component of the energy surface evolve towards the forward hemisphere of the dividing surface $B^{2d-2}_{\mathrm{ds,\,f}}(E)$, cross $B^{2d-2}_{\mathrm{ds,\,f}}(E)$ and evolve into a region of the products component of the energy surface that is enclosed by $W_{\mathrm{f}}(E)$. Similarly, we call the union of the backward branches, $W_{\mathrm{b}}(E) := W^s_{\mathrm{b}}(E)\cup W^u_{\mathrm{b}}(E)$, the *backward reactive spherical cylinder*. Trajectories with initial conditions enclosed by $W_{\mathrm{b}}(E)$ in the products component of the energy surface evolve towards $B^{2d-2}_{\mathrm{ds,\,b}}(E)$, cross $B^{2d-2}_{\mathrm{ds,\,b}}(E)$ and evolve into a region of the reactants component of the energy surface that is enclosed by $W_{\mathrm{b}}(E)$. *All* forward reactive trajectories are enclosed by $W_{\mathrm{f}}(E)$ and *all* backward reactive trajectories are enclosed by $W_{\mathrm{b}}(E)$. As we will see in the next section these structures can be computed from the normal form developed in section 2.

4.2. The normal form coordinates: phase space structures and trajectories of Hamilton's equations

We now describe how the phase space structures mentioned in the previous section can be identified and computed from the normal form algorithm, and how they influence trajectories of Hamilton's equations. From the discussion in section 2.3, after N steps of the normal form algorithm, we have constructed a coordinate transformation from the original, 'physical'

coordinates to new, 'normal form' coordinates $(q_1^{(N)}, \ldots, q_d^{(N)}, p_1^{(N)}, \ldots, p_d^{(N)})$, and in these new coordinates the Hamiltonian truncated at order N takes the form

$$H_{\mathrm{CNF}}^{(N)} = K_{\mathrm{CNF}}^{(N)}(I^{(N)}, J_2^{(N)}, \ldots, J_d^{(N)})$$
$$= E_0 + \lambda I^{(N)} + \omega_2 J_2^{(N)} + \cdots + \omega_d J_d^{(N)} + \text{higher order terms}, \tag{4.1}$$

where

$$I^{(N)} = q_1^{(N)} p_1^{(N)}, \qquad J_k^{(N)} = \frac{1}{2}\left(\left(q_k^{(N)}\right)^2 + \left(p_k^{(N)}\right)^2\right), \qquad k = 2, \ldots, d, \tag{4.2}$$

and the higher order terms are of order greater than 1 and less than or equal to $[N/2]$ (in the integrals), see equation (2.83) in section 2.3.

The quantities (4.2) are integrals of the motion ('conserved quantities'), i.e. they are constant on trajectories of the Hamiltonian vector field given by the Nth order classical normal form Hamiltonian[11]. Henceforth we will drop the superscripts (N) for the sake of a less cumbersome notation, but it should be understood that the normal form procedure is truncated at some fixed order N.

In the normal form coordinates, using (4.1) and (4.2), Hamilton's equations take the form

$$\dot{q}_1 = \frac{\partial K_{\mathrm{CNF}}}{\partial I}(I, J_2, \ldots, J_d)\, q_1 \equiv \Lambda(I, J_2, \ldots, J_d)\, q_1,$$

$$\dot{p}_1 = -\frac{\partial K_{\mathrm{CNF}}}{\partial I}(I, J_2, \ldots, J_d)\, p_1 \equiv -\Lambda(I, J_2, \ldots, J_d)\, p_1,$$

$$\dot{q}_k = \frac{\partial K_{\mathrm{CNF}}}{\partial J_k}(I, J_2, \ldots, J_d)\, p_k \equiv \Omega_k(I, J_2, \ldots, J_d)\, p_k,$$

$$\dot{p}_k = -\frac{\partial K_{\mathrm{CNF}}}{\partial J_i}(I, J_2, \ldots, J_d) q_k \equiv -\Omega_k(I, J_2, \ldots, J_d)\, q_k, \qquad k = 2, \ldots, d. \tag{4.3}$$

These equations appear 'decoupled'. It is important to understand this statement in quotations since the equations are not 'decoupled' in the usual fashion. Nevertheless, effectively, this is the case since the coefficient Λ and the nonlinear frequencies Ω_k, $k = 2, \ldots, d$, are constant on a given trajectory. This follows from the fact that they are functions of the integrals I and J_k, $k = 2, \ldots, d$. Hence, once the initial conditions for a trajectory are chosen, then the coefficients of (4.3) are constant (in time), and in this sense the equations are decoupled and can be easily integrated. The reason we have this property is a result of the d independent integrals given in (4.2). However, Λ and the nonlinear frequencies Ω_k, $k = 2, \ldots, d$, will generally vary from trajectory to trajectory and the equations are hence not decoupled in the classical sense. We could view them as being 'decoupled on trajectories' as a result of the d integrals being constant on trajectories. In mathematical terms this means that the equations of motion are *integrable*. The notion 'integrability' can be viewed as a generalization of the notion 'separability'. The latter refers to the property of the equations of motion that allows the achievement of a decoupling of the form (4.3) from a transformation that involves the configuration space variables q only (which then entails a transformation of the momenta p to give a symplectic transformation of the full phase space coordinates). Historically, separability has played an important role in developing approximate transition state theory and analysing tunnelling effects, see, e.g., [JR61,EM74,Mil76]. Indeed, if the full dynamics is separable near the saddle point (in phase space) then the construction of a dividing surface with no recrossing

[11] The fact that there are d constants of motion is a consequence of the nonresonance assumption on the linear frequencies ω_k, $k = 2, \ldots, d$. If there are resonances amongst the ω_k, then there will be fewer integrals.

is trivial and the choice of reaction coordinate is 'obvious'. However, it is important to point out that in the neighbourhood of a saddle-centre-...-centre equilibrium point the equations of motions are in general *not* separable but the normal form transformation leading to the decoupling in (4.3) in general involves a symplectic transformation which mixes configuration and momentum variables.

The general solution of (4.3) is given by

$$\begin{aligned} q_1(t) &= A_1 \exp(\Lambda(I, J_2, \ldots, J_d)\, t), \\ p_1(t) &= B_1 \exp(-\Lambda(I, J_2, \ldots, J_d)\, t), \\ q_k(t) &= A_k \sin(\Omega_k(I, J_2, \ldots, J_d)\, t + \varphi_k), \\ p_k(t) &= A_k \cos(\Omega_k(I, J_2, \ldots, J_d)\, t + \varphi_k), \qquad k = 2, \ldots, d, \end{aligned} \tag{4.4}$$

where the $A_1, \ldots, A_d$, $\varphi_2, \ldots, \varphi_d$ and B_1 are $2d$ constants determined by the initial conditions $(q_1(0), \ldots, q_d(0), p_1(0), \ldots, p_d(0))$. The constants in (4.4) determine the integrals according to

$$I = A_1\, B_1, \qquad J_k = \tfrac{1}{2} A_k^2, \qquad k = 2, \ldots, d. \tag{4.5}$$

From the general solution (4.4) we see that the motion is generally hyperbolic (i.e. 'saddle like') in the plane of the coordinates (q_1, p_1) associated with the saddle and rotational in the planes of the coordinate pairs (q_k, p_k), $k = 2, \ldots, d$, associated with the centre directions.

In the following, we show how the normal form, which is valid in the neighbourhood of the saddle-centre-...-centre equilibrium point, gives *explicit formulae* for the various manifolds described in section 4.1. At the same time, we show how trajectories of Hamilton's equations expressed in the normal form coordinates, are constrained by these manifolds. Many more details can be found in [UJP+01, WBW04b]. The geometrical illustrations that we give are for three degrees of freedom. In fact, conceptually, the step from two to three degrees of freedom is the big step; once the case of three degrees of freedom is well understood, it is not difficult to incorporate more degrees of freedom. We begin by describing the local structure of the energy surfaces.

The structure of an energy surface near a saddle point. For $E < E_0$, the energy surface consists of two disjoint components. The two components correspond to 'reactants' and 'products.' The top panel of figure 2 shows how the two components project to the various planes of the normal form coordinates. The projection to the plane of the saddle coordinates (q_1, p_1) is bounded away from the origin by the two branches of the hyperbola, $q_1 p_1 = I < 0$, where I is given implicitly by the energy equation with the centre actions J_k, $k = 2, \ldots, d$, set equal to zero: $K_{\mathrm{CNF}}(I, 0, \ldots, 0) = E < E_0$. The projections to the planes of the centre coordinates, (q_k, p_k), $k = 2, \ldots, d$, are unbounded.

At $E = E_0$, the formerly disconnected components merge (the energy surface bifurcates), and for $E > E_0$ the energy surface has locally the structure of a spherical cylinder, $S^{2d-2} \times \mathbb{R}$. Its projection to the plane of the saddle coordinates now includes the origin. In the first and third quadrants it is bounded by the two branches of the hyperbola, $q_1 p_1 = I > 0$, where I is again given implicitly by the energy equation with all centre actions equal to zero, but now with an energy greater than E_0: $K_{\mathrm{CNF}}(I, 0, \ldots, 0) = E > E_0$. The projections to the planes of the centre coordinates are again unbounded. This is illustrated in the bottom panel of figure 2.

The dividing surface and reacting and nonreacting trajectories. On an energy surface with $E > E_0$, we define the dividing surface by $q_1 = p_1$. This gives a $(2d-2)$-sphere which we denote by $S^{2d-2}_{\mathrm{ds}}(E)$. Its projection to the saddle coordinates simply gives a line segment through the origin which joins the boundaries of the projection of the energy surface, as shown in figure 3. The projections of the dividing surface to the planes of the centre coordinates are bounded by circles $(p_k^2 + q_k^2)/2 = J_k$, $k = 2, \ldots, d$, where J_k is determined by the energy equation with the other centre actions, J_l, $l \neq k$, and the saddle integral, I, set equal to zero. The dividing surface divides the energy surface into two halves, $p_1 - q_1 > 0$ and $p_1 - q_1 < 0$, corresponding to reactants and products.

As mentioned above, trajectories project to hyperbolae in the plane of the saddle coordinates, and to circles in the planes of the centre coordinates. The sign of I determines whether a trajectory is nonreacting or reacting, see figure 3. Trajectories which have $I < 0$ are nonreactive and for one branch of the hyperbola $q_1 p_1 = I$ they stay on the reactants side and for the other branch they stay on the products side; trajectories with $I > 0$ are reactive, and for one branch of the hyperbola $q_1 p_1 = I$ they react in the forward direction, i.e. from reactants to products, and for the other branch they react in the backward direction, i.e. from products to reactants. The projections of reactive trajectories to the planes of the centre coordinates are always contained in the projections of the dividing surface. In this, and other ways, the geometry of the reaction is highly constrained. There is no analogous restriction on the projections of nonreactive trajectories to the centre coordinates.

The normally hyperbolic invariant manifold (NHIM) and its relation to the 'activated complex'. On an energy surface with $E > E_0$, the NHIM is given by $q_1 = p_1 = 0$. The NHIM has the structure of a $(2d-3)$-sphere, which we denote by $S^{2d-3}_{\mathrm{NHIM}}(E)$. The NHIM is the equator of the dividing surface; it divides it into two 'hemispheres': the *forward dividing surface*, which has $q_1 = p_1 > 0$, and the *backward dividing surface*, which has $q_1 = p_1 < 0$. The forward and backward dividing surfaces have the structure of $(2d-2)$-dimensional balls, which we denote by $B^{2d-2}_{\mathrm{ds,\,f}}(E)$ and $B^{2d-2}_{\mathrm{ds,\,b}}(E)$, respectively. All forward reactive trajectories cross $B^{2d-2}_{\mathrm{ds,\,f}}(E)$; all backward reactive trajectories cross $B^{2d-2}_{\mathrm{ds,\,b}}(E)$. Since $q_1 = p_1 = 0$ in the equations of motion (4.3) implies that $\dot{q}_1 = \dot{p}_1 = 0$, the NHIM is an invariant manifold, i.e. trajectories started in the NHIM stay in the NHIM for all time. The system resulting from $q_1 = p_1 = 0$ is an invariant subsystem with one degree of freedom less than the full system. In fact, $q_1 = p_1 = 0$ defines the centre manifold associated with the saddle-centre-...-centre equilibrium point, and the NHIM at an energy E greater than the energy of the equilibrium point is given by the intersection of the centre manifold with the energy surface of this energy E [UJP+01, WW04].

This invariant subsystem is the 'activated complex' (in phase space), located between reactants and products (see section 4.1). The NHIM can be considered to be the energy surface of the activated complex. In particular, all trajectories in the NHIM have $I = 0$.

The equations of motion (4.3) also show that $\dot{p}_1 - \dot{q}_1 < 0$ on the forward dividing surface $B^{2d-2}_{\mathrm{ds,\,f}}(E)$, and $\dot{p}_1 - \dot{q}_1 > 0$ on the backward dividing surface $B^{2d-2}_{\mathrm{ds,\,b}}(E)$. Hence, except for the NHIM, which is an invariant manifold, the dividing surface is everywhere transverse to the Hamiltonian flow. This means that a trajectory, after having crossed the forward or backward dividing surface, $B^{2d-2}_{\mathrm{ds,\,f}}(E)$ or $B^{2d-2}_{\mathrm{ds,\,b}}(E)$, respectively, must leave the neighbourhood of the dividing surface before it can possibly cross it again. Indeed, such a trajectory must leave the local region in which the normal form is valid before it can possibly cross the dividing surface again.

The NHIM has a special structure: due to the conservation of the centre actions, it is filled, or *foliated*, by invariant $(d-1)$-dimensional tori, $\mathbb{T}^{d-1}$. More precisely, for $d = 3$

degrees of freedom, each value of J_2 implicitly defines a value of J_3 by the energy equation $K_{\mathrm{CNF}}(0, J_2, J_3) = E$. For three degrees of freedom, the NHIM is thus foliated by a one-parameter family of invariant 2-tori. The end points of the parametrization interval correspond to $J_2 = 0$ (implying $q_2 = p_2 = 0$) and $J_3 = 0$ (implying $q_3 = p_3 = 0$), respectively. At the end points, the 2-tori thus degenerate to periodic orbits, the so-called *Lyapunov periodic orbits*. As we will discuss in more detail in sections 5 and 6, the fact that the NHIM is foliated by invariant tori has important consequences for the corresponding quantum system.

The stable and unstable manifolds of the NHIM forming the phase space conduits for reactions. Since the NHIM is of saddle stability type, it has stable and unstable manifolds, $W^s(E)$ and $W^u(E)$. The stable and unstable manifolds have the structure of spherical cylinders, $S^{2d-3} \times \mathbb{R}$. Each of them consists of two branches: the 'forward branches', which we denote by $W^s_{\mathrm{f}}(E)$ and $W^u_{\mathrm{f}}(E)$, and the 'backward branches', which we denote by $W^s_{\mathrm{b}}(E)$ and $W^u_{\mathrm{b}}(E)$. In terms of the normal form coordinates, $W^s_{\mathrm{f}}(E)$ is given by $q_1 = 0$ with $p_1 > 0$, $W^u_{\mathrm{f}}(E)$ is given by $p_1 = 0$ with $q_1 > 0$, $W^s_{\mathrm{b}}(E)$ is given by $q_1 = 0$ with $p_1 < 0$ and $W^u_{\mathrm{b}}(E)$ is given by $p_1 = 0$ with $q_1 < 0$, see figure 4. Trajectories on these manifolds have $I = 0$.

Since the stable and unstable manifolds of the NHIM are of one less dimension than the energy surface, they enclose volumes of the energy surface. We call the union of the forward branches, $W^s_{\mathrm{f}}(E)$ and $W^u_{\mathrm{f}}(E)$, the *forward reactive spherical cylinder* and denote it by $W_{\mathrm{f}}(E)$. Similarly, we define the *backward reactive spherical cylinder*, $W_{\mathrm{b}}(E)$, as the union of the backward branches, $W^s_{\mathrm{b}}(E)$ and $W^u_{\mathrm{b}}(E)$.

The reactive volumes enclosed by $W_{\mathrm{f}}(E)$ and $W_{\mathrm{b}}(E)$ are shown in figure 5 as their projections to the normal form coordinate planes. In the plane of the saddle coordinates, the reactive volume enclosed by $W_{\mathrm{f}}(E)$ projects to the first quadrant. This projection is bounded by the corresponding hyperbola $q_1 p_1 = I$, with I obtained from $K_{\mathrm{CNF}}(I, 0, \ldots, 0) = E$. Likewise, $W_{\mathrm{b}}(E)$ projects to the third quadrant in the (q_1, p_1)-plane. $W_{\mathrm{f}}(E)$ encloses *all* forward reactive trajectories; $W_{\mathrm{b}}(E)$ encloses *all* backward reactive trajectories. *All* nonreactive trajectories are contained in the complement.

Forward and backward reaction paths. The local geometry of $W_{\mathrm{f}}(E)$ and $W_{\mathrm{b}}(E)$ suggests a natural definition of *dynamical* forward and backward reaction paths as the unique paths in *phase space* obtained by putting all of the energy of a reacting trajectory into the reacting mode, i.e. setting $q_2 = \ldots = q_d = p_2 = \ldots = p_d = 0$. This gives the two branches of the hyperbola $q_1 p_1 = I$, with I obtained from $K_{\mathrm{CNF}}(I, 0, \ldots, 0) = E$, which in phase space are contained in the plane of the saddle coordinates, see figure 5. This way, the forward (respectively, backward) reaction path can be thought of as the 'centre curve' of the relevant volume enclosed by the forward (respectively, backward) reactive spherical cylinder $W_{\mathrm{f}}(E)$ (respectively, $W_{\mathrm{b}}(E)$). These reaction paths are the special reactive trajectories which intersect the dividing surface at the 'poles' (in the sense of North and South poles, where $q_1 = p_1$ assumes its maximum and minimum values on the dividing surface).

The transmission time through the transition state region. The normal form coordinates provide a way of computing the time for *all* trajectories to cross the transition region. We illustrate this with a forward reacting trajectory (a similar argument and calculation can be applied to backward reacting trajectories). We choose the boundary for the entrance to the reaction region to be $p_1 - q_1 = c$ for some constant $c > 0$, i.e. initial conditions which lie on the reactant side of the transition state, and the boundary for exiting the

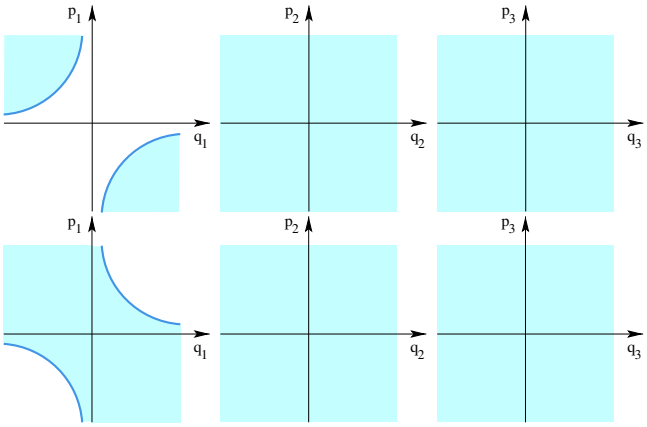

Figure 2. Projection of energy surfaces (turquoise regions) to the planes of the normal form coordinates. The energy surface in the top panel has $E < E_0$; the energy surface in the bottom panel has $E > E_0$.

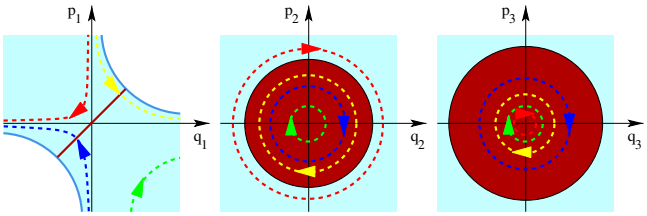

Figure 3. Projection of the dividing surface and reacting and nonreacting trajectories to the planes of the normal form coordinates. In the plane of the saddle coordinates, the projection of the dividing surface is the dark red diagonal line segment, which has $q_1 = p_1$. In the planes of the centre coordinates, the projections of the dividing surface are the dark red discs. Forward and backward reactive trajectories (yellow and blue) project to the first and third quadrants in the plane of the saddle coordinates, respectively, and pass through the dividing surface. The red and green curves mark nonreactive trajectories on the reactant side ($p_1 - q_1 > 0$), and on the product side ($p_1 - q_1 < 0$), of the dividing surface, respectively. The turquoise regions indicate the projections of the energy surface.

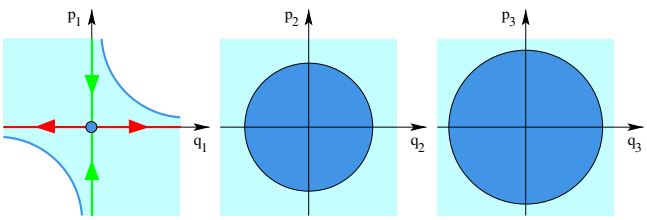

Figure 4. The projection of the NHIM and the local parts of its stable and unstable manifolds, $W^s(E)$ and $W^u(E)$, to the planes of the normal form coordinates. In the plane of the saddle coordinates, the projection of the NHIM is the origin marked by the blue bold point, and the projection of $W^s(E)$ and $W^u(E)$ are the p_1-axis and q_1-axis, respectively. $W^s(E)$ consists of the forward and backward branches $W^s_{\rm f}(E)$ and $W^s_{\rm b}(E)$, which have $p_1 > 0$ and $p_1 < 0$, respectively; $W^u(E)$ consists of $W^u_{\rm f}(E)$ and $W^u_{\rm b}(E)$, which have $q_1 > 0$ and $q_1 < 0$, respectively. In the plane of the centre coordinates, the projections of the NHIM, $W^s(E)$ and $W^u(E)$ (the blue circular discs), coincide with the projection of the dividing surface in figure 3. The turquoise regions mark the projections of the energy surface.

reaction region to be $p_1 - q_1 = -c$ on the product side. We now compute the *time of flight* for a forward reacting trajectory with initial condition on $p_1 - q_1 = c$ to reach $p_1 - q_1 = -c$ on the product side. The solutions are $q_1(t) = q_1(0)\exp(\Lambda(I, J_2, \ldots, J_d)t)$ and $p_1(t) = p_1(0)\exp(-\Lambda(I, J_2, \ldots, J_d)t)$ (see (4.4)), where $\Lambda(I, J_2, \ldots, J_d)$ is determined by the initial conditions. This gives the time of flight as

$$T = (\Lambda(I, J_2, \ldots, J_d))^{-1} \ln\left(\frac{p_1(0)}{q_1(0)}\right). \tag{4.6}$$

The time diverges logarithmically as $q_1(0) \to 0$, i.e. the closer the trajectory starts to the boundary $W_f(E)$. It is not difficult to see that the time of flight is shortest for the centre curve of the volume enclosed by $W_f(E)$, i.e. *the trajectory which traverses the transition state region fastest is precisely our forward reaction path*. A similar construction applies to backward reactive trajectories.

In fact, the normal form can be used to map trajectories through the transition state region, i.e. the phase space point at which a trajectory enters the transition state region can be mapped analytically to the phase space point at which the trajectories exit the transition state region.

4.3. The normal form coordinates: the foliation of the reaction region by Lagrangian submanifolds

In section 4.2 we have indicated that the different types of possible motion near a saddle-centre-...-centre equilibrium point can be described in terms of the integrals. In fact, the existence of the d integrals (4.2) leads to even further constraints on the classical motions and hence to even more detailed structuring of the phase space near a saddle-centre-...-centre equilibrium point than we have already described in section 4.2. As we will see in section 5, this structure will have important consequences for the quantum mechanics of reactions. In order to describe this structure we introduce the so-called *momentum map* $\mathcal{M}$ [Gui94, MR99] which maps a point $(q_1, \ldots, q_d, p_1, \ldots, p_d)$ in the phase space $\mathbb{R}^{2d}$ to the integrals evaluated at this point:

$$\mathcal{M}(q_1, \ldots, q_d, p_1, \ldots, p_d) \mapsto (I, J_2, \ldots, J_d). \tag{4.7}$$

The preimage of a value for the constants of motion $(I, J_2, \ldots, J_d)$ under $\mathcal{M}$ is called a *fibre*. A fibre thus corresponds to the common level set of the integrals in phase space.

A point $(q_1, \ldots, q_d, p_1, \ldots, p_d)$ is called a *regular point* of the momentum map if the linearization of the momentum map, $D\mathcal{M}$, has rank d at this point, i.e. if the gradients of the d integrals $I, J_k, k = 2, \ldots, d$, with respect to the phase space coordinates (q, p), are linearly independent at this point. If the rank of $D\mathcal{M}$ is less than d then the point is called an irregular point. A regular fibre is a fibre which consists of regular points only. The regular fibres of the momentum map in (4.7) are d-dimensional manifolds given by the Cartesian product of a hyperbola $q_1 p_1 = I$ in the saddle plane (q_1, p_1) and $d - 1$ circles S^1 in the centre planes $(q_k, p_k), k = 2, \ldots, d$. Since hyperbola $q_1 p_1 = I$ consists of two branches each of which have the topology of a line $\mathbb{R}$, the regular fibres consist of two disjoint *toroidal cylinders*, $\mathbb{T}^{d-1} \times \mathbb{R}$, which are the Cartesian products of a $(d-1)$-dimensional torus and a line. We denote these toroidal cylinders by

$$\Lambda^+_{I,J_2,\ldots,J_d} = \{(q, p) \in \mathbb{R}^{2d} \,:\, p_1 q_1 = I,\ \tfrac{1}{2}(p_2^2 + q_2^2) = J_2, \ldots, \tfrac{1}{2}(p_d^2 + q_d^2) = J_d, q_1 > 0\} \tag{4.8}$$

and

$$\Lambda^-_{I,J_2,\ldots,J_d} = \{(q, p) \in \mathbb{R}^{2d} \,:\, p_1 q_1 = I,\ \tfrac{1}{2}(p_2^2 + q_2^2) = J_2, \ldots, \tfrac{1}{2}(p_d^2 + q_d^2) = J_d, q_1 < 0\}. \tag{4.9}$$

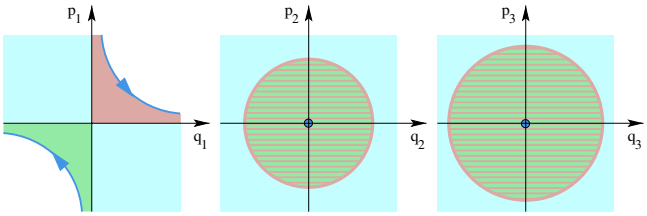

Figure 5. Projections of the reactive volumes enclosed by the forward and backward reactive spherical cylinders, $W_{\mathrm{f}}(E)$ and $W_{\mathrm{b}}(E)$, and the forward and backward reaction paths, to the planes of the normal form coordinates. The volumes enclosed by $W_{\mathrm{f}}(E)$ and $W_{\mathrm{b}}(E)$ project to the dark pink and green regions in the first and third quadrants in the plane of the saddle coordinates, respectively. These volumes project to the dark green/dark pink brindled discs in the planes of the centre coordinates, where their projections coincide with the projection of the NHIM and the dividing surface in figures 3 and 4. The forward and backward reaction paths project to the two branches of a hyperbola marked blue in the first and third quadrants in the plane of the saddle coordinates, respectively, and to the origins (bold blue points) in the planes of the centre coordinates. The turquoise regions mark the projections of the energy surface.

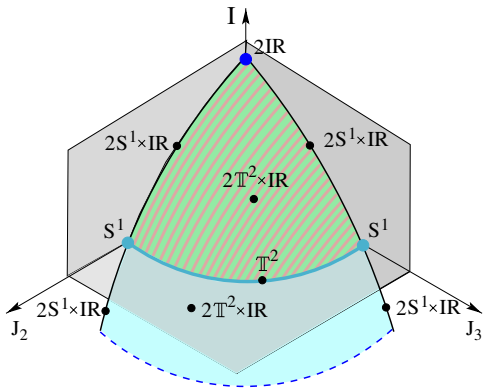

Figure 6. Sketch of the image of the energy surface of energy $E > E_0$ under the momentum map $\mathcal{M}$ in equation (4.7) in the space of the integrals I and J_k, $k = 2, \ldots, d$, for the case of $d = 3$ degrees of freedom. The green/dark pink brindled piece of the image of the energy surface has $I > 0$; the turquoise piece has $I < 0$. The intersections with the planes $I = 0$, $J_2 = 0$ and $J_3 = 0$ (pieces of which are visualized by semitransparent planes for clarity) form the bifurcation diagram of the energy surface. The image of the energy surface is not bounded in the direction of negative I as indicated by the dashed line at the bottom. The topology of the fibres $\mathcal{M}^{-1}(I, J_2, J_3)$ is indicated for the various points (I, J_2, J_3) marked by dots. The fibre of a point (I, J_2, J_3) with $I \neq 0$ consists of two disconnected manifolds as indicated by the factor of 2. The fibre of a point (I, J_2, J_3) with $I = 0$ consists of a single connected manifold.

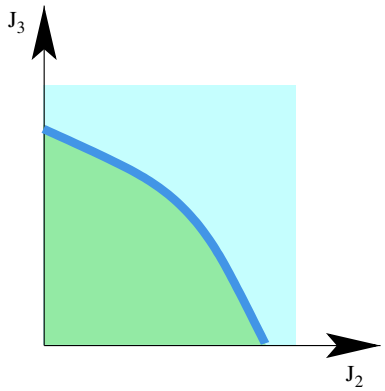

Figure 7. Contour $K_{\mathrm{CNF}}(0, J_2, \ldots, J_d) = E$ (blue line) in the space of the centre integrals $(J_2, \ldots, J_d)$ for $d = 3$ degrees of freedom. Up to the prefactor $(2\pi)^{d-1}$, the area $\mathcal{V}(E)$ of the enclosed region (marked green) gives the directional flux through the dividing surface, see equation (4.10). The green region agrees with the projection of the piece of the image of the energy surface under the momentum map which has $I > 0$ in figure 6. to the (J_2, J_3)-plane.

$\Lambda^+_{I,J_2,\ldots,J_d}$ and $\Lambda^-_{I,J_2,\ldots,J_d}$ are *Lagrangian manifolds* [Arn78]. Prominent examples of Lagrangian manifolds are tori which foliate the neighbourhood of a centre-...-centre equilibrium point and whose semiclassical quantization often lead to a very good approximation of part of the energy spectra of the corresponding bounded system [OdA88]. In our case the

Lagrangian manifolds are unbounded. They are the products of $(d-1)$-dimensional tori $\mathbb{T}^{d-1}$ and unbounded lines $\mathbb{R}$. The toroidal base of these cylinders will again lead to semiclassical quantization conditions and, as we will see in sections 5 and 6, this will have important consequences for the computation of quantum reaction rates and resonances.

If the fibre contains an irregular point then the fibre is called singular. The image of the singular fibres under the momentum map is called the *bifurcation diagram*. It is easy to see that the bifurcation diagram consists of the set of $(I, J_2, \ldots, J_d)$ where one or more of the integrals vanish. In figure 6. we show the image of the energy surface with energy $E > E_0$ under the momentum map $\mathcal{M}$ in the space of the integrals for $d = 3$ degrees of freedom. The bifurcation diagram (of the energy surface) consists of the intersections of the image of the energy surface (the turquoise and green/dark pink brindled surface in figure 6.) with one of the planes $I = 0$, $J_2 = 0$ or $J_3 = 0$. Upon approaching one of the edges that have $J_2 = 0$ or $J_3 = 0$ the circle in the plane (q_2, p_2) or (q_3, p_3), respectively, shrinks to a point, and accordingly the regular fibres $\mathbb{T}^2 \times \mathbb{R}$ reduce to cylinders or 'tubes' $S^1 \times \mathbb{R}$. At the top corner in figure 6. both J_2 and J_3 are zero. Here both circles in the centre planes (q_2, p_2) and (q_3, p_3) have shrunk to points. The corresponding singular fibre consists of two lines, $\mathbb{R}$, which are the forward and backward reaction paths, respectively (see also figure 5).

All the fibres mentioned so far have $I \neq 0$ and each consists of a pair of disconnected components. For $I < 0$, one member of each pair is located on the reactants side and the other on the products side of the dividing surface. For $I > 0$, one member of each pair consists of trajectories evolving from reactants to products and the other member consists of trajectories that evolve from products to reactants. In fact the two members of a fibre which has $I > 0$ are contained in the energy surface volume enclosed by the forward and backward reactive spherical cylinders $W_{\mathrm{f}}(E)$ and $W_{\mathrm{b}}(E)$, see figure 5. For this reason we marked the piece of the image of the energy surface under the momentum map which has $I > 0$ by the same green/dark pink colour in figure 6. that we used in figure 5. Green corresponds to forward reactive trajectories and dark pink corresponds to backward reactive trajectories. Under the momentum map these trajectories have the same image.

The light blue line in figure 6. which has $I = 0$ is the image of the NHIM under the momentum map. For three degrees of freedom the NHIM is a three-dimensional sphere, and as mentioned in section 4.2 and indicated in figure 6., it is foliated by a one-parameter family of invariant 2-tori which shrink to periodic orbits, i.e. circles S^1, at the end points of the parametrization interval. As we have already indicated in section 4.2, this foliation of the NHIM has important consequences for the quantum mechanics of reactions which we will dicuss in sections 5 and 6. Moreover, we will see in section 4.4 that, for $d = 3$ degrees of freedom, the area enclosed by the image of the NHIM in the plane (J_2, J_3) gives, up to a prefactor, the directional flux through the dividing surface.

4.4. The directional flux through the dividing surface

A key ingredient of transition state theory and the classical reaction rate is the directional flux through the dividing surface defined in section 4.1. Given the Hamiltonian function in normal form expressed as a function of the integrals (4.2), and a fixed energy E above the energy of the saddle-centre-...-centre, E_0, it is shown in [WW04] that the directional flux through the dividing surface is given by

$$f(E) = (2\pi)^{d-1}\mathcal{V}(E), \tag{4.10}$$

where $\mathcal{V}(E)$ is the volume in the space of the actions $(J_2, \ldots, J_d)$ enclosed by the contour $H_{\mathrm{CNF}}(0, J_2, \ldots, J_d) = E$. For $E < E_0$, the directional flux is zero. For the case of a system

with three degrees of freedom for which we sketched the image of the energy surface in the space of the integrals in figure 6., the volume $\mathcal{V}(E)$ is given by the area in the (J_2, J_3) plane enclosed by the light blue line corresponding to the NHIM in figure 6.. For clarity we illustrate this area again in figure 7.. As we mentioned in section 4.2, the NHIM can be considered as the energy surface of an invariant subsystem with one degree of freedom less than the full system which is referred to as the activated complex in the chemistry literature. Therefore the flux can be interpreted as the volume enclosed by the energy surface (given by the NHIM) in the phase space of this invariant subsystem. This gives a direct connection between the directional flux through the dividing surface and the activated complex. In fact, the dimensionless quantity

$$N_{\mathrm{Weyl}}(E) = \frac{f(E)}{(2\pi\hbar)^{d-1}}, \tag{4.11}$$

where $2\pi\hbar$ is Planck's constant, is Weyl's approximation of the integrated density of states, or equivalently the mean number of quantum states of the activated complex with energies less than or equal to E (see, e.g., [Gut90]). As we will see in section 5 $N_{\mathrm{Weyl}}(E)$ can be interpreted as the mean number of open quantum 'transition channels' at energy E.

In the case where we take into account only the quadratic part of the normal form or, equivalently, if we linearize Hamilton's equations, we have $H_{\mathrm{CNF}}(I, J_2, \ldots, J_d) = \lambda I + \sum_{k=2}^{d} \omega_k J_k$ and the energy surface $H_{\mathrm{CNF}}(0, J_2, \ldots, J_d) = E$ encloses a simplex in $(J_2, \ldots, J_d)$ whose volume leads to the well-known result [Mac90]

$$f(E) = \frac{E^{d-1}}{(d-1)!} \prod_{k=2}^{d} \frac{2\pi}{\omega_k}. \tag{4.12}$$

This shows, e.g., that the flux scales with E^{d-1} for energies close to the saddle energy. The key advantage of the normal form algorithm that we presented in section 2 is that it allows one to include the nonlinear corrections to (4.12) to any desired order.

Here we give a brief outline of the essential elements of the derivation of the expression for the flux in (4.10) following the discussion [WW04]. It is important to note that our work is firmly rooted in phase space. In particular, we are considering the (directional) flux of a vector field on phase space (Hamilton's equations) through a dividing surface in phase space (which has been proven to have the 'no-recrossing' property as discussed earlier). For this reason the modern notation of differential forms, especially in light of its importance in the modern formulation of Hamiltonian mechanics, proves to be most convenient and notationally economical.

Therefore we begin by considering the phase space volume form $\Omega = \mathrm{d}p_1 \wedge \mathrm{d}q_1 \wedge \cdots \wedge \mathrm{d}p_d \wedge \mathrm{d}q_d$, which in terms of the symplectic 2-form $\omega = \sum_{k=1}^{d} \mathrm{d}p_k \wedge \mathrm{d}q_k$ can be written as $\Omega = \omega^d/d!$. Note that in our case the phase space coordinates (q, p) used here will be Nth order normal form coordinates and we do not use superscripts (N) to indicate this. However the quantities introduced in the following do not depend on the chosen coordinate system. They are invariant under symplectic coordinate transformations. Let η be an energy surface volume form defined via the property $\mathrm{d}H \wedge \eta = \Omega$. Then the flux through a codimension one submanifold of the $(2d-1)$-dimensional energy surface $H = E$ is obtained from integrating over it the 'flux' form Ω' given by the interior product of the Hamiltonian vector field X_H with η [Mac90], i.e.

$$\Omega' = i_{X_H}\eta = \frac{1}{(d-1)!}\omega^{d-1}, \tag{4.13}$$

where $i_{X_H}\eta(\xi_1, \ldots, \xi_{2d-2}) = \eta(\xi_1, \ldots, \xi_{2d-2}, X_H)$ for any $2d-2$ vectors ξ_k. The second equality in (4.13) is easily established on a noncritical energy surface, i.e. on an energy surface

which contains no equilibria. The flux form Ω' is exact. In fact the generalized 'action' form

$$\phi = \sum_{k=1}^{d} p_k \, \mathrm{d}q_k \wedge \frac{1}{(d-1)!}\omega^{d-2}$$

has the property $\mathrm{d}\phi = \Omega'$ and facilitates the use of Stokes' theorem to compute the flux. In the case of two degrees of freedom we simply have $\Omega' = \omega = \mathrm{d}p_1 \wedge \mathrm{d}q_1 + \mathrm{d}p_2 \wedge \mathrm{d}q_2$ and ϕ becomes the usual action form $\phi = p_1 \, \mathrm{d}q_1 + p_2 \, \mathrm{d}q_2$. Since the dividing surface $S_{\mathrm{ds}}^{2d-2}(E)$ is a sphere, that is, a manifold without boundary, it follows from Stokes' theorem that the integral of Ω' over $S_{\mathrm{ds}}^{2d-2}(E)$ is zero. In order to compute reaction rates one has to distinguish between the directions in which the Hamiltonian flow crosses the dividing surface (i.e. distinguish between forward and backward reactive trajectories). Given a normal bundle[12] over $S_{\mathrm{ds}}^{2d-2}(E)$ the direction can be specified by the sign of the scalar product between the normal vectors and the Hamiltonian vector field. This scalar product is strictly positive on one hemisphere of $S_{\mathrm{ds}}^{2d-2}(E)$, strictly negative on the other hemisphere and zero only at the equator of $S_{\mathrm{ds}}^{2d-2}(E)$, i.e. at the normally hyperbolic invariant manifold $S_{\mathrm{NHIM}}^{2d-3}(E)$, where the Hamiltonian vector field is tangent to $S_{\mathrm{ds}}^{2d-2}(E)$. Likewise, the flux form Ω' on $S_{\mathrm{ds}}^{2d-2}(E)$ vanishes nowhere on $B_{\mathrm{ds,\,f}}^{2d-2}(E)$ and $B_{\mathrm{ds,\,b}}^{2d-2}(E)$ and is identically zero on $S_{\mathrm{NHIM}}^{2d-3}(E)$. It is natural to take as the orientation of $B_{\mathrm{ds,\,f}}^{2d-2}(E)$ and $B_{\mathrm{ds,\,b}}^{2d-2}(E)$ the orientation they inherit from the dividing surface. Without restriction we may assume that the orientation of $S_{\mathrm{ds}}^{2d-2}(E)$ is such that Ω' is positive on the forward hemisphere $B_{\mathrm{ds,\,f}}^{2d-2}(E)$ and negative on the backward hemisphere $B_{\mathrm{ds,\,b}}^{2d-2}(E)$, i.e. Ω' and $-\Omega'$ can be considered as *volume forms* on $B_{\mathrm{ds,\,f}}^{2d-2}(E)$ and $B_{\mathrm{ds,\,b}}^{2d-2}(E)$, respectively. It follows from Stokes' theorem that the fluxes through the forward and backward hemispheres, $\int_{B_{\mathrm{ds,\,f}}^{2d-2}(E)} \Omega'$ and $\int_{B_{\mathrm{ds,\,b}}^{2d-2}(E)} \Omega'$, have the same magnitude but opposite signs and can be computed from integrating the action form ϕ over the NHIM:

$$f(E) = \int_{B_{\mathrm{ds,\,f}}^{2d-2}(E)} \Omega' = -\int_{B_{\mathrm{ds,\,b}}^{2d-2}(E)} \Omega' = \left| \int_{S_{\mathrm{NHIM}}^{2d-3}(E)} \phi \right|. \tag{4.14}$$

We call the positive quantity $\int_{B_{\mathrm{ds,\,f}}^{2d-2}(E)} \Omega'$ the *forward flux* and the negative quantity $\int_{B_{\mathrm{ds,\,f}}^{2d-2}(E)} \Omega'$ the *backward flux* through $S_{\mathrm{ds}}^{2d-2}(E)$.

Writing the flux form Ω' in terms of 'angle-action variables' $(\varphi_1, \ldots, \varphi_d, I, J_2, \ldots, J_d)$ (these were derived in terms of the integrals of the normal form in section 2.3.1) we obtain the result that the forward flux through the dividing surface is given by the expression in equation (4.10).

4.5. The normal form coordinates: issues associated with truncation

The final question to address concerns the 'validity' of the normal form transformation. More precisely, this means how large the neighbourhood (in phase space) U of the saddle-centre-...-centre equilibrium point can be taken so that the geometric structures given by the normal form are accurate for the 'full equations'. Actually, there are a number of questions to be answered related to 'validity'.

- In truncating the Taylor expansion of the Hamiltonian at degree N, how do you determine N?
- What is the region of validity of the normal form transformation for the Taylor expanded Hamiltonian truncated at degree N?

[12] Roughly speaking, at each point of the dividing surface we consider the normal vector in the energy surface. The *normal bundle* is the union of all vectors taken over all points on the dividing surface.

- How 'accurate' are the phase space structures (e.g. the dividing surface, the NHIM) for the normal form of the Hamiltonian truncated at degree N?
- How accurate are trajectories of the normal form of the Hamiltonian at order N?

First, general theory assures us that the phase space structures *exist*, and have the properties described above (e.g. normal hyperbolicity, the bottleneck property), *for energies sufficiently close to that of the saddle-centre-...-centre equilibrium point* [Wig94]. The normal form computation is merely an approach for realizing the geometrical structures that the theory tells us must exist.

In practice, one Taylor expands the Hamiltonian and then truncates it at a degree that one *thinks* will provide sufficient accuracy for the range of energies of interest. Experience will generally provide some good 'rules of thumb', e.g. for the HCN isomerization work described in [WBW04b], an expansion up to degree 10 was found to provide sufficient accuracy in the range of energies studied (up to 0.2 eV above the saddle-centre-...-centre equilibrium point).

There is still the question of accuracy. Once the normal form is computed to the desired degree (and, most importantly, the transformation and its inverse between the original coordinates and the 'normal form coordinates'), and the energy is fixed, we have explicit formulae for the dividing surface, the NHIM (the 'equator' of the dividing surface), and the (local) stable and unstable manifolds of the NHIM[13]. We next need to check their 'accuracy'. There are several tests that we employ, and these tests are carried out at *fixed energy*.

- Numerically verify that the dividing surface satisfies the 'bottleneck property', i.e. it (locally) separates the energy surface into two components, and the only way a trajectory can pass between components (while remaining in this region) is by passing through the dividing surface.
- Using the inverse of the normal form transformation map the NHIM and its (local) stable and unstable manifolds back into the original coordinates and check that the full (i.e. not a truncated Taylor expansion) Hamiltonian vector field is tangent to these surfaces. This is a requirement for these surface to be 'invariant manifolds'. The tests are carried out pointwise on a grid of points covering the surfaces.
- The integrals (4.2) are constant in time on trajectories of the normal form of the truncated Taylor expansion. We check how they vary in time on trajectories of the full Hamiltonian.

If the desired accuracy is obtained for this energy, then the energy may be increased and the accuracy tests are repeated at the higher energy. If accuracy is inadequate, then a higher degree Taylor expansion can be computed. As energy is increased, ultimately two factors may lead to break down of this approach for realizing these phase space structures. One is that the energy surface may deform in such a way that the bottleneck property does not hold. Another is that the approach will require such a high degree Taylor expansion that it becomes computationally intractable.

4.6. The global dynamics associated with the manifolds constructed in the reaction region

As we have shown, the normal form transformation to normal form coordinates provides a method for providing a complete understanding of the geometry of reaction dynamics in a neighbourhood U (in phase space) of the saddle-centre-...-centre equilibrium point of Hamilton's equations. By this, we mean that in the normal form coordinates we can give an explicit equation for the surfaces and, as a result of the 'simple' structure of Hamilton's equations in the normal form coordinates, we can describe precisely the influence of these

[13] Here 'local' means that we only have realizations of the stable and unstable manifolds in a neighbourhood of the saddle-centre-...-centre equilibrium point where the normal form transformation has the desired accuracy.

Table 1. Table of phase space surfaces influencing reaction dynamics and their representations in normal form coordinates on an energy surface of energy greater than the energy of the saddle equilibrium point.

Geometrical structure	Equation in normal form coordinates
Dividing surface, $S^{2d-2}_{\mathrm{ds}}(E)$	$q_1 = p_1$
Forward reactive hemisphere, $B^{2d-2}_{\mathrm{ds,f}}(E)$	$q_1 = p_1 > 0$
Backward reactive hemisphere, $B^{2d-2}_{\mathrm{ds,b}}(E)$	$q_1 = p_1 < 0$
NHIM, $S^{2d-3}_{\mathrm{NHIM}}(E)$	$q_1 = p_1 = 0$
Stable manifold of the NHIM, $W^s(E)$	$q_1 = 0, \quad p_1 \neq 0$
Unstable manifold of the NHIM, $W^u(E)$	$p_1 = 0, \quad q_1 \neq 0$
Forward branch of $W^s(E)$, $W^s_{\mathrm{f}}(E)$	$q_1 = 0, \quad p_1 > 0$
Backward branch of $W^s(E)$, $W^s b(E)$	$q_1 = 0, \quad p_1 < 0$
Forward branch of $W^u(E)$, $W^u_{\mathrm{f}}(E)$	$p_1 = 0, \quad q_1 > 0$
Backward branch of $W^u(E)$, $W^u_{\mathrm{b}}(E)$	$p_1 = 0, \quad q_1 < 0$
Forward reactive spherical cylinder $W_{\mathrm{f}}(E) \equiv W^s_{\mathrm{f}}(E) \cup W^u_{\mathrm{f}}(E)$	$p_1 q_1 = 0, \quad p_1, q_1 \geqslant 0, \quad q_1 \neq p_1$
Backward reactive spherical cylinder $W_{\mathrm{b}}(E) \equiv W^s_{\mathrm{b}}(E) \cup W^u_{\mathrm{b}}(E)$	$p_1 q_1 = 0, \quad p_1, q_1 \leqslant 0, \quad q_1 \neq p_1$
Forward reaction path	$q_2 = \ldots = q_d = p_2 = \ldots = p_d = 0, \quad p_1 > 0$
Backward reaction path	$q_2 = \ldots = q_d = p_2 = \ldots = p_d = 0, \quad p_1 < 0$

geometrical structures on trajectories of Hamilton's equations. In table 1 we summarize the results obtained thus far by providing a list of the different surfaces that control the evolution of trajectories from reactants to products in the neighbourhood U in figure 1.

However, all of these surfaces, and associated dynamical phenomena, are only 'locally valid' in the neighbourhood U. The next step is to understand their influence on the dynamics outside U, i.e. their influence on the dynamics of reaction throughout phase space in the original coordinates (as opposed to the normal form coordinates). In order to do this we will need the normal form transformation constructed in section 2 and given in (2.59), to order N (where N is determined according to the desired accuracy following the discussion in section 4.5). We rewrite (2.59) below:

$$\begin{aligned} z^{(1)} &= z - z_0, \\ z^{(2)} &= M z^{(1)}, \\ (q_1^{(N)}, \ldots, q_d^{(N)}, p_1^{(N)}, \ldots, p_d^{(N)}) \equiv z^{(N)} &= \Phi^1_{W_N} \circ \cdots \circ \Phi^1_{W_3}(z^{(2)}). \end{aligned} \tag{4.15}$$

We refer to the original coordinates as the 'physical coordinates' where reading from top to bottom, (4.15) describes the sequence of transformations from physical coordinates to normal form coordinates as follows. We translate the saddle-centre-...-centre equilibrium point to the origin, we 'simplify' the linear part of Hamilton's equations, then we iteratively construct a sequence of nonlinear coordinate transformations that successively 'simplify' the order 3, 4, ..., N terms of the Hamiltonian according to the algorithm described in section 2. We can invert each of these transformations to return from the normal form coordinates to the physical coordinates.

Computation of $W^u_{\mathrm{b}}(E)$ and $W^u_{\mathrm{f}}(E)$. Our approach to computing the stable and unstable manifolds of a NHIM is, in principle, the same as for computing the stable and unstable

manifolds of a hyperbolic trajectory (however, the practical implementation of the algorithm in higher dimensions is a different matter and one that deserves much more investigation).

We describe the computation of $W^u_{\rm f}(E)$ as follows.

- In the normal form coordinates, choose a distribution of initial conditions on the NHIM and displace these initial conditions 'slightly' in the direction of the forward branch of $W^u(E)$ ($p_1 = 0,\ q_1 = \varepsilon > 0, \varepsilon$ 'small').
- Map these initial conditions back into the physical coordinates using the inverse of the normal form transformation.
- Integrate the initial conditions forward in time using Hamilton's equations in the physical coordinates, for the desired length of time (typically determined by accuracy considerations) that will give the manifold of the desired 'size'. Since the initial conditions are in the unstable manifold they will leave the neighbourhood U in which the normal form transformation is valid (which is why we integrate them in the original coordinates with respect to the original equations of motion).

The backward branch of $W^u(E)$ can be computed in an analogous manner by displacing the initial conditions on the NHIM in the direction of the backward branch of $W^u(E)$ ($p_1 = 0,\ q_1 = \varepsilon < 0, \varepsilon$ 'small').

Computation of $W^s_{\rm b}(E)$ and $W^s_{\rm f}(E)$. The forward and backward branches of $W^s(E)$ can be computed in an analogous fashion, except the initial conditions are integrated *backward* in time.

Computation of the forward and backward reaction paths. Here the situation is, numerically, much simpler since we only have to integrate a trajectory. We consider the case of the forward reaction path. The backward reaction path is treated in the same way, after the obvious changes of sign for the appropriate quantities.

Recalling that the dividing surface in normal form coordinates is given by $q_1 = p_1$, the intersection of the forward reaction path with the dividing surface is given by

$$\begin{aligned} &q_2 = \ldots = q_d = p_2 = \ldots = p_d = 0, \\ &q_1^2 = I, q_1 = p_1 > 0, \qquad \text{with } K_{\rm CNF}(I, 0, \ldots, 0) = E. \end{aligned} \tag{4.16}$$

We transform this point in normal form coordinates into physical coordinates using the inverse of the transformations given in (4.15). Integrating this point forward in time using Hamilton's equations in the physical coordinates gives the forward reaction path immediately *after* passage through the dividing surface. Integrating the point backward in time gives the forward reaction path immediately *before* passage through the dividing surface.

Computation of reactive volumes. Consider a region of the energy surface of some fixed energy E whose entrance and exit channels are associated with saddle-centre-...-centre equilibrium points. Near each such equilibrium point we can construct a dividing surface that a trajectory of energy E must cross in order to enter the region. Suppose that the region is compact and simply connected. An example is the phase space region associated with the potential well that corresponds to an isomer in an isomerization reaction [WBW04b]. It is then possible to give a formula for the energy surface volume corresponding to trajectories of the energy E that will leave that region of the energy surface.

This formula is expressed in terms of the phase space flux across the dividing surfaces controlling access to this region of the energy surface and the corresponding 'mean first passage

times' of trajectories entering the region through the dividing surfaces. This theory is described in detail in [WBW05a, WBW05c] and here we just outline the results and show how the phase space structures discussed above in a region of the transition state are 'globalized' to give this result.

We consider an energy surface region to which entrance is possible only through a number of dividing surfaces, $B^{2d-2}_{\mathrm{ds,\,f};i}(E)$ (i is the index for the number of forward dividing surfaces that control access to the region under consideration in the sense that trajectories initialized on this surface and integrated in *forward* time enter the region), and we compute the *energy surface volume* of *reactive initial conditions*, i.e. the initial conditions of trajectories that can leave the region under consideration through one of the dividing surfaces. The phase space transport theory described above is crucial for this computation as it allows us to define entrance and exit channels *uniquely* in terms of dividing surfaces that have the property of 'no recrossing of trajectories' and minimal directional flux.

If the region under consideration is compact and connected it is a simple consequence of the Poincaré recurrence theorem [Arn78] that reactive initial conditions in the region lie (up to a set of measure zero, or 'zero volume') on trajectories which in the future escape from the region *and* in the past entered the region. Hence, for each point on a particular dividing surface hemisphere $B^{2d-2}_{\mathrm{ds,\,f};i}(E)$, there exists a time t (which depends on the point) for the trajectory starting at this point to spend in the region before it escapes through the same, or another, dividing surface. We define the *mean passage time associated with* $B^{2d-2}_{\mathrm{ds,\,f};i}(E)$ as

$$\langle t\rangle_{\mathrm{enter};i}(E) = \left(\int_{B^{2d-2}_{\mathrm{ds,\,f};i}(E)} t\,\Omega\right) \Big/ \left(\int_{B^{2d-2}_{\mathrm{ds,\,f};i}(E)} \Omega\right). \tag{4.17}$$

Here we use the more concise language of differential forms also used in section 4.4 to express the measure on the dividing surface over which we integrate the passage time. This measure is given by $\Omega = \omega^{d-1}/(d-1)!$, where ω denotes the canonical symplectic two-form $\sum_{k=1}^{d} \mathrm{d}p_k \wedge \mathrm{d}q_k$. It then follows from arguments analogous to those that lead to the so-called classical spectral theorem proven by Pollak in the context of bimolecular collisions [Pol81] that the energy surface volume of reactive initial conditions in an energy surface region is given by

$$\mathcal{V}_{\mathrm{react}}(E) = \sum_i \langle t\rangle_{\mathrm{enter};i}(E)\, f_{\mathrm{enter};i}(E), \tag{4.18}$$

where the summation runs over all dividing surfaces $B^{2d-2}_{\mathrm{ds,\,f};i}(E)$ controlling access to the region under consideration, and each entrance/exit channel contributes to the total reactive volume by the product of the associated mean passage time and the (directional) flux,

$$f_{\mathrm{enter};i}(E) = \int_{B^{2d-2}_{\mathrm{ds,\,f};i}(E)} \Omega. \tag{4.19}$$

The mean passage time for a given dividing surface hemisphere can be computed from a Monte Carlo sampling of that hemisphere. Performing such a sampling, uniformly with respect to the measure Ω, is straightforward in the normal form coordinates. The flux through a dividing surface hemisphere is also computed easily from the normal form as described in section 4.4. The efficiency of this procedure has been demonstrated for concrete examples in [WBW05a, WBW05c].

Practical considerations. By their very definition, invariant manifolds consist of trajectories, and the common way of computing them, and visualizing them, that works well in low dimensions is to integrate a distribution of initial conditions located on the invariant manifold

(hence, this illustrates the value of the normal form coordinates and transformation for locating appropriate initial conditions). In high dimensions there are numerical and algorithmic issues that have yet to be fully addressed. How does one choose a mesh on a $2d-3$ dimensional sphere? As this mesh evolves in time, how does one 'refine' the mesh in such a way that the evolved mesh maintains the structure of the invariant manifold?

4.7. The flux–flux autocorrelation function formalism for computing classical reaction probabilities

In the chemistry literature (see [YT60, MST83, Mil98a]) the accepted expression for the flux that goes into the expression for the classical reaction rate is given by

$$f(E) = \int_{\mathbb{R}^d}\int_{\mathbb{R}^d} \delta(E - H(q,p))F(q,p)P_{\mathrm{r}}(q,p)\,\mathrm{d}q\,\mathrm{d}p. \tag{4.20}$$

We want to explain the relation of this expression for the flux to the one derived in section 4.4. We begin by explaining the dynamical significance of each function in (4.20). The function $\delta(E-H)$ restricts the integration to the energy surface of energy E under consideration. The remaining functions in the integral are defined on the basis of a dividing surface which is defined as the zero level set of a function s, i.e. the dividing surface is given by

$$\{(q,p) \in \mathbb{R}^{2d} \,:\, s(q,p) = 0\}. \tag{4.21}$$

It is assumed that this surface divides the phase space into two components: a reactants component which has $s(q,p) < 0$ and a products component which has $s(q,p) > 0$. In the chemistry literature s is usually a function of q only, i.e. 'it is a dividing surface defined in configuration space.' However, it is crucial to note that this restriction is not important.

If we let Θ denote the Heaviside function (which is zero if its argument is negative and one if its argument is positive) then the composition $\Theta \circ s$ can be viewed as a characteristic function on phase space which vanishes on the reactants components and is identically one on the products component. The function F occurring in (4.20) at a point (q,p) is then defined as the time derivative of $\Theta \circ s(\Phi_H^t(q,p))$ at time $t=0$, i.e.

$$F(q,p) = \frac{\mathrm{d}}{\mathrm{d}t}\Theta \circ s(\Phi_H^t(q,p))|_{t=0} = \delta(s(q,p))\{s,H\}(q,p), \tag{4.22}$$

where $\{\cdot,\cdot\}$ again denotes the Poisson bracket. This means that F is a δ function in s that is weighted by the scalar product between the gradient of the surface s and the Hamiltonian vector field X_H,

$$F(q,p) = \delta(s(q,p))\langle \nabla s(q,p), X_H(q,p)\rangle. \tag{4.23}$$

Due to the function $\delta(s)$ in F the integral (4.20) is effectively restricted to the dividing surface (4.21), or if we also take into account the function $\delta(E-H)$, the integral (4.20) is effectively a $(2d-2)$-dimensional integral over the intersection of the dividing surface (4.21) with the energy surface of energy E. It is not difficult to see that if we disregard the factor P_{r} in (4.20), then the restriction of the resulting measure $\{s,H\}\,\mathrm{d}q\,\mathrm{d}p$ to the intersection of the dividing surface with the energy surface agrees with the measure Ω' that we defined in (4.13) in section 4.4. This implies that the expression for the flux (4.20) is invariant under symplectic coordinate transformations.

The function P_{r} in (4.20) is defined as

$$P_{\mathrm{r}}(q,p) = \lim_{t\to\infty} \Theta(s(\Phi_H^t(q,p))), \tag{4.24}$$

which evaluates to one if the trajectory with initial conditions (q,p) has $s(q(t),p(t)) > 0$ and hence proceeds to products for $t \to \infty$ and to zero otherwise. In this way the function P_{r}

in (4.20) acts as a characteristic function on the intersection of the dividing surface with the energy surface.

Equation (4.20) can be rewritten as

$$f(E) = \int_0^\infty C_F(t)\,\mathrm{d}t, \tag{4.25}$$

where

$$C_F(t) = \int_{\mathbb{R}^d}\int_{\mathbb{R}^d} \delta(E - H(q,p))F(q,p)F(q(t),p(t))\,\mathrm{d}q\,\mathrm{d}p, \tag{4.26}$$

which is referred to as the flux–flux autocorrelation function. This result is obtained using the identity

$$P_{\mathrm{r}}(q,p) = \int_0^\infty \frac{\mathrm{d}}{\mathrm{d}t}\Theta\circ s(\Phi_H^t(q,p))\,\mathrm{d}t = \int_0^\infty F(\Phi_H^t(q,p))\,\mathrm{d}t, \tag{4.27}$$

and changing the order of the time and phase space integrals. In (4.27) it is tacitly assumed that $\Theta(s(q,p)) = 0$, which means that if we want to use the form of P_{r} given in (4.27) in the integral (4.20) then it is assumed that $\Theta(s(q,p))$ evaluates to zero on the dividing surface. This means that one assumes that a trajectory with initial condition at a point (q,p) on the dividing surface (4.21) still requires an infinitesimal time to actually cross the dividing surface (4.21), i.e. more correctly (4.25) should be

$$f(E) = \lim_{\epsilon\to 0+}\int_{-\epsilon}^\infty C_F(t)\,\mathrm{d}t. \tag{4.28}$$

We emphasized this point since it is important for understanding the time dependence of the function C_F to which we come back below.

As stated in the chemistry literature (see, e.g., [Mil98a]) the equivalent expressions for the flux in (4.20) and (4.25) do not depend on the particular choice of the dividing surface. To see this recall that an arbitrarily chosen dividing surface will in general have the recrossing problem that we mentioned in section 4.1. This means that there are either

- 'nonreactive recrossings': nonreactive trajectories that cross the dividing surface, or
- 'reactive recrossings': reactive trajectories that cross the dividing surface more than once,

or both.

In fact reactive and nonreactive recrossings are independent, i.e. one can construct a dividing surface that only has nonreactive recrossings or only has reactive recrossings or has both (or no recrossings at all like the dividing surface that we construct). From the definition of the function P_{r} in (4.24) it is clear that those nonreactive recrossings that result from trajectories that approach the dividing surface from the side of reactants, cross the dividing surface (4.21) (two or an even number larger than two times) and return to the side of reactants do not contribute to the integral (4.20). In order to see that the factor P_{r} in the expression for the flux in (4.20) also takes care of nonreactive trajectories that approach the dividing surface from the products side and also of reactive recrossings one needs to note that $F(q,p)$ takes into account the direction in which a trajectory crosses the dividing surface: the sign of the scalar product between the Hamiltonian vector field and the gradient of the function s that defines the dividing surface depend on the direction in which the Hamiltonian vector field pierces the dividing surface (see (4.23)). In this way a family of nonreactive trajectories that approach the dividing surface from the products side crosses the dividing surface (4.21) (two or an even number larger than two times) and returns to the side of products will have a vanishing net contribution to the integral (4.20). Similarly, if a family of reactive trajectories crosses the dividing surface on its way from reactants to products n times (where n must be odd for the

trajectories to be reactive) then the net contribution of the first $n-1$ intersections of this family of trajectories to the integral (4.20) is zero. This can be rigorously proven using the methods described in [WW04] but we omit the details here.

The benefits that result from (4.20) formally not depending on the particular choice of the dividing surface are diminished by the fact that the implementation of the characteristic function P_r is computationally very expensive. In practice (i.e. in numerical computations) one cannot carry out the integration of Hamilton's equations to $t = \infty$ in order to evaluate P_r according to (4.24). Instead one attempts to truncate the integration after a finite time t_0 after which trajectories are *assumed* not to come back to the dividing surface. This is equivalent to assuming that the flux–flux autocorrelation function $C_F(t)$ is essentially zero for times $t > t_0$ such that the integral in (4.25) can be truncated at time t_0. A smaller time t_0 required for this assumption to hold means that the number of numerical computations required is reduced. This implies that some dividing surfaces are better suited for numerical computations than others [PM05], but this is generally not known *a priori*.

We note that our dividing surface is free of recrossings. In order to use expression (4.20) to get our result for the flux in (4.10) we define the function s according to $s(q, p) = q_1 - p_1$, where (q, p) are the normal form coordinates that we used in section 4.2. The delta function $\delta(E - H(q, p))$ in the integral (4.21) then restricts the integration to the isoenergetic dividing surface that we constructed in section 4.2. In our case P_r simply needs to effectively restrict the integral (4.21) to the forward reactive hemisphere of our dividing surface. We therefore set

$$P_\mathrm{r}(q, p) = \Theta(q_1 - p_1). \tag{4.29}$$

In this way we recover the expression for the flux that we have given in (4.10). It is crucial to note that in our case the evaluation of P_r does not require the integration of Hamilton's equations and is therefore computationally much cheaper than using (4.20) with P_r defined according to (4.24) for an arbitrarily chosen dividing surface. Equivalently, using the fact that in our case we have $F = \{H, P_\mathrm{r}\}$ it is easy to see that the flux–flux autocorrelation function $C_F(t)$ becomes the function $\delta(t)$ times our result for the flux given in (4.10). The time integration in (4.28) (or in its corrected version (4.28)) becomes trivial in our case. For an arbitrarily chosen dividing surface C_F will as a function of time gradually approach zero—in a monotonic or an oscillatory manner depending on the portions of reactive and nonreactive recrossings of the dividing surface (see, e.g., [PM05]).

5. Quantum reaction dynamics and cumulative reaction probabilities

As described in the introduction, in this section we develop the quantum version of the classical reaction rate theory developed in section 4. We especially emphasize the roles of the classical and quantum normal forms. In particular, the classical coordinates in this section are the normal form coordinates. Moreover, we will see that the classical phase space structures that are realized through the classical normal form the 'skeleton' on which the quantum dynamics evolves.

5.1. Quantum normal form

We consider a Hamilton operator whose principal symbol has an equilibrium point of saddle-centre-. . .-centre stability type. In section 3.4 we have shown how such a Hamilton operator can be transformed to quantum normal form to any desired order N of its symbol by conjugating it with suitable unitary transformations. The resulting Nth order quantum normal form $\hat{H}^{(N)}_{\mathrm{QNF}}$

is a polynomial of order $[N/2]$ in the operators

$$\hat{I} = \frac{\hbar}{\mathrm{i}}\left(q_1\frac{\mathrm{d}}{\mathrm{d}q_1} + \frac{1}{2}\right) \quad \text{and} \quad \hat{J}_k = -\frac{\hbar^2}{2}\frac{\mathrm{d}^2}{\mathrm{d}q_k^2} + \frac{1}{2}q_k^2, \qquad k = 2, \ldots, d, \tag{5.1}$$

i.e. $\hat{H}^{(N)}_{\mathrm{QNF}}$ is of the form

$$\hat{H}^{(N)}_{\mathrm{QNF}} = K^{(N)}_{\mathrm{QNF}}(\hat{I}, \hat{J}_2, \ldots, \hat{J}_d) = E_0 + \lambda\hat{I} + \omega_2\hat{J}_2 + \cdots + \omega_d\hat{J}_d + c\hbar + \text{higher order terms}, \tag{5.2}$$

where $c \in \mathbb{R}$ is a constant and the higher order terms are of order greater than one and less than $[N/2]$ in the operators $\hat{I}$ and $\hat{J}_k$, $k = 2, \ldots, d$.

From the structure of $\hat{H}^{(N)}_{\mathrm{QNF}}$ in (5.2) it follows that its eigenfunctions are products of the eigenfunctions of the individual operators in (5.1). This structure is the quantum manifestation of the integrability of the classical normal form described in section 2.3.2. In the classical case integrability leads to a particular simple form of Hamilton's equations which provides a complete understanding of the phase space structure and dynamics in a neighbourhood of the saddle-centre-. . .-centre equilibrium point. Similarly, we see that the quantum manifestation of classical integrability will lead to a simple structure for the corresponding quantum Hamilton operators in such a way that multidimensional problems are rendered 'solvable'.

The operators $\hat{J}_k$ are the Hamilton operators of one-dimensional harmonic oscillators (with unit frequency). Their eigenvalues are $\hbar(n_k + 1/2)$, $n_k \in \mathbb{N}_0$, and the corresponding eigenfunctions are given by

$$\psi_{n_k}(q_k) = \frac{1}{(\pi\hbar)^{1/4}\sqrt{2^{n_k}n_k!}}H_{n_k}\left(\frac{x}{\sqrt{\hbar}}\right)\mathrm{e}^{-\frac{q_k^2}{2\hbar}}, \tag{5.3}$$

where H_{n_k} is the n_kth Hermite polynomial [AS65, LL01].

We will choose the eigenfunctions of $\hat{I}$ in such a way that their product with the harmonic oscillator eigenfunctions (5.3) give incoming and outgoing scattering wavefunctions of the system described by the Hamilton operator in (5.2). For clarity, we start with the one-dimensional case.

5.2. Scattering states for one-dimensional systems

The scattering states and S-matrix associated with a saddle equilibrium point in a one-dimensional system have been studied in [CP94a, CP94b, CP99] and in the following we mainly follow their presentation.

For one-dimensional systems a Hamilton operator in quantum normal form is a polynomial function of the operator $\hat{I} = -\mathrm{i}\hbar(q\mathrm{d}/\mathrm{d}q + 1/2)$. The scattering states ψ_I are the eigenfunctions of $\hat{I}$, i.e. solutions of

$$\hat{I}\psi_I(q) \equiv -\mathrm{i}\hbar\left(q\frac{\mathrm{d}}{\mathrm{d}q} + \frac{1}{2}\right)\psi_I(q) = I\psi_I(q) \tag{5.4}$$

with eigenvalues $I \in \mathbb{R}$. Two solutions of this equation are given by

$$\begin{aligned}\psi_{I\mathrm{o;r}}(q) &= \Theta(-q)|q|^{-1/2+\mathrm{i}I/\hbar},\\ \psi_{I\mathrm{o;p}}(q) &= \Theta(\ \ q)|q|^{-1/2+\mathrm{i}I/\hbar},\end{aligned} \tag{5.5}$$

where Θ is the Heaviside function, and the index 'o' is for 'outgoing to' and 'r' and 'p' are for 'reactants' and 'products', respectively. The motivation for this notation becomes clear from viewing the solutions (5.5) as Lagrangian states, i.e. we rewrite them as

$$\psi_{I\mathrm{o;r/p}}(q) = A_{I\mathrm{o;r/p}}(q)\mathrm{e}^{\mathrm{i}\varphi_{I\mathrm{o;r/p}}(q)/\hbar}, \tag{5.6}$$

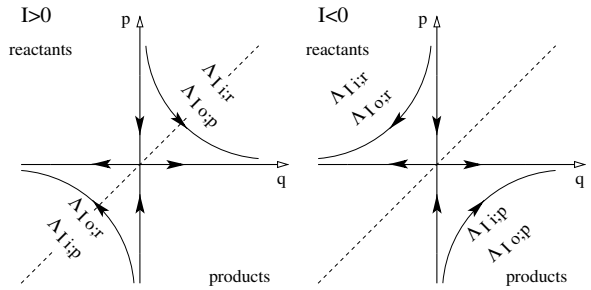

Figure 8. Lagrangian manifolds $\Lambda_{Io/i;r/p}$ associated with the wavefunctions $\psi_{Io/i;r/p}$. The arrows indicate the Hamiltonian vector field generated by $I = pq$.

where the amplitude and phase functions are given by

$$A_{Io;r/p}(q) = \Theta(\mp q)|q|^{-1/2}, \qquad \varphi_{Io;r/p}(q) = I \ln|q|, \tag{5.7}$$

respectively. This way we can associate the one-dimensional Lagrangian manifolds

$$\begin{aligned} \Lambda_{Io;r} &= \left\{(q,p) = \left(q, \frac{\mathrm{d}}{\mathrm{d}q}\varphi_{Io;r}(q)\right) = \left(q, \frac{I}{q}\right) : q < 0\right\}, \\ \Lambda_{Io;p} &= \left\{(q,p) = \left(q, \frac{\mathrm{d}}{\mathrm{d}q}\varphi_{Io;p}(q)\right) = \left(q, \frac{I}{q}\right) : q > 0\right\} \end{aligned} \tag{5.8}$$

with the states $\psi_{Io;r}$ and $\psi_{Io;p}$. From the presentation of $\Lambda_{Io;r}$ and $\Lambda_{Io;p}$ in figure 8 we see that for $q \to -\infty$, $\psi_{Io;r}$ is the outgoing state to reactants, and for $q \to +\infty$, $\psi_{Io;p}$ is the outgoing state to products.

We define another set of eigenfunctions of $\hat{I}$ which will correspond to incoming states by requiring their momentum representations to be given by

$$\bar{\psi}_{Ii;r}(p) = \psi^*_{Io;p}(p), \qquad \bar{\psi}_{Ii;p}(p) = \psi^*_{Io;r}(p). \tag{5.9}$$

Here '$*$' denotes complex conjugation. The corresponding position representations are obtained from the Fourier transforms of (5.9) giving

$$\begin{aligned} \psi_{Ii;r}(q) &= \frac{1}{\sqrt{2\pi\hbar}} \int \bar{\psi}_{Ii;r}(p) \mathrm{e}^{\frac{\mathrm{i}}{\hbar}qp}\,\mathrm{d}p = \frac{1}{\sqrt{2\pi\hbar}} \int_0^\infty p^{-1/2-\mathrm{i}I/\hbar} \mathrm{e}^{\frac{\mathrm{i}}{\hbar}qp}\,\mathrm{d}p, \\ \psi_{Ii;p}(q) &= \frac{1}{\sqrt{2\pi\hbar}} \int \bar{\psi}_{Ii;p}(p) \mathrm{e}^{\frac{\mathrm{i}}{\hbar}qp}\,\mathrm{d}p = \frac{1}{\sqrt{2\pi\hbar}} \int_{-\infty}^0 (-p)^{-1/2-\mathrm{i}I/\hbar} \mathrm{e}^{\frac{\mathrm{i}}{\hbar}qp}\,\mathrm{d}p. \end{aligned} \tag{5.10}$$

The integrals in (5.10) are not absolutely convergent, but can be defined as oscillatory integrals. The motivation for defining incoming states according to equation (5.9) becomes clear from considering the stationary phase contributions to the integrals (5.10). These come from the p satisfying

$$\frac{\mathrm{d}}{\mathrm{d}p}(-I \ln|p| + qp) = 0, \tag{5.11}$$

i.e. $p = I/q$, where $p > 0$ for $\psi_{Ii;r}$ and $p < 0$ for $\psi_{Ii;p}$. This way we can associate with the incoming states the Lagrangian manifolds

$$\begin{aligned} \Lambda_{Ii;r} &= \left\{(q,p) = \left(q, \frac{I}{q}\right) : p > 0\right\}, \\ \Lambda_{Ii;p} &= \left\{(q,p) = \left(q, \frac{I}{q}\right) : p < 0\right\}. \end{aligned} \tag{5.12}$$

These manifolds are also shown in figure 8 and we see that for $p \to +\infty$, $\psi_{I\mathrm{i;r}}$ is an incoming state from reactants and for $p \to -\infty$, $\psi_{I\mathrm{i;p}}$ is an incoming state from products.

In order to evaluate the integrals (5.10) we use the well-known formula

$$\int_0^\infty y^{z-1}\mathrm{e}^{-ky}\,\mathrm{d}y = \mathrm{e}^{-z\ln k}\Gamma(z). \tag{5.13}$$

This is valid for $\mathrm{Re}k > 0$, and we will use the analytic continuation to $\mathrm{Re}k = 0$, in which case the left-hand side is defined as an oscillatory integral. We then obtain

$$\psi_{I\mathrm{i;r}}(q) = \begin{cases} \dfrac{\mathrm{e}^{\mathrm{i}\frac{\pi}{4}}}{\sqrt{2\pi}}\mathrm{e}^{-\mathrm{i}\frac{I}{\hbar}\ln\hbar}\mathrm{e}^{\frac{\pi}{2}\frac{I}{\hbar}}\Gamma\left(\dfrac{1}{2}-\mathrm{i}\dfrac{I}{\hbar}\right)q^{-1/2+\mathrm{i}I/\hbar}, & q > 0, \\ \dfrac{\mathrm{e}^{-\mathrm{i}\frac{\pi}{4}}}{\sqrt{2\pi}}\mathrm{e}^{-\mathrm{i}\frac{I}{\hbar}\ln\hbar}\mathrm{e}^{-\frac{\pi}{2}\frac{I}{\hbar}}\Gamma\left(\dfrac{1}{2}-\mathrm{i}\dfrac{I}{\hbar}\right)(-q)^{-1/2+\mathrm{i}I/\hbar}, & q < 0. \end{cases} \tag{5.14}$$

This can be rewritten as

$$\psi_{I\mathrm{i;r}} = \frac{\mathrm{e}^{\mathrm{i}\frac{\pi}{4}}}{\sqrt{2\pi}}\mathrm{e}^{-\mathrm{i}\frac{I}{\hbar}\ln\hbar}\Gamma\left(\frac{1}{2}-\mathrm{i}\frac{I}{\hbar}\right)(\mathrm{e}^{\frac{\pi}{2}\frac{I}{\hbar}}\psi_{I\mathrm{o;p}} - \mathrm{i}\mathrm{e}^{-\frac{\pi}{2}\frac{I}{\hbar}}\psi_{I\mathrm{o;r}}). \tag{5.15}$$

In the same way we obtain

$$\psi_{I\mathrm{i;p}} = \frac{\mathrm{e}^{\mathrm{i}\frac{\pi}{4}}}{\sqrt{2\pi}}\mathrm{e}^{-\mathrm{i}\frac{I}{\hbar}\ln\hbar}\Gamma\left(\frac{1}{2}-\mathrm{i}\frac{I}{\hbar}\right)(\mathrm{e}^{\frac{\pi}{2}\frac{I}{\hbar}}\psi_{I\mathrm{o;r}} - \mathrm{i}\mathrm{e}^{-\frac{\pi}{2}\frac{I}{\hbar}}\psi_{I\mathrm{o;p}}). \tag{5.16}$$

For what follows in section 5.7 it is useful to discuss how the eigenfunctions $\psi_{I\mathrm{o;r/p}}$ and $\psi_{I\mathrm{i;r/p}}$ are related to the more standard eigenfunctions of the operator $\hat{I}$ in the Q-representation that we introduced in section 3.2 (see (3.36)–(3.38)).

The eigenvalue equation (5.4) then becomes

$$\hat{I}\chi_I(Q) = \left(-\frac{\hbar^2}{2}\frac{\mathrm{d}^2}{\mathrm{d}Q^2} - \frac{1}{2}Q^2\right)\chi_I(Q) = I\chi_I(Q). \tag{5.17}$$

Two solutions of this equation are given by

$$\chi_{I\pm}(Q) = \frac{1}{\sqrt{2\pi^2\hbar}}\left(\frac{1}{2\hbar}\right)^{1/4}\mathrm{e}^{\frac{I}{\hbar}\frac{\pi}{4}}\Gamma\left(\frac{1}{2}-\mathrm{i}\frac{I}{\hbar}\right)D_{-\frac{1}{2}+\mathrm{i}\frac{I}{\hbar}}\left(\pm\mathrm{e}^{-\mathrm{i}\frac{\pi}{4}}\sqrt{\frac{2}{\hbar}}Q\right), \tag{5.18}$$

where D_ν is the parabolic cylinder function [AS65, LL01]. In fact, the eigenfunctions $\psi_{I\mathrm{i;r/p}}$ are the images of $\chi_{I+/-}$ under the unitary transformation $\hat{U}_\mathrm{r}$ that we defined in (3.39), or equivalently

$$\chi_{I+} = \hat{U}_\mathrm{r}^*\psi_{I\mathrm{i;r}}, \qquad \chi_{I-} = \hat{U}_\mathrm{r}^*\psi_{I\mathrm{i;p}}. \tag{5.19}$$

This relationship is discussed in great detail in [Chr03a, Chr03b] where it is also shown that the pairs of eigenfunctions $\psi_{I\mathrm{i;r/p}}$, $\psi_{I\mathrm{o;r/p}}$ and $\chi_{I+/-}$ are orthogonal and fulfil the completeness relations

$$\begin{aligned} &\int_{\mathbb{R}}(\psi^*_{I\mathrm{i;r}}(q)\psi_{I\mathrm{i;r}}(q') + \psi^*_{I\mathrm{i;p}}(q)\psi_{I\mathrm{i;p}}(q'))\,\mathrm{d}I = \delta(q-q'), \\ &\int_{\mathbb{R}}(\psi^*_{I\mathrm{o;r}}(q)\psi_{I\mathrm{o;r}}(q') + \psi^*_{I\mathrm{o;p}}(q)\psi_{I\mathrm{o;p}}(q'))\,\mathrm{d}I = \delta(q-q'), \\ &\int_{\mathbb{R}}(\chi^*_{I+}(Q)\chi_{I+}(Q') + \chi^*_{I-}(Q)\chi_{I-}(Q'))\,\mathrm{d}I = \delta(Q-Q'). \end{aligned} \tag{5.20}$$

5.3. S-matrix and transmission probability for one-dimensional systems

The incoming and outgoing wavefunctions defined in section 5.2 are not independent. Each solution ψ_I of (5.4) can be written as a linear combination of $\psi_{I\mathrm{o;r/p}}$ or $\psi_{I\mathrm{i;r/p}}$,

$$\psi_I = \alpha_p \psi_{I\mathrm{o;p}} + \alpha_r \psi_{I\mathrm{o;r}}, \tag{5.21}$$

$$\psi_I = \beta_p \psi_{I\mathrm{i;p}} + \beta_r \psi_{I\mathrm{i;r}}. \tag{5.22}$$

These representations are connected by the S-matrix,

$$\begin{pmatrix} \alpha_p \\ \alpha_r \end{pmatrix} = \mathcal{S}(I) \begin{pmatrix} \beta_p \\ \beta_r \end{pmatrix}. \tag{5.23}$$

We can read off the entries of the S-matrix from (5.15) and (5.16) and obtain

$$\mathcal{S}(I) = \frac{\mathrm{e}^{\mathrm{i}\frac{\pi}{4}}}{\sqrt{2\pi}} \mathrm{e}^{-\mathrm{i}\frac{I}{\hbar}\ln\hbar} \Gamma\left(\frac{1}{2} - \mathrm{i}\frac{I}{\hbar}\right) \begin{pmatrix} -\mathrm{i}\mathrm{e}^{-\frac{\pi}{2}\frac{I}{\hbar}} & \mathrm{e}^{\frac{\pi}{2}\frac{I}{\hbar}} \\ \mathrm{e}^{\frac{\pi}{2}\frac{I}{\hbar}} & -\mathrm{i}\mathrm{e}^{-\frac{\pi}{2}\frac{I}{\hbar}} \end{pmatrix}. \tag{5.24}$$

Using the relation $\Gamma(1/2+\mathrm{i}y)\Gamma(1/2-\mathrm{i}y) = \pi/\cosh(\pi y)$ it is easy to see that $\mathcal{S}(I)^*\mathcal{S}(I) = 1$, i.e. $\mathcal{S}(I)$ is unitary.

From the S-matrix we can determine the transmission coefficient

$$\mathcal{T}(I) = |\mathcal{S}_{12}(I)|^2 = \frac{\mathrm{e}^{\pi\frac{I}{\hbar}}}{\mathrm{e}^{\pi\frac{I}{\hbar}} + \mathrm{e}^{-\pi\frac{I}{\hbar}}} = \frac{1}{1+\mathrm{e}^{-2\pi\frac{I}{\hbar}}} \tag{5.25}$$

and the reflection coefficient

$$\mathcal{R}(I) = |\mathcal{S}_{11}(I)|^2 = \frac{\mathrm{e}^{-\pi\frac{I}{\hbar}}}{\mathrm{e}^{\pi\frac{I}{\hbar}} + \mathrm{e}^{-\pi\frac{I}{\hbar}}} = \frac{1}{1+\mathrm{e}^{2\pi\frac{I}{\hbar}}}. \tag{5.26}$$

As required we have $\mathcal{T}(I) + \mathcal{R}(I) = 1$. We see that the relevant scale is $I/\hbar$. $\mathcal{T}$ tends to 1 if $I \gg \hbar$ and to 0 if $I \ll -\hbar$.

We can generalize this now easily to operators $\hat{H}_{\mathrm{QNF}} = K_{\mathrm{QNF}}(\hat{I})$, where K_{QNF} is a polynomial function of $\hat{I}$. In this case the incoming and outgoing states defined in section 5.2 are also eigenfunctions of $\hat{H}_{\mathrm{QNF}}$. We have

$$\hat{H}_{\mathrm{QNF}} \psi_{I\mathrm{i/o;r/p}} = E \psi_{I\mathrm{i/o;r/p}}, \tag{5.27}$$

where $E = K_{\mathrm{QNF}}(I)$ with I being the corresponding eigenvalue of $\hat{I}$. The expression for the S-matrix in (5.24) remains valid with I replaced by $I(E) := K_{\mathrm{QNF}}^{-1}(E)$, where we have to assume that the energy is close enough to the equilibrium energy so that $K_{\mathrm{QNF}}(E)$ is invertible. We thus obtain the S-matrix for the scattering problem described by the Hamilton operator $\hat{H}_{\mathrm{QNF}} = K_{\mathrm{QNF}}(\hat{I})$,

$$S(E) = \mathcal{S}(I(E)). \tag{5.28}$$

The corresponding transmission coefficient is given by

$$T(E) = \mathcal{T}(I(E)) = \frac{1}{1+\exp\left(-2\pi\dfrac{I(E)}{\hbar}\right)}, \tag{5.29}$$

and similarly the reflection coefficient is given by $R(E) = \mathcal{R}(I(E))$. This is a simple generalization of the previous example. However, it is a very important result because we see that we can use the quantum normal form to compute the local S-matrix and the transmission

and reflection coefficients to any desired order of the symbol of the Hamilton operator that describes the scattering problem.

5.4. S-matrix and cumulative reaction probability for multi-dimensional systems

We now consider the multi-dimensional case. In this case the Hamilton operator in quantum normal form is given by $\hat{H}_{\mathrm{QNF}} = K_{\mathrm{QNF}}(\hat{I}, \hat{J}_2, \ldots, \hat{J}_d)$, where K_{QNF} is a polynomial function, and $\hat{J}_k = (-\hbar^2\partial_{q_k}^2 + q_k^2)/2$, $k = 2, \ldots, d$, are one-dimensional harmonic oscillators. Let ψ_{n_k}, $n_k \in \mathbb{N}_0$, be the n_kth harmonic oscillator eigenfunction (5.3), i.e.

$$\hat{J}_k\psi_{n_k} = \hbar(n_k + 1/2)\psi_{n_k}. \tag{5.30}$$

Then the incoming and outgoing scattering states are given by

$$\begin{aligned}\psi_{(I,n_{\mathrm{sca}})\,\mathrm{i;r/p}}(q_1, \ldots, q_d) &= \psi_{I\mathrm{i;r/p}}(q_1)\psi_{n_2}(q_2)\cdots\psi_{n_d}(q_d),\\ \psi_{(I,n_{\mathrm{sca}})\,\mathrm{o;r/p}}(q_1, \ldots, q_d) &= \psi_{I\mathrm{o;r/p}}(q_1)\psi_{n_2}(q_2)\cdots\psi_{n_d}(q_d),\end{aligned} \tag{5.31}$$

where $n_{\mathrm{sca}} = (n_2, \ldots, n_d) \in \mathbb{N}_0^{d-1}$ is a $(d-1)$-dimensional vector of scattering quantum numbers.

The S-matrix connecting incoming to outgoing states is then block-diagonal with

$$S_{n_{\mathrm{sca}},m_{\mathrm{sca}}}(E) = \delta_{n_{\mathrm{sca}},m_{\mathrm{sca}}}\mathcal{S}(I_{n_{\mathrm{sca}}}(E)), \tag{5.32}$$

where $\delta_{n_{\mathrm{sca}},m_{\mathrm{sca}}}$ is the multi-dimensional Kronecker symbol, $\mathcal{S}(I)$ is given by (5.24) and $I_{n_{\mathrm{sca}}}(E)$ is determined by

$$K_{\mathrm{QNF}}(I_{n_{\mathrm{sca}}}(E), \hbar(n_2 + 1/2), \ldots, \hbar(n_d + 1/2)) = E. \tag{5.33}$$

We will assume that this equation has a unique solution $I_{n_{\mathrm{sca}}}(E)$, which is guaranteed if the energy is close enough to the equilibrium energy since K_{QNF} starts linearly in the actions, see (5.2).

We can now define the transition matrix T as the diagonal sub-block of the S-matrix which has the $(1, 2)$-components of the matrices in (5.32) on the diagonal, i.e.

$$T_{n_{\mathrm{sca}},m_{\mathrm{sca}}}(E) = \delta_{n_{\mathrm{sca}},m_{\mathrm{sca}}}\mathcal{S}_{1,2}(I_{n_{\mathrm{sca}}}(E)) = \delta_{n_{\mathrm{sca}},m_{\mathrm{sca}}}\left[1 + \exp\left(-2\pi\frac{I_{n_{\mathrm{sca}}}(E)}{\hbar}\right)\right]^{-1}. \tag{5.34}$$

The *cumulative reaction probability* $N(E)$ is then defined as (see, e.g., [Mil98a])

$$N(E) = \mathrm{Tr}T(E)T(E)^{\dagger}. \tag{5.35}$$

Using (5.34) we thus get

$$N(E) = \sum_{n_{\mathrm{sca}}} T_{n_{\mathrm{sca}},n_{\mathrm{sca}}}(E) = \sum_{n_{\mathrm{sca}}\in\mathbb{N}_0^{d-1}}\left[1 + \exp\left(-2\pi\frac{I_{n_{\mathrm{sca}}}(E)}{\hbar}\right)\right]^{-1}. \tag{5.36}$$

The cumulative reaction probability $N(E)$ is the quantum analogue of the classical flux $f(E)$ or, more precisely, of the dimensionless quantity $N_{\mathrm{Weyl}}(E) = f(E)/(2\pi\hbar)^{d-1}$ that we defined in equation (4.11) in section 4.4. To see this let us consider $N(E)$ in the semiclassical limit $\hbar \to 0$. To this end first note that

$$\left[1 + \exp\left(-2\pi I/\hbar\right)\right]^{-1} \to \Theta(I) \qquad \text{as } \hbar \to 0, \tag{5.37}$$

where Θ is the Heaviside function. This means that the transmission coefficients $T_{n_{\mathrm{sca}},n_{\mathrm{sca}}}(E)$ in (5.36) are essentially characteristic functions, i.e. in the semiclassical limit, $T_{n_{\mathrm{sca}},n_{\mathrm{sca}}}(E)$ is 0 or 1 if the solution of $K(I_{n_{\mathrm{sca}}}, \hbar(n_2 + 1/2), \ldots, \hbar(n_d + 1/2)) = E$ for $I_{n_{\mathrm{sca}}}$ is negative or

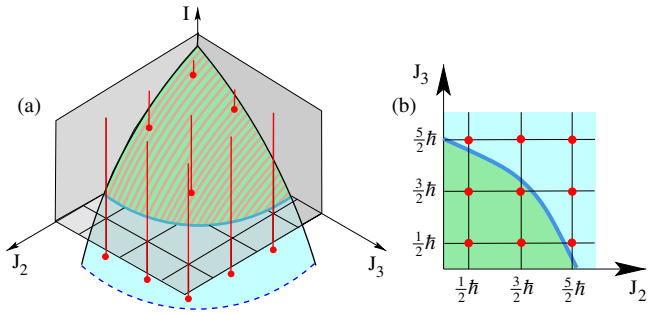

Figure 9. (*a*) Lines $(I, \hbar(n_2 + 1/2), \ldots, \hbar(n_d + 1/2))$, $I \in \mathbb{R}$, $n_k \in \mathbb{N}_0$, $k = 2, \ldots, d$, in the space $(I, J_2, \ldots, J_d) \in \mathbb{R} \times [0, \infty)^{d-1}$ for $d = 3$ and their intersections with the surface $K_{\mathrm{QNF}(I,J_2,J_3)} = E$. (*b*) Grid points $(\hbar(n_2 + 1/2), \ldots, \hbar(n_d + 1/2))$ in the space $(J_2, \ldots, J_d)$ for $d = 3$. The blue line marks the contour $K_{\mathrm{QNF}}(0, J_2, \ldots, J_d) = E$. In this plot only the scattering states for which the quantum numbers (n_2, n_3) have the values $(0, 0)$, $(0, 1)$, $(1, 0)$ or $(1, 1)$ correspond to 'open transmission channels', see text.

positive, respectively. This way the cumulative reaction probability can be considered to be a counting function. For a given energy E, it counts how many of the solutions $I_{n_{\mathrm{sca}}}$ of the equations $K_{\mathrm{QNF}}(I_{n_{\mathrm{sca}}}, \hbar(n_2 + 1/2), \ldots, \hbar(n_d + 1/2)) = E$ with scattering quantum numbers $n_{\mathrm{sca}} = (n_2, \ldots, n_d) \in \mathbb{N}_0^{d-1}$ are positive:

$$N(E) \to \#\{I_{n_{\mathrm{sca}}} > 0 \,:\, K_{\mathrm{QNF}}(I_{n_{\mathrm{sca}}}, \hbar(n_2 + \tfrac{1}{2}), \ldots, \hbar(n_d + \tfrac{1}{2})) = E,\ n_{\mathrm{sca}} \in \mathbb{N}_0^{d-1}\}, \qquad (5.38)$$

as $\hbar \to 0$. In other words, $N(E)$ can be considered to count the number of open 'transmission channels', where a transmission channel with quantum numbers n_{sca} is open if the corresponding transmission coefficient $T_{n_{\mathrm{sca}}, n_{\mathrm{sca}}}(E)$ is close to 1.

We can interpret $N(E)$ graphically as the number of grid points $(\hbar(n_2 + 1/2), \ldots, \hbar(n_d + 1/2))$ in the space of $(J_2, \ldots, J_d) \in [0, \infty)^{d-1}$ that are enclosed by the contour $K_{\mathrm{QNF}}(0, J_2, \ldots, J_d) = E$, see figure 9. The number of grid points is approximately given by the volume in the space of $(J_2, \ldots, J_d) \in [0, \infty)^{d-1}$ enclosed by $K_{\mathrm{QNF}}(0, J_2, \ldots, J_d) = E$ divided by $\hbar^{d-1}$. Using the fact that for $\hbar \to 0$, K_{QNF} becomes the function K_{CNF} which gives the classical energy as a function of the classical integrals $(I, J_2, \ldots, J_d)$ we find that the volume in the space of $(J_2, \ldots, J_d)$ enclosed by $K_{\mathrm{CNF}}(0, J_2, \ldots, J_d) = E$ is given by the classical flux $f(E)$ divided by $(2\pi)^{d-1}$, see (4.10) in section 4.4, and the cumulative reaction probability $N(E)$ is thus approximately given by $N_{\mathrm{Weyl}}(E) = f(E)/(2\pi\hbar)^{d-1}$ defined in (4.11) in section 4.4. This way we verified our statement in section 4.4 that $N_{\mathrm{Weyl}}(E)$ gives the mean number of open transmission channels. In fact, as mentioned in section 4.4, the classical flux $f(E)$ can be considered to be the phase space volume enclosed by the energy contour of energy E of the invariant subsystem which has one degree of freedom less than the full scattering system and which as the so-called activated complex is located between reactants and products. $N_{\mathrm{Weyl}}(E)$ counts how many elementary quantum cells of volume $(2\pi\hbar)^{d-1}$ fit into this phase space volume and this way gives the Weyl approximation of the cumulative reaction probability $N(E)$.

It is important to note here that like the flux in the classical case the cumulative reaction probability is determined by local properties of the Hamilton operator embodied in its symbol in the neighbourhood of the equilibrium point only. All one needs to know is the quantum normal form, which enters through the relation (5.33) and which determines $I_{n_{\mathrm{sca}}}(E)$.

5.5. Distribution of the scattering states in phase space

At the end of the previous section we have seen how the cumulative reaction probability is related to the classical flux. In this section we want to further investigate the quantum–classical correspondence by studying the distribution of the scattering states in phase space and relating these distributions to the classical phase space structures that control classical reaction dynamics as discussed in sections 4.1 and 4.2.

The standard tool to describe the phase space distribution of a wavefunction is the Wigner function, but since the scattering wavefunctions are not square-integrable the Wigner functions will be distributions. Therefore it is more convenient to study the phase space distribution in terms of their *Husimi representation* which is obtained from projecting the scattering states onto a coherent state basis (see [Har88, Bal98]) and this way leads to smooth functions. For a point $(q_0, p_0) \in \mathbb{R}^d \times \mathbb{R}^d$ we define a coherent state with wavefunction

$$\psi_{q_0,p_0}(q) = \frac{1}{(\pi\hbar)^{d/4}} \mathrm{e}^{\frac{\mathrm{i}}{\hbar}(\langle p_0,q\rangle - \langle q_0,p_0\rangle/2)} \mathrm{e}^{-\frac{1}{2\hbar}\langle q-q_0,q-q_0\rangle}. \tag{5.39}$$

This wavefunction is concentrated around $q = q_0$ and its Fourier transform, i.e. its momentum representation, is concentrated around $p = p_0$. In phase space the coherent state (5.39) is thus concentrated around (q_0, p_0). The Husimi function of a state ψ is now defined by the modulus square of the projection onto a coherent state,

$$H_\psi(q, p) := \frac{1}{(2\pi\hbar)^d} |\langle \psi_{p,q}, \psi\rangle|^2. \tag{5.40}$$

It has the important property that the expectation value of an operator $\mathrm{Op}[A]$ with respect to a state ψ is given by

$$\langle \psi, \mathrm{Op}[A]\psi\rangle = \iint_{\mathbb{R}^d\times\mathbb{R}^d} A(q, p) H_\psi(q, p)\, \mathrm{d}q\mathrm{d}p + O(\hbar). \tag{5.41}$$

Furthermore, we have $H_\psi(q, p) \geqslant 0$, i.e. the Husimi function can be considered to be a probability density on phase space and describes how a quantum state is distributed in phase space.

The Husimi functions of the scattering states $\psi_{(I,n_{\mathrm{sca}})\,\mathrm{i/o;r/p}}$ inherit the product structure (5.31), i.e. we have

$$H_{\psi_{(I,n_{\mathrm{sca}})\,\mathrm{i/o;r/p}}}(q_1, \ldots, q_d, p_1, \ldots, p_d) = H_{\psi_{I\mathrm{i/o;r/p}}}(q_1, p_1) H_{\psi_{n_2}}(q_2, p_2) \cdots H_{\psi_{n_d}}(q_d, p_d). \tag{5.42}$$

The Husimi functions of the eigenfunctions ψ_{n_k} of the one-dimensional harmonic oscillators $\hat{J}_k$ are well known (see, e.g., [KMW97]),

$$H_{\psi_{n_k}}(q_k, p_k) = \frac{1}{2\pi\hbar 2^{n_k} n_k!} \frac{(p_k^2 + q_k^2)^{n_k}}{\hbar^{n_k}} \mathrm{e}^{-\frac{p_k^2+q_k^2}{2\hbar}}. \tag{5.43}$$

The first three of these Husimi functions are shown in figure 10. They are concentrated on the circles $p_k^2 + q_k^2 = 2n_k\hbar$ and have an n_k-fold zero at the origin.

The computation of the Husimi functions for the one-dimensional scattering states $\psi_{I\mathrm{o;r/p}}$ in (5.5) can be found in [NV97] where it is shown that for the linear combination

$$\psi^{\alpha,\beta} = \alpha\psi_{I\mathrm{o;p}} + \beta\psi_{I\mathrm{o;r}}, \qquad \alpha, \beta \in \mathbb{C}, \tag{5.44}$$

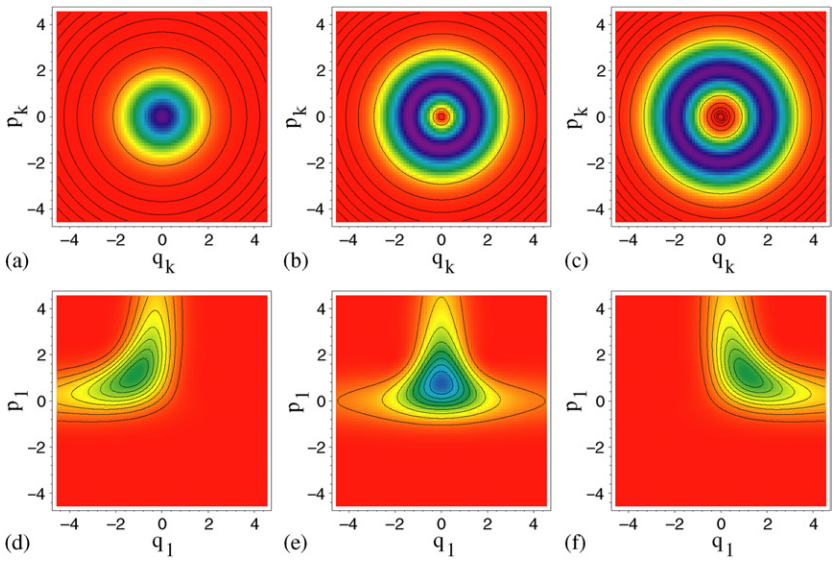

Figure 10. Contour plots of the harmonic oscillator Husimi functions $H_{\psi_{n_k}}$ in the (q_k, p_k)-plane for $n_k = 0$ (a), $n_k = 1$ (b) and $n_k = 2$ (c), and contour plots of the Husimi functions $H_{\psi_{I\,\mathrm{i;r}}}$ in the (q_1, p_1)-plane for $I = -1$ (d), $I = 0$ (e) and $I = 1$ (f). Red corresponds to low values; blue corresponds to high values. In (a)–(c) the spacing between the values of the contour lines is decreasing exponentially ($\hbar = 0.1$).

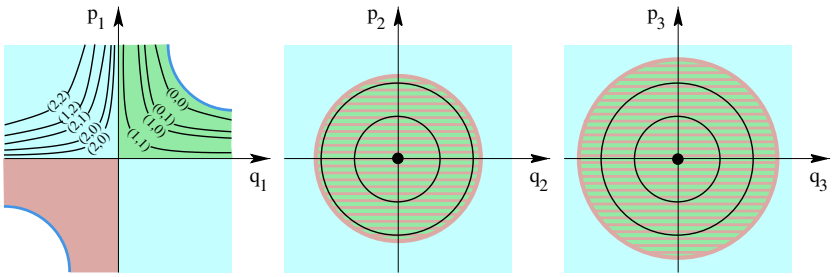

Figure 11. Projections of the Lagrangian manifolds $\Lambda_{(I,n_{\mathrm{sca}})\,\mathrm{i;r}}$ defined in equation (5.46) to the normal form coordinate planes for the same set-up as in figure 9. The scattering quantum numbers are $n_{\mathrm{sca}} = (n_2, n_3)$ with $0 \leqslant n_2, n_3 \leqslant 3$. For the values $(0, 0)$, $(0, 1)$, $(1, 0)$ and $(1, 1)$ of the quantum numbers (n_2, n_3), the Lagrangian manifolds $\Lambda_{\psi^{\mathrm{in}}_{n_{\mathrm{sca}}\,\mathrm{react}}}$ are contained in the energy surface volume (green region) enclosed by the forward reactive spherical cylinder $W_{\mathrm{f}}(E)$ defined in section 4. For the other values of the quantum numbers the Lagrangian manifolds $\Lambda_{(I,n_{\mathrm{sca}})\,\mathrm{i;r}}$ are located in the reactants component of the energy surface.

one gets

$$H_{\psi^{\alpha,\beta}}(q, p) = \frac{\sqrt{\pi}}{2\pi\hbar\cosh(\pi I/\hbar)} \mathrm{e}^{-\frac{1}{2\hbar}(p^2+q^2)} \left| \alpha D_{-\frac{1}{2}-\frac{\mathrm{i}I}{\hbar}}\left(-\frac{q-\mathrm{i}p}{\sqrt{\hbar}}\right) + \beta D_{-\frac{1}{2}-\frac{\mathrm{i}I}{\hbar}}\left(\frac{q-\mathrm{i}p}{\sqrt{\hbar}}\right)\right|^2, \tag{5.45}$$

where D_ν again denotes the parabolic cylinder function [AS65]. Figure 10 shows contour plots of the Husimi representation of the state $\psi_{I\,\mathrm{i;r}}$ for different values of the eigenvalue I. Here α and β in (5.44) are determined from (5.15). In accordance with the classical dynamics

where trajectories with $I < 0$ are nonreactive and trajectories with $I > 0$ are reactive, most of the state $\psi_{I\mathrm{i;r}}$ is reflected to the reactants side for $I < 0$ while it is transmitted mainly to the products side for $I > 0$. The borderline case between these two situations is given by $I = 0$. Here the state is localized in phase space at the hyperbolic equilibrium point with ridges along the reactants branches of the stable and unstable manifolds and the products branch of the unstable manifold.

Figure 10 indicates that the Husimi functions of the scattering states $\psi_{I\mathrm{i;r}}$ are localized on the Lagrangian manifolds

$$\Lambda_{(I,n_{\mathrm{sca}})\,\mathrm{i/o;r/p}} = \Lambda_{I\mathrm{i/o;r/p}} \times \Lambda_{n_2} \times \cdots \times \Lambda_{n_d}, \tag{5.46}$$

where the $\Lambda_{I\mathrm{i/o;r/p}}$ are defined in (5.8) and (5.12), and

$$\Lambda_{n_k} = \{(q_k, p_k) \in \mathbb{R}^2 \,:\, q_k^2 + p_k^2 = 2\hbar n_k\}, \qquad k = 2, \ldots, d, \tag{5.47}$$

are the Lagrangian manifolds associated with one-dimensional harmonic oscillator eigenfunctions. Quantum mechanics thus picks out those Lagrangian manifolds $\Lambda^{\pm}_{I,J_2,\ldots,J_d}$ foliating the classical phase space (see section 4.3) for which the actions, $J_2, \ldots, J_d$, fulfil Bohr–Sommerfeld quantization conditions. More precisely we find that the outgoing scattering states $\psi_{I;\mathrm{o;r/p}}$ are localized on the Lagrangian manifolds

$$\begin{aligned} \Lambda_{(I,n_{\mathrm{sca}})\,\mathrm{o;r}} &= \Lambda^{-}_{I,\hbar n_2,\ldots,\hbar n_d}, \\ \Lambda_{(I,n_{\mathrm{sca}})\,\mathrm{o;p}} &= \Lambda^{+}_{I,\hbar n_2,\ldots,\hbar n_d}, \end{aligned} \tag{5.48}$$

and the incoming scattering states $\psi_{I;\mathrm{i;r/p}}$ are localized on the Lagrangian manifolds

$$\begin{aligned} \Lambda_{(I,n_{\mathrm{sca}})\,\mathrm{i;r}} &= \begin{cases} \Lambda^{+}_{I,\hbar n_2,\ldots,\hbar n_d}, & I > 0, \\ \Lambda^{-}_{I,\hbar n_2,\ldots,\hbar n_d}, & I < 0, \end{cases} \\ \Lambda_{(I,n_{\mathrm{sca}})\,\mathrm{i;p}} &= \begin{cases} \Lambda^{-}_{I,\hbar n_2,\ldots,\hbar n_d}, & I > 0, \\ \Lambda^{+}_{I,\hbar n_2,\ldots,\hbar n_d}, & I < 0. \end{cases} \end{aligned} \tag{5.49}$$

The projection of the Lagrangian manifolds $\Lambda_{(I,n_{\mathrm{sca}})\,\mathrm{i/o;r/p}}$ to the centre planes (q_k, p_k), $k = 2, \ldots, d$, is thus restricted to the discrete circles $p_k^2 + q_k^2 = 2n_k\hbar$, $n_k \in \mathbb{N}_0$. If we fix the total energy E then this also entails a discretization of the projection of the manifolds (5.46) to the saddle plane (q_1, p_1) since the eigenvalue I needs to satisfy the energy equation $K_{\mathrm{QNF}}(I, \hbar(n_2 + 1/2), \ldots, \hbar(n_d + 1/2)) = E$. For the Lagrangian manifold $\Lambda_{(I,n_{\mathrm{sca}})\,\mathrm{i;r}}$ this is depicted in figure 11. Depending on whether I is positive or negative the Lagrangian manifold $\Lambda_{(I,n_{\mathrm{sca}})\,\mathrm{i;r}}$ is either located inside or outside the energy surface volume enclosed by the forward reactive spherical cylinder $W_{\mathrm{f}}(E)$ defined in section 4, and hence is either composed of reactive or nonreactive trajectories of the classical dynamics. From our discussion at the end of section 5.4 it then follows that the cumulative reaction probability $N(E)$ is approximately given by the total number of Lagrangian manifolds $\Lambda_{(I,n_{\mathrm{sca}})\,\mathrm{i;r}}$ which, for scattering quantum numbers $n_{\mathrm{sca}} = (n_2, \ldots, n_d) \in \mathbb{N}_0^{d-1}$, are located inside the energy surface volume enclosed by $W_{\mathrm{f}}(E)$.

5.6. The global S-matrix

It is important to emphasize again that, so far, our approach to quantum reaction dynamics has been local, i.e. it is derived completely from the properties of the quantum normal form that is valid in the neighbourhood of the saddle-centre-. . .-centre equilibrium point. The property

of the resulting S-matrix in (5.32) being block-diagonal reflects the fact that the quantum normal form is integrable in the sense that the basis of scattering states can be chosen in the product form (5.31). In a different basis the matrix will lose this feature, and phenomena like mode mixing are related to how other incoming and outgoing scattering states are related to this special basis. It is natural to embed the study of this phenomenon in a study of the global dynamics which we will describe in this section. The global formalism is in particular required in order to compute general state-to-state reaction rates.

Let us start by describing the scattering or reaction process in classical mechanics by using Poincaré sections. Recall that a Poincaré section at energy E is given by a smooth hypersurface $\Sigma(E)$ of the energy surface with energy E which is transversal to the flow ($\Sigma(E)$ is allowed to have several components). If we have two such Poincaré sections $\Sigma_1(E)$ and $\Sigma_2(E)$ such that all the flow lines intersecting $\Sigma_1(E)$ intersect at a later time $\Sigma_2(E)$, too, then moving along the flow from $\Sigma_1(E)$ to $\Sigma_2(E)$ defines a Poincaré map

$$P^{(2,1)}(E) : \Sigma_1(E) \to \Sigma_2(E). \tag{5.50}$$

Such Poincaré maps can be composed. If $\Sigma_3(E)$ is another Poincaré section which lies behind $\Sigma_2(E)$ in the sense that the flow lines that intersect $\Sigma_2(E)$ also intersect $\Sigma_3(E)$ at a later time, and if $P^{(3,2)}(E) : \Sigma_2(E) \to \Sigma_3(E)$ is the corresponding Poincaré map, then the Poincaré map

$$P^{(3,1)}(E) : \Sigma_1(E) \to \Sigma_3(E) \tag{5.51}$$

is given by

$$P^{(3,1)}(E) = P^{(3,2)}(E) \circ P^{(2,1)}(E). \tag{5.52}$$

Using this construction we can describe transport through phase space regions by a sequence of maps. Given some Poincaré section $\Sigma_{\text{initial}}(E)$ located in the area of initial points in the reactants region where we prepare the system and a Poincaré section $\Sigma_{\text{final}}(E)$ in the products region where we measure the outcome, a succession of Poincaré maps

$$\Sigma_{\text{initial}}(E) \to \Sigma_1(E) \to \Sigma_2(E) \to \cdots \to \Sigma_{\text{final}}(E) \tag{5.53}$$

tells us how the initial points are transported through the system[14].

The advantage of subdividing the flow into a sequence of maps lies in the fact that different regions in phase space might need different techniques to compute the flow. In our case of interest Poincaré sections can be constructed to the products and reactants side of a saddle-centre-. . .-centre equilibrium point. The dynamics 'across' this equilibrium point can then be described by the normal form while the dynamics between neighbourhoods of different saddle points can be obtained from integrating the original equations of motions [Cre04, Cre05, WBW05b]. Moreover, the phase space structures obtained from the local normal form can be 'globalized' following the discussion in section 4.6.

A similar procedure can be developed in the quantum case. The Poincaré maps

$$P^{(j,i)}(E) : \Sigma_i(E) \to \Sigma_j(E) \tag{5.54}$$

are symplectic maps, and as such can be quantized using the theory of Fourier integral operators. The quantizations will be unitary operators which we interpret as local S-matrices,

$$S^{(j,i)}(E) : L^2_{\Sigma_i(E)} \to L^2_{\Sigma_j(E)}, \tag{5.55}$$

[14] We here ignore the difficulties involved in constructing global Poincaré sections (see, e.g., [DW95]); we assume that the sequence of Poincaré sections (5.53) is intersected transversally by the trajectories with initial points from a suitable open subset in the reactants region.

where $L^2_{\Sigma(E)}$ is a Hilbert space obtained by geometric quantization of $\Sigma(E)$, see, e.g., [Kir01]. This is similar to the quantization developed in [Bog92]. As in classical dynamics we can compose these matrices to obtain a global S-matrix

$$S^{(\text{final,initial})}(E) = S^{(\text{final},n)}(E)S^{(n,n-1)}(E)\cdots S^{(1,\text{initial})}(E), \tag{5.56}$$

which tells us how initial states in $L^2_{\Sigma_{\text{initial}}(E)}$ are transformed into final states in $L^2_{\Sigma_{\text{final}}(E)}$. The reasons for introducing this splitting of the S-matrix are the same as in the classical case. We can employ different techniques for computing the S-matrices according to different local properties of the system. Near equilibrium points the dynamics can be described by the quantum normal form we developed in this paper. Notice that the neighbourhoods of the saddle-centre-...-centre equilibrium points are the regions where we expect quantum effects to be of most importance due to partial reflection at and tunnelling through the barriers associated with saddle points. The quantum transport between neighbourhoods of different equilibrium points can be described by a standard van Vleck type formalism, using, e.g., *initial value representations* (IVRs) which are very common in theoretical chemistry (see, e.g., [Mil98a, Mil98b] for references).

5.7. The flux–flux autocorrelation function formalism to compute quantum reaction probabilities

The main approach to computing quantum mechanical reaction rates that is most heavily pursued in the chemistry literature is the quantum version of the flux–flux autocorrelation function formalism that we reviewed in section 4.7. This approach was developed by Miller and others (see [YT60, MST83, Mil98a]) and in the following we will mainly follow their presentation. We will see that the cumulative reaction probability $N(E)$ is the quantum mechanical flux through a dividing surface and hence is the analogue of the classical flux. The goals of this section are twofold. Firstly, we will show that we recover our result for the cumulative reaction probability in (5.36) when we evaluate the quantum flux–flux autocorrelation function expression for the cumulative reaction probability $N(E)$ in terms of the quantum normal form and for our choice of the dividing surface that we discussed in section 4. This way will ensure that the flux–flux autocorrelation function formalism and our result for the cumulative reaction probability are formally equivalent and hence, our result for $N(E)$ can be viewed as a quantum mechanical flux through a dividing surface. Secondly, we will argue that, as in the classical case, the application of the flux–flux autocorrelation formalism in its original form, which does not depend on the specific choice of a dividing surface, is computationally much more expensive than our quantum normal form approach.

Following [YT60, MST83, Mil98a], a quantization of the flux–flux autocorrelation function formalism in section 4.7, or more precisely of the dimensionless quantity

$$N_{\text{Weyl}}(E) = f(E)/(2\pi\hbar)^{d-1} = 2\pi\hbar \int_{\mathbb{R}^d}\int_{\mathbb{R}^d} \delta(E - H)F P_{\text{r}} \frac{\mathrm{d}q\,\mathrm{d}p}{(2\pi\hbar)^d} \tag{5.57}$$

is obtained by replacing the classical phase space integral in (5.57) by the trace of the associated operators in the form

$$N(E) = 2\pi\hbar\,\mathrm{Tr}\,\delta(E - \hat{H})\hat{F}\hat{P}_{\text{r}}. \tag{5.58}$$

Following the quantum–classical correspondence principle the operator $\hat{F}$ is obtained from its classical counterpart F by replacing the Poisson bracket in the classical expression $F = \{\Theta(s), H\}$ by the corresponding commutator to give

$$\hat{F} = -\frac{\mathrm{i}}{\hbar}[\widehat{\Theta(s)}, \hat{H}]. \tag{5.59}$$

Here $\widehat{\Theta(s)}$ is a quantization (to which we will come back below) of the composition of the Heaviside function with a function s that defines the dividing surface according to $s(q, p) = 0$ as discussed in section 4.7. Similarly, the quantization of the projection function $P_\mathrm{r} = \lim_{t\to\infty} \Theta(s(\Phi^t))$ in (4.24) is given by the operator

$$\hat{P}_\mathrm{r} = \lim_{t\to\infty} \mathrm{e}^{\frac{\mathrm{i}}{\hbar}\hat{H}t}\widehat{\Theta(s)}\mathrm{e}^{-\frac{\mathrm{i}}{\hbar}\hat{H}t}. \tag{5.60}$$

The application of $\hat{P}_\mathrm{r}$ to a state ψ is thus obtained from taking the limit $t \to \infty$ in the process of letting the time evolution operator, $\exp(-\frac{\mathrm{i}}{\hbar}\hat{H}t)$, act on ψ for the time t, then apply $\widehat{\Theta(s)}$ to determine whether ψ has evolved to products after time t (see below for the details) and then evolve the state ψ backward in time by applying the inverse of the time evolution operator, $\exp(\frac{\mathrm{i}}{\hbar}\hat{H}t)$. In fact, the operator $\hat{P}_\mathrm{r}$ is given by the limit $t \to \infty$ of the Heisenberg picture of the operator $\widehat{\Theta(s)}$.

Using

$$\hat{P}_\mathrm{r} = \int_0^\infty \frac{\mathrm{d}}{\mathrm{d}t}\left(\mathrm{e}^{\frac{\mathrm{i}}{\hbar}\hat{H}t}\widehat{\Theta(s)}\mathrm{e}^{-\frac{\mathrm{i}}{\hbar}\hat{H}t}\right)\mathrm{d}t = \int_0^\infty \mathrm{e}^{\frac{\mathrm{i}}{\hbar}\hat{H}t}\hat{F}\mathrm{e}^{-\frac{\mathrm{i}}{\hbar}\hat{H}t}\,\mathrm{d}t, \tag{5.61}$$

we find that analogously to (4.25) the cumulative reaction probability can be rewritten as an autocorrelation function[15]:

$$N(E) = 2\pi\hbar\int_0^\infty C_{\hat{F}}(t)\,\mathrm{d}t, \tag{5.62}$$

where

$$C_{\hat{F}}(t) = \mathrm{Tr}\,\delta(E - \hat{H})\hat{F}\mathrm{e}^{\frac{\mathrm{i}}{\hbar}\hat{H}t}\hat{F}\mathrm{e}^{-\frac{\mathrm{i}}{\hbar}\hat{H}t}. \tag{5.63}$$

We illustrate the application of the flux–flux autocorrelation function formalism in the following sections.

5.7.1. Example: 1D parabolic barrier. As a first example we consider a one-dimensional system and a surface defined according to $s(q, p) = q - q_0 = 0$. In the position representation the quantization of the function $\Theta(s)$ is then defined by its action on a wavefunction $\psi(q)$ according to

$$\widehat{\Theta(s)}\psi(q) = \Theta(q - q_0)\psi(q). \tag{5.64}$$

A state ψ thus is an eigenfunction with eigenvalue 1 of the operator $\hat{P}_\mathrm{r}$ if its wavefunction $\psi(q)$ is concentrated in $q > q_0$ if evolved forward in time to time $t = \infty$. Likewise, ψ is an eigenfunction with eigenvalue 0 of the operator $\hat{P}_\mathrm{r}$ if its wavefunction $\psi(q)$ is concentrated in $q < q_0$ if evolved forward in time to time $t = \infty$. For a Hamilton operator of type 'kinetic plus potential', $\hat{H} = \frac{1}{2m}\hat{p}^2 + V(\hat{q})$, with the quantization of the operators $\hat{q}$ and $\hat{p}$ given in (3.38), the operator $\hat{F}$ becomes

$$\begin{aligned}\hat{F} &= -\frac{\mathrm{i}}{\hbar}[\hat{\Theta(s)}, \hat{H}] = -\frac{\mathrm{i}}{\hbar}[\hat{\Theta(s)}, \frac{1}{2m}\hat{p}^2] = -\frac{\mathrm{i}}{\hbar}\frac{1}{2m}(\hat{p}[\hat{\Theta(s)}, \hat{p}] + [\hat{\Theta(s)}, \hat{p}]\hat{p}) \\ &= \frac{1}{2m}(\hat{p}\delta(q_0) + \delta(q_0)\hat{p}).\end{aligned} \tag{5.65}$$

[15] Formally equation (5.61) still contains a term $\widehat{\Theta(s)}$. But this term will give no contribution to $N(E)$ for the same reason as in the classical flux–flux autocorrelation formalism (see the discussion after (4.27)). In the examples below this can be seen explicitly since we define the operator $\widehat{\Theta(s)}$ in normal form coordinates as a multiplication operator by a characteristic function. Then the same reasoning as in the classical case applies.

For the expectation value of $\hat{F}$ with respect to a state ψ we thus get[16]

$$\langle\psi|\hat{F}|\psi\rangle = -\mathrm{i}\frac{\hbar}{2m}(\psi^*(q_0)\psi'(q_0) - \psi'^*(q_0)\psi(q_0)), \tag{5.66}$$

where the primes denote the derivatives. This agrees with the standard definition of the quantum probability current density that can be found in any quantum mechanics textbook (see, e.g., [LL01]).

To make the example more concrete we consider a parabolic barrier described by the Hamilton operator

$$\hat{H} = -\frac{\hbar^2}{2m}\frac{\mathrm{d}^2}{\mathrm{d}q^2} - \frac{1}{2}m\lambda^2 q^2. \tag{5.67}$$

The spectrum of $\hat{H}$ is $\mathbb{R}$. We choose energy eigenfunctions $\psi_{E\pm}$ such that they correspond to wavefunctions moving in the positive and negative q directions, respectively, i.e. besides

$$\hat{H}\psi_{E\pm} = E\psi_{E\pm} \tag{5.68}$$

we have

$$\hat{P}_\mathrm{r}\psi_{E+} = \psi_{E+}, \qquad \hat{P}_\mathrm{r}\psi_{E-} = 0. \tag{5.69}$$

For the trace (5.58) to be well defined we need to require that the states $\psi_{E\pm}$ are normalized in such a way that they satisfy the completeness relation

$$\int_{\mathbb{R}} (\psi^*_{E+}(q)\psi_{E+}(q') + \psi^*_{E-}(q)\psi_{E-}(q'))\,\mathrm{d}E = \delta(q-q'). \tag{5.70}$$

The eigenfunctions $\psi_{E\pm}$ having the properties (5.69) and (5.70) are given by

$$\psi_{E\pm}(q) = \frac{1}{\sqrt{2\pi^2\hbar}}\left(\frac{m}{2\hbar\lambda}\right)^{1/4} \mathrm{e}^{\frac{E}{\lambda\hbar}\frac{\pi}{4}}\Gamma\left(\frac{1}{2} - \mathrm{i}\frac{E}{\hbar\lambda}\right) D_{-\frac{1}{2}-\mathrm{i}\frac{E}{\hbar\lambda}}\left(\pm\mathrm{e}^{-\mathrm{i}\frac{\pi}{4}}\sqrt{\frac{2m\lambda}{\hbar}}q\right), \tag{5.71}$$

where D_ν again denotes the parabolic cylinder function [AS65]. In fact, the wavefunctions $\psi_{E\pm}$ can be obtained from a suitable scaling of the wavefunctions $\chi_{I\pm}$ that we defined in (5.18) and which satisfy the completeness relations (5.20). For $\psi_{E\pm}$, we have

$$-\mathrm{i}\frac{\hbar}{2m}(\psi^*_{E\pm}\psi'_{E\pm} - \psi'^*_{E\pm}\psi_{E\pm}) = \pm\frac{1}{2\pi\hbar}\frac{1}{1+\mathrm{e}^{-2\pi E/(\lambda\hbar)}}, \tag{5.72}$$

and hence using (5.66) and (5.69) we get for the cumulative reaction probability,

$$\begin{aligned} N(E) &= 2\pi\hbar\mathrm{Tr}\delta(E-\hat{H})\hat{F}\hat{P}_\mathrm{r} \\ &= 2\pi\hbar\int_{\mathbb{R}}(\langle\psi_{E'+}|\delta(E-\hat{H})\hat{F}\hat{P}_\mathrm{r}|\psi_{E'+}\rangle + \langle\psi_{E'-}|\delta(E-\hat{H})\hat{F}\hat{P}_\mathrm{r}|\psi_{E'-}\rangle)\,\mathrm{d}E' \\ &= 2\pi\hbar\int_{\mathbb{R}}\delta(E-E')\langle\psi_{E'+}|\hat{F}|\psi_{E'+}\rangle\,\mathrm{d}E' = \frac{1}{1+\mathrm{e}^{-2\pi E/(\lambda\hbar)}}, \end{aligned} \tag{5.73}$$

which is the exact quantum mechanical reflection coefficient for a parabolic barrier [LL01].

We now want to repeat the calculation above by inserting for $\hat{H}$ the quantum normal form of the parabolic barrier in (5.58). This will show two things. Firstly, this will lead to our result for the cumulative reaction probability $N(E)$ that we have given in (5.36) (which for the one-dimensional case reduces the reflection coefficient derived in section 5.3). Secondly, we will see that our result agrees with $N(E)$ in (5.73), i.e. our result for $N(E)$ in terms of the quantum normal form is exact for parabolic barriers.

[16] In the following it will be notationally more convenient to use the Dirac notation for scalar products. Here $\langle\psi|A|\psi\rangle$ is the same as $\langle\psi, A\psi\rangle$ for any operator A and state ψ.

From our discussion in section 3.5 it follows that the quantum normal form of (5.67) is given by

$$\hat{H}_{\mathrm{QNF}} = K_{\mathrm{QNF}}(\hat{I}) = \lambda \hat{I}. \tag{5.74}$$

In order to evaluate (5.58) for our dividing surface which in terms of the normal form coordinates is given by $s(q, p) = q - p = 0$ (see section 4.2) it is convenient to work with the rotated coordinates

$$(Q, P) = \frac{1}{\sqrt{2}}(q - p, q + p). \tag{5.75}$$

The Q representation of the operator $\widehat{\Theta(s)}$ is then defined analogously to (5.64), i.e.

$$\widehat{\Theta(s)}\psi(Q) = \Theta(Q)\psi(Q). \tag{5.76}$$

As we have seen in the example of the application of lemma 6 (exact Egorov) in section 3.2 the Q representation of the operator $\hat{I}$ reads

$$\hat{I} = -\frac{\hbar^2}{2}\frac{\mathrm{d}^2}{\mathrm{d}Q^2} - \frac{1}{2}Q^2 \tag{5.77}$$

(see equation (3.38)). In section 5.2 we showed that the eigenfunctions of (5.77) are given by $\chi_{I\pm}$ defined in (5.18). In fact, the eigenfunctions $\chi_{I\pm}$ formally agree with the eigenfunctions $\psi_{E\pm}$ in (5.71) if m and λ are replaced by 1 and E is replaced by I. Analogously to (5.65) we have

$$-\frac{\mathrm{i}}{\hbar}[\widehat{\Theta(s)}, \hat{I}] = \frac{1}{2}(\hat{P}\delta(Q) + \delta(Q)\hat{P}), \tag{5.78}$$

and for an arbitrary state ψ,

$$\langle\psi| - \frac{\mathrm{i}}{\hbar}[\widehat{\Theta(s)}, \hat{I}]|\psi\rangle = -\mathrm{i}\frac{\hbar}{2}(\psi^*(0)\psi'(0) - \psi'^*(0)\psi(0)). \tag{5.79}$$

Evaluating this expression for the eigenfunctions $\chi_{I\pm}$ we get

$$-\mathrm{i}\frac{\hbar}{2}(\chi^*_{I\pm}\chi'_{I\pm} - \chi'^*_{I\pm}\chi_{I\pm}) = \pm\frac{1}{2\pi\hbar}\frac{1}{1 + \mathrm{e}^{-2\pi I/\hbar}}. \tag{5.80}$$

Using this result and the fact that χ_{I+} and χ_{I-} are moving in positive and negative Q directions and hence are eigenfunctions of $\hat{P}_{\mathrm{r}}$ with eigenvalues 1 and 0, respectively, we get

$$\begin{aligned} N(E) &= 2\pi\hbar \mathrm{Tr}\delta(E - K_{\mathrm{QNF}}(\hat{I}))\hat{F}\hat{P}_{\mathrm{r}} \\ &= 2\pi\hbar\int_{\mathbb{R}} \left(\langle\chi_{I+}|\delta(E - K_{\mathrm{QNF}}(\hat{I}))\hat{F}\hat{P}_{\mathrm{r}}|\chi_{I+}\rangle + \langle\chi_{I-}|\delta(E - K_{\mathrm{QNF}}(\hat{I}))\hat{F}\hat{P}_{\mathrm{r}}|\chi_{I-}\rangle\right)\mathrm{d}I \\ &= 2\pi\hbar\int_{\mathbb{R}} \delta(E - K_{\mathrm{QNF}}(I))\lambda\langle\chi_{I+}| - \frac{\mathrm{i}}{\hbar}[\widehat{\Theta(s)}, \hat{I}]|\chi_{I+}\rangle\,\mathrm{d}I = \frac{1}{1 + \mathrm{e}^{-2\pi E/(\lambda\hbar)}}. \end{aligned} \tag{5.81}$$

This formally agrees with the expression for $N(E)$ that we have given in (5.36) and also with the exact result in (5.73), i.e. our quantum normal form computation of $N(E)$ is exact for parabolic barriers.

5.7.2. Example: general barriers in 1D. Let us now use the quantum normal form in the flux–flux autocorrelation formalism in the more general case of a one-dimensional system with a Hamilton operator whose principal symbol has a saddle equilibrium point but is not necessarily quadratic. As in the previous section we again work in the Q representation, i.e. our

dividing surface is defined by $s(Q, P) = Q = 0$, and the operators $\widehat{\Theta(s)}$ and $\hat{I}$ are defined by (5.76) and (5.77), respectively. In order to evaluate (5.58) for a general Hamilton operator in quantum normal form, $\hat{H}_{\mathrm{QNF}} = K_{\mathrm{QNF}}(\hat{I})$, where $K_{\mathrm{QNF}}(\hat{I})$ is a polynomial in $\hat{I}$, we use that for $n \in \mathbb{N}$, we have

$$[\widehat{\Theta(s)}, \hat{I}^n] = \sum_{k=0}^{n-1} \hat{I}^{n-k-1} [\widehat{\Theta(s)}, \hat{I}] \hat{I}^k. \tag{5.82}$$

This can be shown by direct calculation. For the eigenfunction $\chi_{I\pm}$ of $\hat{I}$ we thus have

$$\langle \chi_{I\pm} | [\widehat{\Theta(s)}, \hat{I}^n] | \chi_{I\pm} \rangle = \langle \chi_{I\pm} | [\widehat{\Theta(s)}, \hat{I}] | \chi_{I\pm} \rangle n I^{n-1}, \tag{5.83}$$

and hence

$$\langle \chi_{I\pm} | [\widehat{\Theta(s)}, K_{\mathrm{QNF}}(\hat{I})] | \chi_{I\pm} \rangle = \langle \chi_{I\pm} | [\widehat{\Theta(s)}, \hat{I}] | \chi_{I\pm} \rangle \frac{\mathrm{d}K_{\mathrm{QNF}}(I)}{\mathrm{d}I}. \tag{5.84}$$

Using this together with (5.79) and (5.80) we find that the cumulative reaction probability is given by

$$\begin{aligned} N(E) &= 2\pi\hbar \left(\langle \chi_{I+} | \delta(E - K_{\mathrm{QNF}}(\hat{I})) \hat{F} \hat{P}_{\mathrm{r}} | \chi_{I+} \rangle + \langle \chi_{I-} | \delta(E - K_{\mathrm{QNF}}(\hat{I})) \hat{F} \hat{P}_{\mathrm{r}} | \chi_{I-} \rangle \right) \\ &= 2\pi\hbar \int_{\mathbb{R}} \delta(E - K_{\mathrm{QNF}}(I)) \langle \chi_{I+} | - \frac{\mathrm{i}}{\hbar} [\widehat{\Theta(s)}, \hat{I}] | \chi_{I+} \rangle \frac{\mathrm{d}K_{\mathrm{QNF}}(I)}{\mathrm{d}I} \, \mathrm{d}I \\ &= \frac{1}{1 + \mathrm{e}^{-2\pi I(E)/\hbar}}, \end{aligned} \tag{5.85}$$

where $I(E)$ is the solution of $E = K_{\mathrm{QNF}}(I(E))$, and we have assumed that there is only one such solution (compare with the remark after (5.33). We thus recover our result for $N(E)$ that we have given in (5.36).

5.7.3. Example: general barriers in arbitrary dimensions. We now consider the d-dimensional case with a Hamilton operator in quantum normal form given by $\hat{H}_{\mathrm{QNF}} = K_{\mathrm{QNF}}(\hat{I}, \hat{J}_2, \ldots, \hat{J}_d)$. Again we work in the Q representation in terms of which our dividing surface is defined as $s(Q_1, \ldots, Q_d, P_1, \ldots, P_d) = Q_1 = 0$. The quantization of $\Theta(s)$ is then defined by its action on a wavefunction $\psi(Q_1, \ldots, Q_d)$ according to

$$\widehat{\Theta(s)} \psi(Q_1, \ldots, Q_d) = \Theta(Q_1) \psi(Q_1, \ldots, Q_d). \tag{5.86}$$

The Q representation of the incoming eigenfunctions (5.31) is given by

$$\begin{aligned} \chi_{(I,n_{\mathrm{sca}})\,\mathrm{i;r}}(Q_1, \ldots, Q_d) &:= \chi_{I+}(Q_1) \psi_{n_2}(Q_2) \cdots \psi_{n_d}(Q_d), \\ \chi_{(I,n_{\mathrm{sca}})\,\mathrm{i;p}}(Q_1, \ldots, Q_d) &:= \chi_{I-}(Q_1) \psi_{n_2}(Q_2) \cdots \psi_{n_d}(Q_d) \end{aligned} \tag{5.87}$$

with $I \in \mathbb{R}$ and scattering quantum numbers $n_{\mathrm{sca}} = (n_2, \ldots, n_d) \in \mathbb{N}_0^{d-1}$. It then follows from the one-dimensional case discussed in the previous section that

$$\begin{aligned} &\langle \chi_{(I,n_{\mathrm{sca}})\,\mathrm{i;r}} | [\widehat{\Theta(s)}, K_{\mathrm{QNF}}(\hat{I}, \hat{J}_2, \ldots, \hat{J}_d)] | \chi_{(I,n_{\mathrm{sca}})\,\mathrm{i;r}} \rangle \\ &\quad = \langle \chi_{(I,n_{\mathrm{sca}})\,\mathrm{i;r}} | [\widehat{\Theta(s)}, \hat{I}] | \chi_{(I,n_{\mathrm{sca}})\,\mathrm{i;r}} \rangle \frac{\partial}{\partial I} K_{\mathrm{QNF}} \left(I, \hbar \left(n_2 + \frac{1}{2} \right), \ldots, \hbar \left(n_d + \frac{1}{2} \right) \right) \end{aligned} \tag{5.88}$$

(see equation (5.84)). Using the completeness of the states $\chi_{(I,n_{\rm sca})\,{\rm i;r/p}}$ we find for the cumulative reaction probability,

$$\begin{aligned} N(E) &= 2\pi\hbar \sum_{n_{\rm sca}\in\mathbb{N}_0^{d-1}} \int_{\mathbb{R}} (\langle \chi_{(I,n_{\rm sca})\,{\rm i;r}} | \delta(E - K_{\rm QNF}(\hat{I}, \hat{J}_2, \ldots, \hat{J}_d))\hat{F}\hat{P}_{\rm r} | \chi_{(I,n_{\rm sca})\,{\rm i;r}} \rangle \\ &\quad + \langle \chi_{(I,n_{\rm sca})\,{\rm i;p}} | \delta(E - K_{\rm QNF}(\hat{I}, \hat{J}_2, \ldots, \hat{J}_d))\hat{F}\hat{P}_{\rm r} | \chi_{(I,n_{\rm sca})\,{\rm i;p}} \rangle)\, {\rm d}I \\ &= 2\pi\hbar \sum_{n_{\rm sca}\in\mathbb{N}_0^{d-1}} \int_{\mathbb{R}} \delta\left(E - K_{\rm QNF}\left(I, \hbar\left(n_2 + \frac{1}{2}\right), \ldots, \hbar\left(n_d + \frac{1}{2}\right)\right)\right) \\ &\quad \times \left\langle \chi_{(I,n_{\rm sca})\,{\rm i;r}} \right| -\frac{\rm i}{\hbar}[\widehat{\Theta(s)}, K_{\rm QNF}(\hat{I}, \hat{J}_2, \ldots, \hat{J}_d)] \left| \chi_{(I,n_{\rm sca})\,{\rm i;r}} \right\rangle {\rm d}I \\ &= \sum_{n_{\rm sca}\in\mathbb{N}_0^{d-1}} \left[1 + \exp\left(-2\pi \frac{I_{n_{\rm sca}}(E)}{\hbar}\right)\right]^{-1}, \end{aligned} \tag{5.89}$$

where $I_{n_{\rm sca}}(E)$ solves $K_{\rm QNF}(I, \hbar(n_2 + 1/2), \ldots, \hbar(n_d + 1/2)) = E$ for $n_{\rm sca} = (n_2, \ldots, n_d) \in \mathbb{N}_0^{d-1}$, and we assume there is only one such solution (compare, again, with the remark after (5.33). We thus recover our result in (5.36).

Though we showed that if the flux–flux autocorrelation function formalism is evaluated in terms of the quantum normal form then it reproduces our results for the cumulative reaction probability that we developed in section 5.4, it is important to point out the computational differences between the flux–flux autocorrelation function formalism in its original form and the quantum normal form approach to computing cumulative reaction probabilities. The main problem with the implementation of the flux–flux autocorrelation function formalism is the occurrence of the projection operator $\hat{P}_{\rm r}$ in the trace in (5.58). The presence of the operator $\hat{P}_{\rm r}$ is crucial in order to ensure that only states that evolve from reactants to products contribute to the trace in (5.58). The extraction of this information for an arbitrarily chosen dividing surface and without any insight into the quantum dynamics requires one to look at the full time evolution of states as embodied in the definition of the operator $\hat{P}_{\rm r}$ in (5.60). Though various techniques like Monte Carlo path integration and *initial value representation* (IVR) [Mil98a, Mil98b] have been developed in order to solve this time evolution problem that is involved in the evaluation of the trace in (5.58) due to the presence of $\hat{P}_{\rm r}$, it remains a formidable numerical task to apply (5.58) to specific systems. In contrast to this, the computation of the cumulative reaction probability from the quantum normal form does not involve the solution of a time evolution problem. The reason for this is that the quantum normal form yields an unfolding of the quantum dynamics in the reaction region. As a result the S-matrix expressed in terms of the corresponding scattering states is diagonal, i.e. the scattering states can be immediately classified and the reaction probabilities can be immediatedly determined without explicitly looking at the time evolution. The numerical effort to implement and evaluate the quantum normal form is comparable to the classical normal form computation described in sections 2 and 4. In section 7 we will illustrate the efficiency of the quantum normal form computation of the cumulative reaction probability for several concrete examples.

6. Quantum resonances

In this section we consider quantum resonances and the corresponding resonance states. The role of quantum resonances in the context of chemical reactions was explicitly studied for the first time in the chemistry literature by Friedman and Truhlar [FT91] and Miller [SM91].

The quantum resonances are viewed as another imprint of the activated complex in addition to the quantization of the cumulative reaction probability discussed in the previous section, section 5. Recent developments in high-resolution spectroscopic techniques allow one to probe the dynamics of quantum mechanical reactions with unprecedented accuracy. There is therefore immense interest in quantum resonances both in experimental and computational chemistry [Zar06, SY04, SSM+00].

We will show that the quantum normal form provides us with a very efficient algorithm for computing quantum resonances and also the corresponding resonance states. In our discussion of the classical reaction dynamics we could identify the activated complex with the centre manifold of the saddle-centre-...-centre equilibrium point, i.e. with an invariant subsystem with one degree of freedom less than the full system located between reactants and products (see section 4.1). As we will discuss in detail in section 6.3, the Heisenberg uncertainty relation excludes the existence of an invariant quantum subsystem. In fact, the quantum resonances will describe how a wavepacket initialized near the classically invariant subsystem will decay in time.

Quantum resonance can be introduced in several ways. A common definition is based on the S-matrix. If one can extend the S-matrix analytically to complex energies, then the resonances are defined as its poles in the complex energy plane. We could therefore use the results of the previous section to determine the resonances from the quantum normal form. However, we will choose a different approach to introduce resonances which will make their dynamical meaning much more clear.

6.1. Definition of quantum resonances

We will define resonances as the poles of the resolvent operator. This is in line with the the convention in the mathematical literature (see, e.g., [Zwo99]). Let us recall the necessary notions.

For an operator $\hat{H} : L^2(\mathbb{R}^d) \to L^2(\mathbb{R}^d)$, the resolvent set $r(\hat{H})$ of $\hat{H}$ is defined as the set of $E \in \mathbb{C}$ such that $\hat{H} - E$ is invertible. The spectrum of $\hat{H}$ is the complement of the resolvent set. For $E \in r(\hat{H})$, the resolvent of $\hat{H}$ is defined as

$$\hat{R}(E) = (\hat{H} - E)^{-1} : L^2(\mathbb{R}^d) \to L^2(\mathbb{R}^d). \tag{6.1}$$

If $\hat{H}$ is self-adjoint, then the spectrum of $\hat{H}$ is contained in $\mathbb{R}$. The resolvent is thus defined at least for all $E \in \mathbb{C}\backslash\mathbb{R}$. The resolvent is related to the time evolution operator $\hat{U}(t) = \exp(-\frac{\mathrm{i}}{\hbar} t\hat{H})$ by Laplace transformation. For $\mathrm{Im}E \geqslant 0$,

$$\hat{R}(E) = \frac{\mathrm{i}}{\hbar} \int_0^\infty \mathrm{e}^{\frac{\mathrm{i}}{\hbar} Et} \hat{U}(t)\, \mathrm{d}t, \tag{6.2}$$

and by Mellin transform

$$\hat{U}(t) = \frac{1}{2\pi\mathrm{i}} \int_{\mathrm{Im}E=c} \hat{R}(E)\mathrm{e}^{\frac{\mathrm{i}}{\hbar} tE}\, \mathrm{d}E, \tag{6.3}$$

where $c > 0$. The path of integration in the Mellin integral should be thought of as encircling the spectrum of $\hat{H}$. Hence, if $\hat{H}$ has only isolated eigenvalues E_n then Cauchy's theorem gives

$$\hat{U}(t) = \sum \mathrm{e}^{-\frac{\mathrm{i}}{\hbar} tE_n} \hat{P}_n \tag{6.4}$$

with the projectors

$$\hat{P}_n := \frac{1}{2\pi\mathrm{i}} \int_{C_n} \hat{R}(E)\, \mathrm{d}E, \tag{6.5}$$

where the C_n are closed paths encircling only E_n. This is the usual spectral theorem which shows how eigenvalues and eigenfunctions (contained in the projectors $\hat{P}_n$) determine the time evolution of a system with discrete spectrum.

In the case where the spectrum of $\hat{H}$ is not discrete the sum over eigenvalues is replaced by an integral, and it becomes harder to read off properties of the time evolution directly. Physically, a continuous spectrum corresponds to an open system like a scattering system where wavepackets can decay by spreading out to infinity. This will be described by resonances.

Let us assume $\hat{H}$ has continuous spectrum. The resolvent $\hat{R}(E)$ is an analytic function of E for $\mathrm{Im}E > 0$, and the resonances are defined as the poles of the meromorphic continuation of $\hat{R}(E)$ to the region $\mathrm{Im}E \leqslant 0$. Since the operator $\hat{H}$ is self-adjoint on $L^2(\mathbb{R}^d)$ and has continuous spectrum, there is no meromorphic continuation of $\hat{R}(E)$ as an operator from $L^2(\mathbb{R}^d) \to L^2(\mathbb{R}^d)$. Instead one looks for a continuation of $\hat{R}(E)$ as an operator

$$\hat{R}(E) : L^2_{\mathrm{comp}}(\mathbb{R}^d) \to L^2_{\mathrm{loc}}(\mathbb{R}^d), \tag{6.6}$$

where $L^2_{\mathrm{comp}}(\mathbb{R}^d)$ and $L^2_{\mathrm{loc}}(\mathbb{R}^d)$ denote the spaces of functions that are in $L^2(\mathbb{R}^d)$ and have compact support, or that are locally in $L^2(\mathbb{R}^d)$, respectively. More directly, let $\varphi, \psi \in L^2_{\mathrm{comp}}(\mathbb{R}^d)$, then *quantum resonances* are the poles of the meromorphic continuation of the matrix elements

$$\langle \varphi, \hat{R}(E)\psi \rangle \tag{6.7}$$

from the region $\mathrm{Im}E > 0$ to $\mathrm{Im}E \leqslant 0$. Assuming we have found such a meromorphic continuation with poles at $E_n \in \mathbb{C}$, $n \in \mathbb{N}$, $\mathrm{Im}E_n < 0$, then we can use (6.3) to get

$$\langle \varphi, \hat{U}(t)\psi \rangle = \frac{1}{2\pi \mathrm{i}} \int_{\mathrm{Im}E=c} \langle \varphi, \hat{R}(E)\psi \rangle \mathrm{e}^{\frac{\mathrm{i}}{\hbar}tE} \, \mathrm{d}E. \tag{6.8}$$

Shifting the contour of integration and picking up the contribution from the poles gives us an expansion in terms of the resonances E_n

$$\langle \varphi, \hat{U}(t)\psi \rangle \sim \sum \mathrm{e}^{-\frac{\mathrm{i}}{\hbar}tE_n} \langle \varphi, \hat{P}_n \psi \rangle \tag{6.9}$$

with the projectors

$$\hat{P}_n := \frac{1}{2\pi \mathrm{i}} \int_{C_n} \hat{R}(E) \, \mathrm{d}E, \tag{6.10}$$

where C_n is a closed path encircling only the resonance E_n. This looks formally like (6.4), but there are two important differences. Firstly, $\mathrm{Im}E_n < 0$ which means that $|\mathrm{e}^{-\frac{\mathrm{i}}{\hbar}tE_n}| = \mathrm{e}^{t\mathrm{Im}E_n}$, and hence the terms in the sum are exponentially decreasing for $t \to \infty$ (since $\mathrm{Im}E_N < 0$). Secondly, the projectors $\hat{P}_n$ are no longer orthogonal projectors in $L^2(\mathbb{R}^d)$. Futhermore, we can take the expansion only as far as the meromorphic continuation allows us to, and even if it extends to $\mathbb{C}$, the resulting sum could be divergent. The range of the meromorphic continuation and the convergence properties of the sum can depend on φ and ψ (see [Zwo99] for a more detailed description).

The relation (6.9) reveals the dynamical meaning of the resonances. Resonance states are not stationary, and the reciprocal value of the imaginary part of the resonance energies determines their lifetime.

6.2. Computation of resonances of the quantum normal form

We now turn to explicit calculations and show how one can compute quantum resonances of the quantum normal form.

6.2.1. Resonances of one-dimensional systems. We start with the simplest one-dimensional example ($d = 1$) and consider the operator

$$\hat{H} = \lambda \hat{I} = \lambda \frac{\hbar}{\mathrm{i}} \left(q\partial_q + \frac{1}{2} \right), \tag{6.11}$$

where $\lambda > 0$. For this operator the Schrödinger equation can be solved explicitly and the time evolution operator is given by

$$\hat{U}(t)\psi(q) = \mathrm{e}^{-\frac{\lambda t}{2}} \psi(\mathrm{e}^{-\lambda t} q). \tag{6.12}$$

This operator is of course unitary, i.e. it preserves the L^2-norm. In time, the state $\hat{U}(t)\psi(q)$ spreads out at an exponential rate. If we look at the overlap of $\hat{U}(t)\psi(q)$ with another localized state we expect an exponential decay, and this is exactly what the resonances describe. Let $\varphi, \psi \in C_0^\infty(\mathbb{R})$, then

$$\langle \varphi, \hat{U}(t)\psi \rangle = \mathrm{e}^{-\frac{\lambda t}{2}} \int \varphi^*(q)\psi(\mathrm{e}^{-\lambda t} q)\, \mathrm{d}q \tag{6.13}$$

and if we insert for ψ its Taylor series

$$\psi(q) = \sum_{n=0}^{N} \frac{1}{n!} \psi^{(n)}(0) q^n + R_{N+1}(q), \tag{6.14}$$

with $|R_{N+1}(q)| \leqslant C_{N+1}|q|^{N+1}$, then we obtain

$$\langle \varphi, \hat{U}(t)\psi \rangle = \sum_{n=0}^{N} \mathrm{e}^{-\lambda(n+1/2)t} \frac{1}{n!} \psi^{(n)}(0) \int \varphi^*(q) q^n \, \mathrm{d}q + O(\mathrm{e}^{-\lambda(N+1+1/2)t}) \tag{6.15}$$

for $t \geqslant 0$. Inserting this equation into (6.2) leads to the meromorphic continuation of $\hat{R}(E)$ to the domain $\mathrm{Im}E > -\hbar\lambda(N + 1 + 1/2)$ with poles at

$$E_n = -\mathrm{i}\hbar\lambda(n + 1/2), \qquad n = 0, \ldots, N. \tag{6.16}$$

These are the resonances of the operator $\hat{H}$ given in (6.11).

We can furthermore read off the projection operators

$$\hat{P}_n \psi(q) := \frac{1}{n!} \psi^{(n)}(0) q^n, \tag{6.17}$$

and a direct calculation shows that q^n is an eigenfunction with complex eigenvalue $E_n = -\mathrm{i}\hbar\lambda(n + 1/2)$,

$$\hat{H} q^n = -\mathrm{i}\hbar\lambda(n + 1/2) q^n. \tag{6.18}$$

We now extend this analysis to the case of a Hamilton operator in quantum normal form for $d = 1$, i.e. $\hat{H} = K(\hat{I})$, where K is a polynomial or an analytic function in I. We will require furthermore the condition

$$\mathrm{Im}K(-\mathrm{i}x) < 0, \qquad \text{for} \quad x > 0. \tag{6.19}$$

By expanding K in a power series we find

$$\hat{H} q^n = K(-\mathrm{i}\hbar(n + 1/2)) q^n \tag{6.20}$$

and solving the Schrödinger equation yields $\hat{U}(t)q^n = \exp[-\frac{\mathrm{i}}{\hbar} t K(-\mathrm{i}\hbar(n + 1/2))] q^n$. Hence, if $\psi(q)$ is analytic, we have

$$\hat{U}(t)\psi(q) = \sum_{n=0}^{\infty} \frac{1}{n!} \psi^{(n)}(0) \mathrm{e}^{-\frac{\mathrm{i}}{\hbar} t K(-\mathrm{i}\hbar(n+1/2))} q^n, \tag{6.21}$$

and by condition (6.19) we can use (6.2) to see that the resonances are given by

$$E_n = K(-\mathrm{i}\hbar(n+1/2)), \qquad n = 0, 1, 2, \ldots. \tag{6.22}$$

This can be regarded as a kind of imaginary Bohr–Sommerfeld quantization condition for the resonances. Moreover, we can formally write the resonance states $\phi_n(q) = q^n$ as 'complex' Lagrangian states,

$$\phi_n(q) = q^n = (\operatorname{sgn} q)^n |q|^{-1/2+\mathrm{i}I_n/\hbar} \tag{6.23}$$

with $I_n = -\mathrm{i}\hbar(n+1/2)$. This reveals the formal similarity of the resonance states to the scattering states (5.5) with the main difference being that in the case of resonances I fulfils an imaginary Bohr–Sommerfeld quantization condition while in the case of scattering the spectrum of $\hat{I}$ is continuous and real. With the states (6.23) we can associate the complex Lagrangian manifolds

$$\Lambda_{\phi_n} = \{(q, p) = (q, I_n/p) \,:\, q \in \mathbb{R}\} \subset \mathbb{R} \times \mathrm{i}\mathbb{R}. \tag{6.24}$$

6.2.2. Resonances of multi-dimensional quantum normal form. Finally, we consider the case of a d-dimensional system in quantum normal form, i.e. let $\hat{H} = K(\hat{I}, \hat{J}_2, \ldots, \hat{J}_d)$ and φ_{n_k} denote the n_kth harmonic oscillator eigenfunction (see (5.30)).

For $n = (n_1, \ldots, n_d) \in \mathbb{N}_0^d$, set

$$\psi_n(q) = q_1^{n_1} \varphi_{n_2}(q_2) \cdots \varphi_{n_d}(q_d). \tag{6.25}$$

Then we have

$$\hat{H}\psi_n = K\big(-\mathrm{i}\hbar(n_1+1/2), \hbar(n_2+1/2), \ldots, \hbar(n_d+1/2)\big)\psi_n, \tag{6.26}$$

and if we assume $\operatorname{Im} K(-\mathrm{i}x_1, x_2 \ldots, x_d) < 0$ for $x_1 > 0$ and $x_2, \ldots, x_d$ in a neighbourhood of 0, we can conclude as before that the resonances of $\hat{H}$ are given by

$$E_n = K(-\mathrm{i}\hbar(n_1+1/2), \hbar(n_2+1/2), \ldots, \hbar(n_d+1/2)), \qquad n \in \mathbb{N}_0^d. \tag{6.27}$$

To summarize, we have shown theorem 4.

Theorem 4. *Suppose $\hat{H} = K(\hat{I}, \hat{J}_2, \cdots, \hat{J}_d)$ and that K satisfies the condition*

$$\operatorname{Im} K(-\mathrm{i}x_1, x_2, \ldots, x_d) < 0 \tag{6.28}$$

for $x_1 > 0$ and $x_2, \ldots x_d$ in some neighbourhood of 0. Then the resonances in a neighbourhood of 0 are given by

$$E_n = K(-\mathrm{i}\hbar(n_1+1/2), \hbar(n_1+1/2), \ldots, \hbar(n_d+1/2)), \qquad n \in \mathbb{N}_0^d, \tag{6.29}$$

and the corresponding resonance eigenstates are

$$\psi_n(q) = q_1^{n_1} \varphi_{n_2}(q_2) \cdots \varphi_{n_d}(q_d). \tag{6.30}$$

Following (6.24) the resonance eigenstate can be interpreted as Lagrangian states associated with the complex Lagrangian manifolds

$$\Lambda_{\psi_n} = \{(q, p) \in \mathbb{R}^{2d} \,:\, p_1 = I_{n_1}/q_1,\ (p_k^2 + q_k^2) = 2n_k\hbar,\ k = 2, \ldots, d\}. \tag{6.31}$$

6.3. Lifetime of the activated complex

The geometric object in classical phase space associated with the activated complex is the centre manifold, a $(2d-2)$-dimensional invariant submanifold. As mentioned in section 4.4 this submanifold can be considered as the phase space of a $(d-1)$ DoF invariant subsystem related to the supermolecule poised between reactants and products in the chemistry literature [Pec76, Mar92]. This invariant subsystem is unstable, i.e. a trajectory with initial condition near but not in the subsystem will leave the neighbourhood of this subsystem.

For the corresponding quantum system the Heisenberg uncertainty relation excludes the existence of a quantum analogue of the classical invariant subsystem. This is because in normal form coordinates the invariant manifold is defined by $q_1 = p_1 = 0$ and in quantum mechanics we have the uncertainty relation $\Delta p_1 \Delta q_1 \geqslant \hbar/2$, i.e. p_1 and q_1 cannot be 0 simultaneously. The closest one can get to a state which initially has $q_1 = p_1 = 0$ is a minimal uncertainty state which is a Gaussian of the form

$$\psi_0(q_1) = \frac{1}{(\pi\hbar)^{1/4}} \mathrm{e}^{-\frac{1}{\hbar}\frac{q_1^2}{2}}. \tag{6.32}$$

In order to obtain a state which at time $t = 0$ is localized on the centre manifold we choose

$$\psi(q_1, \ldots, q_d) = \frac{1}{(\pi\hbar)^{1/4}} \mathrm{e}^{-\frac{1}{\hbar}\frac{q_1^2}{2}} \varphi_{n_2}(q_2) \cdots \varphi_{n_d}(q_d) \tag{6.33}$$

for some fixed quantum numbers $n_2, \ldots, n_d \in \mathbb{N}_0$, where φ_{n_k} again denote the harmonic oscillator eigenfunctions.

A suitable quantity for measuring the lifetime of such a state is the decay of the autocorrelation function

$$|\langle \psi, \hat{U}(t)\psi \rangle|^2. \tag{6.34}$$

We will compute the autocorrelation function for the case that the Hamiltonian is in quantum normal form. Inserting the expression (6.33) for ψ and expanding the Gaussian into a Taylor series gives

$$\begin{aligned} \langle \psi, \hat{U}(t)\psi \rangle &= \sum_{k=0}^{\infty} \frac{1}{k!} \frac{(-1)^k}{(2\hbar)^k} \frac{1}{(\pi\hbar)^{1/4}} \langle \psi_0 \varphi_{n_2} \cdots \varphi_{n_d}, \hat{U}(t) q^{2k} \varphi_{n_2} \cdots \varphi_{n_d} \rangle \\ &= \sum_{k=0}^{\infty} \frac{1}{k!} \frac{(-1)^k}{(2\hbar)^k} \frac{1}{(\pi\hbar)^{1/2}} \int \mathrm{e}^{-\frac{1}{\hbar}\frac{q_1^2}{2}} q_1^{2k} \, \mathrm{d}q_1 \mathrm{e}^{-\frac{\mathrm{i}}{\hbar} t H(-\mathrm{i}\hbar(2k+1/2), \hbar(n_2+1/2), \ldots, \hbar(n_d+1/2))}, \end{aligned} \tag{6.35}$$

where we have used as well that q^{2k} is a resonance state (6.26). The integral over q_1 gives $\int \mathrm{e}^{-\frac{1}{\hbar}\frac{q_1^2}{2}} q_1^{2k} \, \mathrm{d}q_1 = \Gamma(k+1/2)(2\hbar)^{k+1/2}$, and we thus find

$$\langle \psi, \hat{U}(t)\psi \rangle = \left(\frac{2}{\pi}\right)^{1/2} \sum_{k=0}^{\infty} \frac{\Gamma(k+1/2)}{k!} (-1)^k \mathrm{e}^{-\frac{\mathrm{i}}{\hbar} t H(-\mathrm{i}\hbar(2k+1/2), \hbar(n_2+1/2), \ldots, \hbar(n_d+1/2))}. \tag{6.36}$$

The leading term in this sum for $t \to \infty$ is given by the smallest resonance with $k = 0$. Hence,

$$|\langle \psi, \hat{U}(t)\psi \rangle|^2 \sim 2\mathrm{e}^{\frac{1}{\hbar} t 2 \mathrm{Im} H(-\mathrm{i}\hbar/2, \hbar(n_2+1/2), \ldots, \hbar(n_d+1/2))}, \tag{6.37}$$

and this determines the maximal lifetime of a quantum state of the activated complex, i.e. a state initially localized on the invariant subsystem given by the centre manifold.

For small $\hbar$ the quantum normal form is dominated by its quadratic part and that gives

$$\lim_{\hbar \to 0} \frac{1}{\hbar} 2 \mathrm{Im} H(-\mathrm{i}\hbar/2, \hbar(n_2 + 1/2), \ldots, \hbar(n_d + 1/2)) = -\lambda \tag{6.38}$$

and therefore for small $\hbar$

$$|\langle\psi, \hat{U}(t)\psi\rangle|^2 \sim 2\mathrm{e}^{-t\lambda}. \tag{6.39}$$

The quantum lifetime of the activated complex is in leading order for $\hbar \to 0$ thus given by the reciprocal value of the classical Lyapunov exponent associated with the saddle equilibrium point.

6.4. On the relation between the resonances of the quantum normal form and the full system

We have seen that the resonances of an operator in quantum normal form can be computed explicitly. They are obtained from the Bohr–Sommerfeld type quantization condition (6.27). In section 3 we have shown how to approximate a Hamilton operator near an equilibrium point of the principal symbol by an operator in quantum normal form. We now want to discuss under which conditions this quantum normal form can be used to compute the resonances of the full Hamilton operator. This question has been studied in [KK00] and we will mainly cite their results.

One would expect that resonances of the full system are close to the one of the quantum normal form around an equilibrium point if that equilibrium point dominates the reaction, i.e. if it is the only equilibrium point at that energy, and all other trajectories come from infinity or can escape to infinity. This idea is formalized by using the trapped set of the classical Hamiltonian, whose definition we now recall.

Let $H(q, p)$ be a Hamilton function and Φ_H^t the Hamiltonian flow generated by it. The *trapped set* at energy E is defined by

$$\mathrm{TS}^E(H) := \{(q, p) \in \mathbb{R}^d \times \mathbb{R}^d \,:\, H(q, p) = E, \quad |\lim_{t\to\pm\infty} \Phi_H^t(q, p)| < \infty\}. \tag{6.40}$$

It consists of the trajectories which stay in some bounded region for $t \to \pm\infty$.

Theorem 5 ([KK00]). *Assume H satisfies the general conditions of [HS86] and has an equilibrium point at z_0 with energy E_0 and $\mathrm{TS}^{E_0}(H) = \{z_0\}$. Let $K_{\mathrm{QNF}}^{(N)}$ be the Nth order quantum normal form of H with respect to z_0. Then the resonances of $\mathrm{Op}[H]$ in a $\hbar^\delta$ neighbourhood of E_0, $1 \geqslant \delta > 0$, are $\hbar^{\delta N}$ close to the resonances of $K_{\mathrm{QNF}}^{(N)}$.*

The conditions from [HS86] referred to above are conditions on H which ensure that the resonances can be defined by a complex deformation of phase space, a generalization of the complex dilation method [Sim79, Rei82, Moi98] which we will use in section 7 to compute numerically exact quantum resonances. For a more recent and more accessible presentation see [LBM02].

More explicitly, the main consequence of theorem 5 is that for every $n \in \mathbb{N}_0^d$, there is a resonance $E_n \in \mathbb{C}$ of $\mathrm{Op}[H]$ with

$$E_n = K_{\mathrm{QNF}}^{(N)}(-\mathrm{i}\hbar(n_1 + 1/2), \hbar(n_1 + 1/2), \ldots, \hbar(n_d + 1/2)) + O((|n|\hbar)^{N+1}). \tag{6.41}$$

The quantum normal form thus provides an asymptotic expansion of the resonances for small $\hbar$. If we want to have all resonances in a neighbourhood of E_0 of radius $\hbar^\delta$, then we must go in n up to a size determined by $\hbar|n| \sim \hbar^\delta$ in which case the error term becomes of order $\hbar^{\delta N}$. Since we are interested in the first few resonances only we can take $\delta = 1$.

We note that the resonances (6.41) coincide with the poles of the S-matrix which we computed in (5.24) and (5.32). As can be seen from (5.24) the poles of the S-matrix are simply given by the poles of the gamma function at nonpositive integers.

In cases when the trapped set is larger, e.g. when there are several equilbrium points at the same energy, the situation is more complicated and the structure of the set of resonances is

no longer necessarily determined by the contributions from the individual equilibrium points. Instead one has to use the methods sketched in section 5.6 to construct a global S-matrix which will bring the global geometry into play.

6.5. Distribution of the resonance states in phase space

We now want to study the distribution of the resonance states in phase space in terms of Husimi functions. As in the case of the scattering states in section 5.5 the Husimi functions of the resonance states (6.25) is given by the product of the Husimi functions of harmonic oscillator eigenfunctions φ_{n_k} and the Husimi function of $\phi_{n_1}(q_1) = q_1^{n_1}$. We have already discussed the Husimi functions of the φ_{n_k} in section 5.5. The computation of the Husimi function of the ϕ_{n_1} is rather straightforward, and we obtain

$$\langle \psi_{p_1,q_1}, \phi_{n_1} \rangle = \frac{\sqrt{2\pi\hbar}}{(\pi\hbar)^{1/4}} \left(\frac{\hbar}{2}\right)^{n/2} \mathrm{i}^n H_{n_1}\left(\frac{p_1 - \mathrm{i}q_1}{\sqrt{2\hbar}}\right) \mathrm{e}^{\frac{\mathrm{i}}{2\hbar} p_1 q_1 - \frac{1}{2\hbar} p_1^2}, \tag{6.42}$$

where H_{n_1} is the n_1th Hermite polynomial. Therefore we have

$$H_{\phi_{n_1}}(q_1, p_1) = \frac{1}{\sqrt{\pi\hbar}} \left(\frac{\hbar}{2}\right)^{n_1} \left| H_{n_1}\left(\frac{p_1 - \mathrm{i}q_1}{\sqrt{2\hbar}}\right)\right|^2 \mathrm{e}^{-p_1^2/\hbar}. \tag{6.43}$$

Figure 12 shows contour plots of the Husimi functions of the first five resonance states. Due to the exponential damping in the direction of p_1 the Husimi functions H_{ϕ_n} are concentrated along $p_1 = 0$. Along $p_1 = 0$ they increase in leading order in q_1 as

$$H_{\phi_n}(q_1, 0) \sim \frac{1}{\sqrt{\pi\hbar}} \left(\frac{\hbar}{2}\right)^{n/2} q_1^n + O(q_1^{n-2}). \tag{6.44}$$

It follows from (6.43) that $H_{\phi_{n_1}}$ has n_1 zeroes located near the origin on $q_1 = 0$.

For $n = (n_1, \ldots, n_d) \in \mathbb{N}_0^d$ the Husimi function of a multi-dimensional scattering wavefunction ψ_n defined in (6.25) is simply given by the product of the functions defined in (5.43) and (6.43), i.e.

$$H_{\psi_n}(q, p) = H_{\phi_{n_1}}(q_1, p_1) H_{\varphi_{n_2}}(q_2, p_2) \cdots H_{\varphi_{n_d}}(q_d, p_d). \tag{6.45}$$

From the distribution of the functions (5.43) and (6.43) it thus follows that the resonance states ψ_n are concentrated on the real projections of the complex Lagrangian manifolds Λ_{ψ_n} in (6.31)

$$\{(q, p) \in \mathbb{R}^{2d} \,:\, p_1 = 0,\ (p_k^2 + q_k^2) = 2n_k\hbar,\ k = 2, \ldots, d\}. \tag{6.46}$$

7. Examples

In the following we illustrate the classical and quantum reaction dynamics for concrete examples with one, two and three degrees of freedom. As we will see, the reaction dynamics in systems with one or two degrees of freedom still has certain features that do not persist in the multidimensional case (of three or more degrees of freedom). We will use the classical normal form to realize the phase space structures that control classical reaction dynamics for these systems and compute the classical flux. Likewise we will use the quantum normal form to compute cumulative reaction probabilities and quantum resonances. We note that we implemented the procedures to compute the classical and quantum normal forms in the programming language C++. In our object-oriented implementation the number of degrees of freedom and the order of the normal form can be chosen arbitrarily.

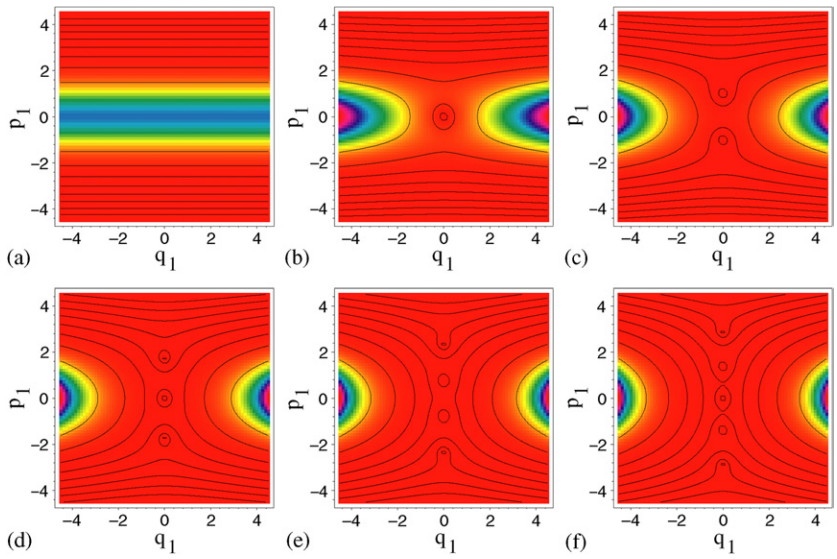

Figure 12. Contour plots of the Husimi functions $H_{\phi_{n_1}}$ in the (q_1, p_1)-plane for $n_1 = 0, \ldots, 5$. Red corresponds to low values; blue corresponds to high values. The spacing between the values of the contour lines is decreasing exponentially ($\hbar = 0.1$).

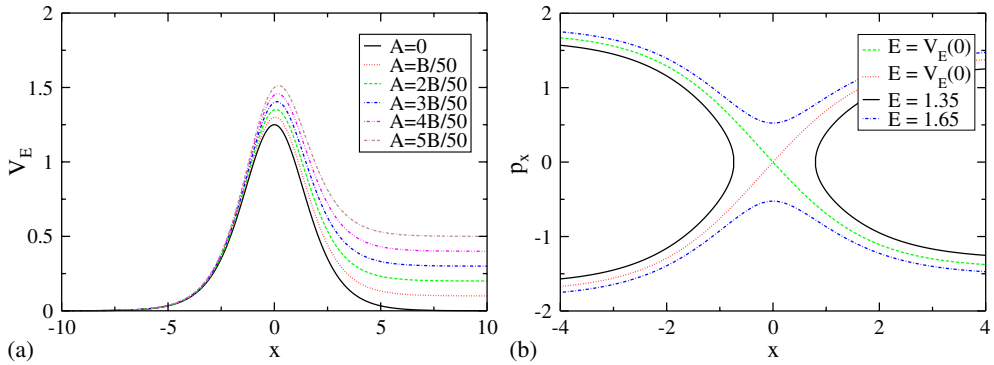

Figure 13. (*a*) Graph of the Eckart potential V_{E} defined in (7.2) with parameters $a = 1$, $B = 5$ and different values of A. (*b*) Phase portaits for the Eckart potential with parameters $a = 1$, $A = 0.5$, $B = 5$ and $m = 1$. The green and red lines mark the stable and unstable manifolds of the equilibrium point $(x, p_x) = 0$.

7.1. Example with 1 DoF

The most frequently used systems to model one-dimensional reaction problems, like the paradigm hydrogen exchange reaction $H_2 + H \rightarrow H + H_2$, are the parabolic barrier and the Eckart potential (see, e.g., [SM91,SY04]). The reason for choosing these model systems is that the reflection coefficient and the quantum resonances can be computed analytically for these systems. We have already seen that the quantum normal form computation of the reflection coefficient and the resonances is exact for a parabolic barrier. We therefore focus here on the Eckart barrier which provides a much more realistic model of reactions than the parabolic barrier.

The Hamilton function for an Eckart barrier [Eck30] is given by

$$H = p^2/(2m) + V_{\mathrm{E}}(x), \tag{7.1}$$

where V_{E} is defined as

$$V_{\mathrm{E}}(x) = A\frac{\exp((x+x_0)/a)}{1+\exp((x+x_0)/a)} + B\frac{\exp((x+x_0)/a)}{(1+\exp((x+x_0)/a))^2} \tag{7.2}$$

with

$$x_0 = a\ln\frac{B+A}{B-A}. \tag{7.3}$$

For $B > A \geqslant 0$ the Eckart potential possesses a maximum which we shifted to $x = 0$ for convenience. The value of the potential at its maximum is

$$V_{\mathrm{E}}(0) = \frac{(A+B)^2}{4B}. \tag{7.4}$$

The potential monotonically decreases to 0 as $x \to -\infty$ and to A as $x \to \infty$ (see figure 13(*a*)). For $A = 0$, the potential is symmetric.

The Weyl quantization of the Hamilton function (7.1) gives the Hamilton operator

$$\mathrm{Op}[H] = -\frac{\hbar^2}{2m}\frac{\partial^2}{\partial x^2} + V_{\mathrm{E}}. \tag{7.5}$$

The Hamilton function H in (7.1) is then the principal symbol of the Hamilton operator $\mathrm{Op}[H]$.

7.1.1. Computation of the classical and quantum normal forms. In order to compute the quantum normal form we can follow the calculation for one-dimensional potential barriers described in section 3.5. Using the notation of section 3.5 the coefficients of the Taylor expansion to fourth order are

$$\lambda = \frac{1}{\sqrt{8ma^2B^3}}(B^2 - A^2), \tag{7.6}$$

and

$$V_{30} = -\frac{1}{16}A\frac{\sqrt{B^2-A^2}}{B^{7/4}}\left(\frac{2}{ma^2}\right)^{3/4}, \qquad V_{40} = \frac{1}{96}\frac{2B^2 - 9A^2}{ma^2B^2}. \tag{7.7}$$

We refrain from giving the analytical expressions for the higher order terms as the actual computation of the classical and quantum normal form implemented in our C++ program is carried out numerically. However, we used the coefficients above together with equation (3.143) to check the numerically computed 4th order quantum normal form. To give the reader the opportunity to verify our results we list in table 2 in appendix B the coefficients of the symbol of the 10th order quantum normal form of the Eckart barrier with parameters $a = 1$, $B = 5$, $A = 1/2$ and $m = 1$. The classical normal form can be obtained from the symbol by discarding all terms that involve a factor $\hbar$.

7.1.2. Classical reaction dynamics. Since the energy surface of a 1 DoF system is one-dimensional, the classical reaction dynamics of 1 DoF systems is trivial. The question of whether a trajectory is reactive or nonreactive is determined by the energy alone, i.e. in the case of the Eckart barrier trajectories are forward or backward reactive if they have energy $E > V_{\mathrm{E}}(0)$, and they are nonreactive localized in reactants or products if $E < V_{\mathrm{E}}(0)$ (see figure 13(*b*)). Fixing an energy $E > V_{\mathrm{E}}(0)$ one can choose any point $x_{\mathrm{ds}} \in \mathbb{R}$ to define a

dividing 'surface' on the energy surface according to $\{(x, p_x) : x = x_{\rm ds},\ H(x, p_x) = E\} = \{(x, p_x) = (x_{\rm ds}, \pm\sqrt{2m(E - V_{\rm E}(x))}\}$. This dividing 'surface' consists of two points which have $p_x > 0$ and $p_x < 0$ and are crossed by all forward reactive trajectories and backward reactive trajectories, respectively. In fact the two points can be considered to form a zero-dimensional sphere, S^0, with each point forming by itself a zero-dimensional ball, B^0. Note that many of the other phase space structures that we discussed in section 4 do not make sense for the case of $d = 1$ degree of freedom. Moreover, the case of one degree of freedom is special because it is the only case for which the location of the dividing surface is not important.

Note that the formalism to compute the classical flux $f(E)$ developed in section 4.4 does not apply either to the case $d = 1$. Still it is useful to view the classical flux to be given by the step function $f(E) = \Theta(E - V_{\rm E}(0))$, i.e. classically, we have full transmission for $E > V_{\rm E}(0)$ and full reflection for $E < V_{\rm E}(0)$.

7.1.3. Quantum reaction dynamics. The effect of quantum mechanical tunnelling makes the quantum reaction dynamics even of 1 DoF systems more complicated than the corresponding classical reaction dynamics. The quantum mechanically exact transmission coefficient $T_{\rm exact}$ can be computed analytically for the Eckart potential [Eck30]. One finds

$$T_{\rm exact}(E) = 1 - \frac{\cosh[2\pi(\alpha - \beta)] + \cosh[2\pi\delta]}{\cosh[2\pi(\alpha + \beta)] + \cosh[2\pi\delta]}, \tag{7.8}$$

where

$$\alpha = \frac{1}{2}\sqrt{\frac{E}{C}}, \qquad \beta = \frac{1}{2}\sqrt{\frac{E - A}{C}}, \qquad \delta = \frac{1}{2}\sqrt{\frac{B - C}{C}}, \qquad C = \frac{\hbar^2}{8ma^2}. \tag{7.9}$$

Note that $T_{\rm exact}(E) \to 0$ when the energy E approaches the limiting value A of the potential from above. Figure 14 shows the graph of $T_{\rm exact}(E)$ versus the energy E. Following section 5.3 we can compute the transmission coefficient from the Nth order quantum normal form $K^{(N)}_{\rm QNF}$ according to

$$T^{(N)}_{\rm QNF}(E) = \left[1 + \exp\left(-2\pi\frac{I^{(N)}(E)}{\hbar}\right)\right]^{-1}, \tag{7.10}$$

where $I^{(N)}(E)$ is obtained from inverting the equation

$$K^{(N)}_{\rm QNF}(I^{(N)}(E)) = E. \tag{7.11}$$

We illustrate the high quality of the quantum normal form computation of the transmission coefficient in figure 15(*a*) which shows the difference between $T_{\rm exact}$ and $T^{(N)}_{\rm QNF}$ for different orders, N, of the quantum normal form. Though the quantum normal form expansion is not expected to converge, the difference between $T_{\rm exact}$ and $T^{(N)}_{\rm QNF}$ decreases as N increases to the maximum value of 10 at which we stopped the quantum normal form computation. In fact, the difference decreases from the order of 1% for the 2nd order quantum normal form to the order of 10^{-11} for the 10th order quantum normal form.

We can also compute the quantum mechanically exact resonances analytically. They are given by the poles of the transmission coefficient (7.8). We find

$$E_{{\rm exact},n} = C\frac{\left((\delta - {\rm i}(n + \frac{1}{2}))^2 + \frac{A}{4C}\right)^2}{(\delta - {\rm i}(n + \frac{1}{2}))^2}, \qquad n = 0, 1, 2, \ldots. \tag{7.12}$$

We illustrate the location of the quantum resonances in the complex energy plane in the bottom panel of figure 14. Following section 6.2.1 we can compute the resonances from the Nth order quantum normal form according to

$$E^{(N)}_{{\rm QNF},n} = K^{(N)}_{\rm QNF}(-{\rm i}\hbar(n + 1/2)), \qquad n = 0, 1, 2, \ldots. \tag{7.13}$$

For the 2nd order quantum normal form this reduces to

$$E^{(2)}_{\mathrm{QNF},n} = V_{\mathrm{E}}(0) - \mathrm{i}\lambda\hbar(n + \tfrac{1}{2}), \qquad n = 0, 1, 2, \ldots. \tag{7.14}$$

As mentioned earlier the 2nd order quantum normal form resonances would be exact for a parabolic potential barrier. For comparison we also show the location of these resonances in the complex energy plane in the bottom panel of figure 14. Note that the 2nd order resonances have a constant real part. The 'bending' of the series of exact resonances in figure 14 is a consequence of the nonlinearity of the Eckart potential. The quantum normal form is able to describe this effect very accurately. The approximation of the exact resonances by the 4th order quantum normal is already so good that the error is no longer visible on the scale of figure 14. We therefore show the differences between the exact and quantum normal form resonances for different orders of the quantum normal form in a separate graph in figure 15(*b*). Again, up to the maximal order shown, the accuracy of the quantum normal form increases with the order. As is to be expected, for a fixed order of the quantum normal form N, the error of the quantum normal form increases with the quantum number n. Note that the sequence of resonances is localized in the complex energy plane in figure 14 in such a way that the real part of the resonance closest to the real axis coincides with the position of the (smooth) step of the transmission coefficient on the (real) energy axis.

7.2. Example with 2 DoF

We now illustrate the quantum normal form computation for a 2 DoF model system which consists of an Eckart barrier in the x-direction that is coupled to a Morse oscillator in the y-direction. A Morse oscillator is a typical model for a chemical bond. The Hamilton function is

$$H = \frac{1}{2m}(p_x^2 + p_y^2) + V_{\mathrm{E}}(x) + V_{\mathrm{M}}(y) + \epsilon H_{\mathrm{c}}, \tag{7.15}$$

where V_{E} is the Eckart potential from (7.2)) and V_{M} is the Morse potential

$$V_{\mathrm{M}}(y) = D_e(\exp(-2a_{\mathrm{M}}y) - 2\exp(-a_{\mathrm{M}}y)) \tag{7.16}$$

with positive valued parameters D_{e} (the *dissociation energy*) and a_{M} (see figure 16(*a*)). For the coupling term H_{c} we choose a so-called *kinetic coupling* (see, e.g., [Hel95])

$$H_{\mathrm{c}} = p_x\, p_y. \tag{7.17}$$

The strength of the coupling is controlled by the parameter ϵ in (7.15). The vector field corresponding to the Hamilton function (7.15) has an equilibrium point at $(x, y, p_x, p_y) = 0$. For $|\epsilon|$ sufficiently small (for given parameters of the Eckart and Morse potentials), the equilibrium point is of the saddle-centre stability type. Contours of the Eckart–Morse potential $V(x, y) = V_{\mathrm{E}}(x) + V_{\mathrm{M}}(y)$ are shown in figure 16(*b*). These indicate the bottleneck-type structure of the energy surfaces with energies slightly above the energy of the saddle-centre equilibrium point. Note that the relation between the saddle of the potential $V(x, y) = V_{\mathrm{E}}(x) + V_{\mathrm{M}}(y)$ at $(x, y) = 0$ and the equilibrium point of Hamilton's equations at $(x, y, p_x, p_y) = 0$ is complicated by the kinetic coupling in (7.15).

The Weyl quantization of the Hamilton function H in (7.15) gives the operator

$$\mathrm{Op}[H] = -\frac{\hbar^2}{2m}\left(\frac{\partial^2}{\partial x^2} + \frac{\partial^2}{\partial y^2}\right) + V_{\mathrm{E}} + V_{\mathrm{M}} - \epsilon\hbar^2\frac{\partial^2}{\partial x\,\partial y}. \tag{7.18}$$

The Hamilton function (7.15) is the principal symbol of the operator $\mathrm{Op}[H]$.

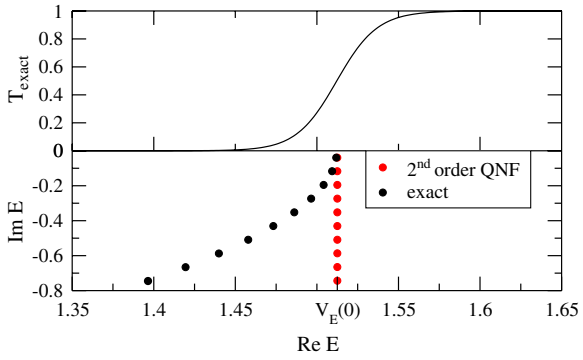

Figure 14. Exact transmission coefficient $T_{\rm exact}(E)$ (top panel) and resonances in the complex energy plane (bottom panel) for the Eckart potential. The parameters a, B, C and m are the same as in figure 13(b), and $\hbar = 0.1$.

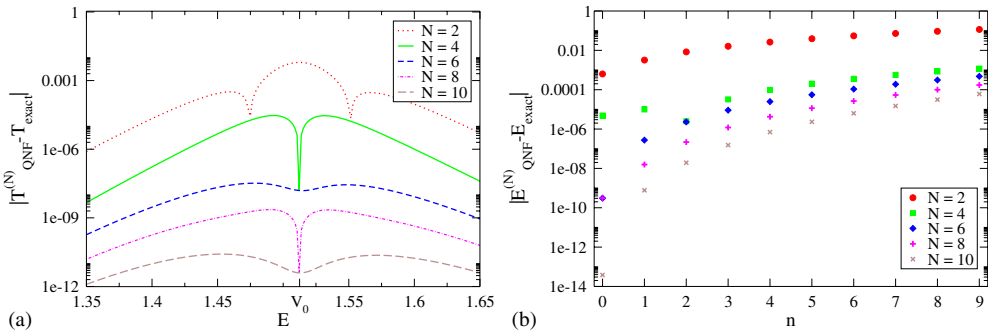

Figure 15. (a) Error for the transmission coefficient of the Eckart potential computed from quantum normal forms of different orders N. (b) Errors for the resonances of the Eckart potential computed from quantum normal forms of different orders N as a function of the quantum number n. The parameters for the Eckart potential are the same as in figure 14.

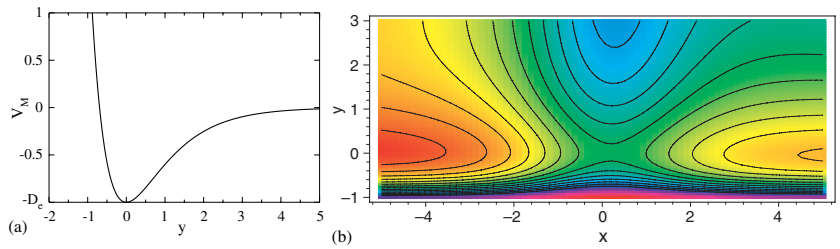

Figure 16. (a) Morse potential $V_{\rm M}(y) = D_{\rm e}\,(\exp(-2\,a_{\rm M}\,y) - 2\exp(-2a_{\rm M}\,y))$. The potential approaches 0 for $y \to \infty$. The parameter $D_{\rm e} = V_{\rm M}(\infty) - V_{\rm M}(0)$ gives the depth of the potential well while $a_{\rm M}$ determines the width of the well. (b) Contours of the Eckart–Morse potential $V_{\rm E}(x) + V_{\rm M}(y)$. Red corresponds to small values of the potential; blue corresponds to large values. The parameters for the Eckart potential are the same as in figure 14. The parameters for the Morse potential are $D_{\rm e} = 1$ and $a_{\rm M} = 1$.

7.2.1. Computation of the classical and quantum normal forms. Since the equilibrium point is already at the origin of the coordinate system we can skip the first step in the classical and quantum normal form transformation sequences (2.27) and (3.65), and start with the second step which consists of simplifying the quadratic part of the Hamilton function or symbol,

respectively. To this end we follow section 2.3 and compute the matrix $J\,\mathrm{D}^2H$ associated with the linearization of Hamilton's equations about $(x, y, p_x, p_y) = 0$. This gives

$$J\,\mathrm{D}^2H(0) = \begin{pmatrix} 0 & 0 & 1/m & \epsilon \\ 0 & 0 & \epsilon & 1/m \\ m\lambda_{\mathrm{E}}^2 & 0 & 0 & 0 \\ 0 & -m\omega_{\mathrm{M}}^2 & 0 & 0 \end{pmatrix}, \tag{7.19}$$

where λ_{E} is defined as in (7.6) and

$$\omega_{\mathrm{M}} = \sqrt{\frac{1}{m}V_{\mathrm{M}}'(0)} = a_{\mathrm{M}}\sqrt{\frac{2D_{\mathrm{e}}}{m}} \tag{7.20}$$

is the linear frequency of the Morse oscillator. The matrix in (7.19) has eigenvalues

$$\lambda := e_1 = \tfrac{1}{2}\sqrt{2\lambda_{\mathrm{E}}^2 - 2\omega_{\mathrm{M}}^2 + 2\sqrt{\omega_{\mathrm{M}}^4 + 2\lambda_{\mathrm{E}}^2\omega_{\mathrm{M}}^2 + \lambda_{\mathrm{E}}^4 - 4\epsilon m^2\lambda_{\mathrm{E}}^2\omega_{\mathrm{M}}^2}}, \tag{7.21}$$

$$e_3 = -\lambda, \tag{7.22}$$

$$\mathrm{i}\omega := e_2 = \mathrm{i}\tfrac{1}{2}\sqrt{2\omega_{\mathrm{M}}^2 - 2\lambda_{\mathrm{E}}^2 + 2\sqrt{\omega_{\mathrm{M}}^4 + 2\lambda_{\mathrm{E}}^2\omega_{\mathrm{M}}^2 + \lambda_{\mathrm{E}}^4 - 4\epsilon m^2\lambda_{\mathrm{E}}^2\omega_{\mathrm{M}}^2}}, \tag{7.23}$$

$$e_4 = -\mathrm{i}\omega, \tag{7.24}$$

where as mentioned above, for given parameters of the Eckart and Morse potentials and $|\epsilon|$ sufficiently small, the eigenvalues e_1 and e_3 (and hence λ) are real, and e_2 and e_4 are purely imaginary (and hence ω is real). For $\epsilon \to 0$, λ and ω converge to λ_{E} and ω_{M}, respectively.

The corresponding eigenvectors are

$$v_k = (e_k(e_k^2 + \omega^2), \epsilon m\lambda_{\mathrm{E}}^2 e_k, m\lambda_{\mathrm{E}}^2(e_k^2 + \omega^2), -\epsilon m^2\lambda_{\mathrm{E}}^2\omega^2)^{\mathrm{T}}, \qquad k = 1, 2, 3, 4. \tag{7.25}$$

Following section 2.3 we obtain a real linear symplectic change of coordinates by using the v_k to define the columns of a matrix M according to

$$M = (c_1 v_1, c_2\mathrm{Re}v_2, c_1 v_3, c_2\mathrm{Im}v_2) \tag{7.26}$$

with the coefficients c_1 and c_2 defined as

$$c_1^{-2} := \langle v_1, J v_3\rangle, \qquad c_2^{-2} := \langle \mathrm{Re}v_2, J\mathrm{Im}v_2\rangle. \tag{7.27}$$

Now set

$$(q_1, q_2, p_1, p_2)^T = M^{-1}(x, y, p_x, p_y)^T. \tag{7.28}$$

Then the Hamilton function (7.15) becomes

$$H = V(0) + \lambda q_1 p_1 + \frac{\omega}{2}\left(q_2^2 + p_2^2\right) + \cdots, \tag{7.29}$$

where the neglected terms are of order greater than 2. The constant term is

$$V(0) = V_{\mathrm{E}}(0) + V_{\mathrm{M}}(0) = \frac{(A+B)^2}{4B} - D_{\mathrm{e}}. \tag{7.30}$$

The truncation of (7.29) at order 2 is the symbol of the 2nd order quantum normal form of (7.15).

The classical and quantum normal forms are then computed from the algorithms described in sections 2.3 and 3.3, respectively. For the parameters $a = 1$, $B = 5$, $A = 1/2$ for the Eckart potential and $D_{\mathrm{e}} = 1$ and $a_{\mathrm{M}} = 1$ for the Morse potential, $\epsilon = 0.3$ for the coupling strength, and $m = 1$, we list the coefficients of the symbol of the 10th order quantum normal from table 3 of appendix B. The classical normal form can be obtained from the symbol by neglecting all terms that involve a factor $\hbar$.

7.2.2. Classical reaction dynamics. For a 2 DoF system the NHIM is a one-dimensional sphere, S^1, i.e. a periodic orbit. This is the Lyapunov periodic orbit associated with the saddle point. As discussed in the introduction, for 2 DoF systems with time-reversal symmetry, the periodic orbit can be used to define a dividing surface without recrossing—the so-called periodic orbit dividing surface—from the projection of the periodic orbit to configuration space [PM73, PP78]. Note that, as mentioned earlier, such a construction in configuration space does not work for systems with 3 or more DoF [WW04].

The NHIM has stable and unstable manifolds with the structure of cylinders or 'tubes', $S^1 \times \mathbb{R}$. They inclose the forward and backward reactive trajectories as discussed in detail in, e.g., [WBW05b, WBW05c]. The flux is given by the action of the periodic orbit [WW04]. In the uncoupled case ($\epsilon = 0$) the periodic orbit (p.o.) is contained in the (y, p_y)-plane and its action can be computed analytically. One finds

$$f(E) = \oint_{\text{p.o.}} p_y \, \mathrm{d}y = \frac{2\pi}{a}(\sqrt{2mD_e} - \sqrt{-2m(E - V_{\text{E}}(0))}) \tag{7.31}$$

for $-D_{\text{e}}+V_{\text{E}}(0) < E < V_{\text{E}}(0)$ and $f(E) = 0$ (no classical transmission) for $E \leqslant -D_{\text{e}}+V_{\text{E}}(0)$.

7.2.3. Quantum reaction dynamics. For the uncoupled case we can compute the cumulative transmission probability analytically. We have

$$N_{\text{exact}}(E) = \sum_{n_2} T_{\text{Eckart;exact}}(E - E_{\text{Morse};n_2}), \tag{7.32}$$

where $T_{\text{Eckart;exact}}$ denotes the transmission coefficient for the Eckart barrier given in (7.8) and $E_{\text{Morse};n_2}$ are the energy levels of a one-dimensional Morse oscillator

$$E_{\text{Morse};n_2} = -\frac{a_{\text{M}}^2\hbar^2}{2m}\left(n_2 + \frac{1}{2} - \frac{\sqrt{2mD_{\text{e}}}}{a_{\text{M}}\hbar}\right)^2, \qquad n_2 = 0, 1, 2, \ldots. \tag{7.33}$$

The graph of N_{exact} in the top panel of figure 17 shows that N_{exact} is 'quantized', i.e. it increases in integer steps each time a new transition channel opens. The opening of a Morse oscillator mode (n_2) as a transition channel can be defined as the energy where $T_{\text{Eckart;exact}}(E - E_{\text{Morse};n_2}) = 1/2$. The quantization of the cumulative reaction probability has been observed experimentally, e.g. in molecular isomerization experiments [LM93] and also in ballistic electron transport problems in semiconductor nanostructures where the analogous effect leads to a quantized conductance [vWvHB+88, WTN+88]. As mentioned in sections 4.4 and 5.4, the quantity

$$N_{\text{Weyl}}(E) = f(E)/(2\pi\hbar) \tag{7.34}$$

can be interpreted as the mean number of open transmission channels at energy E. This is illustrated in the top panel of figure 17 which shows N_{Weyl} together with N_{exact}. Note the nonlinear increase of $N_{\text{Weyl}}(E)$ with E which is an indication of the strong anharmonicity of the Morse oscillator.

In order to compute the cumulative reaction probability from the quantum normal form we follow the procedure described in section 5.4. We get

$$N_{\text{QNF}}^{(N)}(E) = \sum_{n_2}\left[1 + \exp\left(-2\pi\frac{I_{n_2}^{(N)}(E)}{\hbar}\right)\right]^{-1}, \tag{7.35}$$

where $I_{n_2}^{(N)}(E)$ is obtained from inverting

$$K_{\text{QNF}}^{(N)}(I_{n_2}^{(N)}(E), \hbar(n_2 + 1/2)) = E, \qquad n_2 = 0, 1, 2, \ldots. \tag{7.36}$$

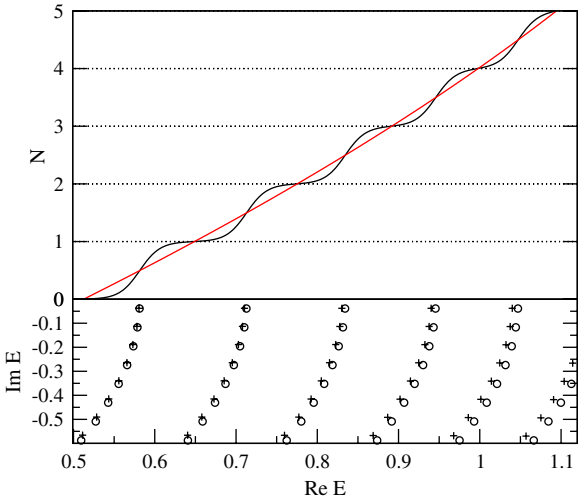

Figure 17. The top panel shows the cumulative reaction probabilities $N_{\rm exact}(E)$ (oscillatory curve) and $N_{\rm Weyl}(E)$ for the Eckart–Morse potential defined in the text with $\epsilon = 0$. The bottom panel shows the (numerically) exact resonances computed from the complex dilation method in the complex energy plane. Circles mark resonances for the uncoupled case $\epsilon = 0$ and crosses mark resonances for the strongly coupled case $\epsilon = 0.3$. The parameters for the potential are the same as in figure 16. Again we choose $m = 1$ and $\hbar = 0.1$.

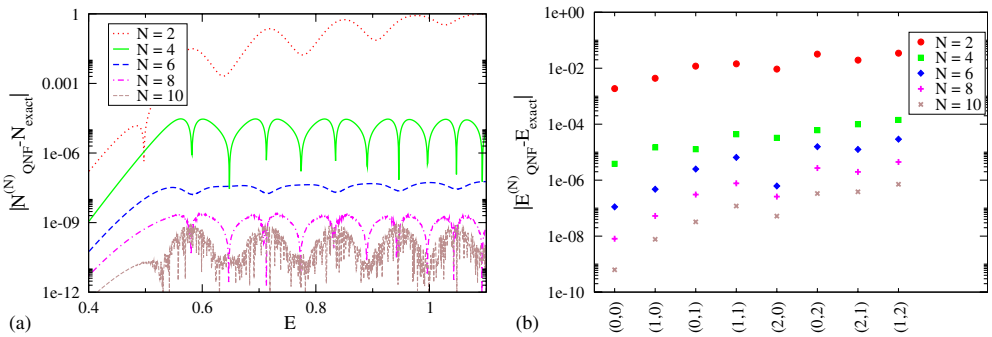

Figure 18. (*a*) Errors for the cumulative reaction probability in the top panel of figure 17 for different orders N of the quantum normal form. (*b*) Difference $|E^{(N)}_{\rm QNF} - E_{\rm exact}|$ for a selection of resonances with quantum numbers (n_1, n_2) for the resonances shown in the bottom panel of figure 17 for the coupled case $\epsilon = 0.3$.

The high quality of the quantum normal form computation of the cumulative reaction probability is illustrated in figure 18(*a*) which shows $|N_{\rm QNF}(E) - N_{\rm exact}(E)|$ versus the energy E for quantum normal forms with $N = 2$ to $N = 10$. As in the 1 DoF example in section 7.1, we find that up to the orders shown, the accuracy of the quantum normal form increases with the order of the quantum normal form. The error is of order 10^{-10} for the 10th order quantum normal form.

For the coupled case $\epsilon \neq 0$ we also make a comparison of the quantum mechanically exact resonances and the resonances computed from the quantum normal form. The exact resonances cannot be computed analytically for the coupled case. To get them numerically we use the *complex dilation method* [Sim79, Rei82, Moi98] whose implementation for the present

system we describe in section C of the appendix. The bottom panel in figure 17 shows the (numerically) exact resonances for the uncoupled case and the strongly coupled case $\epsilon = 0.3$. In both cases the resonances form a distorted lattice in the complex energy plane. The quantum normal form computation of the resonances is given by

$$E^{(N)}_{\mathrm{QNF},(n_1,n_2)} = K^{(N)}_{\mathrm{QNF}}(-\mathrm{i}\hbar(n_1 + 1/2), \hbar(n_2 + 1/2)), \qquad n_1, n_2 = 0, 1, 2, \ldots . \tag{7.37}$$

One of the benefits of the quantum normal form is that it leads to an assignment of the resonance lattice by quantum numbers. The quantum number n_1 labels the resonances in the vertical direction, and the quantum number n_2 labels the resonances in the horizontal direction. Each vertical string of resonances (i.e. sequence of resonances for fixed n_2) gives rise to one quantization step of the cumulative reaction probability. Note that an assignment of the resonances is very difficult to obtain only from the exact quantum computation. Figure 18(*b*) illustrates the high accuracy of the quantum normal form computation for a selection of resonances.

7.3. Example with 3 DoF

Our final example is a 3 DoF model system consisting of an Eckart barrier in the x-direction that is coupled to Morse oscillators in the y-direction and in the z-direction. The Hamilton function is

$$H = \frac{1}{2m}(p_x^2 + p_y^2 + p_z^2) + V_{\mathrm{E}}(x) + V_{\mathrm{M};2}(y) + V_{\mathrm{M};3}(z) + \epsilon H_{\mathrm{c}}, \tag{7.38}$$

where V_{E} is the Eckart potential from (7.2) and $V_{\mathrm{M};k}$, $k = 2, 3$, are Morse potentials of the form (7.16) with parameters $D_{\mathrm{e};k}$ and $a_{M;k}$, $k = 2, 3$, respectively. For H_{c} we choose the mutual kinetic coupling

$$H_{\mathrm{c}} = p_x p_y + p_x p_z + p_y p_z. \tag{7.39}$$

The strength of the coupling is again controlled by the parameter ϵ in (7.38). The vector field generated by the Hamilton function has an equilibrium point at $(x, y, z, p_x, p_y, p_z) = 0$. For $|\epsilon|$ sufficiently small (for given parameters of the Eckart and Morse potentials), the equilibrium point is of the saddle-centre-centre stability type. Figure 19 shows contours of the potential $V(x, y, z) = V_{\mathrm{E}}(x) + V_{\mathrm{M};2}(y) + V_{\mathrm{M};3}(z)$ which, for energies slightly above the saddle-centre-centre equilibrium point, indicate the bottleneck-type structure of the corresponding energy surfaces.

The Weyl quantization of the Hamilton function H in (7.38) gives the operator

$$\mathrm{Op}[H] = -\frac{\hbar^2}{2m}\left(\frac{\partial^2}{\partial x^2} + \frac{\partial^2}{\partial y^2} + \frac{\partial^2}{\partial z^2}\right) + V_{\mathrm{E}} + V_{\mathrm{M};2} + V_{\mathrm{M};3} - \epsilon\hbar^2\left(\frac{\partial^2}{\partial x \partial y} + \frac{\partial^2}{\partial x \partial z} + \frac{\partial^2}{\partial y \partial z}\right). \tag{7.40}$$

The Hamilton function (7.15) is the principal symbol of the operator $\mathrm{Op}[H]$.

7.3.1. Computation of the classical and quantum normal forms. As in section 7.2 the equilibrium point is again already at the origin of the coordinate system. For the computation of the classical and quantum normal forms we therefore again start with the second step in the sequences (2.27) and (3.65), respectively. Following again section. 2.3, we compute the Hamiltonian matrix associated with the linearization of Hamilton's equations about the

equilibrium point $(x, y, z, p_x, p_y, p_z) = 0$. This gives

$$J\mathrm{D}^2H(0) = \begin{pmatrix} 0 & 0 & 0 & 1/m & \epsilon & \epsilon \\ 0 & 0 & 0 & \epsilon & 1/m & \epsilon \\ 0 & 0 & 0 & \epsilon & \epsilon & 1/m \\ m\lambda_{\mathrm{E}}^2 & 0 & 0 & 0 & 0 & 0 \\ 0 & -m\omega_{\mathrm{M};2}^2 & 0 & 0 & 0 & 0 \\ 0 & 0 & -m\omega_{\mathrm{M};3}^2 & 0 & 0 & 0 \end{pmatrix}, \tag{7.41}$$

where λ_{E} is defined in (7.6) and

$$\omega_{\mathrm{M};k} = \sqrt{\frac{1}{m}V'_{\mathrm{M};k}(0)} = a_{\mathrm{M};k}\sqrt{\frac{2D_{\mathrm{e};k}}{m}}, \qquad k = 2, 3, \tag{7.42}$$

are the linear frequencies of the Morse oscillators. The matrix $J\,\mathrm{D}^2H(0)$ has six eigenvalues, one pair of real eigenvalues of opposite signs and two pairs of imaginary eigenvalues with opposite signs. We label them according to

$$e_1 = \lambda, \qquad e_4 = -\lambda, \qquad e_2 = \mathrm{i}\omega_2, \qquad e_5 = -\mathrm{i}\omega_2, \qquad e_3 = \mathrm{i}\omega_3, \qquad e_6 = -\mathrm{i}\omega_3, \tag{7.43}$$

where λ, ω_2 and ω_3 are real positive constants that converge to λ_{E} and the linear frequencies $\omega_{\mathrm{M};2}$ and $\omega_{\mathrm{M};3}$, respectively, when $\epsilon \to 0$. We assume that the parameters $D_{\mathrm{e};k}$ and $a_{\mathrm{M};k}$, $k = 2, 3$, are chosen such that ω_2 and ω_3 are linearly independent over $\mathbb{Z}$. Let us again denote the corresponding eigenvectors by v_k, $k = 1, \ldots, 6$. In order to define a real linear symplectic change of coordinates we use the eigenvectors v_k to define the columns of a matrix M according to

$$M = (c_1 v_1, c_2\mathrm{Re}v_2, c_3\mathrm{Re}v_3, c_1 v_4, c_2\mathrm{Im}v_2, c_3\mathrm{Im}v_3) \tag{7.44}$$

with the coefficients c_1, c_2 and c_3 defined as

$$c_1^{-2} := \langle v_1, Jv_4\rangle, \qquad c_2^{-2} := \langle \mathrm{Re}v_2, J\mathrm{Im}v_2\rangle, \qquad c_3^{-2} := \langle \mathrm{Re}v_3, J\mathrm{Im}v_3\rangle. \tag{7.45}$$

We choose the eigenvectors v_1 and v_3 such that $\langle v_1, Jv_3\rangle$ is positive (if $\langle v_1, Jv_2\rangle < 0$ then multiply v_2 by -1). As mentioned in section 2.2 the coefficients c_2^{-2} and c_3^{-2} in (7.45) are automatically positive and the matrix M is symplectic. For

$$(q_1, q_2, q_3, p_1, p_2, p_3)^{\mathrm{T}} = M^{-1}(x, y, z, p_x, p_y, p_z)^{\mathrm{T}} \tag{7.46}$$

the Hamilton function (7.38) becomes

$$H = V(0) + \lambda q_1 p_1 + \frac{\omega_2}{2}\left(q_2^2 + p_2^2\right) + \frac{\omega_3}{2}\left(q_3^2 + p_3^2\right) + \cdots, \tag{7.47}$$

where the neglected terms are of order greater than 2. The constant term is

$$V(0) = V_{\mathrm{E}}(0) + V_{\mathrm{M};2}(0) + V_{\mathrm{M};3}(0) = \frac{(A+B)^2}{4B} - D_{\mathrm{e};2} - D_{\mathrm{e};3}. \tag{7.48}$$

The truncation of (7.47) at order 2 is the symbol of the 2nd order quantum normal form of (7.38). The higher order classical and quantum normal forms are then computed from the algorithm described in sections 2.3 and 3.3. For the parameters $a = 1$, $B = 5$, $A = 1/2$ for the Eckart potential and $D_{\mathrm{e};1} = 1$, $D_{\mathrm{e};2} = 3/2$ and $a_{\mathrm{M};1} = a_{\mathrm{M};2} = 1$ for the Morse potential, $\epsilon = 0.3$ for the coupling strength and $m = 1$, we list the coefficients of the symbol of the 10th order quantum normal form in table 4 of appendix B. The classical normal form is obtained from discarding terms involving a factor $\hbar$.

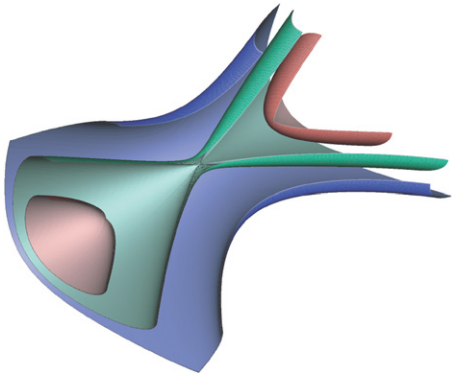

Figure 19. Contours $V_{\mathrm{E}}(x) + V_{\mathrm{M};2}(y) + V_{\mathrm{M};3}(z) = \text{const}$ of the Eckart–Morse–Morse potential. The parameters for the Eckart potential are the same as in figure 14. The parameters for the Morse potentials are $D_{\mathrm{e};2} = a_{\mathrm{M};2} = a_{\mathrm{M};3} = 1$ and $D_{\mathrm{e};3} = 2/3$.

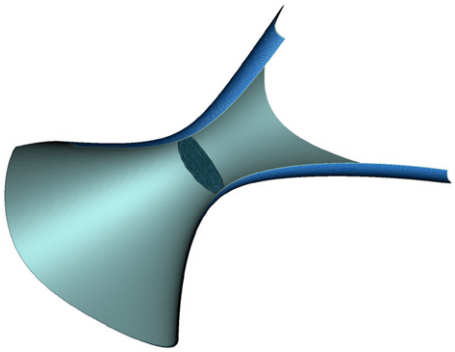

Figure 20. The NHIM projected into configuration space. The energy is 0.1 above the energy of the saddle-centre-centre equilibrium point.

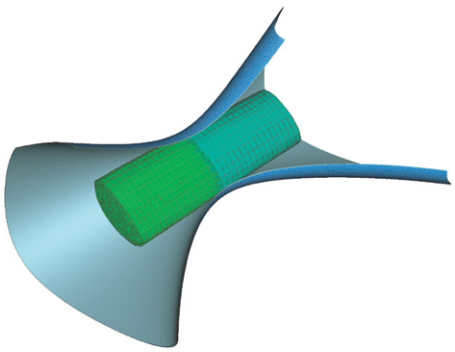

Figure 21. The stable and unstable manifolds of the NHIM projected into configuration space. Due to the time-reversal symmetry, these manifolds project onto each other in configuration space. The two colours represent the forward and backward branches of the manifolds, and they are 'joined' at the NHIM. The energy is 0.1 above the energy of the saddle-centre-centre equilibrium point.

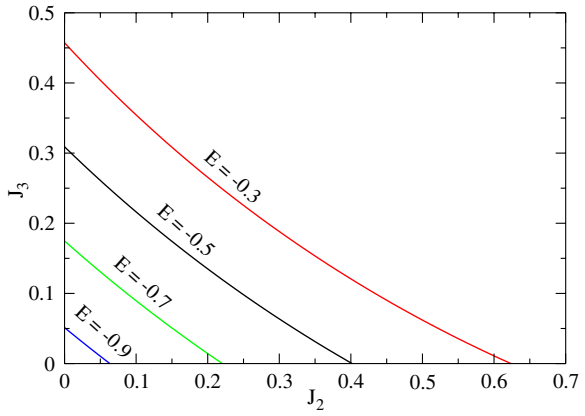

Figure 22. Energy contours in the plane of the Morse oscillator actions (J_2, J_3). The Morse oscillators have energies E_y and E_z such that $V_E(0) + E_y + E_z = E$ with $V_E(0)$ being the height of the one-dimensional Eckart barrier (see text). The parameters for the potential are the same as in figure 19. The mass m is 1.

7.3.2. Classical reaction dynamics. The NHIM is a three-dimensional sphere, S^3. In figure 20 we show the NHIM with the energy 0.1 above the energy of the saddle-centre-centre equilibrium point projected into configuration space, with the equipotential at the same energy for reference. Note that the projection of the NHIM to configuration space is a three-dimensional object. This can be viewed as an indication that the construction of a (in this case two-dimensional) dividing surface 'in configuration space' without recrossing is not possible for a system with 3 (or more) DoF since, as explained in detail in [WW04], a dividing surface without recrossing needs to contain the NHIM (as its equator).

The NHIM's stable and unstable manifolds have the structure of spherical cylinders, $S^3 \times \mathbb{R}$. In figure 21 we show projections into configuration space of local pieces of the backward branch of the stable manifold of the NHIM, the forward branch of the stable manifold of the NHIM, the backward branch of the unstable manifold of the NHIM and the forward branch of the unstable manifold of the NHIM. Due to the time-reversal symmetry of the system the stable and unstable manifolds project onto each other in configuration space. The stable and unstable manifolds enclose the forward and backward reactive trajectories as discussed in section 4.

The NHIM is foliated by invariant 2-tori. According to section 4.4 the classical flux for an energy E is given by

$$f(E) = (2\pi)^2 \mathcal{V}(E), \tag{7.49}$$

where $\mathcal{V}(E)$ is the area enclosed by the energy contour in the plane of the corresponding action variables J_2 and J_3. In the uncoupled case the 2-tori are given by the Cartesian products of two circles that are contained in the (y, p_y)-plane and (z, p_z)-plane, respectively. The corresponding action variables J_2 and J_3 can be easily computed in this case. Let E_y and E_z be the energies contained in these two DoF. Then

$$J_2(E_y) = \frac{1}{2\pi} \oint_{\text{p.o.}} p_y \, \mathrm{d}y = \frac{1}{a_2}(\sqrt{2m D_{e;2}} - \sqrt{-2m E_y}), \qquad -D_e < E_y < 0, \tag{7.50}$$

and similarly for $J_3(E_z)$. The NHIM has energy $E = V_E(0) + E_y + E_z$, where $V_E(0) = (A + B)^2/(4B)$ is the height of the one-dimensional Eckart barrier. Figure 22 shows some

energy contours in the (J_2, J_3)-plane. The fact that the energy contours are not straight lines is an indication of the strong nonlinearity of the Morse oscillators for the energies shown. For an energy $V_{\mathrm{E}}(0) - D_{\mathrm{e};2} - D_{\mathrm{e};3} < E < V_{\mathrm{E}}(0) - D_{\mathrm{e};3}$, the inclosed area is given by

$$\mathcal{V}(E) = \int_{-D_{\mathrm{e};2}}^{E+D_{\mathrm{e};3}-V_{\mathrm{E}}(0)} J_3(E - V_{\mathrm{E}}(0) - E_y)\frac{\mathrm{d}J_2(E_y)}{\mathrm{d}E_y}\,\mathrm{d}E_y \tag{7.51}$$

$$= \frac{2m\sqrt{D_{\mathrm{e};3}}}{a_2\,a_3}(\sqrt{D_{\mathrm{e};2}} - \sqrt{V_{\mathrm{E}}(0) - D_{\mathrm{e};3} - E}) - \frac{m}{a_2\,a_3}(g(E - V_{\mathrm{E}}(0) + D_{\mathrm{e};3}) - g(-D_{\mathrm{e};2})), \tag{7.52}$$

where

$$g(E_y) := \sqrt{-E_y(E_y - E + V_{\mathrm{E}}(0))} - \frac{1}{2}(E - V_{\mathrm{E}}(0))\ \arctan\left(\frac{E - V_{\mathrm{E}}(0) - 2E_y}{2\sqrt{-E_y(E_y - E + V_{\mathrm{E}}(0))}}\right). \tag{7.53}$$

For $E \leqslant V_{\mathrm{E}}(0) - D_{\mathrm{e};2} - D_{\mathrm{e};3}$ the classical flux is zero. The graph of $N_{\mathrm{Weyl}}(E) = f(E)/(2\pi\hbar)^2$ is shown in the top panel of figure 23.

7.3.3. Quantum reaction dynamics. In the uncoupled case the exact cumulative reaction probability N_{exact} can be computed analytically. We have

$$N_{\mathrm{exact}}(E) = \sum_{n_2,n_3} T_{\mathrm{Eckart;exact}}(E - E_{\mathrm{Morse};2,n_2} - E_{\mathrm{Morse};3,n_3}), \tag{7.54}$$

where $T_{\mathrm{Eckart;exact}}$ denotes the transmission coefficient for the Eckart barrier given in (7.8) and $E_{\mathrm{Morse;k},n_k}$, $k = 2, 3$, are the energy levels of the one-dimensional Morse oscillators,

$$E_{\mathrm{Morse};k,n_k} = -\frac{a_{\mathrm{M};k}^2\hbar^2}{2m}\left(n_k + \frac{1}{2} - \frac{\sqrt{2m\,D_{\mathrm{e};k}}}{a_{\mathrm{M};k}\hbar}\right)^2, \qquad n_k = 0, 1, 2, \ldots. \tag{7.55}$$

The graph of N_{exact} gives the oscillatory curve shown in the top panel of figure 23.

For the quantum normal form computation of the cumulative reaction probability we get

$$N_{\mathrm{QNF}}^{(N)}(E) = \sum_{n_2,n_3}\left[1 + \exp\left(-2\pi\,\frac{I_{n_2,n_3}^{(N)}(E)}{\hbar}\right)\right]^{-1}, \tag{7.56}$$

where $I_{(n_2,n_3)}^{(N)}(E)$ is obtained from inverting

$$K_{\mathrm{QNF}}(I_{(n_2,n_3)}^{(N)}(E), \hbar(n_2 + 1/2), \hbar(n_3 + 1/2)) = E, \qquad n_2, n_3 = 0, 1, 2, \ldots. \tag{7.57}$$

The high quality of the quantum normal form approximation of the cumulative reaction probability is illustrated in figure 24(*a*) which shows $|N_{\mathrm{QNF}}^{(N)}(E) - N_{\mathrm{exact}}(E)|$ versus the energy E.

For the coupled case $\epsilon \neq 0$ we again make a comparison of the exact resonances and the resonances computed from the quantum normal form. We again compute the (numerically) exact resonances from the complex dilation method whose implementation is described in appendix C. The bottom panel in figure 23 shows the exact resonances for the uncoupled case and the strongly coupled case $\epsilon = 0.3$. In both cases the resonances now

form a superposition of distorted lattices. The quantum normal form computation of the resonances

$$E^{(N)}_{\mathrm{QNF},(n_1,n_2,n_3)} = K^{(N)}_{\mathrm{QNF}}(-\mathrm{i}\hbar(n_1+1/2), \hbar(n_2+1/2), \hbar(n_3+1/2)), \qquad n_1, n_2, n_3 \in \mathbb{N}_0, \tag{7.58}$$

allows one to organize the resonance by quantum numbers. The quantum numbers n_1 label the resonances in the vertical direction, and the pairs of Morse oscillator mode quantum numbers (n_2, n_3) label the resonances in the horizontal direction. Here each vertical string of resonances (i.e. sequence of resonances for fixed (n_2, n_3)) gives rise to one step of the cumulative reaction probability. In the top panel of figure 23 we mark the energies at which a mode (n_2, n_3) opens as a transmission channel. These energies are defined in the same way as in section 7.2.

Since the density of the resonances in the complex energy plane is higher for the 3 DoF case than it is in the 2 DoF case the quantization of the cumulative reaction probability is more 'washed out'. Again note that an assignment of the resonances is very difficult to obtain only from the exact quantum computation. The resonances computed from the quantum normal form are again of a very high accuracy as shown for a selection of resonances with quantum numbers (n_1, n_2, n_3) in figure 24(*b*).

8. Conclusions and outlook

In this paper we have developed a phase space version of Wigner's dynamical transition state theory for both classical and quantum systems. In the setting of Hamiltonian classical mechanics, reaction type dynamics is induced by the presence of a saddle-centre-...-centre equilibrium point ('saddle' for short). For a fixed energy slightly above the energy of the saddle, the energy surface has a wide–narrow–wide structure in the neighbourhood of the saddle. Trajectories must pass through this bottleneck in order to evolve from reactants to products. We provided a detailed study of the phase space structures which for such an energy, exist near the saddle and control the dynamics in the neighbourhood of the saddle. In particular we showed the existence of a dividing surface which is free of local recrossings, i.e. it has the property that all trajectories extending from reactants to products (or vice versa) intersect this dividing surface exactly once without leaving a neighbourhood of the saddle and nonreactive trajectories which enter the neighbourhood from the side of reactants (respectively, products) and exit the neighbourhood back to reactants (respectively, products) do not intersect the dividing surface. This dividing surface minimizes the directional flux in the sense that a (generic) deformation of the dividing surface leads to an increase of the directional flux through the dividing surface. Such a dividing surface is a prerequisite for the computation of reaction rates from the directional flux and its construction for multi-degree-of-freedom systems was considered a major problem in transition state theory. We showed that the existence of such a dividing surface is related to the presence of a normally hyperbolic invariant manifold (NHIM) which exists near the saddle. The NHIM has the structure of a sphere of two dimensions less than the energy surface. It can be considered to form the equator of the dividing surface which itself is a sphere of one dimension less than the energy surface. This way the NHIM divides the dividing surface into two hemispheres of which one is intersected by all trajectories evolving from reactants to products and the other is crossed by all trajectories evolving from products to reactants.

The NHIM is the mathematical manifestation of what is referred to as activated complex in the chemistry literature. In fact, the NHIM, which is the intersection of the centre manifold of the saddle with the energy surface of the (full) system, can itself be viewed as the energy surface of an unstable invariant subsystem (the subsystem given by the centre manifold). This

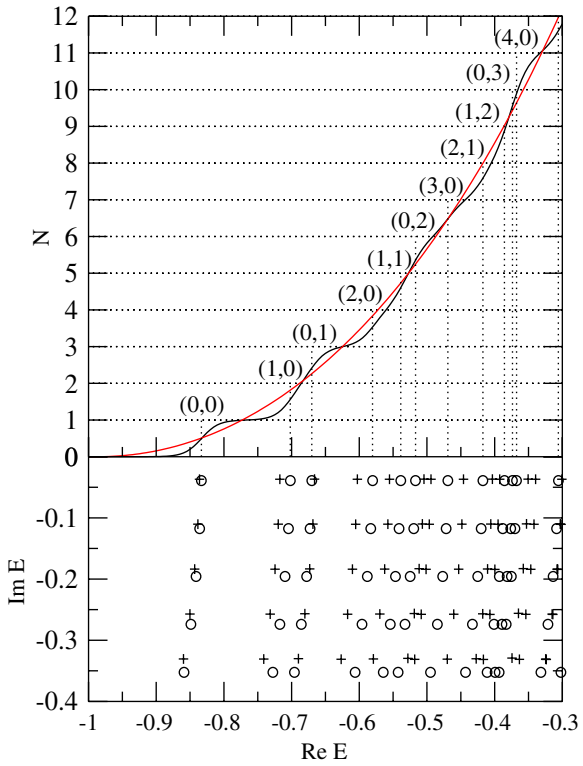

Figure 23. The top panel shows the cumulative reaction probabilities $N_{\mathrm{exact}}(E)$ (oscillatory curve) and $N_{\mathrm{Weyl}}(E)$ (smooth curve) for the Eckart–Morse–Morse potential defined in the text with $\epsilon = 0$. It also shows the quantum numbers (n_2, n_3) of the Morse oscillators that contribute to the quantization steps. The bottom panel shows the resonances in the complex energy plane marked by circles for the uncoupled case $\epsilon = 0$ and by crosses for the strongly coupled case $\epsilon = 0.3$. The parameters for the Eckart potential are the same as in figure 14. The parameters for the Morse potential are $D_{\mathrm{e};2} = 1$, $D_{\mathrm{e};3} = 3/2$, $a_{\mathrm{M};2} = 1$ and $a_{\mathrm{M};3} = 1$. Again we choose $m = 1$ and $\hbar = 0.1$.

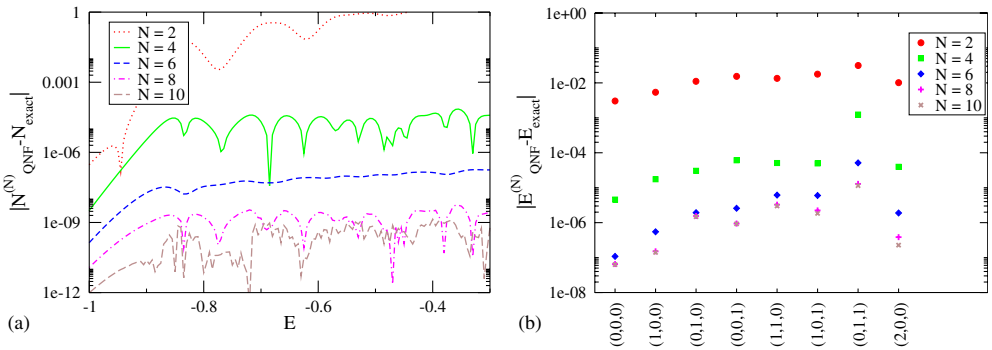

Figure 24. (*a*) Errors for the cumulative reaction probability in the top panel figure 23 for different orders N of the quantum normal form. (*b*) Errors $|E^{(N)}_{\mathrm{QNF}} - E_{\mathrm{exact}}|$ for a selection of resonances with quantum numbers (n_1, n_2, n_3) for the coupled case $\epsilon = 0.3$ in the bottom panel of figure 23.

subsystem has one degree of freedom less than the full system and as a kind of super molecule is poised between reactants and products. The theoretical background presented in this paper thus shows that the activated complex is not merely a heuristic concept utilized by transition state theory, but a geometric object of precise significance for the dynamics. In particular, the NHIM has stable and unstable manifolds which have sufficient dimensionality to act as separatrices. They form the phase space conduits for reactions in the sense that they enclose the reactive volumes (which consist of trajectories evolving from reactants to products or vice versa) and separate them from the nonreactive volumes (which consist of nonreactive trajectories). They have the structure of spherical cylinders (i.e. cylinders where the base is a sphere). We discussed how the centre lines of the reactive volumes enclosed by these spherical cylinders naturally lead to the definition of a reaction path, i.e. as a kind of guiding trajectory about which other reactive trajectories rotate in phase space (observed as an oscillation when projected to configuration space) in a well-defined manner. In contrast to the usual, often heuristic definitions of a reaction path, the reaction path presented in this paper incorporates the full dynamics in a mathematically precise way.

We showed that all the phase space structures mentioned above can be realized through an efficient algorithm based on a standard Poincaré–Birkhoff normal form. This algorithm allows one to transform the Hamilton function which describes the classical reaction dynamics to a simpler ('normal') form to any order of its Taylor expansion about the saddle point through a succession of symplectic transformations. In several examples we showed that the normal form computation truncated at a suitable order leads to a very accurate description of the dynamics near the saddle. In the generic situation where there are no resonances between the linear frequencies associated with the centre direction of the saddle the normal form is integrable and explains the regularity of the motion near the saddle which has been discovered in the chemistry literature [HB93, KB99, Mil77]. The integrability leads to a foliation of the neighbourhood of the saddle by invariant Lagrangian manifolds. These Lagrangian manifolds have the structure of toroidal cylinders, i.e. cylinders where the base is formed by a torus.

We showed that similarly to the unfolding of the classical dynamics in the neighbourhood of a saddle point we can obtain an unfolding of the corresponding quantum dynamics. We therefore reviewed some basic tools from the theory of micro local analysis which allow one to study properties of quantum operators in a region of interest in the phase space of the corresponding classical system. The main idea is to use the Weyl calculus to relate Hamilton operators to phase space functions (symbols) and vice versa. This way one can extract properties of a Hamilton operator resulting from some classical phase space region by studying its symbol restricted to (or 'localized at') this phase space region. In the case of reaction dynamics the region of interest is the neighbourhood of a saddle point. We showed that in the neighbourhood of a saddle the Hamilton operator can be transformed to a simple form—the quantum normal form—to any order of the Taylor expansion of its symbol about the saddle by conjugating the Hamilton operator by a succession of suitable unitary transformations. We showed that the quantum normal form computation can be cast into an explicit algorithm based on the Weyl calculus. This algorithm consists of two parts of which the first part takes place on the level of the symbols and is therefore very similar in nature to the classical normal form computation. The main difference is that the Poisson bracket involved in the symplectic transformation in the classical case is replaced by the Moyal bracket. In the second part of the quantum normal form algorithm the symbols are quantized to obtain the corresponding quantum operators. For this part we also developed an explicit algorithm.

Through applications to several examples we illustrated the efficiency of the quantum normal form algorithm for computing quantum reaction quantities like the cumulative reaction

probability and quantum resonances. The cumulative reaction rate is the quantum analogue of the classical flux. Quantum resonances describe the decay of wavepackets initialized on the centre manifold. In fact, quantum mechanically, the Heisenberg uncertainty principle excludes the existence of an invariant subsystem representing the activated complex analogously to the classical case. So quantum mechanically a state initially localized on the centre manifold is unstable and will spread out. The quantum resonances describe the lifetimes of such states. We showed that these resonances are also related to the stepwise increase ('quantization') of the cumulative reaction probability as a function of energy. The dependence of the cumulative reaction probability on the energy and also the resonances are viewed as the quantum signatures of the activated complex, and there is huge experimental interest in these quantities [SY04]. In fact, recent advances in spectroscopic techniques allow one to study quantum scattering with unprecedented detail (see, e.g., [Zar06]). We hope that the results presented and the methods developed in this paper will contribute to the understanding and a better interpretation of such experiments.

The benefit of the quantum normal form presented in this paper is not only to give a firm theoretical framework for a quantum version of an activated complex but it moreover leads to a very efficient method for computing quantum reaction rates and the associated resonances.

In fact, the quantum normal form computation of reaction probabilities and resonances is highly promising since it opens the way to study high dimensional systems for which other techniques based on the *ab initio* solution of the quantum scattering problem like the complex dilation method [Sim79, Rei82, Moi98] or the utilization of an absorbing potential [NM01] do not seem feasible. We mention that in order to compute resonances from the complex dilation method that are sufficiently accurate to facilitate a comparison with our quantum normal form computations for the three-degree-of-freedom example studied in this paper we had to diagonalize matrices of size 2500×2500, and this way we reached the limits of our numerical computation capabilities. Furthermore, the complex dilation method requires the 'tuning' of the scaling angle which is not straightforward but has to be worked out by repeating the numerical computation for different scaling angles. In contrast to this, the quantum normal form computation can be implemented in a similarly transparent and efficient way as the classical normal form. The quantum normal form then gives an explicit formula for the resonances from which they can be computed directly by inserting the corresponding quantum numbers. In particular, this leads to a direct assignment of the resonances which one cannot obtain from the *ab initio* methods mentioned above.

We used the Weyl calculus as a tool to systematically study several further aspects of the quantum–classical correspondence. One such aspect is the relation between the quantum mechanics of reactions to the phase space structures that control classical reaction dynamics. We showed that the scattering wavefunctions are concentrated on those Lagrangian manifolds foliating the neighbourhood of a saddle whose toroidal base fulfils Bohr–Sommerfeld quantization conditions. The location of such a 'quantized' Lagrangian manifold relative to the NHIM's stable and unstable manifold, i.e. the question of whether the classical trajectories on such a Lagrangian manifold are reactive or nonreactive, determines whether the scattering wavefunction corresponds to an open or a closed transmission channel. In fact, the cumulative reaction probability can be interpreted as a counting function of the number of open transmission channels (i.e. the number of quantized Lagrangian manifolds in the reactive volume of phase space) at a given energy. We showed that the Weyl approximation of this number is obtained from dividing the phase space volume of the invariant subsystem representing the activated complex enclosed by the NHIM of the given energy by elementary quantum cells, i.e. quantum cells with sidelength given by Planck's constant.

We moreover showed that the resonance states can be viewed to be localized on Lagrangian manifolds for which in addition to the Bohr–Sommerfeld quantization of the toroidal base the remaining degree of freedom fulfils a complex Bohr–Sommerfeld quantization condition. These complex Lagrangian manifolds project to the NHIM and its unstable manifolds (the direction of the decay of the resonance states) in real phase space.

Most of the theory discussed in this paper, both classically and quantum mechanically, is local in nature. In fact, the flux in the classical case, and the cumulative reaction probability and the associated resonances in the quantum case only require local information derived from properties of the Hamilton function or operator, respectively, in the neighbourhood of the saddle point. This information can therefore be extracted from the classical and quantum normal forms. Some of the classical phase space structures in the neighbourhood of the saddle where they are accurately described by the normal form are nonlocal in nature. This concerns the stable and unstable manifolds and the Lagrangian manifolds mentioned above. In fact they can extend to regions far away from the saddle point. This 'global' information is important for the study of state specific reactivity and the control of reactions. Since these phase space structures are invariant manifolds and hence consist of trajectories they can be obtained by 'growing' them out of the neighbourhood described by the (classical) normal form by integrating the equations of motion generated by the original Hamilton function. For the classical case we used this, as we mentioned in this paper, to develop an efficient procedure to determine, e.g., the volume of reactive initial conditions in a system. For the quantum case we mention the recent work by Creagh [Cre04, Cre05] who developed a semiclassical theory of a reaction operator from a kind of normal form expansion about what we defined as the dynamical reaction path in this paper. Our own future work will follow similar ideas by extending the Bohr–Sommerfeld quantized Lagrangian manifolds that carry the scattering wavefunctions to the Lagrangian structures associated with the asymptotic states of reactants and products. The goal is to develop an efficient semiclassical procedure to compute full scattering matrices. This would not only allow one to compute state-specific reactivities but also give a clearer idea of how the quantum signatures of the activated complex are manifested in scattering experiments.

Acknowledgments

HW is grateful to Andrew Burbanks for many helpful discussions on the numerical implementation of the normal form computation in the programming language C++. Furthermore, HW and SW would like to thank Peter Collins for comparing the results for the normal forms presented in this paper with the results of his numerical computations. RS, HW and SW acknowledge individual support by EPSRC. SW also acknowledges support by ONR (Grant No N00014-01-1-0769).

Appendix A. Proof of lemma 9

We here provide a short sketch of the proof of lemma 9.

Proof. Let $A \in \mathcal{S}_\hbar(\mathbb{R}^d \times \mathbb{R}^d)$ and A' be the symbol of $\mathrm{e}^{\frac{\mathrm{i}}{\hbar}\mathrm{Op}[W]}\mathrm{Op}[A]\mathrm{e}^{-\frac{\mathrm{i}}{\hbar}\mathrm{Op}[W]}$ with $W \in \mathcal{W}^s_{\mathrm{qm;loc}}$. We need to show that $A' \in \mathcal{S}_\hbar(\mathbb{R}^d \times \mathbb{R}^d)$. To this end define for $s \geqslant 0$,

$$\mathcal{H}^s(\mathbb{R}^d) := \{\psi \in L^2(\mathbb{R}^d) \,:\, \mathrm{Op}[B]\psi \in L^2(\mathbb{R}^d)\, \forall B \in \mathcal{W}^{s'}_{\mathrm{qm}} \text{ with } 0 \leqslant s' \leqslant s\}, \tag{A.1}$$

and let $\mathcal{H}^{-s}(\mathbb{R}^d)$ denote the dual of $\mathcal{H}^s(\mathbb{R}^d)$. Then a variant of the usual Beals characterization of pseudodifferential operators gives that $A \in \mathcal{S}_\hbar(\mathbb{R}^d \times \mathbb{R}^d)$ if and only if for all $s, s' \in \mathbb{Z}$,

$$\mathrm{Op}[A] : \mathcal{H}^{s'}(\mathbb{R}^d) \to \mathcal{H}^s(\mathbb{R}^d). \tag{A.2}$$

This follows because (A.2) implies that for any $B_j \in \mathcal{W}^{s_j}_{\mathrm{qm}}$, $j = 1, \ldots, N$ with $s_j \geqslant 0$, we have

$$[\mathrm{Op}[B_N], [\mathrm{Op}[B_{N-1}], \ldots, [\mathrm{Op}[B_1], \mathrm{Op}[A]]]] : L^2(\mathbb{R}^d) \to L^2(\mathbb{R}^d), \tag{A.3}$$

and this implies that $A \in \mathcal{S}_\hbar(\mathbb{R}^d \times \mathbb{R}^d)$ (see [DS99]).

For a real valued $W \in \mathcal{W}^s_{\mathrm{qm;loc}}$, we define $\hat{U}(\epsilon) := \mathrm{e}^{-\frac{\mathrm{i}}{\hbar}\epsilon \mathrm{Op}[W]}$. Then $\hat{U}(\epsilon) : L^2(\mathbb{R}^d) \to L^2(\mathbb{R}^d)$ since $\hat{U}(\epsilon)$ is unitary. Moreover, we have that

$$\hat{U}(\epsilon) : \mathcal{H}^s(\mathbb{R}^d) \to \mathcal{H}^s(\mathbb{R}^d) \tag{A.4}$$

for all s. To see this, let $\psi \in \mathcal{H}^s(\mathbb{R}^d)$. Then we have to show that $\mathrm{Op}[B]\hat{U}(\epsilon)\psi \in L^2(\mathbb{R}^d)$ for all $B \in \mathcal{W}^{s'}_{\mathrm{qm}}$ with $s' \leqslant s$. But $\mathrm{Op}[B]\hat{U}(\epsilon) = \hat{U}(\epsilon)\hat{U}(-\epsilon)\mathrm{Op}[B]\hat{U}(\epsilon)$ and

$$\begin{aligned}\hat{U}(-\epsilon)\mathrm{Op}[B]\hat{U}(\epsilon) - \mathrm{Op}[B] &= \int_0^\epsilon \frac{\mathrm{d}}{\mathrm{d}\epsilon'}\Big(\hat{U}(-\epsilon')\mathrm{Op}[B]\hat{U}(\epsilon')\Big)\,\mathrm{d}\epsilon' \\ &= \int_0^\epsilon \hat{U}(-\epsilon')\frac{\mathrm{i}}{\hbar}[\mathrm{Op}[W], \mathrm{Op}[B]]\hat{U}(\epsilon')\,\mathrm{d}\epsilon'. \end{aligned}\tag{A.5}$$

Hence

$$\mathrm{Op}[B]\hat{U}(\epsilon) = \hat{U}(\epsilon)\Big(\mathrm{Op}[B] + \int_0^\epsilon \hat{U}(-\epsilon')\frac{\mathrm{i}}{\hbar}[\mathrm{Op}[W], \mathrm{Op}[B]]\hat{U}(\epsilon')\,\mathrm{d}\epsilon'\Big). \tag{A.6}$$

Since W is localized, the commutator $\frac{\mathrm{i}}{\hbar}[\mathrm{Op}[W], \mathrm{Op}[B]]$ is a bounded operator, and therefore $\mathrm{Op}[B]\hat{U}(\epsilon)\psi \in L^2(\mathbb{R}^d)$.

By (A.4) we see then that if $\mathrm{Op}[A]$ satisfies (A.2) then $\hat{U}(-\epsilon)\mathrm{Op}[A]\hat{U}(\epsilon)$ satisfies (A.2), too, and therefore $A' \in \mathcal{S}_\hbar(\mathbb{R}^d \times \mathbb{R}^d)$. □

Appendix B. Symbols of the quantum normal forms of the systems studied in section 7

Table 2. Nonvanishing coefficients of the symbol $H^{(10)}_{\mathrm{QNF}}(\hbar, x, \xi) = \sum_{\alpha+\beta+2\gamma\leqslant 10} h_{(\alpha,\beta,\gamma)} x^\alpha \xi^\beta \hbar^\gamma$ of the 10th order quantum normal form of the one DoF Eckart barrier with the potential (7.2) studied in section 7.1. Recall that the nonvanishing terms in the normal form have $\alpha = \beta$.

α	γ	$h_{(\alpha,\beta,\gamma)}$	α	γ	$h_{(\alpha,\beta,\gamma)}$
0	0	1.512 500 000 000 000 000	4	0	0.000 625 000 000 000 000
1	0	0.782 663 720 891 674 056	2	2	0.002 375 000 000 000 005
2	0	0.128 750 000 000 000 027	0	4	0.000 250 000 000 000 000
0	2	0.001 250 000 000 000 000	5	0	−0.000 237 170 824 512 630
3	0	−0.001 581 138 830 084 187	3	2	−0.001 877 602 360 724 986
1	2	−0.012 155 004 756 272 212	1	4	−0.001 098 767 960 437 415

Table 3. Nonvanishing coefficients of the symbol $H^{(10)}_{\mathrm{QNF}} = \sum_{|\alpha|+|\beta|+2\gamma\leqslant 10} \times h_{(\alpha,\beta,\gamma)} x_1^{\alpha_1} x_2^{\alpha_2} \xi_1^{\beta_1} \xi_2^{\beta_2} \hbar^{\gamma}$ of the 10th order quantum normal form of the coupled 2 DoF Eckart–Morse system defined in equation (7.15) in section 7.2. Recall that the nonvanishing terms in the normal form have $\alpha = \beta$.

α_1	α_2	γ	$h_{(\alpha,\beta,\gamma)}$	α_1	α_2	γ	$h_{(\alpha,\beta,\gamma)}$
0	0	0	0.512 500 000 000 000 000	1	3	0	−i 0.011 273 157 211 934 359
1	0	0	0.754 753 936 565 858 878	1	1	2	−i 0.011 172 831 518 205 997
0	1	0	i 1.398 960 687 353 887 473	0	4	0	0.002 732 350 157 899 168
2	0	0	0.123 785 339 782 523 858	0	2	2	0.007 186 254 008 569 981
1	1	0	−i 0.001 065 319 634 986 676	0	0	4	0.000 687 695 639 095 786
0	2	0	0.502 213 521 058 802 562	5	0	0	−0.000 214 239 042 469 975
0	0	2	0.125 449 608 038 641 072	4	1	0	−i 0.000 985 595 001 405 555
3	0	0	0.000 021 351 350 002 054	3	2	0	0.003 423 967 215 023 733
2	1	0	i 0.008 176 183 587 983 269	3	0	2	−0.000 782 323 582 246 664
1	2	0	−0.013 717 963 053 750 142	2	3	0	i 0.001 688 243 381 394 164
1	0	2	−0.014 142 331 760 119 375	2	1	2	i 0.000 302 145 176 622 814
0	3	0	−i 0.002 237 031 129 850 027	1	4	0	0.003 334 954 065 262 960
0	1	2	−i 0.002 154 732 890 857 193	1	2	2	0.011 718 284 130 545 851
4	0	0	0.000 388 266 134 708 556	1	0	4	0.000 106 782 020 240 749
3	1	0	i 0.001 167 305 695 975 092	0	5	0	i 0.001 836 329 386 792 953
2	2	0	−0.007 789 574 828 129 416	0	3	2	i 0.011 444 002 354 002 782
2	0	2	0.000 318 492 327 523 421	0	1	4	i 0.004 314 246 915 341 055

Table 4. Nonvanishing coefficients of the symbol $H^{(10)}_{\mathrm{QNF}} = \sum_{|\alpha|+|\beta|+2\gamma\leqslant 10} \times h_{(\alpha,\beta,\gamma)} x_1^{\alpha_1} x_2^{\alpha_2} x_3^{\alpha_3} \xi_1^{\beta_1} \xi_2^{\beta_2} \xi_3^{\beta_3} \hbar^{\gamma}$ of the coupled 3 DoF Eckart–Morse–Morse system defined in equation (7.38) in section 7.3. Recall that the nonvanishing terms in the normal form have $\alpha = \beta$.

α_1	α_2	α_3	γ	$h_{(\alpha,\beta,\gamma)}$	α_1	α_2	α_3	γ	$h_{(\alpha,\beta,\gamma)}$
0	0	0	0	−0.987 500 000 000 000 000	0	2	0	2	0.152 783 733 769 442 116
1	0	0	0	0.734 955 236 108 148 115	0	1	3	0	0.310 986 515 383 694 741
0	1	0	0	i 1.822 517 936 036 739 209	0	1	1	2	−4.151 328 593 608 719 646
0	0	1	0	i 1.267 290 444 967 990 459	0	0	4	0	0.006 137 865 049 515 079
2	0	0	0	0.118 038 678 383 844 813	0	0	2	2	0.859 423 987 882 411 768
1	1	0	0	−i 0.012 334 879 342 872 699	0	0	0	4	−0.265 855 011 175 839 773
1	0	1	0	i 0.005 310 192 075 685 135	5	0	0	0	−0.000 210 376 032 140 816
0	2	0	0	0.393 832 730 618 103 493	4	1	0	0	−i 0.000 284 795 393 758 395
0	1	1	0	0.909 582 776 314 433 320	4	0	1	0	−i 0.000 337 276 968 652 946
0	0	2	0	0.173 096 436 125 076 552	3	2	0	0	−0.000 627 685 605 556 083
0	0	0	2	0.266 664 869 446 484 871	3	1	1	0	0.003 281 135 664 719 332
3	0	0	0	0.000 552 036 804 498 563	3	0	2	0	0.000 026 178 720 039 055
2	1	0	0	i 0.002 430 126 450 332 083	3	0	0	2	−0.000 809 539 163 262 948
2	0	1	0	i 0.004 886 339 438 884 285	2	3	0	0	−i 0.001 666 813 854 950 104
1	2	0	0	−0.000 569 612 518 570 350	2	2	1	0	−i 0.011 060 027 951 060 662
1	1	1	0	−0.039 861 920 250 395 527	2	1	2	0	i 0.021 558 200 542 697 081
1	0	2	0	0.005 117 262 453 168 276	2	1	0	2	−i 0.001 561 080 497 427 406
1	0	0	2	−0.015 343 995 286 930 709	2	0	3	0	−i 0.004 089 992 505 729 545
0	3	0	0	−i 0.063 077 949 720 773 535	2	0	1	2	−i 0.000 973 333 949 567 230
0	2	1	0	i 0.851 786 534 413 891 081	1	4	0	0	0.002 350 577 380 299 191
0	1	2	0	−i 1.430 298 863 449 648 912	1	3	1	0	0.165 841 199 916 935 531
0	1	0	2	−i 0.085 082 314 838 682 922	1	2	2	0	0.544 009 061 075 099 235

Table 4. Continued.

0	0	3	0	i 0.243 714 959 199 355 560	1	2	0	2	−0.126 519 607 942 211 641
0	0	1	2	i 0.066 628 105 873 760 135	1	1	3	0	−0.182 508 361 502 375 351
4	0	0	0	0.000 459 055 390 142 951	1	1	1	2	2.075 443 875 730 594 886
3	1	0	0	i 0.002 154 242 685 324 458	1	0	4	0	−0.016 321 552 385 758 725
3	0	1	0	i 0.000 532 155 590 347 800	1	0	2	2	−0.493 860 447 549 943 396
2	2	0	0	−0.004 840 046 450 845 588	1	0	0	4	0.100 323 914 200 990 955
2	1	1	0	−0.008 696 277 962 945 819	0	5	0	0	−i 0.035 437 158 103 964 192
2	0	2	0	−0.001 521 249 367 386 827	0	4	1	0	−i 1.098 730 518 769 317 535
2	0	0	2	−0.000 729 166 304 792 555	0	3	2	0	−i 16.346 415 113 011 525 772
1	3	0	0	−i 0.005 625 488 538 854 559	0	3	0	2	i 3.112 191 195 399 140 660
1	2	1	0	−i 0.042 200 218 044 352 362	0	2	3	0	i 25.261 986 404 397 997 857
1	1	2	0	i 0.035 856 221 513 981 255	0	2	1	2	−i 79.663 024 974 498 432 059
1	1	0	2	−i 0.019 385 123 066 852 090	0	1	4	0	−i 3.564 332 805 428 819 594
1	0	3	0	−i 0.005 485 448 552 764 268	0	1	2	2	i 91.718 400 582 446 722 291
1	0	1	2	i 0.005 553 350 862 328 742	0	1	0	4	−i 7.653 275 405 441 236 619
0	4	0	0	−0.022 779 283 170 516 708	0	0	5	0	−i 0.071 898 162 267 093 398
0	3	1	0	−0.382 813 075 268 433 553	0	0	3	2	−i 8.612 377 204 404 908 782
0	2	2	0	−0.852 347 953 691 774 933	0	0	1	4	i 6.544 597 476 333 204 031

Appendix C. Computation of quantum resonances from the complex dilation method

We here provide some details on the *complex dilation method* [Sim79, Rei82, Moi98] that we used to numerically compute the quantum resonances of the 2 DoF coupled Eckart–Morse system in section 7.2 and the 3 DoF coupled Eckart–Morse–Morse system in section 7.3. We illustrate the method for the 2 DoF system. The generalization to 3 DoF is straightforward.

Let $\hat{H} = \mathrm{Op}[H]$ be the Weyl quantization of the Hamilton function H defined in (7.15). For an angle $\alpha \geqslant 0$, we define the scaled operator $\hat{H}^\alpha$ that is obtained from the operator $\hat{H}$ by substituting for the coordinate x the scaled coordinate $\exp(\mathrm{i}\alpha)x$, i.e.

$$\hat{H}^\alpha = -\frac{\hbar^2}{2m}\left(\mathrm{e}^{-2\mathrm{i}\alpha}\frac{\partial^2}{\partial x^2} + \frac{\partial^2}{\partial y^2}\right) + V_{\mathrm{E}}(\mathrm{e}^{\mathrm{i}\alpha}x) + V_{\mathrm{M}}(y) - \epsilon\hbar^2\mathrm{e}^{-\mathrm{i}\alpha}\frac{\partial^2}{\partial x\,\partial y}. \tag{C.1}$$

For $\alpha \neq 0$ this operator is no longer Hermitian. The effect of the complex scaling is that, for suitable $\alpha > 0$, the generalized eigenfunctions of $\hat{H}$ that correspond to resonances become square-integrable after the substitution $x \mapsto \exp(\mathrm{i}\alpha)x$, i.e. they become genuine elements of the Hilbert space $L^2(\mathbb{R}^2)$. The resonances are then given by the eigenvalues of the operator $\hat{H}^\alpha$ which can be computed from a standard variational principle using a finite matrix representation in which $\hat{H}^\alpha$ is expanded in terms of some truncated basis set.

We choose the basis set given by the product states $|n_{\mathrm{dv}}, n_{\mathrm{M}}\rangle := |n_{\mathrm{dv}}\rangle \otimes |n_{\mathrm{M}}\rangle$, where, using the Dirac notation, the states $|n_{\mathrm{dv}}\rangle$ and $|n_{\mathrm{M}}\rangle$ with quantum numbers n_{dv} and n_{M} form 1D basis states in the directions of x and y, respectively. For the y-direction, we choose the eigenstates that correspond to the discrete part of the spectrum of the 1D Morse oscillator $\hat{H}_{\mathrm{M}} := -(\hbar^2/2m)\partial_y^2 + V_{\mathrm{M}}(y)$. The quantum number n_{M} then runs from 0 to $n_{\mathrm{M\,max}} - 1$, where

$$n_{\mathrm{M\,max}} = \left[\frac{\sqrt{2mD_e}}{a_{\mathrm{M}}\hbar} + \frac{1}{2}\right] \tag{C.2}$$

is the number of bound states of the 1D Morse oscillator. The matrix with elements $\langle n_{\mathrm{M}}|\hat{H}_{\mathrm{M}}|n'_{\mathrm{M}}\rangle$ is then diagonal with the Morse oscillator energies on the diagonal, i.e.

$$\langle n_{\mathrm{M}}|\hat{H}_{\mathrm{M}}|n'_{\mathrm{M}}\rangle = E_{\mathrm{M}}(n_{\mathrm{M}})\delta_{n_{\mathrm{M}}n'_{\mathrm{M}}}, \qquad E_{\mathrm{M}}(n_{\mathrm{M}}) = -\frac{a_{\mathrm{M}}^2\hbar^2}{2m}\left(n_{\mathrm{M}} + \frac{1}{2} - \frac{\sqrt{2mD_e}}{a_{\mathrm{M}}\hbar}\right)^2. \tag{C.3}$$

In order to compute the matrix elements of $\hat{H}^\alpha$ with respect to the product states we also need the matrix elements $\langle n_\mathrm{M}|\hat{p}_y|n'_\mathrm{M}\rangle$, where $\hat{p}_y$ is the momentum operator $\hat{p}_y = -\mathrm{i}\hbar\partial_y$. For the elements above the diagonal, we get (see, e.g., [vJBv85])

$$\langle n_\mathrm{M}|\hat{p}_y|n'_\mathrm{M}\rangle = (-1)^{n_\mathrm{M}-n'_\mathrm{M}-1}\mathrm{i}\left(\frac{b_{n_\mathrm{M}}b_{n'_\mathrm{M}}n_\mathrm{M}!\Gamma(2\beta-n_\mathrm{M})}{2\beta^2 n'_\mathrm{M}!\Gamma(2\beta-n'_\mathrm{M})}mD\right)^{1/2}, \qquad n_\mathrm{M} > n'_\mathrm{M}, \tag{C.4}$$

where

$$b_{n_\mathrm{M}} = 2\beta - 2n_\mathrm{M} - 1, \qquad \beta = \frac{\sqrt{2mD_e}}{a_\mathrm{M}\hbar}. \tag{C.5}$$

The diagonal elements vanish and the elements below the diagonal can be obtained from the elements above the diagonal,

$$\langle n_\mathrm{M}|\hat{p}_y|n_\mathrm{M}\rangle = 0, \qquad \langle n'_\mathrm{M}|\hat{p}_y|n_\mathrm{M}\rangle = -\langle n_\mathrm{M}|\hat{p}_y|n'_\mathrm{M}\rangle. \tag{C.6}$$

In the x-direction we choose a so-called *discrete value representation* [LHL85] which consists of a basis set $|n_\mathrm{dv}\rangle$, $n_\mathrm{dv} \in \mathbb{Z}$, for which the wave functions $\langle x|n_\mathrm{dv}\rangle$ are localized in space on a discrete grid. Concretely, we choose the 'sinc' functions

$$\langle x|n_\mathrm{dv}\rangle = \sqrt{\Delta x}\frac{\sin\left(\dfrac{\pi}{\Delta x}(x - n_\mathrm{dv}\Delta x)\right)}{\pi(x - n_\mathrm{dv}\Delta x)}, \tag{C.7}$$

where Δx is a positive constant (the grid spacing). The states $|n_\mathrm{dv}\rangle$ are normalized and orthogonal. The matrix elements of the kinetic energy operator $\hat{p}_x^2/(2m)$ are easily worked out to give

$$\left\langle n_\mathrm{dv}\middle|\frac{\hat{p}_x^2}{2m}\middle|n'_\mathrm{dv}\right\rangle = \begin{cases} \dfrac{1}{6}\dfrac{\hbar^2\pi^2}{m\Delta x^2}, & n_\mathrm{dv} = n'_\mathrm{dv}, \\ (-1)^{n_\mathrm{dv}-n'_\mathrm{dv}}\dfrac{\hbar^2}{m\Delta x^2(n_\mathrm{dv}-n'_\mathrm{dv})^2}, & n_\mathrm{dv} \neq n'_\mathrm{dv}. \end{cases} \tag{C.8}$$

Similarly, we get for the above-diagonal matrix elements of the momentum operator $\hat{p}_x$ in this representation

$$\langle n_\mathrm{dv}|\hat{p}_x|n'_\mathrm{dv}\rangle = (-1)^{n'_\mathrm{dv}-n_\mathrm{dv}}\mathrm{i}\frac{\hbar}{(n'_\mathrm{dv}-n_\mathrm{dv})\Delta x}, \qquad n_\mathrm{dv} > n'_\mathrm{dv}. \tag{C.9}$$

The diagonal elements vanish and the elements below the diagonal can be obtained from the elements above the diagonal,

$$\langle n_\mathrm{dv}|\hat{p}_x|n_\mathrm{dv}\rangle = 0, \qquad \langle n'_\mathrm{dv}|\hat{p}_x|n_\mathrm{dv}\rangle = -\langle n_\mathrm{dv}|\hat{p}_x|n'_\mathrm{dv}\rangle. \tag{C.10}$$

The matrix elements of the potential V_E, or more precisely the complexified potential $V_\mathrm{E}^\alpha(x) = V_\mathrm{E}(\exp(\mathrm{i}\alpha)\,x)$, have to be computed from numerical quadrature.

Using the results above, we find that the matrix elements $\hat{H}^\alpha_{(n_\mathrm{dv},n_\mathrm{M};n'_\mathrm{dv},n'_\mathrm{M})} := \langle n_\mathrm{M}, n_\mathrm{dv}|\hat{H}^\alpha|n_\mathrm{dv}, n_\mathrm{M}\rangle$ of the full operator $\hat{H}^\alpha$ are given by

$$\begin{aligned}\hat{H}^\alpha_{(n_\mathrm{dv},n_\mathrm{M};n'_\mathrm{dv},n'_\mathrm{M})} &= \mathrm{e}^{-2\mathrm{i}\alpha}\langle n_\mathrm{dv}|\frac{\hat{p}_x^2}{2m}|n'_\mathrm{dv}\rangle\delta_{n_\mathrm{M}n'_\mathrm{M}} + \langle n_\mathrm{dv}|\hat{V}_\mathrm{E}^\alpha|n'_\mathrm{dv}\rangle\delta_{n_\mathrm{M}\,n'_\mathrm{M}} \\ &\quad + E_\mathrm{M}(n_\mathrm{M})\delta_{n_\mathrm{dv}\,n'_\mathrm{dv}}\delta_{n_\mathrm{M}\,n'_\mathrm{M}} + \mathrm{e}^{-\mathrm{i}\alpha}\langle n_\mathrm{dv}|\hat{p}_x|n'_\mathrm{dv}\rangle\langle n_\mathrm{M}|\hat{p}_y|n'_\mathrm{M}\rangle.\end{aligned} \tag{C.11}$$

In our numerical study of the 2 DoF system we chose $n_\mathrm{M} \in \{0, \ldots, 13\}$ (for our choice of parameters in section 7.2 the Morse oscillator has 14 bound states), $n_\mathrm{dv} \in \{-50, \ldots, 50\}$ and $\Delta_x = 0.1$. This led to a matrix of size 1414×1414. In our numerical study of the 3 DoF system we chose $n_\mathrm{dv} \in \{-25, \ldots, 25\}$, $\Delta_x = 0.16$, $n_{\mathrm{M};2} \in \{0, \ldots, 6\}$ and $n_{\mathrm{M};3} \in \{0, \ldots, 6\}$

(for our choice of parameters in section 7.3 the 1D Morse oscillators have 14 and 17 bound states, respectively). This led to a matrix of size 2499×2499. We computed the eigenvalues of these matrices using the function eigs in Matlab. For both systems we chose the scaling angle to be $\alpha = 1.2$.

References

[AKN88] Arnol'd V I, Kozlov V V and Neishtadt A I 1988 Mathematical aspects of classical and celestial mechanics *Dynamical Systems III* (*Encyclopaedia of Mathematical Sciences* vol 3) ed V I Arnol'd (Berlin: Springer)

[Ali85] Ali M K 1985 The quantum normal form and its equivalents *J. Math. Phys.* **26** 2565–72

[AM78] Abraham R and Marsden J E 1978 *Foundations of Mechanics* 2 edn (Reading, MA: Benjamin-Cummings)

[Arn78] Arnold V I 1978 *Mathematical Methods of Classical Mechanics* (*Graduate Texts in Mathematics* vol 60) (Berlin: Springer)

[AS65] Abramowitz M and Stegun I A 1965 *Handbook of Mathematical Functions* (New York: Dover)

[AYAD03] Ammal S C, Yamataka H, Aida M and Dupuis M 2003 Dynamics-driven reaction pathway in an intramolecular rearrangement *Science* **299** 1555–7

[Bal98] Ballentine L E 1998 *Quantum Mechanics* revised edn (River Edge, NJ: World Scientific) (A modern development. (MR MR1629320 (99k:81001))

[BGP99] Bambusi D, Graffi S and Paul T 1999 Normal forms and quantization formulae *Commun. Math. Phys.* **207** 173–95 (MR MR1724855 (2001f:81048))

[BHC05] Bach A, Hostettler J M and Chen P 2005 Quasiperiodic trajectories in the unimolecular dissociation of ethyl radicals by time frequency analysis *J. Chem. Phys.* **123** 021101

[BHC06] Bach A, Hostettler J M and Chen P 2005 Nonstatistical effects in the dissociation of ethyl radical: finding order in chaos *J. Chem. Phys.* **125** 024304

[BJ05] Bligaard T and Jónsson H 2005 Optimization of hyperplanar transition states: application to 2D test problems *Comput. Phys. Commun.* **169** 284–8

[Bog92] Bogomolny E B 1992 Semiclassical quantization of multidimensional systems *Nonlinearity* **5** 805–66

[Bow06] Bowman J M 2006 Skirting the transition state, a new paradigm in reaction rate theory *Proc. Natl Acad. Sci.* **103** 16061–2

[Bru71] Bruno A D 1971 Analytical forms of differential equations *Trans. Moscow Math. Soc.* **25** 131–288

[BV90] Bellissard J and Vittot M 1990 Heisenberg's picture and noncommutative geometry of the semiclassical limit in quantum mechanics *Ann. Inst. H Poincaré Phys. Théor.* **52** 175–235 (MR MR1057445 (91f:81035))

[Car05] Carpenter B K 2005 Nonstatistical dynamics in thermal reactions of polyatomic molecules *Ann. Rev. Phys. Chem.* **56** 57–89

[CdV77] Colin de Verdière Y 1997 Quasi-modes sur les variétés Riemanniennes *Invent. Math.* **43** 15–52 (MR MR0501196 (58 #18615))

[CGSL+05] Cargo M, Gracia-Saz A, Littlejohn R G, Reinsch M W and de M Mios P 2005 Quantum normal forms, Moyal star product and Bohr–Sommerfeld approximation *J. Phys. A: Math. Gen.* **38** 1977–2004

[Chr03a] Chruściński D 2003 Quantum mechanics of damped systems *J. Math. Phys.* **44** 3718–33

[Chr03b] Chruściński D 2003 Quantum mechanics of damped systems: II. Damping and parabolic barrier *J. Math. Phys.* **45** 841–54

[CK99] Churchill R C and Kummer M 1999 A unified approach to linear and nonlinear normal forms for Hamiltonian systems *J. Symb. Comput.* **27** 49–131

[CP80] Child M S and Pollak E 1980 Analytical reaction dynamics: origin and implications of trapped periodic orbits *J. Chem. Phys.* **73** 4365–72

[CP94a] Colin de Verdière Y and Parisse B 1994 Équilibre instable en régime semi-classique I *Commun. Partial Diff. Eqns* **19** 1535–63

[CP94b] Colin de Verdière Y and Parisse B 1994 Équilibre instable en régime semi-classique II *Ann. Inst. H Poincaré* (*Phys. Théor.*) **61** 347–67

[CP99] Colin de Verdière Y and Parisse B 1999 Singular Bohr–Sommerfeld rules (III) *Commun. Math. Phys.* **205** 459–500

[Cre90] Crehan P 1990 The proper quantum analogue of the Birkhoff–Gustavson method of normal forms *J. Phys. A: Math. Gen.* **23** 5815–28

[Cre04] Creagh S C 2004 Classical transition state theory in quantum theory *Nonlinearity* **17** 1261–303
[Cre05] Creagh S C 2005 Semiclassical transmission across transition states *Nonlinearity* **18** 2089–110
[Dep69] Deprit A 1969 Canonical transformations depending on a small parameter *Celest. Mech.* **1** 12–30
[DH72] Duistermaat J J and Hörmander L 1972 Fourier integral operators. II *Acta Math.* **128** 183–269 (MR MR0388464 (52 #9300))
[dOdAST02] de Olivieira H P, Ozorio de Almeida A M, Damião Soares I and Tonini E V 2002 Homoclinic chaos in the dynamics of a general Bianchi type-IX model *Phys. Rev.* D **65** 083511
[DS99] Dimassi M and Sjöstrand J 1999 *Spectral Asymptotics in the Semi-classical Limit* (*London Mathematical Society Lecture Note Series* vol 268) (Cambridge: Cambridge University Press)
[DF76] Dragt A J and Finn J M 1976 Lie series and invariant functions for analytic symplectic maps *J. Math. Phys.* **17** 2215–27
[DW95] Dullin H R and Wittek A 1995 Complete Poincaré sections and tangent sets *J. Phys. A: Math. Gen.* **28** 7157–80
[Eck30] Eckart C 1930 The penetration of a potential barrier by electrons *Phys. Rev.* **35** 1303–9
[Eck86] Eckhardt B 1986 Birkhoff–Gustavson normal form in classical and quantum mechanics *J. Chem. Phys.* A **19** 2961–72
[Eck95] Eckhardt B 1995 Transition state theory for ballistic electrons *J. Phys. A: Math. Gen.* **28** 3469
[EGH91] Esposti M D, Graffi S and Herczyński J 1991 Quantization of the classical Lie algorithm in the Bargmann representation *Ann. Phys.* **209** 364–92 (MR MR1117300 (92h:81037))
[Ego69] Ju V Egorov 1969 The canonical transformations of pseudodifferential operators *Usp. Mat. Nauk* **24** 235–6 (MR MR0265748 (42 #657))
[EM74] Eastes W and Marcus R A 1974 Semiclassical calculation of bound states of a multidimensional system *J. Chem. Phys.* **61** 4301–6
[Eyr35] Eyring H 1935 The activated complex in chemical reactions *J. Chem. Phys.* **3** 107–15
[FE88a] Fried L E and Ezra G S 1988 Generalized algebraic quantization: corrections to arbitrary order in Planck's constant *J. Chem. Phys.* **92** 3144–54
[FE88b] Fried L E and Ezra G S 1988 Perturb: a program for calculating vibrational energies by generalized algebraic quantization *Comput. Phys. Commun.* **51** 103–14
[Fol89] Folland G B 1989 *Harmonic Analysis in Phase Space* (*Annals of Mathematics Studies* vol 122) (Princeton, NJ: Princeton University Press)
[FT91] Friedman R S and Truhlar D G 1991 Chemical reaction thresholds are resonances *Chem. Phys. Lett.* **183** 539–46
[Gar00] Garrett B C 2000 Perspective on 'The transition state method,' Wigner E. (1938) Trans. Faraday Soc. 34:29-41 *Theor. Chem. Acc.* **103** 200–4
[GB05] Giménez X and Bofill J M 2005 The canonical transformation theory and its application to the reaction path Hamiltonian *J. Mol. Struct. Theochem.* **727** 21–7
[GGB01] González J, Giménez X and Bofill J M 2001 On the reaction-path Hamiltonian for polyatomic molecules *J. Phys. Chem.* A **105** 5022–9
[GGB04] González J, Giménez X and Bofill J M 2004 Generalized reaction-path Hamiltonian dynamics *Theor. Chem. Acc.* **112** 75–83
[GL77] Grimmelmann E K and Lohr L L Jr 1977 On the exactness of classical transition state theory for collinear collisions *Chem. Phys. Lett.* **48** 487–90
[GS87] Gérard C and Sjöstrand J 1987 Semiclassical resonances generated by a closed trajectory of hyperbolic type *Commun. Math. Phys.* **108** 391–421 (MR MR874901 (88k:58151))
[Gui94] Guillemin V 1994 *Moment Maps and Combinatorial Invariants of Hamiltonian T^n-spaces* (Boston, MA: Birkhäuser)
[Gut90] Gutzwiller M C 1990 *Chaos in Classical and Quantum Mechanics* (*Interdisciplinary Applied Mathematics* vol 1) (Berlin: Springer)
[Har88] Harriman J E 1988 Some properties of the Husimi function *J. Chem. Phys.* **88** 6399–408
[Hel95] Heller E J 1995 Dynamical tunneling and molecular spectra *J. Chem. Phys.* **99** 2625–34
[HB93] Hinde R J and Berry R S 1993 Chaotic dynamics in small inert-gas clusters—the influence of potential-energy surfaces *J. Chem. Phys.* **99** 2942–63
[HK06] Houston P L and Kable S H 2006 Photodissociation of acetaldehyde as a second example of the roaming mechanism *Proc. Natl Acad. Sci.* **103** 16079–82
[Hör71] Hörmander L 1971 Fourier integral operators. I *Acta Math.* **127** 79–183 (MR MR0388463 (52 #9299))
[Hör85a] Hörmander L 1985 The analysis of linear partial differential operators. III *Grundlehren der Mathematischen Wissenschaften* (*Fundamental Principles of Mathematical Sciences* vol 274) (Berlin: Springer) (Pseudodifferential operators. MR MR781536 (87d:35002a))

[Hör85b] Hörmander L 1985 The analysis of linear partial differential operators. IV *Grundlehren der Mathematischen Wissenschaften* (*Fundamental Principles of Mathematical Sciences* vol 275) (Berlin: Springer) (Fourier integral operators. MR MR781537 (87d:35002b))

[HS86] Helffer B and Sjöstrand J 1986 Résonances en limite semi-classique *Bull. Soc. Math. France Mém.* **24–25** Suppl. 114(3) (MR MR871788 (88i:81025))

[IS02] Iantchenko A and Sjöstrand J 2002 Birkhoff normal forms for Fourier integral operators II *Am. J. Math.* **124** 817–50

[JFU00] Jaffé C, Farrelly D and Uzer T 2000 Transition state theory without time-reversal symmetry: chaotic ionization of the hydrogen atom *Phys. Rev. Lett.* **84** 610–3

[JJ01] Jóhannesson G H and Jónsson H 2001 Optimization of hyperplanar transition states *J. Chem. Phys.* **115** 9644–56

[JR61] Johnston H S and Rapp D 1961 Large tunnelling corrections in chemical reaction rates. II *J. Ann. Chem. Soc.* **83** 1–9

[JRL+02] Jaffé C, Ross S D, Lo M W, Marsden J, Farrelly D and Uzer T 2002 Statistical theory of asteriod escape rates *Phys. Rev. Lett.* **89** 011101

[JTDF84] Jacucci G, Toller M, DeLorenzi G and Flynn C P 1984 Rate theory, return jump catastrophes, and center manifolds *Phys. Rev. Lett.* **52** 295–8

[KB99] Komatsuzaki T and Berry R S 1999 Regularity in chaotic reaction paths: I. Ar_6 *J. Chem. Phys.* **110** 9160–73

[KB02] Komatsuzaki T and Berry R S 2002 Chemical reactions dynamics: many-body chaos and regularity *Adv. Chem. Phys.* **123** 79–152

[Kec67] Keck J C 1967 Variational theory of reaction rates *J. Chem. Phys.* **13** 85–121

[Kir01] Kirillov A A 2001 Geometric quantization, Dynamical systems IV *Encyclopaedia of Mathametical Sciences* vol 4 (Berlin: Springer) pp 139–76 (MR MR1866632)

[KK00] Kaidi N and Kerdelhué P 2000 Forme normale de Birkhoff et résonances *Asymptotic Anal.* **23** 1–21 (MR MR1764337 (2001h:35198))

[KMM04] Kaczynski T, Mischaikow K and Mrozek M 2004 *Computational Homology* (*Applied Mathematical Sciences* vol 157) (New York: Springer)

[KMW97] Korsch H J, Müller C and Wiescher H 1997 On the zeros of the Husimi distribution *J. Phys. A: Math. Gen.* **20** L677–84

[LBM02] Lahmar-Benbernou A and Martinez A 2002 *On Helffer–Sjöstrand's Theory of Resonances* (*International Mathematical Research Notices*) (MR MR1890848 (2003m:35258))

[LCZ+07] Lahankar S A, Chambreau S D, Zhang X, Bowman J M and Suits A G 2007 Energy dependence of the roaming atom pathway in formaldehyde decomposition *J. Chem. Phys.* **126** 044314

[LHL85] Light J C, Hamilton I P and Lill J V 1985 Generalized discrete variable approximation in quantum mechanics *J. Chem. Phys.* **82** 1400–9

[LK83] Laidler K J and King M C 1983 The development of transition state theory *J. Phys. Chem.* **87** 2657–64

[LL01] Landau L D and Lifschitz E M 2001 *Quantum Mechanics* (*Non-Relativistic Theory*) (*Course of Theoretical* vol 3) (Dordrecht: Elsevier)

[LM93] Lovejoy E R and Moore C B 1993 Structures in the energy dependence of the rate constant for ketene isomerization *J. Chem. Phys.* **98** 7846–54

[Mac90] MacKay R S 1990 Flux over a saddle *Phys. Lett.* A **145** 425–7

[Mac91] MacKay R S 1991 A variational principle for invariant odd-dimensional submanifolds of an energy surface for Hamiltonian systems *Nonlinearity* **4** 155–7

[Mah74] Mahan B H 1974 Activated complex theory of bimolecular reactions *J. Chem. Educ.* **51** 709–11

[Mar66a] Marcus R A 1966 On the analytical mechanics of chemical reactions. Classical mechanics of linear collisions *J. Chem. Phys.* **45** 4500–4

[Mar66b] Marcus R A 1968 On the analytical mechanics of chemical reactions. Quantum mechanics of linear collisions *J. Chem. Phys.* **45** 4493–9

[Mar68] Marcus R A 1968 On the analytical mechanics of chemical reactions: III Natural collision coordinates *J. Chem. Phys.* **49** 2610–6

[Mar92] Marcus R A 1992 Skiing the reaction slope *Science* **256** 1523–4

[Mar02] Martinez A 2002 *An Introduction to Semiclassical and Microlocal Analysis (Universitext)* (New York: Springer) (MR MR1872698 (2003b:35010))

[Mey70] Meyer K 1970 Generic bifurcation of periodic points *Trans. Am. Math. Soc.* **149** 95–107

[MH92] Meyer K R and Hall G R 1992 *Introduction to Hamiltonian Dynamical Systems and the N-Body Problem* (Berlin: Springer)

[MHA80] Miller W H, Handy N C and Adams J E 1980 Reaction path Hamiltonian for polyatomic molecules *J. Chem. Phys.* **72** 99–112

[Mil76] Miller W H 1976 Importance of nonseparability in quantum mechanical transition-state theory *Acc. Chem. Res.* **9** 306–12

[Mil77] Miller W H 1977 Semiclassical theory for non-separable systems-construction of good action-angle variables for reaction-rate constants *Faraday Discuss.* **62** 40–6

[Mil83] Miller W H 1983 Reaction-path dynamics for polyatomic systems *J. Phys. Chem.* **87** 3811–19

[Mil98a] Miller W H 1998 Direct and correct calculation of canonical and microcanonical rate constants for chemical reactions *J. Phys. Chem.* A **102** 793–806

[Mil98b] Miller W H 1998 Spiers Memorial Lecture. Quantum and semiclassical theory of reaction rates *Farad. Discuss.* **110** 1–21

[MM97] Makarov D E and Metiu H 1997 The reaction rate constant in a system with localized trajectories in the transition region: classical and quantum dynamics *J. Chem. Phys.* **107** 7787–99

[MMW98] McCord C K, Meyer K R and Wang Q D 1998 The integral manifolds of the three body problem *Mem. Am. Math. Soc.* **628** 1–91

[Moi98] Moiseyev N 1998 Quantum theory of resonances: calculating energies, widths and cross-sections by complex scaling *Phys. Rep.* **302** 211–93

[MR99] Marsden J E and Ratiu T S 1999 *Introduction to Mechanics and Symmetry* 2nd edn (Heidelberg: Springer)

[MST83] Miller W H, Schwartz S D, and Tromp J W 1983 Quantum mechanical rate constants for bimolecular reactions *J. Chem. Phys.* **79** 4889–98

[Mur03] Murdock J 2003 *Normal Forms and Unfoldings for Local Dynamical Systems* (Berlin: Springer)

[Nat91] Natanson G A 1991 A reduction of the reaction path formalism to the space of internal variables *Chem. Phys. Lett.* **178** 49–54

[Nat92a] Natanson G A 1992 A new definition for the reaction coordinate via adiabatic dividing surfaces formed by classical trajectories *Chem. Phys. Lett.* **190** 215–24

[Nat92b] Natanson G A 1992 Optimum choice of the reaction coordinate for adiabatic calculations of the tunneling probabilities *Chem. Phys. Lett.* **190** 209–14

[Nat04] Natanson G A 2004 Explicit definition of the reaction coordinate for the Jackels–Gu–Truhlar projection technique to compute harmonic vibrational frequencies along the intrinsic reaction path *Theor. Chem. Acc.* **112** 68–74

[Neu92] Neumark D M 1992 Transition state spectroscopy of bimolecular chemical reactions *Ann. Rev. Phys. Chem.* **43** 153–76

[NGT+91] Natanson G A, Garrett B C, Truong T N, Joseph T and Truhlar D G 1991 The definition of reaction coordinate for reaction-path dynamics *J. Chem. Phys.* **94** 7875–92

[NM01] Neumaier A and Mandelshtam V A 2001 Pseudotime Schrödinger equation with absorbing potential for quantum scattering calculations *Phys. Rev. Lett.* **86** 5031–4

[NV97] Nonnenmacher S and Voros A 1997 Eigenstate structures around a hyperbolic point *J. Phys. A: Math. Gen.* **30** 295–315 (MR MR1447118 (98e:81063))

[OdA88] Ozorio de Almeida A M 1988 *Hamiltonian Systems: Chaos and Quantization* (Cambridge, UK: Cambridge University Press)

[PC80] Pollak E and Child M S 1980 Classical mechanics of a collinear exchange reaction: a direct evaluation of the reaction probability and product distribution *J. Chem. Phys.* **73** 4373–80

[PCC+05] Pomerantz A E, Camden J P, Chiou A S, Ausfelder F, Chawla N, Hase W L and Zare R N 2005 Reaction products with internal energy beyond the kinematic limit result from trajectories far from the minimum energy path: an example from $H + HBr \rightarrow H_2 + Br$ *J. Am. Chem. Soc.* **127** 16368–9

[PCP80] Pollak E, Child M S and Pechukas P 1980 Classical transition state theory: a lower bound to the reaction probability *J. Chem. Phys.* **72** 1669–78

[Pec76] Pechukas P 1976 *Dynamics of Molecular Collisions* ed W H Miller (New York: Plenum)

[Pec81] Pechukas P 1981 Transition state theory *Ann. Rev. Phys. Chem.* **32** 159–77

[Pet00] Petersson G A 2000 Perspective on 'The activated complex in chemical reactions', Eyring, H. (1995) J. Chem. Phys. 3: 107 *Theor. Chem. Acc.* **103** 190–5

[PM73] Pechukas P and McLafferty F J 1973 On transition-state theory and the classical mechanics of collinear collisions *J. Chem. Phys.* **58** 1622–5

[PM03] Pérez-Marco R 2003 Convergence or generic divergence of the Birkhoff normal form *Ann. Math.* **157** 557–74

[PM05] Predescu C and Miller W H 2005 Optimal choice of dividing surface for the computation of quantum reaction rates *J. Phys. Chem.* B **109** 6491–9

[PMOE06] Pearce J K, Murray C and Orr-Ewing A J 2006 How do the structures of polyatomic molecules affect their reaction dynamics? *Phys. Scr.* **73** C14–19

[Poi93a] Poincaré H 1993 *New Methods of Celestial Mechanics Vol. 1* (*History of Modern Physics and Astronomy* vol 13) (New York: American Institute of Physics) *Periodic and Asymptotic Solutions* (Translated from the French) Revised reprint of the 1967 English translation (With endnotes by V I Arnol′d, edited and with an introduction by D L Goroff)

[Poi93b] Poincaré H 1993 *New Methods of Celestial Mechanics Vol. 2* (*History of Modern Physics and Astronomy* vol 13) (New York: American Institute of Physics) *Approximations by Series* (Translated from the French) Revised reprint of the 1967 English translation (With endnotes by V M Alekseev, edited and with an introduction by D L Goroff)

[Poi93c] Poincaré H 1993 *New Methods of Celestial Mechanics. Vol. 3* (*History of Modern Physics and Astronomy* vol 13) (New York: American Institute of Physics) *Integral Invariants and Asymptotic Prperties of Certain Solutions* (Translated from the French) Revised reprint of the 1967 English translation (With endnotes by G A Merman, edited and with an introduction by D L Goroff)

[Pol81] Pollak E 1981 Spectral theorem in bimolecular collisions *J. Chem. Phys.* **74** 6763–4

[PP77] Pechukas P and Pollak E 1977 Trapped trajectories at the boundary of reactivity bands in molecular collisions *J. Chem. Phys.* **67** 5976–7

[PP78] Pechukas P and Pollak E 1978 Transition states, trapped trajectories, and classical bound states embedded in the continuum *J. Chem. Phys.* **69** 1218–26

[PP79a] Pechukas P and Pollak E 1979 Classical transition state theory is exact if the transition state is unique *J. Chem. Phys.* **71** 2062–8

[PP79b] Pollak E and Pechukas P 1979 Unified statistical model for 'complex' and 'direct' reaction mechanisms: a test on the collinear $H + H_2$ exchange reaction *J. Chem. Phys.* **70** 325–33

[Pri05] Pritchard H O 2005 Recrossings and transition state theory *J. Phys. Chem.* A **109** 1400–4

[PT05a] Pollak E and Talkner P 2005 Reaction rate theory: what is was, where it is today, and where is it going? *Chaos* **15** 026116

[PT05b] Pollak E and Talkner P 2005 Reaction rate theory: what it was, where it is today, and where is it going? *Chaos* **15** 026116

[PZ95] Polanyi J C and Zewail A H 1995 Direct observation of the transition state *Acc. Chem. Res.* **28** 119–32

[Rei82] Reinhardt W P 1982 Complex coordinates in the theory of atomic and molecular structure and dynamics *Annu. Rev. Phys. Chem.* **33** 223–55

[Rob84] Robnik M 1984 The algebraic quantisation of the Birkhoff–Gustavson normal form *J. Phys. A: Math. Gen.* **17** 109–30

[Rüs67] Rüssmann H 1967 Über die Normalform analytischer Hamiltonscher Differentialgleichungen in der Nähe einer Gleichgewichtslösung *Math. Ann.* **169** 55–72

[Sim79] Simon B 1979 The definition of molecular resonance curves by the method of exterior complex scaling *Phys. Lett.* A **71** 211–4

[Sjö87] Sjöstrand J 1987 Semiclassical resonances generated by nondegenerate critical points *Pseudodifferential Operators* (*Oberwolfach, 1986*), (*Lecture Notes in Mathametics* vol 256) (Berlin: Springer) pp 402–429 (MR MR897789 (88m:35003))

[Sjö92] Sjöstrand J 1992 Semi-excited states in nondegenerate potential wells *Asymptot. Anal.* **6** 29–43 (MR MR1188076 (93m:35052))

[Sjö03] Sjöstrand J 2003 Resonances associated to a closed hyperbolic trajectory in dimension 2 *Asymptot. Anal.* **36** 93–113 (MR MR2021528 (2004j:35214))

[SK78] Sverdlik D I and Koeppl G W 1978 An energy limit of transition state theory *Chem. Phys. Lett.* **59** 449–53

[SM71] Siegel C L and Moser J K 1971 *Lectures on Celestial Mechanics* (Berlin: Springer)

[SM91] Seideman T and Miller W H 1991 Transition state theory, Siegert eigenvalues, and quantum mechanical reaction rates *J. Chem. Phys.* **95** 1768–80

[SSH02] Sun L, Song K and Hase W L 2002 A S_N2 reaction that avoids the deep potential energy minimum *Science* **296** 875–8

[SSM+00] Skodje R T, Skouteris D, Manolopoulos D E, Lee S-H, Dong F and Liu K 2000 Resonances-mediated chemical reaction: $F + HD \rightarrow HF + D$ *Phys. Rev. Lett.* **85** 1206–9

[SY04] Skodje R T and Yang X 2004 The observation of quantum bottleneck states *Int. Rev. Phys. Chem.* **23** 253–87

[TG84] Truhlar D G and Garrett B C 1984 Variational transition state theory *Ann. Rev. Phys. Chem.* **35** 159–89

[TGK96] Truhlar D G, Garrett B C and Klippenstein S J 1996 Current status of transition state theory *J. Chem. Phys.* **100** 12771–800

[TLL+04] Townsend D, Lahankar S A, Lee S K, Chambreau S D, Suits A G, Zhang Z, Rheinecker J, Harding L B and Bowman J M 2004 The roaming atom: straying from the reaction path in formaldehyde decomposition *Science* **306** 1158–61

[Tru98] Truhlar D G 1998 General discussion *Faraday Discuss.* **110** 91–104

[UJP+01] Uzer T, Jaffé C, Palacián J, Yanguas P and Wiggins S 2001 The geometry of reaction dynamics *Nonlinearity* **15** 957–92

[vJBv85] Špirko V, Jensen P, Bunker P R and Čejchan A 1985 The development of a new Morse-oscillator based rotation–vibration Hamiltonian for H_3^+ *J. Mol. Spectrosc.* **112** 183–202

[VMG02] Voter A F, Montalenti F and Germann T C 2002 Extending the time scale in atomistic simulation of materials *Ann. Rev. Mater. Res.* **32** 321–46

[vWvHB+88] vann Wees B J, van Houten H, Beenakker C W J, Williamson J G, Kouwenhoven L P, van der Marel D and Foxon C T 1988 Quantized conductance of point contacts in a two-dimensional electron gas *Phys. Rev. Lett.* **60** 848–50

[Wal04] Wales D J 2004 *Energy Landscapes: Applications to Clusters, Biomolecules and Glasses* (Cambridge, UK: Cambridge University Press)

[WBW04a] Waalkens H, Burbanks A and Wiggins S 2004 A computational procedure to detect a new type of high-dimensional chaotic saddle and its application to the 3D Hill's problem *J. Phys. A: Math. Gen.* **37** L257–65

[WBW04b] Waalkens H, Burbanks A and Wiggins S 2004 Phase space conduits for reaction in multidimensional systems: HCN isomerization in three dimensions *J. Chem. Phys.* **121** 6207–25

[WBW05a] Waalkens H, Burbanks A and Wiggins S 2005 Efficient procedure to compute the microcanonical volume of initial conditions that lead to escape trajectories from a multidimensional potential well *Phys. Rev. Lett.* **95** 084301

[WBW05b] Waalkens H, Burbanks A and Wiggins S 2005 Escape from planetary neighborhoods *Mon. Not. R. Astron. Soc.* **361** 763–75

[WBW05c] Waalkens H, Burbanks A and Wiggins S 2005 A formula to compute the microcanonical volume of reactive initial conditions in transition state theory *J. Phys. A: Math. Gen.* **38** L759–68

[Wig38] Wigner E 1938 The transition state method *Trans. Faraday Soc.* **34** 29–48

[Wig94] Wiggins S 1994 *Normally Hyperbolic Invariant Manifolds in Dynamical Systems* (Berlin: Springer)

[WTN+88] Wharam D A, Thornton T J, Newbury R, Pepper M, Ahmed H Frost J E F, Hasko D G, Peacock D C, Ritchie D A and Jones G A 1988 One-dimensional transport and the quantisation of the ballistic resistance *J. Phys. C: Solid State Phys.* **21** L209

[WW04] Waalkens H and Wiggins S 2004 Direct construction of a dividing surface of minimal flux for multi-degree-of-freedom systems that cannot be recrossed *J. Phys. A: Math. Gen.* **37** L435–45

[WWJU01] Wiggins S, Wiesenfeld L, Jaffé C and Uzer T 2001 Impenetrable barriers in phase-space *Phys. Rev. Lett.* **86** 5478–81

[YT60] Yanao T and Takatsuka K 1960 Quantum statistical mechanical theory of the rate of exchange chemical reactions in the gas phase *J. Chem. Phys.* **33** 281–9

[Zar06] Zare R N 2006 Resonances in reaction dynamics *Science* **311** 1383–5

[Zew00] Zewail A H 2000 Femtochemistry: atomic-scale dynamics of the chemical bond *J. Phys. Chem.* **104** 5660–94

[Zwo99] Zworski M 1999 Resonances in physics and geometry *Not. Am. Math. Soc.* **46** 319–28